Complexes of Platinum(II) and Iridium(III) with Liquid Crystal and Luminescent Properties

Submitted by **Amedeo Santoro**

University of York   29 August 2010
Department of Chemistry

Thesis for the degree of Doctor of Philosophy in Chemistry.

Abstract

   This thesis is concerned with the search for luminescent metallomesogens, a class of materials that presents the combination of two different properties, luminescence (triplet emission) and liquid crystallinity. The motivation is two-fold. One possibility is that these materials could be used as polarised back-light emitters in liquid crystal displays, which would mean that the back polariser could be removed, so improving light throughput through the device. The other is that, owing to the order inherent in liquid crystal phases, the use of liquid-crystalline components will lead to better charge-carrier mobilities, this enhancing the overall efficiency of the devices in which they are used.

The research is based around cyclometallated 2-phenylpyridine complexes of two metals, platinum(II) with its square planar geometry, and iridium(III) with its octahedral geometry, and the aim is to modify the ligand structures so that, in combination with the metal, liquid-crystalline complexes result that retain the emissive properties of the 2-phenylpyridine-metal chromophore..

All the complexes have been characterise using different technique. Chemical characterisation used NMR spectroscopy, elemental analysis, mass spectrometry and in some cases single crystal X-ray diffraction. Liquid crystal phases were characterised using combinations of polarised optical microscopy, differential scanning calorimetry and powder X-ray diffraction.

Chapter 1

Chapter 1 commences with the introduction to OLED devices, with a general description of the working principle and materials requirements. A brief description of the reasons behind the use of luminescent liquid crystal material for OLED and other application is given, along with an introduction to the liquid crystal world where particular structural requirements and some of the more common phases are describe in detail. Furthermore, a detailed description of the techniques to recognise the different liquid crystal phases is given.

Chapter 2

Chapter 2 deals with the reasons behind the choice of 2-phenylpyridine-type ligands and platinum(II) as metal centre. Furthermore the synthesis of the ligand with the use of a Diels-Alder methodology for the insertion of side substituents on the ligand are discussed. The synthetic strategy for obtaining the platinum complexes is given along with the discovery of the synthesis of new class of dinuclear Pt^{III} liquid crystal complex. The liquid crystal properties of ligands and complexes are reported, with a full discussion of their phases and a comparison with similar materials reported in literature.

Chapter 3

Chapter 3 describes work directed at realising liquid-crystalline complexes of iridium(III) given the challenge of working with octahedral complexes. The successes and failures are described and are discussed in the light of the repeated formation of an as yet unidentified complex, which seems to result when monodentate ligands are present. The liquid crystal properties of some complexes are described.

Chapter 4

Chapter 4 discusses fully the luminescent properties of the platinum complexes including a detailed comparison with the similar material present in the literature, and the modification that can be used to improve the quantum yield and/or tune the emission. Less characterisation has been carried out with the iridium complexes because of their instability, but such results that have been obtained are discussed.

Chapter 5

Chapter 5 gives a summative, critical conclusion to the project.

Chapter 6

Chapter 6 present all the experimental information and characterisation data of the materials synthesised in this thesis project along with details of the instrumentation used.

Paper published in connection with this thesis

-*Oxidation of Organoplatinum(II) by Coordinated Dimethylsulfoxide: Dinuclear, Liquid-Crystalline Complexes of Platinum(III)*, A. Santoro, M. Wegrzyn, A. C. Whitwood, B. Donnio and D. W. Bruce, *J. Am. Chem. Soc.*, 2010, **132**, 10689.

-*Luminophores*, UK Patent Appl. No. GB1004151.5 (13 **March** 2010) D. W. Bruce, V. N. Kozhevnikov, A. M. Prokhorov and A. Santoro.

-*Luminophores*, UK Patent Appl. No. PCT/GB2010/000349 (26 **February** 2010) D. W. Bruce, V. N. Kozhevnikov and A. Santoro.

-*Synthesis, Mesomorphism, and Luminescent Properties of Calamitic 2-Phenylpyridines and Their Complexes with Platinum(II),* A. Santoro, A. C. Whitwood, J. A. G. Williams, V. N. Kozhevnikov and D. W. Bruce, *Chem. Mater.*, 2009, **21**, 3871.

-*Synthesis of Cyclometallated Platinum(II) Complexes with Substituted Thienylpyridines and Detailed Characterization of Their Luminescence Properties,* D. N. Kozhevnikov, V. N. Kozhevnikov, M. M. Ustinova, *A. Santoro*, D. W. Bruce, B. Koenig, R. Czerwieniec, T. Fischer, M. Zabel and H. Yersin, *Inorg. Chem.,* 2009, **48**, 4179.

-*From 1,2,4-triazines towards substituted pyridines and their cyclometallated Pt(II) complexes,* V. N. Kozhevnikov, M. M. Ustinova, P. A. Slepukhin, A. Santoro, D. W. Bruce and D. N. Kozhevnikov, *Tetrahedron Lett.*, 2008, **49**, 4096.

Abbreviations

The following abbreviations will be used throughout this thesis:

EL	Electroluminescence
OLEDs	Organic Light Emitting Diodes
LCD	Liquid Crystal Display
PL	Photoluminescence
HOMO	Highest Occupied Molecular Orbital
LUMO	Lowest Unoccupied Molecular Orbital
EML	Emitting Layer
ETL	Electron Transport Layer
HTL	Hole Transport Layer
EIL	Electron Injection Layer
HIL	Hole Injection Layer
Cr	Crystal
N	Nematic
SmA	Smectic A phase
SmC	Smectic C phase
SmI	Smectic I phase
SmF	Smectic F phase
SmB	Smectic B phase
L	Lamellar
Col	Columnar (*e.g.* Col_h = columnar hexagonal)
I	Isotropic
NMR	Nuclear Magnetic Resonance
s	Singlet
d	Doublet
t	Triplet
m	Multiplet
DSC	Differential Scanning Calorimetry
DMSO	Dimethylsulfoxide
DMS	Dimethylsulfaide
phpy	2-Phenylpyridine
acac	acetylacetonate
hfac	hexafluoro acetylacetonate
tfac	trifluoro acetylacetonate
LC	Ligand Centre (1= singlet, 3 = triplet)
MC	Metal Centre (1= singlet, 3 = triplet)
MLCT	Metal Ligand Charge Transfer
CT	Charge Transfer

Chapter 1: Introduction to Organic Light Emitting Diodes and Liquid Crystals

1.1 Organic Light Emitting Diodes.

1.1.1 History.

1.1.1.1 Definition.

Electroluminescence (EL) is the production of light by the flow of electrons, as within certain crystals. EL is one of the few instances in which direct conversion of electric energy into visible light takes place without the generation of heat.[1]

1.1.1.2 Key points

The demonstration of electroluminescence (EL) in organic compound, discovered by Bernanose and co-workers in the early 1950s through applying a high-voltage (alternating current) to crystalline thin films of acridine orange[I] and quinacridone,[I,2] was the first step to open a new, large field of interesting research. In 1960, researchers at Dow Chemicals developed AC-driven electroluminescent cells using doped anthracene[I,3], but the technology developed significantly after the 1987 when Tang and Van Slyke[4] constructed the first EL device, employing tris(8-hydroxyquinolato)aluminium(III) as the luminescent material. Since then, many studies of EL material have been carried out, and above all, in the last 20 years, EL

compounds have found more and more applications in modern technology. But one in particular is the driving force of recent research: Organic Light Emitting Diodes, a new technology to the world of displays. Organic electroluminescent materials have been the subject of intense research for use in light-emitting diodes (LEDs) in general, in the last 10 years. When compared with liquid crystals displays, the prototype of organic light emitting diodes show faster response time, and have improved colour contrast. But the greatest benefit of OLED displays over traditional liquid crystal displays (LCDs) is that OLEDs do not require a backlight to work and can be made much thinner.[3] The OLEDs are already better also in response time, viewing angle and contrast ratio. The weak points are those connected with the production, essentially high cost of manufacturing, lifetime of the displays, and resolution, especially for large size displays. Nowadays, with the development of better multilayer system, the difference in power consuming is hugely decreased (Figure 1).
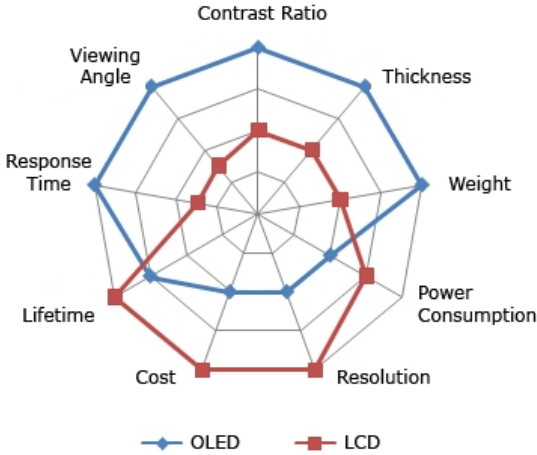
Figure 1-I Schematic comparison of LCD and OLED displays. The radial axes are in arbitrary units and represent the relative efficiency of the two devices. (http://digidelve.com accessed 6/05/2010)

But all these improvement are still far to be addressed in commercially available displays even if some small and monochromatic displays are already on the market. Therefore, as will be discussed in the next sections, a lot of effort in the research is needed to find solution to several different problem such as blue-emitters, matching different energetic level in multilayer systems, electrostability and photostability of the compound, all these aspect and some other will be discussed in the following part of the thesis.

1.1.2 Why use Liquid Crystals for OLEDs?

Recently, there has been great attention for the development of new liquid crystalline materials for new areas such as thin-film transistors,[5] solid organic lasers[6] and photovoltaic devices;[7] this is due to the self-assembling properties and the various supramolecular structures of liquid crystals.[8] It is without any doubt that some materials require organised structures to improve their performance, and consequently it is logical to think that the intrinsic ability of the liquid crystals to self organise into well-defined supramolecular structures could be one of the key advantages to increase the desired property. A remarkable characteristic of liquid crystals is that different phases can be used in order to obtain different physical effect. For example, some discotic liquid crystal oriented in columns act as molecular wires and they proved to have highly anisotropic hole mobility along the columns.[9] Therefore with appropriate functionalisation of *disc-like* molecules, it is possible to achieve a self-organised structure that forms specific channels for the transport of electrons or holes. *Rod-like* liquid crystal are no less important, indeed they can be used in all the applications that

required a highly anisotropic material. Indeed, if luminescent molecules are used that organise themselves in a nematic or smectic phase, because all the molecules are oriented in the same direction it is possible to obtain polarised emission.[8c] This could be of great advantage for new generation of LCDs and is discussed below.

Another example is that luminescent and charge-transporting liquid crystal polymer networks formed from nematic liquid crystal monomers provide a low-cost option to fabricate multilayer OLEDs with the added advantage of being photolithographically patternable.[10]

A further interesting effect of luminescent liquid crystal materials is that the aliphatic side-chain acts as spacer in the solid state reducing intermolecular forces of attraction due to steric effects; this can result in a high solid-state luminescence efficiency (quantum yield).[11]

1.1.3 Device Structure

The simplest OLED device, where the light is generated by electrical excitation, is a thin film of luminescent material sandwiched between two electrodes. The cathode typically consists of a thin film of a metal such as calcium or aluminium, while the most commonly used anode is a semi-transparent indium-tin oxide (ITO)-coated glass or polymer substrate. If a polymer substrate is used, the possibility of creating an ultra-thin, flexible display becomes achievable.
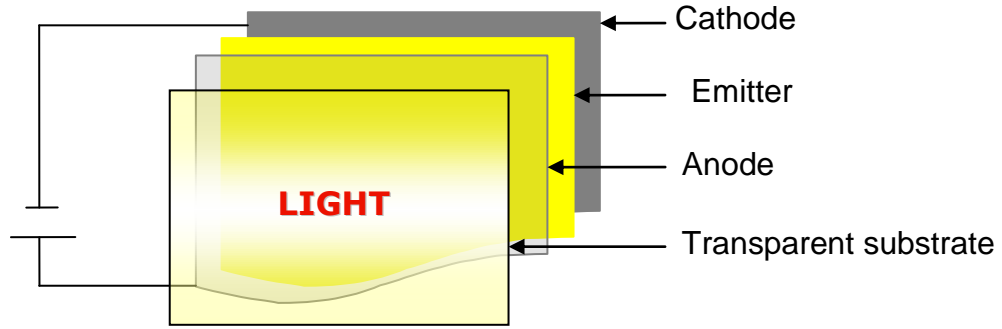
Figure 2-I Simplest OLED device construction.

A simple OLED device construction is shown in Figure 2. The material sandwiched between the cathode and the anode has to be an emissive material.

The working concept of these devices is very simple. When an electrical current is applied across the device, electrons are injected into the lowest unoccupied molecular orbital (LUMO) of the EL material at the cathode generating an electronically excited state, and holes are injected into the highest occupied molecular orbital (HOMO) of the EL material at the anode,[12] which relaxes with the emission of light as either fluorescence or phosphorescence, depending on the material used. The luminous power efficiency (L_{eff}) is defined through the equation (1):

$$L_{eff} = \frac{\pi L}{JV}$$

(1)

where L is the luminance with units $cd \cdot m^{-2}$, J is the current density in $A \cdot m^{-2}$, and V is the applied voltage in V. The external quantum efficiency (Φ_{ext}) of the electroluminescent device is defined as the number of photons emitted per number of injected charge carriers, and is

expressed by equation (2):[13]

$$\Phi_{ext} = \frac{\pi L \int \frac{F^{'}(\lambda)\lambda}{hc} d\lambda}{\int F^{'}(\lambda) K_m y(\lambda) d\lambda} \div \frac{J}{e} \qquad (2)$$

where e is elementary charge (in C), λ is the wavelength (in nm), h is the Planck constant (in J·s), c is the velocity of light (in m·s^{-1}), K_m is the maximum luminous efficiency, $F^{'}(\lambda)$ is the EL spectrum, and $y(\lambda)$ is the normalised photonic spectral response function.

The main factors that contribute to L_{eff} and Φ_{ext} are:

- efficiency of charge carrier injection;

- charge balance;

- spin multiplicity of luminescent state (singlet, triplet);

- photoluminescent (PL) quantum yield;

- extraction of the light emitted out of the device.

Therefore, it is possible to say that $\Phi_{ext} = \alpha(\Phi_{re} \cdot \Phi_{spin} \cdot \Phi_{em})$, where α is the light extraction factor, Φ_{re} is the probability of recombination of injected holes and electrons, Φ_{spin} represents the probability of generating an electronically excited state, either singlet or triplet (the value is 0.25 for singlet and 0.75 for triplet formation) and Φ_{em} represents the photoluminescent quantum yield from either the singlet excited state or the triplet excited state.[14] To improve Φ_{re}, multilayer systems have been developed (Figures 3 and 4).
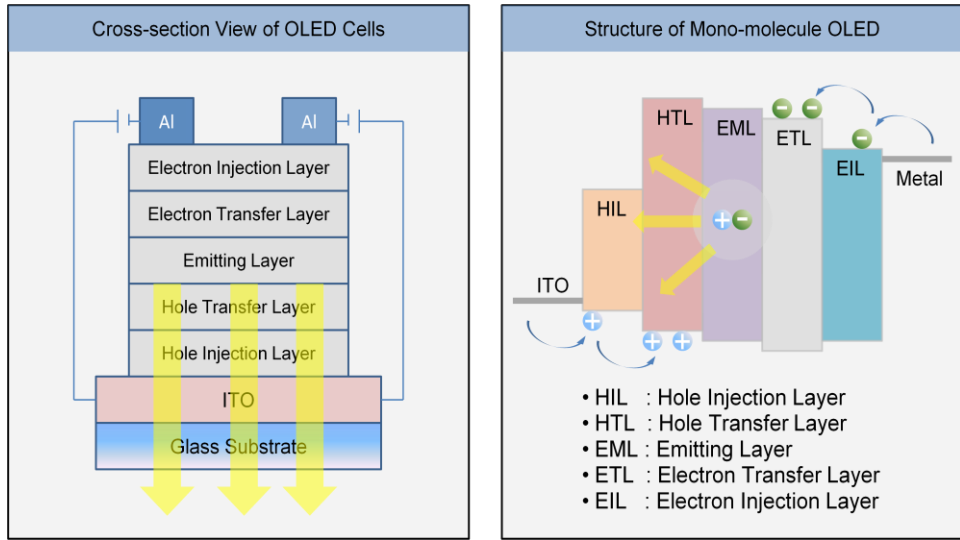
Figure 3-I Structure of OLED.
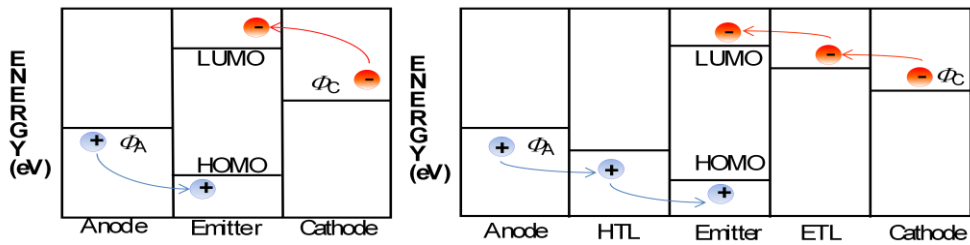
Figure 4-I Energy-level diagram of single-layer OLED and multilayer OLED device.

These multilayer systems are very important because efficient devices require the matching of energy to minimise the barrier between anode and EML (emitting layer), and between cathode and EML. Indeed, if there is a large gap in energy between the HOMO and the anode work function (Φ_a) or the LUMO and the cathode work function (Φ_c), charge injection will be poor[15] (Figures 3 and 4).

Two other important requirements for efficient OLED devices are the carrier mobility (μ) for ETL (electron transport layer) and HTL (hole transport layer), defined as the electron or hole velocity per unit of electric field. It is possible to calculate μ using equation (3):

$$\mu = \frac{d^2}{V\tau} \tag{3}$$

where d is the sample thickness, τ is the transit time, namely the time that a sheet of charge carriers generated near to one electrode take to arrive to the other electrode, and V is the potential applied to the device.

The other important requirement is to have high quantum efficiency for EML. Therefore, incorporation of a layer with either good hole or electron affinity between the emissive layer and the electrode reduces the energy barrier to charge injection.

1.1.4 Materials

In considering the device operation laid out in the present section, a broad spectrum of material requirements for OLEDs emerge:

(a) the materials should possess suitable ionisation potentials and electron affinities;

(b) they should have energy levels well matched for the injection of charge carriers from the electrodes or the organic layer in to the adjacent organic layers;

(c) they should be capable of giving a smooth, uniform, thin film without pinholes;

(d) they should be thermally, photochemically and electrochemically stable;

(e) the material should have a high viscosity which can lead to an amorphous glass, required for long-term stability;

(f) materials should have specific properties based on the role they will play in the device, for example: materials which have low ionisation potentials together with low electron

affinities usually function as hole-transporting materials, whereas materials which have high electron affinities together with high ionisation potentials, usually function as electron-transporting materials.

The two main classes of organic materials normally used (small molecules and conjugated main-chain polymers) involve two different methods of layer deposition, and there are many review articles that examine these issues.[16]

The deposition method used with low molecular weight OLEDs was the first to be developed, and employed thermal evaporation of the material forming thermally stable glasses, with the other thin films being deposited in sequence to obtain the device. This method gives very good results for both luminous power efficiency, (L_{eff} = 60 lm·W^{-1}) and external quantum efficiency (Φ_{ext} = 19%).[17] Unfortunately this multilayer approach by physical vapour deposition is expensive and difficult to realise.

Alternative methods to deposit electroluminescent and charge-transporting films of main-chain conjugated polymers (POLEDs) are ink-jet printing or spin-coating. These thin films of polymers are stabilised in the glassy state and the method is cheaper and scalable, but the results are poorer (L_{eff} = 20 lm·W^{-1}).[18] This method can also lead to problems with layers because the solvent used to deposit the next layer could dissolve the underlying film deposited previously.

As the device performance is highly dependent on the morphology of the materials, control over morphology is of crucial importance in materials science and practical applications. Indeed, in recent years, another method has started to be tested along these two well established and commercially viable technologies, namely the use of liquid crystal materials for applications different from the LCD displays. Therefore a combination of different

properties start to be investigated, such as fluorescent and phosphorescent liquid crystal materials, liquid crystal materials for charge transport, and several others.[9]

1.2 Current State of the Art.

The continued dominance of LCDs (Liquid Crystal Displays) in the area of flat-panel displays is starting to be challenged by the rapid improvements in OLED displays.[19] Monochromatic screens based on these device have been available since 1997, but in November 2007, Sony started to sell the XEL-1, the world's first OLED TV[20] with an 11-inch display, (1300 units in one day in Japan alone, Figure 5). Recently, Sony demonstrated a wireless, battery-powered version of the XEL-1 to highlight what is possible with a low-power TV.[21] (http://www.pcworld.co.uk - the XEL-1 is on sale for £2499)

Figure 5-I The XEL-1, the world's first OLED TV with an 11-inch display by Sony.
(http://www.sony.co.uk/product/tvp-oled-tv/xel-1) (accessed 8/06/10)

1.2.1 Triplet Emitter for OLEDs

The first OLED devices utilised small, fluorescent, organic molecules and dopant compounds.[4] However, in the last ten years transition metal complexes with luminescence properties have become highly attractive, in particular due to their applicability in electro-luminescence devices such as OLEDs. Attention has been focused more specifically on triplet

emitters, because one of the requirements of all the new technologies, but especially of displays, is low power consumption and high efficiency, and organo-transition metal complexes may potentially improve the luminescence efficiency[22] by a factor of four.

Fluorescence is a radiative relaxation with the retention of the electron spin and typically involves a transition between singlet excited state and ground state. On the other hand phosphorescence results from a spin-forbidden transition where the electron spin is not conserved, usually between a triplet exited state and singlet ground state. Under electrical excitation both excited states, singlet and triplet, are populated; therefore harvesting luminescence only from singlet state emission significantly compromises the efficiency of the displays.[23] Thus, if the formation of a spin-forbidden state through the introduction of electron from the cathode and hole from the anode are considered there are four possible combinations of the electronic spin of the two charge carriers.[19,24] Of these, three give a resultant spin of one, a triplet state, and one gives zero, a singlet state. Therefore, if organometallic compounds containing heavy atoms are used, the efficient spin-orbit coupling (SOC) leads to rapid conversion between the singlet and triplet state, facilitating the intersystem crossing leading to an enhanced triplet formation. As both states, singlet and triplet, are used, the theoretical possibility exists to achieve an internal quantum yield of up to 100%.[25,26]

Nowadays, probably the most studied complexes are cyclometalated derivatives of Ir[III], and more than 100 reports are published every year.[27] In this context other metals are more recently becoming a source of attention, such as Ru and Pt.[21] Depending on the specific compound, the emission can show widely different properties. The wavelength can be tuned from blue to red and, in some cases, ultraviolet or infrared emission is achievable. Further, the quantum yield and the excited state lifetime are found over a wide range, from an attractive

99%[28] to less than 1%,[29] and from less than 1 μs[24] to as long as several milliseconds.[21] This will be discussed in more detail in Chapter 4. Only a few groups are working to obtain liquid-crystalline metals complexes with good luminescent (phosphorescent) properties.[30] In general some properties from the metal, such as geometry, can be helpful to drive the liquid crystal properties of the compounds and these will be described in more details in the following chapters.

1.2.2 Polarised Emission

As mentioned before, a powerful application for luminescent LC materials is that they can be used as a source of polarised light.[8c] Indeed there is a considerable recent interest in the possibility of using oriented compounds as polarised emitters in display technology.

The use of liquid crystal as source of polarised light will help to reduce the amount of power required from the actual LCDs, will improve the quality of the contrast and the brightness of the displays and moreover will help to obtain displays much more thinner and lighter. The use of uniformly oriented liquid crystals for polarised electroluminescence was reviewed for the first time in 1999[31] and recently in 2009 by Holmes *et al.*[25]

There are different possibilities to achieve polarised emission for use as a backlight source in the displays, but before discussing them, an explanation of the reason behind the interest and the benefit of applying polarised light on displays has to be made. In Figure 6 a general liquid crystal display is shown.

White
Unpolarized
Light

Rear Glass

Polarizing Film

Liquid Crystals

Front Glass

Polarizing Film

Color Filter

Colored
Light

© Lon Koenig
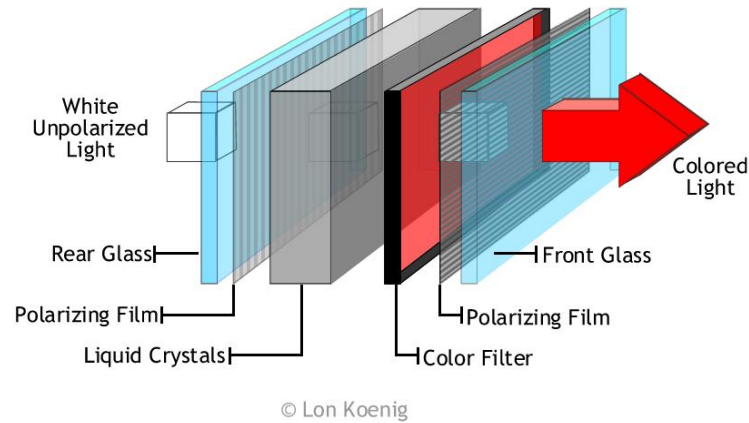
Figure 6-I Structure of a common liquid crystal display. http://tv09.org/ (09/06/10)

The LCDs are constituted by a sequence of different layers. The first layer is the light source (backlight) and it can be made up of different source such as incandescent light bulbs, light-emitting diodes (LEDs), electroluminescent panel (ELP), one or more cold cathode fluorescent lamps (CCFL), each of them is used in specific designed devices. Behind it, there is a rear glass and a back filter; this filter polarises the incoming light. Then there is a layer of liquid crystalline molecules aligned between two layers of transparent electrodes. The surfaces of the electrodes are treated so as to align the liquid crystal molecules in a particular direction. Electrodes are made of the transparent conductor called indium tin oxide (ITO). The most common liquid crystal device uses a twisted nematic configuration. The surface alignment directions at the two electrodes are perpendicular to each other, and so the molecules arrange themselves in a twisted, helical structure. Then there are the colour filters in the case of polychromatic displays, and the second polarising filter, usually set at 90° with respect to the back polariser. Finally there is the front glass. The working concept is exemplified in Figure 7. If the voltage is applied and is large enough (Figure 7 green filter), the liquid crystal molecules in the centre of the layer are almost completely untwisted and the polarisation of the incident

light is not rotated as it passes through the liquid crystal layer. This light will then interact with the front polariser, perpendicular to the back filter, and thus will block the light and the pixel will appear black. On the other hand, when the voltage is off (Figure 7 red filter) the liquid crystal material will be oriented in a helical structure. This will induce the rotation of the polarised light and the pixel will appear grey or coloured, depending if it is a monochromatic or polychromatic display.
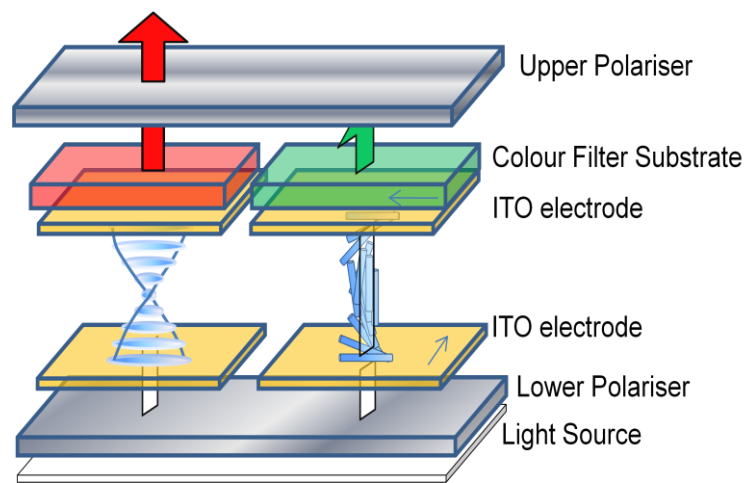
Figure 7-I Interaction between the polarised light and the LC material in LCDs.

In all new technologies, reduction in power consumption is one of the most important key factors. The clear environmental benefit, but especially the possibility to obtain better portable displays, pushes companies to research new, energy-saving approaches. In this context, one of the most energy-consuming parts is the presence of the back and front polarisers; indeed each of them is responsible of the loss of 40% or more of the light intensity. The most comprehensive solution to the backlight problem is a backlight that emits linearly polarised light, which is the basis for the idea of using oriented luminescent materials as the backlight in

LCDs. Indeed, with one polariser removed, at least 40% more light emerges from the device, resulting in a lower power consumption. There are a variety of methods that can be used to achieve orientation and thus polarised emission, and all of the following have been utilized for organic EL materials:

- mechanical alignment;

- Langmuir-Blodgett (LB) deposition;

- liquid-crystalline self-organisation;

- alignment on specific substrates.

The anisotropy of liquid crystal materials and their good processability allows direct preparation of well-aligned, thin films due also to their self-assembly properties, in particular nematic and smactic phases.[32] The use of uniformly oriented liquid crystals for polarised electroluminescence was first established in 1995, Inganas *et al.*[33] who demonstrated emission of polarised light based on an aligned, conjugated polymer. They suggested that such compounds would be particularly useful as the backlight in a conventional liquid crystal display.

Since then the field has developed rapidly as a new branch of material/applied science, and nowadays several reports are published of different compounds, especially polymers, that meet these requirements.[25]

1.3 An Introduction to Liquid Crystals.

As the name suggests, the liquid crystal state is a state of organisation between the liquid and crystal states. This fluid state has been known for nearly one hundred and fifty years, but the fundamental realisation of a novel behaviour of matter was introduced about hundred years ago. Thus, Reinitzer[34] was measuring the melting point of cholesteryl benzoate and he discovered that, at 145 °C, the compound melted to form a turbid fluid that became clear at 178 °C. The turbid fluid was the liquid crystal state. The term *liquid crystal* (*flüssigekristall*) was coined one year later by Lehmann,[35] a specialist in polarising microscopy. Liquid crystal phases are also known as *mesophases*; this word having a Greek root which means 'between phases' (Figure 8). The properties of this discrete state of matter are in fact intermediate between those of the solid and liquid states, and it is possible to classify it as a very disordered solid or as a rather ordered liquid. As a matter of fact, there is only a slight tendency for the molecules to orient in one direction more than in another, or to adopt some positional order, so it is a dynamic system where the molecules are relatively free to move from one position to another. Evidence of this is also revealed from the latent heat of transition, so that for a Cr-LC transition, ΔH is around 40-60 kJ·mol^{-1} whereas for a LC-I, so isotropic, it is typically about 1-5 kJ·mol^{-1}.[30]

| Crystal | Liquid Crystal | Liquid |
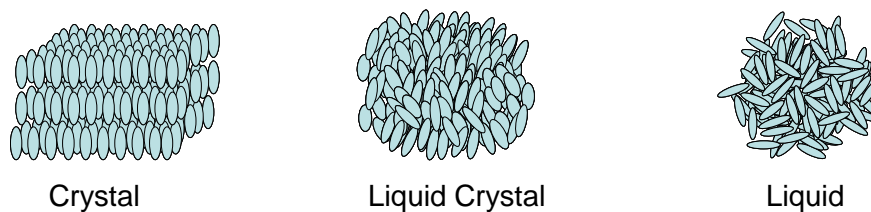
Figure 8-I Degree of order and disorder in the liquid, liquid crystal and crystalline states.

Liquid crystals can be divided in two main classes, thermotropic[36] and lyotropic.[37] Thermotropic liquid crystals are all those compounds where phase transitions are driven by temperature, whereas for lyotropic liquid crystals, mesophases are induced by the action of a solvent. In this thesis, only thermotropic liquid crystal will be discussed as lyotropic properties have not formed part of the investigations.

1.3.1 Thermotropic Liquid Crystals

Thermotropic LCs are generally classified into two main categories (Scheme 1), low-molar-mass and high-molar-mass, which means non-polymeric and polymeric material, respectively. Each class can then be represented by further sub-divisions. Thus, high-molar-mass systems include the *side-chain* and *main-chain* polymers,[32] and dendritic molecules,[38] while for low-molar-mass systems there are *rod-like*, *disc-like* and *bent-core* molecules.[39] The nature of liquid crystal phases depends strongly on the shape of the molecules, and on the stereochemistry. Rod-like molecules are also called *calamitic* whereas the disc-like molecules are usually called *discotic*. In the liquid crystal molecules, the structural anisotropy is the determinant factor and indeed, calamitic molecules have one long axis and two short axes, while discotic molecules have two long axes and one short.

In the simplest LC phase, all the molecules tend to arrange in one direction, usually along the main axis; this preferred direction is called the director and is denoted with the unit vector **n**. It represents the average local direction and the optic axis of the system.
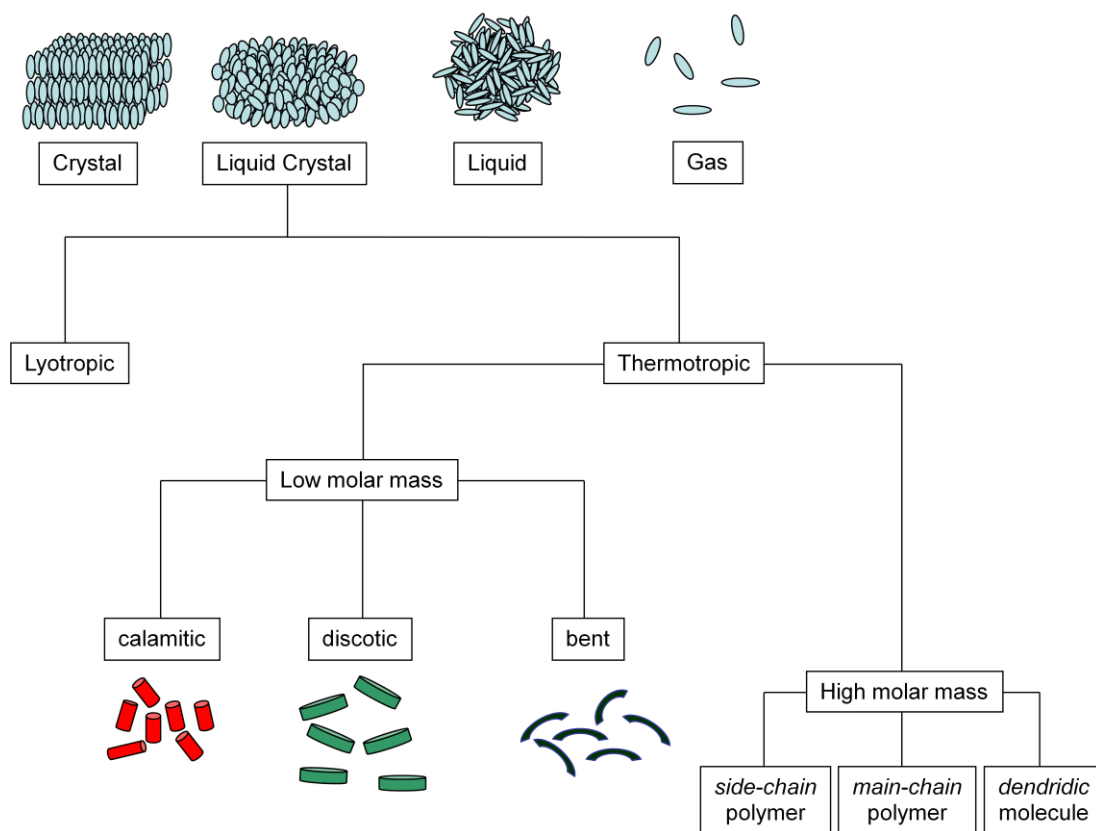
Scheme 1-I LC classification diagram.

1.3.1.1 Rod-like molecules

As mentioned above, in order to show a mesophase, a molecule must be structurally anisotropic. In *rod-like* molecules, there is one long axis and two short one (Figure 9).
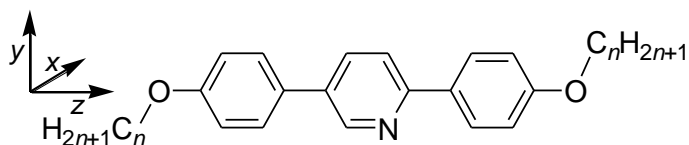
Figure 9-I Typical *rod-like* structure

The nematic phase (N) is the most disordered mesophase. Here the molecules are all

oriented, on average, in the same direction, which is given by the director, **n**. However, there is only orientational order and the molecular centres of mass are distributed isotropically so that there is no positional order.

To specify the amount of orientational order in a LC phase it is necessary to define an order parameter, *S*. The equation (4), is one of the best functions to describe the system composed of many molecules at the same time or one molecule averaged over time.

$$S = \frac{1}{2}\left\langle 3\cos^2\theta - 1\right\rangle \tag{4}$$

The angle, *θ*, is the average angle formed between the projection of the molecular long axes with the director **n**. Usually, for a nematic phase (N) the value of *S* stands between 0.4 and 0.7 (Figure 10). *S* for crystal state is equal to 1 and in the isotropic state is equal to 0.
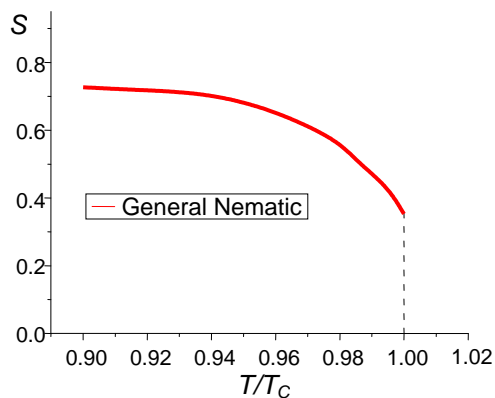
Figure 10-I Typical temperature dependence of the order parameter in a general nematic phase. *T* is the actual temperature and T_C is the transition temperature between liquid crystal phase and liquid phase.
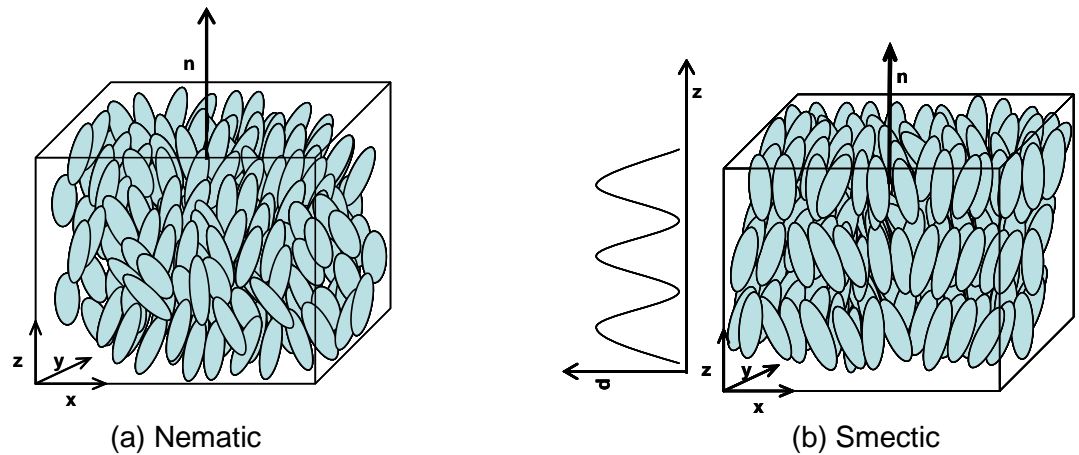
Figure 11-I Structure of a nematic and smectic phases shown by a calamitic material.

The introduction of partial positional order due to the organisation into layers of the molecular centres of mass, leads to the formation of smectic phases (Figure 11b and 12). For a more realistic representation, the layer organisation should be described as a density function (**d**) of the molecular centres of mass along the *z* direction. The period (**p**) of this sinusoidal function is usually in good agreement with the length, *l*, of the extended conformation of the molecules. It is possible to have different smectic phases, (SmA, SmB, SmC, SmF and SmI); the simplest are the SmA and SmC phases (Figure 12).
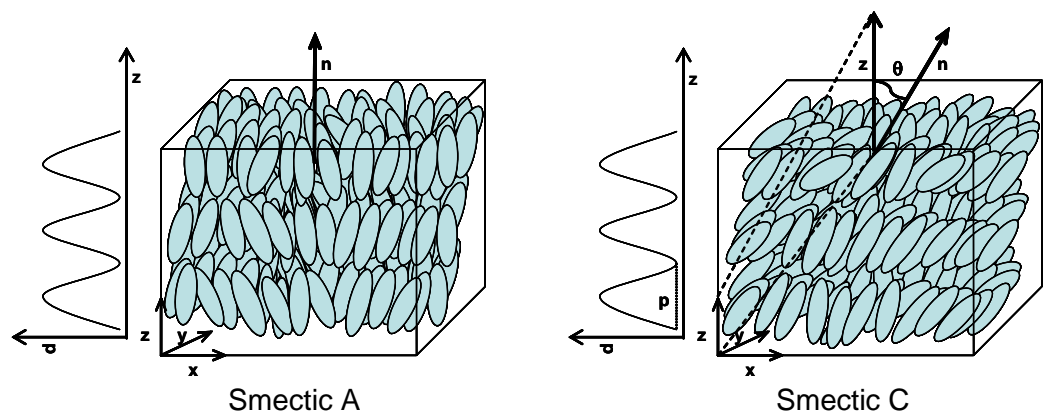
Figure 12-I Structure of SmA and SmC phases.

In the SmA mesophase, the molecules are, on average, oriented with their long axes perpendicular to the layer direction, while in the SmC phase, the molecules are tilted, so that the director makes an angle, θ, with the z-axis, perpendicular to the plane of the smectic layers.

The other smectic mesophase show a higher degree of organisation within the layers, having the molecules organised into an hexagonal array. The simplest phase is the SmB, an orthogonal phase in which the lattice is organised as a regular hexagon, whereas in the SmF and SmI, the hexagonal lattice is tilted. In the case of SmF the lattice is tilted towards the edge of the hexagonal net, while in the SmI phase the lattice is tilted to the apex of the hexagonal net. Figure 13

Smectic B   Smectic I   Smectic F
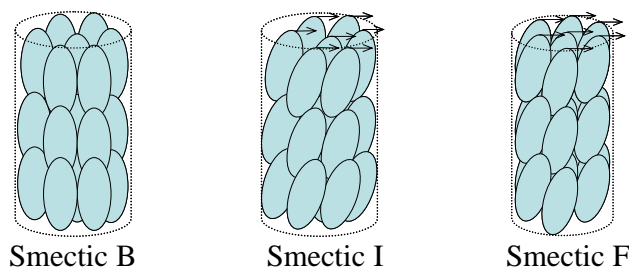
Figure 13-I Model structure of hexagonal packing. The SmI phase is tilted towards the apex of the hexagon, the SmF is tilted towards the side.

1.3.1.2 Disc-like molecules

Disc-like molecules posses two long axes and one short. The phases are formed from molecules having a flat core, often constituted by aromatic units surrounded by alkyl chain, with at least five carbon atoms (Figure 14). The interaction between the molecules is shown along their shortest axis. The simplest mesophase formed by discotic molecules is a nematic phase (N_D), whose organisation is very similar to the nematic phase shown for calamitic

molecules, although it is much less common than its calamitic analogue.
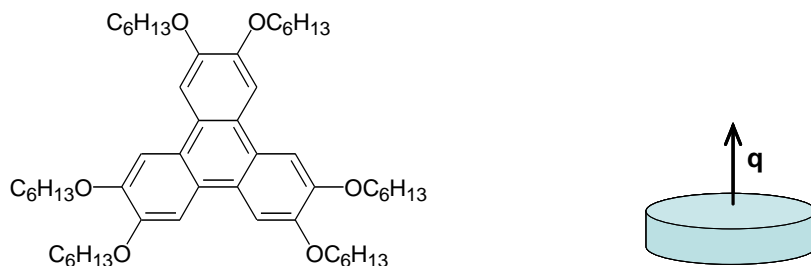
Figure 14-I General shape of a discotic molecule, **q** represents the direction of the shortest axis.

In the N_D phase, the molecules are organised with their short axes correlated about the director **n**, and, as for calamitic systems, there is no positional order of the molecular centres of mass. The columnar nematic phase (N_C) is characterised by an association of the *disc-like* molecules into columns, which then dispose themselves to rise into a nematic phase, displaying short-range positional order and long-range orientational order (Figure 15).[40]
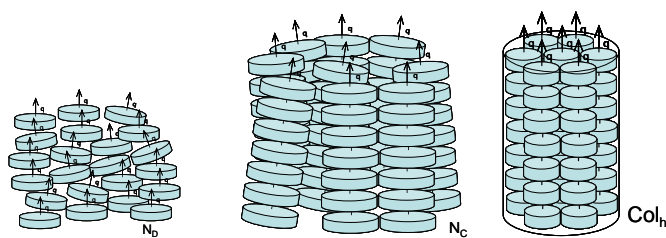
Figure 15-I Structure of different mesophases of discs, (a) nematic discotic, (b) column nematic, (c) columnar hexagonal.

However, the most common phases of *disc-like* molecules are those where columns of molecules are arranged in a two-dimensional fashion, giving rise to columnar phases. The most common examples are the columnar hexagonal (Col_h), columnar rectangular (Col_r), and columnar oblique (Col_{obl}) phases. These are illustrated below (Figure 16) as projections with

28

the main columnar axes pointing out of the page. Elliptical shapes imply that the molecules are tilted within the columns. In the column hexagonal phase structure, all the columns are parallel through their main axes and they are characterised by an hexagonal packing of their column.
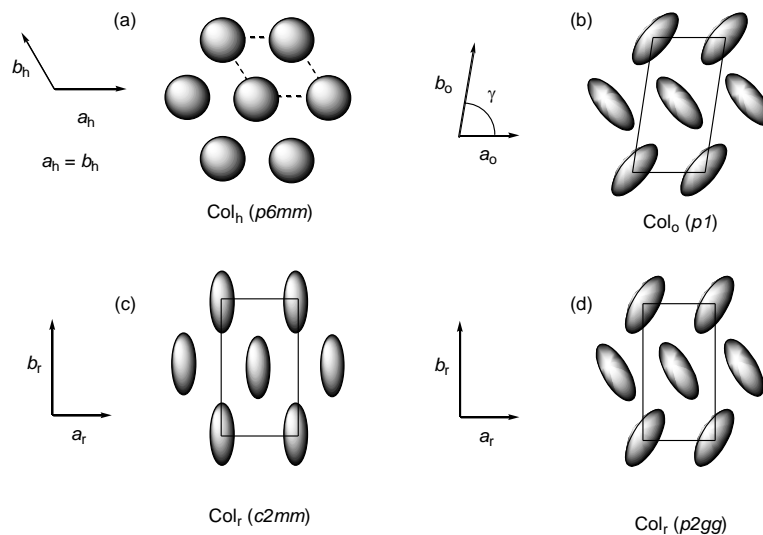
Figure 16-I Representations of the lattices of (a) hexagonal, (b) oblique, and (c) and (d) rectangular columnar phases

The columnar rectangular mesophase consists of the stacking of the aromatic cores of the molecules in columns surrounded by the disordered aliphatic chains and packed in a rectangular fashion. The columnar oblique mesophase then consist of columns that are tilted in respect to the direction perpendicular to the molecules. Lamellar mesophases are also known.[38]

1.3.2 Characterisation of the mesophases.

Different methods are used to characterise the mesophases formed by liquid crystalline materials: *Polarised Optical Microscopy*, *Differential Scanning Calorimetry (DSC)* and *X-Ray Diffraction*. These methods are often used at the same time, indeed for the same samples could happen that a transition is easily detectable in the DSC but very difficult to appreciate using POM, the classical case is the transition SmA-SmB.

1.3.2.1 Polarised optical microscopy.

The fastest and the simplest method used to recognise a liquid crystal phase is *polarised optical microscopy*; this technique uses the phenomenon of *birefringence* (Figure 17), one of the physical properties of a mesophase. This property is due to the anisotropy of the phase. Mesophases posses at least two different refractive indexes, so that when the light passes through the material, it will be refracted in two different directions and with two different speeds.
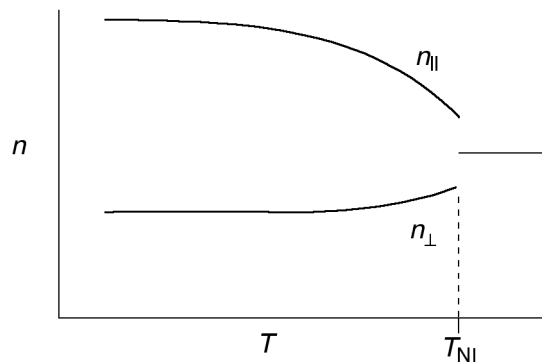
Figure 17-I Diagram of birefringence versus temperature for one wavelength in a liquid crystal material.

There will be, therefore, two rays; one perpendicular to the director, **n**, which is usually called ordinary ray, n_o (or $n\perp$), and the other one is parallel to **n** and is called extraordinary ray, n_e (or n_{ll}). The maximum difference between these two refractive indexes, is called the *birefringence* ($\Box n$) and is given by $\Delta n = n_e - n_o$.

The optical microscope is equipped with two polarisers, one between the light and the sample, and the other between the sample and the observer, and they are oriented at 90° to each other. The sample is usually sandwiched between two glass cover slips and then placed on a hot-stage whose temperature can be controlled. The samples can aligned in homeotropic fashion (the main axes of the molecules are perpendicular to the plane of the cover glasses) or homogeneously (the main axes of the molecules lie in the same plane as the cover glasses). The light impinging the sample is plane polarised by the first filter, then the polarised light passes through the sample and through the other filter. If the sample is in the isotropic phase or in the homeotropic state, it appears black because no interference pattern is formed. This is because isotropic liquids are not birefringent, possessing only one refractive index, while when viewing a sample that is aligned homeotropically, viewing is down one of the optic axes and so again, no interference is seen. In this case, then, the polarised light passing through it is stopped by the analyser (Figure 18). However, if the sample in the liquid crystal phase is ot aligned homeotropically, the polarised light passing through it will be split into two different beams that will interfere. This interference destroys the plane polarisation and creates an interference pattern from which it is possible to recognise a mesophase.

To identify the phases with POM not only the formed pictures are important, what is even more important is the behaviour of the samples in the liquid crystal phase and during the transitions. For example a Nematic phase in full homeotropic alignment will result in a black

spot, but a normal, unaligned sample does not usually have a director **n** that points in the same direction in all the regions of the material. The director changes through the whole samples and where the changes are drastic no specific order can be defined and a defect is generated. These defects are shown as black point (point defects) or line defects (disclination line). These defects appear black because of the optical extinction caused by the cross polarisers. For optical extinction to occur the molecules must be aligned or homeotropically or in the direction of either of the two cross polarisers. In Figure 19 some of these alignments are shown. In the first two cases (s = 1) the defect result in the four-brush dhlieren (red ring in Figure 20 c), in the other two cases (s = 1/2) there are two regions from the point defect where the molecules are aligned with the polariser and so these two regions are optically extinguished, generating a two-brush schlieren. (Figure 20 c green ring). The other phases are just described by their peculiar characteristic and their behaviour in the phase transition.

The SmA phase are characterise by the presence of black part due to the homotropical alignment and by the presence of clean and smooth focal conical fan texture, the transition to a SmC phase will be visible by the appearance of a schlieren texture in the homotropic alignment, as the SmC is a tilted phase therefore no extinguished is possible, and by the appearance of brushes on the focal conical fan texture. The presence of a SmI phase is characterised by the presence of even larger brushes on the focal conical texture and by a difficulty to focus on the phase. All these difference, herein mentioned, several time are not so easy to be detected and a lot of experience is required to recognise the different phase.[32] Thus, although this is a powerful method of characterisation, sometimes other analyses are required to characterise a mesophase completely.
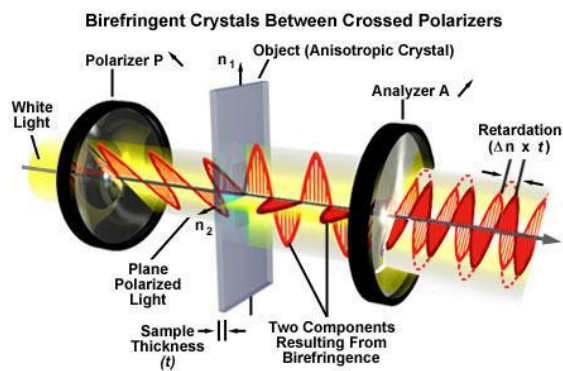
Figure 18-I Working scheme of POM
(http://www.molecularexpressions.com/optics/lightandcolor/birefringence.html accessed 10/06/10)
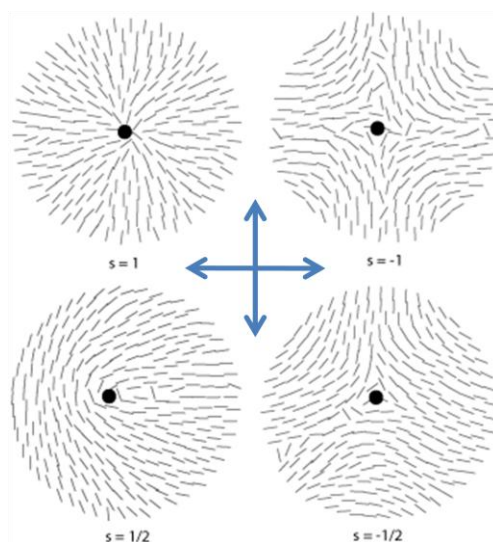
Figure 19-I Molecular alignment resulting in a schlieren brushes. Blue arrows indicate the direction of the cross polarisers.

| (a) | (b) | (c) |
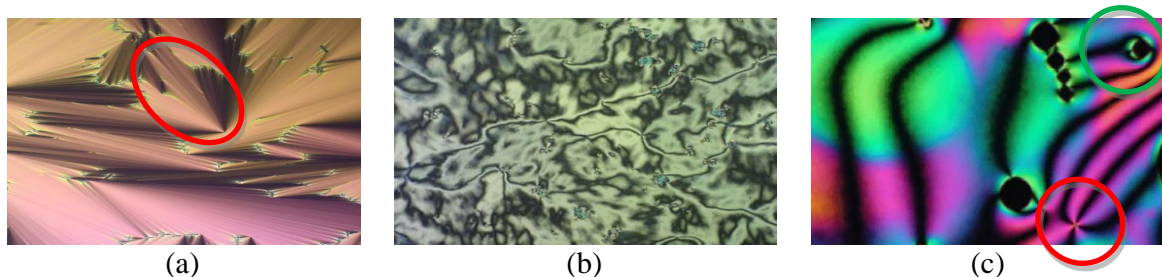
Figure 20-I Liquid crystal imagines of: (a) smectic A phase where the smooth focal conical fan texture has been highlighted, (b) brushed schlieren texture of smectic I phase of **1(6)** at 198 °C and (c) classic nematic phase with the clear presence of defects. All the structure are shown in the next chapter.

1.3.2.2 Differential Scanning Calorimetry

Differential scanning calorimetry is normally used in parallel with optical microscopy, as sometimes a phase transition is not easily detected in the microscope, or an apparent textural change is not actually a real phase transition. Indeed some time the defect textures can be very similar, such as at the SmA-SmB transition, and also the retention of the defect of the preceding phase in the new phase can contribute to the difficulty to identify and attribute unequivocally the liquid crystal phase. In this case, through utilisation of DSC, it is possible to see the occurrence of the transition. At the same time, a change detected by microscopy may or not be real and so DSC can be used to confirm it. These two methods should be used together, because they are complementary. The DSC technique measures the power that the instrument has to supply to the sample to maintain the same temperature against a reference during a phase transition. Usually, the sample (2-3 mg) is placed in an aluminium pan which is covered with an aluminium slip and sealed. This is inserted in the sample heater plate, while an empty pan is placed in the reference heater. The two independent heaters are controlled by platinum sensors and through these sensors, or using a thermocouple, the instrument checks the amount of power that has to be added (Figure 21).
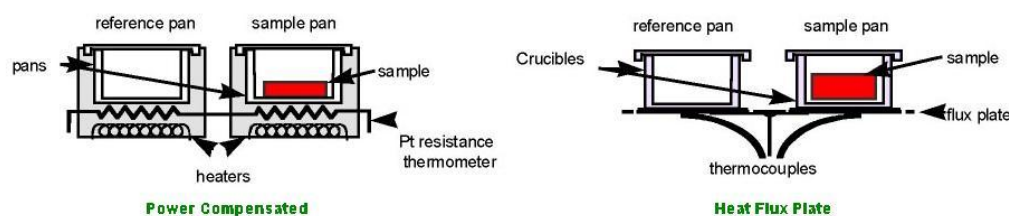
Figure 21-I Scheme of generic differential scanning calorimeters

When, on heating, a phase transition occurs in the sample, the heat given is used by the

sample to change phase, and there is no change in temperature. The calorimeter has to supply more power to the sample pan to maintain the same temperature as the reference pan. This heat supply will then result in a peak on a plot of the power against temperature.
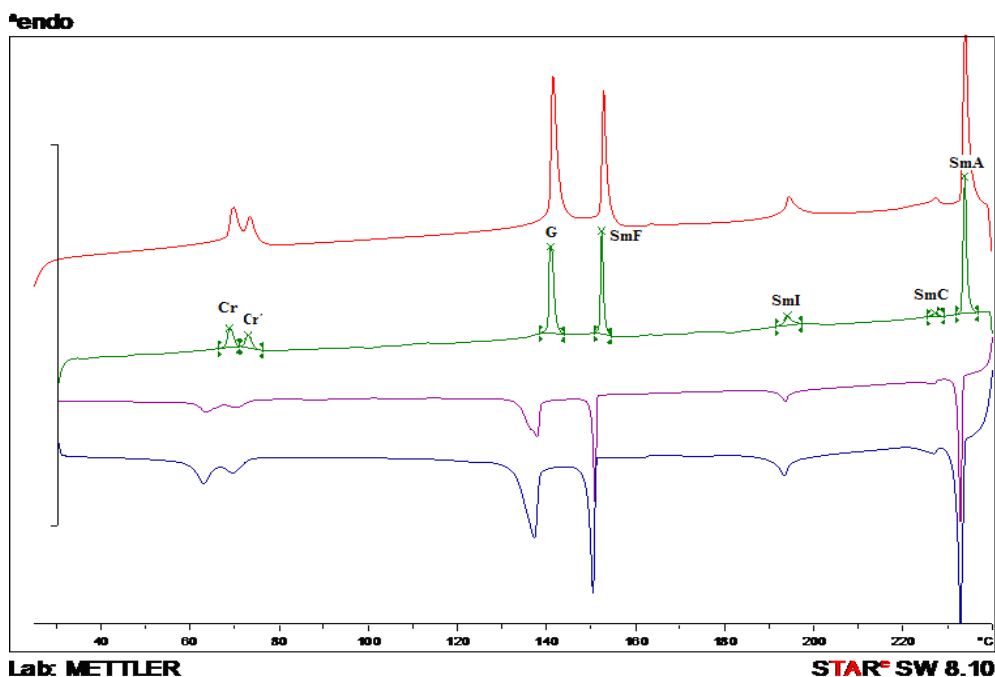
Figure 22-I DSC diagram of ligand **1(6)**. The green and the red lines are the heating cycle and the blue and the violet lines are the cooling cycle. Cr and Cr' are a crystal phase, G is a soft-crystal phase, SmF is a smectic F phase. SmI is a smectic I phase, SmC is a smectic C phase and SmA is a smectic A phase.

The Figure 22 shows a classical example of a DCS plot. Heating the sample there is a first transition from a crystal phase (Cr) to another crystal phase (Cr') around 70 ℃ (unidentified phases) then another transition take place just few degree later from the crystal phase (Cr') to a soft-crystal G phase assigned as predicted phase to follow a SmF phase on cooling. Now at 140 ℃ there is a proper melting point with the transition from crystal G phase to liquid crystal SmF phase, then there are a SmF to SmI transition at 150 ℃ and a SmI to SmC at 195 ℃ few degree later there is the transition from the SmC phase to the SmA phase and then there is the

clearing point, namely the transition from liquid crystal phase SmA to a liquid phase I. The assignments of these transitions and liquid crystal phases were done on the phase of the POM analysis and the energy of the transition.

1.3.2.3 X-ray Diffraction

X-Ray diffraction is a powerful technique to investigate the microscopic structure of liquid crystal phases.[30] In the mesophase, the molecules are partially ordered and form periodic structures. When the beam from an X-ray source passes through a sample of a mesogen, each molecule can be considered as a point in a net; each point can scatter the incident plane wave of X-rays in different directions. All these reflected rays will interfere with each other and the result of this interference is then detected on a film placed after the samples. The resulted figure is called a diffraction pattern (Figure 23).
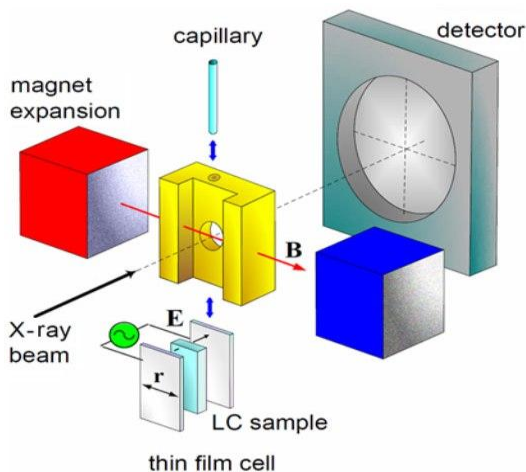
Figure 23-I Schematic representation of a X-ray diffractometer. The thin film sample could be aligned by a magnetic (**B**) or electric (**E**) field applied either perpendicular to the beam direction or parallel to it. The other possibility is to have an heating system. http://www.esrf.eu/news/spotlight/spotlight86/spotlight86/ (10/05/10).

Figure 23 shows an incident beam with wavelength λ striking a structure with period d in a direction perpendicular to the beam. Imagine that some of the X-rays are diffracted by an angle θ, toward a detector very far away compared to d; the path length difference for the scattered waves is $2d\sin(\theta)$. This is because the rays of the incident beam are always in phase and parallel up to the point at which the top beam strikes the top layer at atom z (Figure 24). The second beam continues to the next layer where it is scattered by atom B. The second beam must travel the extra distance AB + BC if the two beams have to continue travelling adjacent and parallel. This extra distance has to be an integer (n) multiple of the wavelength λ. Therefore:

$n\lambda$ = AB + BC, and AB = $d\sin\theta$ but because AB = BC, $n\lambda$ = 2AB.

Therefore, $n\lambda = 2d\sin\theta$.

Thus, if the distance is equal to a multiple of the wavelength, then constructive interference occurs, and a peak is expected in the diffraction pattern. If the interference is not constructive, no signal is detected. Thus, following Bragg's Law, only diffraction at certain angle, θ, or its multiples will give constructive interference.
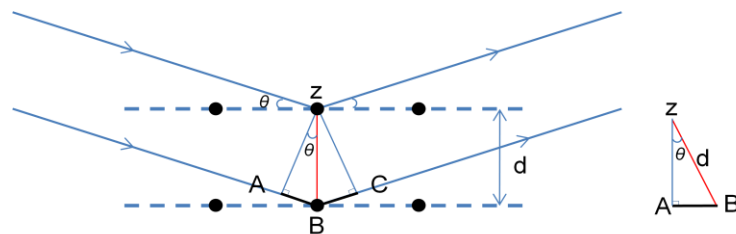
Figure 24-I Illustration of Bragg's Law using the reflection geometry and applying trigonometry. The lower beam must travel the extra distance (AB + BC) to continue traveling parallel and adjacent to the top beam.

X-Ray diffraction from liquid crystals is just like Bragg scattering from crystals, in which periodicities in the structure of the phase give rise to constructive interference and therefore

peaks in the scattering of X-ray. One example, for a Col$_h$ phase, is shown in Figure 24. The assignment of the two-dimensional symmetry of the mesophase arises from the analysis of the *d*-spacings from these data. In the small-angle region ($0 < 2\theta < 5°$), three different reflections peak were observed corresponding to the fundamental, harmonics, and higher orders of diffraction and indicative of the two-dimensional lattice of the hexagonal phases. Furthermore, in Figure 25 at high angles ($2\theta \sim 20°$) a broad, diffuse scattering peak is present, corresponding to the liquid-like order of the aliphatic chains.
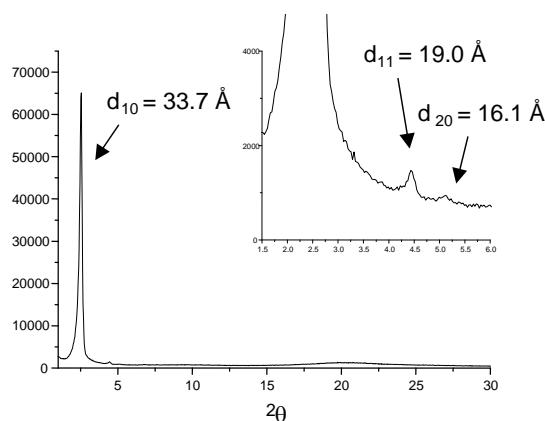
Figure 25-I General X-ray diffraction of a Col$_h$ liquid crystal material.

1.3 Aims and Objectives

The purpose of this research project is based on the design and synthesis of new materials that posses the coexistence of luminescent and liquid crystal properties. Until now, only few materials are reported to deal with both properties, but the growing interest in this field is indicated by the timely review by Binnemans in 2009.[30] Moreover, there are specific challenges in aiming to retain the luminescent properties of good chromophores, while

imparting liquid crystallinity. Moreover, there can be particular effects associated with the combination of the two properties, for example the way in which the liquid crystal properties can influence emission behaviour.[41,42]

It has been reported that, in general, liquid crystal phases, can be of great advantage in several areas such as thin-film transistors[5], solid organic lasers[6] and photovoltaic devices[7]. Thus, the objectives of this research are to produce materials, mainly for two applications: polarised emitters and emitters in OLED devices.

The use of liquid crystals as polarised emitters has been well reported in literature (paragraph 1.2.2) and here the principal objective is to have a *rod-like triplet emitter* with low transition temperature to be applied as polarised emitter. Indeed its liquid crystal alignment, classically SmA, will result in an emission linearly polarised. Therefore the use of a *quasi*-planar ligand with a square planar metal complex will assure the presence of calamitic liquid crystal phases, and moreover the presence of platinum(II) will guarantee the great performance in the triplet emission.

Other kind of liquid crystals, such as *disk-like* and *bent-core* do not posses this ability. Furthermore other kinds of liquid crystal such as *disk-like* can be successful applied in OLED devices because their supramolecular organisation can be an advance in the charge mobility (both holes and electrons); thus the main object here is to develop *disk-like* system that can be organised in column for their application in OLED. Thus with appropriate modifications on the ligands, such as introduction of other chains with the formation of a polycatenar system, could be used to induce a *disk-like* phase on platinum complexes, or used in other metal system with a different geometry, such as iridium(III) that, as for platinum, will assure good spin orbit coupling with the formation of triplet emitters.

Therefore both the properties (EL and LC) of these materials have to be at high standard to compete with all the exceptional luminescent material and liquid crystal material present in the corresponding research field.

References

1   http://www.britannica.com/EBchecked/topic/183108/electroluminescence   acessed 23/06/09.

2   (a) A. Bernanose, M. Comte and P. Vouaux, *J. Chim. Phys.*, 1953, **50**, 64; (b) A. Bernanose and P. Vouaux, *J. Chim. Phys.*, 1953, **50**, 261; (c) A. Bernanose, *J. Chim. Phys.*, 1955, **52**, 396; (d) A. Bernanose and P. Vouaux, *J. Chim. Phys.*, 1955, **52**, 509.

3   U. Mitschke and P. Bäuerle, *J. Mater. Chem.*, 2000, **10**, 1471.

4   C. Tang and S. VanSlyke, *Appl. Phys. Lett.*, 1987, **51**, 913.

5   H. Sirringhaus, N. Tessler and R. H. Friend, *Science*, 1998, **280**, 1741.

6   F. Hide, M. A. Diaz-Garcia, B. J. Schwartz, M. R. Andersson, Q. B. Pei and A. J. Heeger, *Science*, 1996, **273**, 1833.

7   J. J. M. Halls, C. A. Walsh, N. C. Greenham, E. A. Marseglia, R. H. Friend, S. C. Moratti and A. B. Holmes, *Nature*, 1995, **376**, 498.

8   (a) W. Pisula, M. Zorn, J. Y. Chang, K. Mullen and R. Zentel, *Macromol. Rap. Comm.*, 2009, **30**, 1179 (b) M. O'Neill and S. M. Kelly, *Adv. Mater.*, 2003, **15**, 1135; (c) A. E. A. Contoret, S. R. Farrar, M. O'Neill, J. E. Nicholls, G. J. Richards, S. M. Kelly and A. W. Hall, *Chem. Mater.*, 2002, **14**, 1477; (d) V. I. Kopp, B. Fan, H. K. M. Vithana and A. Z. Genack, *Optics Lett.*, 1998, **21**, 1707.

9   L. Schmidt-Mende, A. Fechtenkotter, K. Mullen, E. Moons, R. H. Friend and J. D. MacKenzie, *Science*, 2001, **293**, 1833.

10 (a) A. E. A. Contoret, S. R. Farrar, M. O'Neill, J. E. Nicholls, G. J. Richards, S. M. Kelly and A. W. Hall, *Adv. Mater.*, 2002, **14**, 1477; (b) A. E. A. Contoret, S. R. Farrar, P. O. Jackson, L. May, M. O'Neill, J. E. Nicholls, G. J. Richards and S. M. Kelly, *Adv. Mater.*, 2000, **12**, 971.

11 J. Cornil, D. Beljonne, J. –P. Calbert and J. L. Bredas, *Adv. Mater.*, 2001, **13**, 1053.

12 A. Kraft, A. C. Grimsdale and A. B. Holmes, *Angew. Chem. Int. Ed.*, 1998, **37**, 402.

13 D. O'Brien, A. Bleyer, D. G. Lidzey, D. D. C. Bradley and T. Tsutsui, *Appl. Phys.*,

1997, **82**, 2662.

14   (a) M. A. Baldo, D. F. O'Brien, Y. You, A. Shoustikov, S. Sibley, M. E. Thompson and S. R. Forrest, *Nature*, 1998, **395**, 151; (b) M. A. Baldo, S. Lamansky, P. E. Thompson and S. R. Forrest, *Appl. Phys. Lett.*, 1999, **75**, 4; (c) S. Lamansky, P. Djurovich, D. Murphy, F. Abdel-Razzaq, H. -E. Lee, C. Adachi, P. E. Burrows, S. R. Forrest and M. E. Thompson, *J. Am. Chem. Soc.*, 2001, **123**, 4304; (d) V. Cleave, G. Yahioglu, P. Le Barny, R. H. Friend and N. Tessler, *Adv. Mater.*, 1999, **11**, 285.

15   A. P. Kulkarni, C. J. Tonzola, A. Babel and S. A. Jenekhe, *Chem. Mater.*, 2004, **16**, 4556.

16   (a) N.K. Patel, S. Cina and J. H. Burroughes, *IEEE J. Select. Topics Quantum Electron*, 2002, **8**, 346; (b) J. Cornil, D. Beljonne, J. –P. Calbert and J. L. Bredas, *Adv. Mater.*, 2001, **13**, 1053; (c) R. H. Friend, R. W. Gymer, A. B. Holmes, J. H. Burroughes, R. N. Marks, C. Taliani, D. D. C. Bradley, D. A. Dos Santos, J. L. Bredas, M. Longdlund and W. R. Salaneck, *Nature*, 1999, **397**, 121; (d) C. H. Chen, J. Shi and C. W. Tang, *Macromol. Symp.*, 1997, **125**, 1.

17   C. Adachi, M. A. Baldo, M. E. Thompson and S. R. Forrest, *J. Appl. Phys.*, 2001, **90**, 5048.

18   J. S. Kim, P. K. H. Ho, C. E. Murphy, N. Baynes and R. H. Friend, *Adv. Mater.*, 2002, **14**, 206.

19   J. H. Burroughes, D. D. C. Bradley, A. R. Brown, R. N. Marks, K. Mackay, R. H. Friend, P. L. Burns and A. B. Holmes, *Nature*, 1990, **347**, 539.

20   http://www.oled-info.com/sony/sony_starts_selling_the_xel_1 accessed 02/10/2008.

21   http://www.sonystyle.com accessed 16/10/09.

22   R. C. Evans, P. Dougles and C. J. Winscom, *Coord. Chem. Rev.*, 2006, **250**, 2093

23   M. A. Balbo, M. E. Thompson and S. R. Forrest, *Pure Appl. Chem.*, 1999, **71**, 2095.

24   A. I. Burshtein, A. A. Neufeld and K. L. Ivanov, *J. Chem. Phys.*, 2001, **115**, 10464.

25   A. C. Grimsdale, K. L. Chan, R. E. Martin, P. G. Jokisz and A. B. Holmes, *Chem. Rev.*, 2009, **109**, 897.

26   (a) Y. Kawamura, K. Goushi, J. Brooks, J. J. Brown, H. Sasabe and C. Adachi, *Appl.*

Phys. Lett., 2005, **86**, 071104-1; (b) H. Yersin, *Top Curr. Chem.*, 2004, **241**, 1.

27 L. Flamigni, A. Barbieri, C. Sabatini, B. Ventura and F. Barigelletti, *Top Curr. Chem.*, 2007, **281**, 143.

28 M. K. Nazeeruddin, R. Humphrey-Baker, D. Berner, S. River, L. Zuppiroli and M. Graetzel, *J. Am. Chem. Soc.*, 2003, **121**, 5009.

29 A. B. Tamayo, S. Garon, T. Sajoto, P. I. Djurovich, I. M. Tsyba, R. Bau and M. E. Thompson, *Inorg. Chem.*, 2005, **44**, 8723.

30 K. Binnemans, *J. Mater. Chem.*, 2009, **19**, 448.

31 M. Grell and D. D. C. Bradley, *Adv. Mater.*, 1999, **11**, 895

32 P. J. Collings and M. Hird, in *Introduction to Liquid Crystals*, Taylor&Francis, 1997.

33 P. Dyreklev, M. Berggren, O. Inganas, M. R. Andersson, O. Wennerstrom and T. Hjertberg, *Adv. Mater.*, 1995, **7**, 43.

34 F. Reinitzer, *Monatsh. Chem.*, 1888, **9**, 421.

35 O. Lehmann, *Z. Phys. Chem.*, 1889, **4**, 462.

36 (a) A. J. Leadbetter, in *Thermotropic Liquid Crystal*, Ed. G. W. Gray, Wiley, Chichester, 1987; (b) D. Demus, *Liq. Cryst.*, 1989, **5**, 75.

37 G. J. T. Tiddy, *Phys. Rev.*, 1980, **57C**, 1.

38 I. M. Saez and J. W. Goodby, *J. Mater. Chem.*, 2004, **15**, 26.

39 (a) S. Chandrasekhar and G. S. Ranganath, *Rep. Prog. Phys.*, 1990, **53**, 57; (b) K. J. Toyne, in *Thermotropic Liquid Crystal*, Ed. G. W. Gray, Wiley, Chichester, 1987.

40 S. Kumar, *Chem. Soc. Rev.*, 2006, **35**, 83.

41 V. N. Kozhevnikov, B. Donnio and D. W. Bruce, *Angew. Chem. Inter. Ed.*, 2008, **47**, 6286.

42 Y. Sagara, and T. Kato, *Angew. Chem., Int. Ed.*, 2008, **47**¸ 5175.

Chapter 2: Preparation and Liquid Crystal Properties of Substituted 2-Phenylpyridine and their Complexes with Platinum(II)

2.1 Background

2.1.1 Introduction

Phosphorescent transition metal complexes are attracting significant attention with respect to their potential application in OLED devices.[1] Thus, as described in the introduction, the aim of the project was to synthesise some third-row transition metal complexes with luminescent properties in the liquid crystal state, using derivatives of 2-phenylpyridine to form metal complexes. There are almost 400,000 publications based on 2-phenylpyridine or its derivatives, which are spread over many different research fields, from medicinal chemistry to photochemistry, and from polymers to catalytic chemistry. One reason for their choice in this project is related to their strong ligand-field effect.[2] The importance arises from the necessity to have luminescence, specifically phosphorescence, at room temperature and in the solid state. Indeed the consequence of such a ligand is that its strong ligand-field increases the energy of the non-luminescent *d-d* transition so that the LUMO is a mix of metal-ligand orbitals. As such there will be a higher probability of a metal-ligand charge transfer (MLCT) transition with extensive spin-orbit coupling therefore facilitating emission from the triplet state. Therefore comparing the luminescent properties of Pt complexes with neutral bidentate

ligands, many cyclometalleted Pt complexes prove to be luminescent in solution at room temperature.[2] More attention will be dedicated to this aspect in the Chapter 4 that will discuss the luminescent properties of the synthesised complexes. These interesting and promising properties are based on the fact that the anionic carbon is a strong σ-donor and the nitrogen is both a σ donor and a π-acceptor. These molecules act as anionic, bidentate ligands whose coordination sites are the nitrogen atom of the pyridine ring and the *ortho*-carbon atom of the phenyl ring. As such they can complex a variety of second- and third-row transition metal ions, and the complexes so formed are rather inert due both to chelate effect and the good ligating ability of both donor atoms (Figure 1).[2]
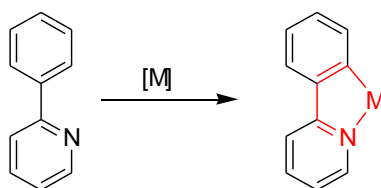
Figure 1-II Generic example of cycloemetallated reaction with phenylpyridine

On the other hand, one of the most important properties in designing molecules with liquid crystal properties is the anisotropy, so that, as described in the introduction, one axis should be longer that the other two (*rod-like* system) or *vice versa* (*disc-like* system). Therefore, the introduction of a further ring on the 5-position of the 2-phenylpyridine and also the presence of alkoxy chains will increase the length of the principal axis (*z*) (Figure 2), increasing the anisotropy of the ligand. These three-ring ligand systems with alkoxy functional group in the *para* position of the phenyl ring are present with their derivatives in about forty reports between patents[3] and academic[4,5] publications.
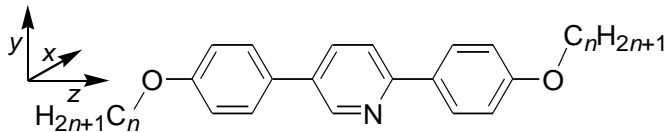
Figure 2-II 2,5-Di(4-alkoxyphenyl)pyridine, **1(*n*)**. Four different molecules have been synthesised: $n = 6, 8, 10$ and 12

These materials may be synthesised using different methodologies. The most common way[6] is described in Scheme 1, which is a straightforward reaction for symmetric substitution of the 2,5-dihalopyridine using palladium cross-coupling chemistry and presents an average yield of 50-60%, for the particular system described in this thesis.
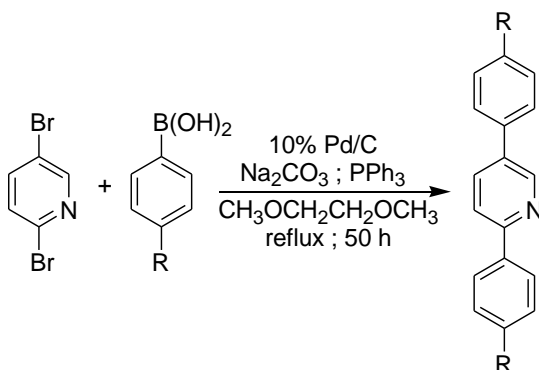
Scheme 1-II Example of Suzuki-Miyaura coupling.

However, in this work the ligands have been synthesised using a novel application of a very interesting reaction described for the first time in the early 1970s[7] by Saraswathi and Srinivasan. The reasons behind this choice are connected with the possibility to introduce a different substituent on the central ring. The presence of further, lateral substituents placed on the pyridine ring of the ligand has also been investigated in order to influence the liquid crystal properties and to control the transition temperatures.

For the metal, attention was concentrated on third-row metals, mainly Pt and Ir, because their strong spin-orbit coupling allows intersystem crossing between singlet to triplet states that, as described in the introduction, could be of great advantage in OLED devices. Another important attribute possessed by platinum, and in general by the metals of Group 10, is that in their d^8 electronic configuration with the presence of strong-field ligands they acquire the thermodynamically favourable square-planar geometry (Figure 3). This splitting, considering the crystal field theory (CFT) and the ligand field theory (LFT), is due to the stabilisation of the orbitals having a z-component where there are no ligands. This square-planar conformation is responsible for many of the characteristic luminescent properties of the platinum(II) complexes and, furthermore, it is very important for the realisation of liquid crystal properties.
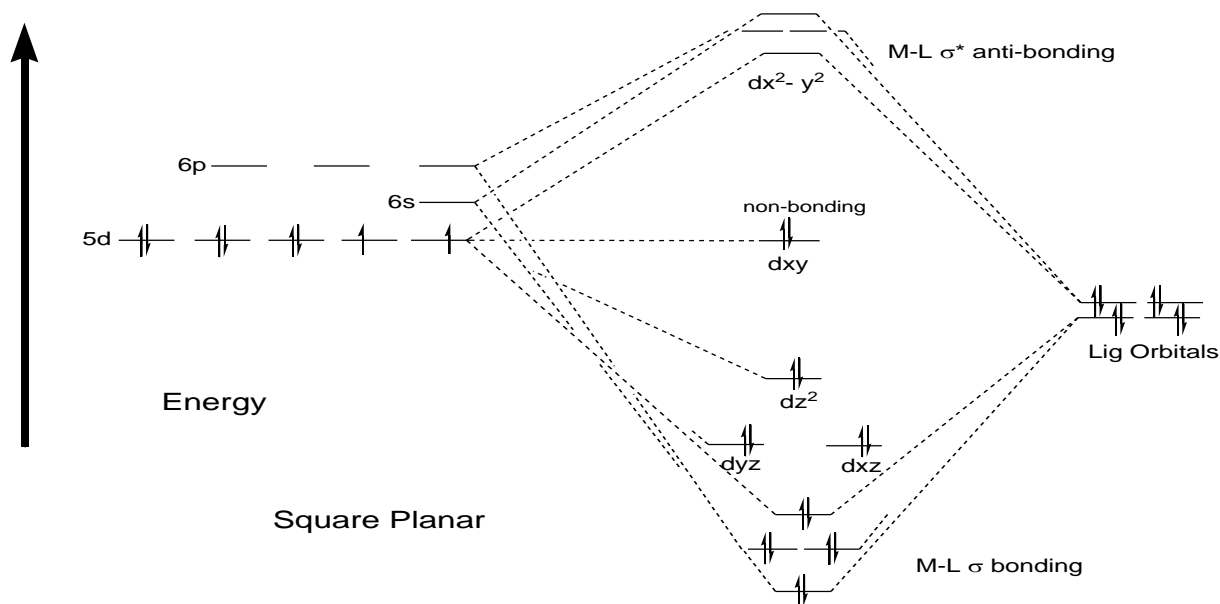
Figure 3-II Ligand field-splitting diagram for metal d-orbital in a square-planar geometry. The order of the lower energy levels depends on the ligand set (*e.g.*, relative importance of σ− and π− effect) but the $d_{x^2-y^2}$ is always the highest in energy.

Many complexes of Group 10 metals with different type of ligands and for many different applications and purposes are reported in the literature,[8] but it is interesting to note that surprisingly only a few are reported to be emissive in solution and there is no reference to measurements made in the solid state.[2] Only Pt^{II} species chelated with aromatic ligands, such as bipyridine, phenanthroline, 2-phenylpyridine, or similar derivatives, emit in fluid solution or in the solid state. A very interesting article written by Brooks *et al.*[9] reported a series of different Pt^{II} complexes with a general formula [Pt(C^N)(O^O)] where O^O is a monoanionic ancillary ligand, essentially a β-diketonate, and C^N is a monoanionic cyclometallating ligand, such as 2-phenylpyridine, 2-(2-thienyl)pyridyl, 2-(4,6-difluorophenyl)pyridyl, and related compounds. Although these complexes are easily prepared, neutral, stable in air and sublimable, making them good materials for use in optoelectronic devices, they do not present any liquid-crystalline properties, not having been so designed. Therefore they are not of particular interest for this project.

The use of metals in the liquid crystal field is well known[10] and is still an area of large interest, because metallomesogens combine the properties of metal complexes with the order and the mobility of the liquid-crystalline state. Thus, with the huge diversity of organic structures that could be used in coordination chemistry, the potential of this field is evident.
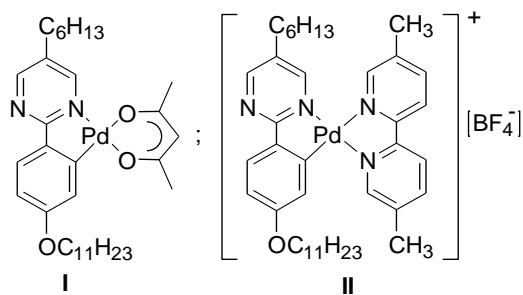
Figure 4-II Complex **I** have monotropic behaviour with melting point at 83 °C (SmA below 68 °C), while complex **II** exhibits a nematic phase (Cr·146·N·158·Iso).

The pioneers in the development of square planar β-diketonate complexes, using 2-phenylpyridine-like ligand, having liquid crystal properties, were Ghedini and Pucci,[11] in the 1990s (Figure 4).

Tschierske and co-worker[12] reported a series of Pd^{II} and Pt^{II} complexes of phenylpyrimidines, imines and phenylpyridines containing a substituted diphenyl-1,3-diketonate ligand (Figure 5). For all the complexes, the metal centre could be Pt^{II} or Pd^{II}. For complexes (**III**) R is $C_{10}H_{21}$, in some cases also a fluorinated chain was used and R`, R`` could be OR or just H. For complexes (**IV**), R^1, R^2, R^3 and R^4 could be a different combination of H or $OC_{10}H_{21}$ and finally, for complexes of series **V**, R^1, R^2, R^3, R^4 and R^5 could be a different combination of H or $OC_{10}H_{21}$. These materials exhibited mainly hexagonal columnar mesophases with the liquid crystallinity being driven by the attendant hexasubstituted β-diketonate, although some, less substituted examples, were found to show a SmA phase and in rare cases the SmC and N phase. Tschierske also reported a similar three-ring system (Figure 2) bearing the same polycatenar diphenyl-1,3-diketonate showing different liquid crystal phases, shown in Figure 6.
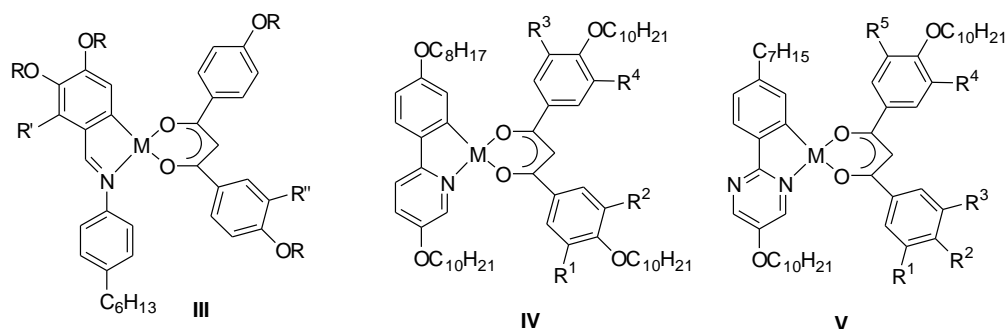
Figure 5-II Complexes prepared by Tschierske and co-workers.
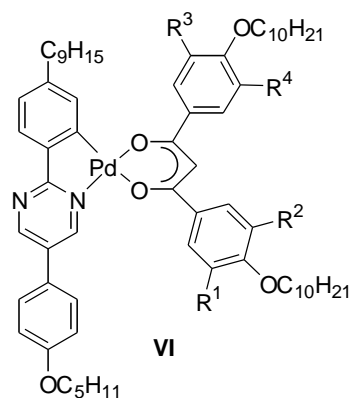
Figure 6-II Complexes (**VI**) R^1, R2, R^3 and R^4 could be a different combination of H or $OC_{10}H_{21}$

On the other hand, Thomas *et al.*[13] reported low emission efficiencies and very short lifetimes for Pt^{II} complexes with diphenyl-1,3-diketonate, as opposed to acetylacetonate, due to the lowering in energy of the non-emissive charge transfer state involving the β-diketonate ligand. This is due to the presence of phenyl groups on β-diketonate ligand, which results in a termally accessible equilibrium with the triplet excited state. This effect has been also reported in the case of cyclometallated Ir^{III} complexes.[14] This will be discussed in detail in Chapter 4.

Similar classes of three rings system, described previously (Figure 2), have been also used by Rourke and co-workers.[15] Some Pd complexes with pyridazine, tetrazine, pyrazines and pyrimidine derivatives (Figure 7), have been synthesised and some of them show liquid crystal properties.[15b] Also, two platinum complexes, one with pyridazine and the other with tetrazine have been reported but there was no report of any liquid crystal or luminescent characterisation. A detailed comparison with the new Pt complexes reported here will be given in § 2.3.2.
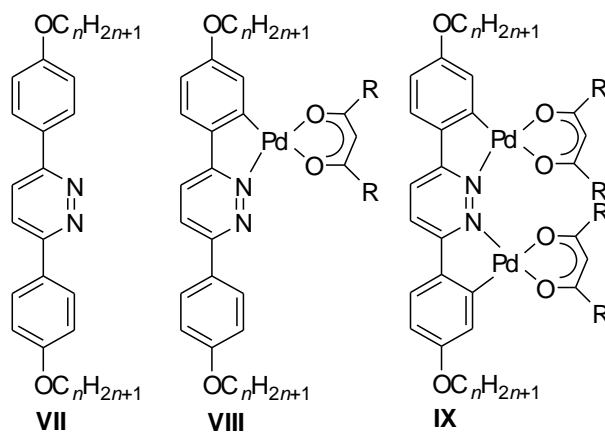
Figure 7-II Pyridazines ligands and their palladium β-diketonate complexes, n = 4, 5, 6, 7, 8 and 10
R = -CH$_3$ or -CH$_2$(CH$_2$)$_2$CH$_3$

2.1.2 Target Compounds

Based on the above background, attention was focused on a material that can deal with both phosphorescent emission and liquid crystal properties at the same time. Therefore, a metal with high spin-orbit coupling to deal with the triplet emission and with an appropriate geometry to deal with the liquid crystal properties was required and, as explained the platinum(II) seemed to be the perfect combination of these characteristics. The choice of the 2-phenylpyridines as ligands is well documented being, its superb characteristic as a strong-field ligand with orbitals of appropriate energy. Thus, the idea came to modify the structure of 2-phenylpyridine inserting another phenyl ring in 5-position of the pyridine and inserting two alkoxy chains in 4-position of the two phenyl groups, so that the increased anisotropy of the ligand could compensate the lateral distortion due to the presence on the ligand of the square-planar platinum group (Pt and acetylacetonate).

These complexes should show liquid crystal phases typical of *rod-like* compounds, therefore they will be apply as polarised emitter, and the presence of acetylacetonate instead of diphenyl diketonate should ensure that the luminescent properties are not compromised.

Platinum complexes (**4(n)** and **8(n)**) were synthesised with two different ligands, with and without a cyclopentene ring fused on the central pyridine (Figure 8). The fused five-member ring has been used previously in studies of luminescent, liquid-crystalline complexes and has been shown to affect both emission behaviour and liquid crystal behaviour.[16] As such, it was of interest to study it here too.
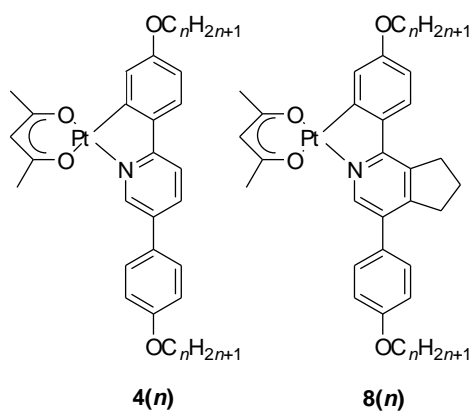
Figure 8-II Pt-complexes of the 2-phenylpyridine derivatives

2.2 Ligands

2.2.1 Synthesis

Scheme 2, gives an overview of the ligands synthesis which is very similar for series **1(*n*)**, **2(*n*)** and **3(*n*)** (Figure 9).
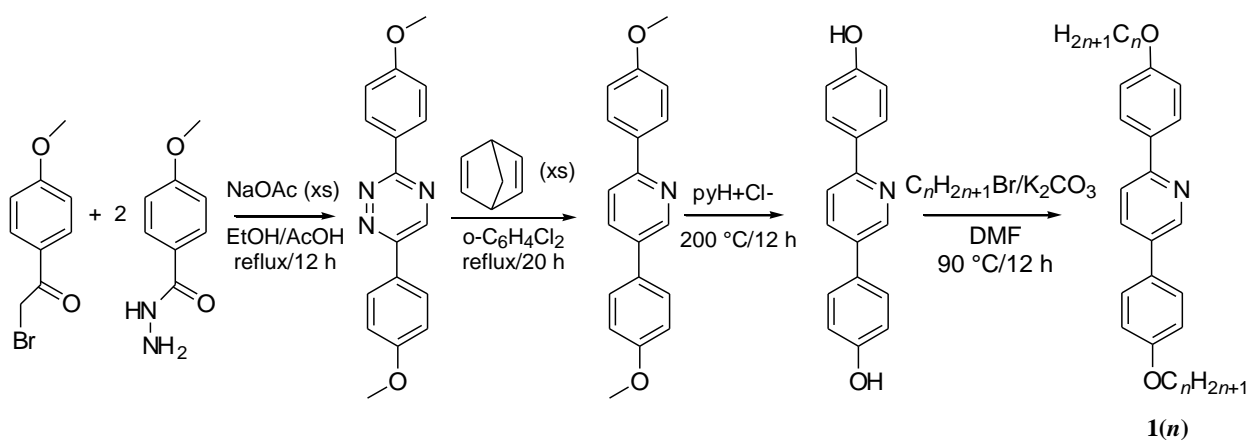
Scheme 2-II Synthetic route to the ligands **1(*n*)**, *n* = 6,8,10 or 12 and represents the number of carbon atoms in the terminal chain.
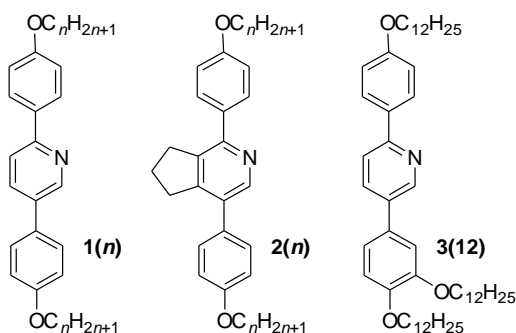
Figure 9-II Ligands synthesised in this project.

The first reaction, which underpins the method, was first described by Saraswathi and Srinivasan in 1971[7] where 2-bromoacetophenone has reacted with two equivalents of 4-methoxybenzohydrazide in the presence of base to give 3,6-di(4-methoxyphenyl)-1,2,4-triazide. The product obtained is as a yellow, crystalline solid and the reaction proceeds in a moderate yield (56%). The second step is an application of an inverse electron demand Diels-Alder reaction, first demonstrated by Carboni and Lindsey in 1959.[17] This methodology has been applied to triazines since 1969,[18] but in this report, it was used a variation called the Boger reaction, applied for the first time in 1981[19] and further developed by Kozhevnikov *et al.* in 2005.[20] In our system, the diene is the electron-deficient heterocycle 1,2,4-triazide possessing a reactive azadiene, and the corresponding electron-rich dienophile is bicyclo[2.2.1]hepta-2,5-diene (norbornadiene) or 1-morpholino-1-cyclopentene. Figure 10 shows the mechanism of this particular Diels-Alder reaction. The use of morpholino-1-cyclopentene or the more reactive 1-pyrrolidino-1-cyclopentene rather than the simple alkene is due to the effect of the morpholino or pyrrolidino moiety as a donating group, making the alkene more electron-rich and hence, producing the desired products in a good or moderate yield.
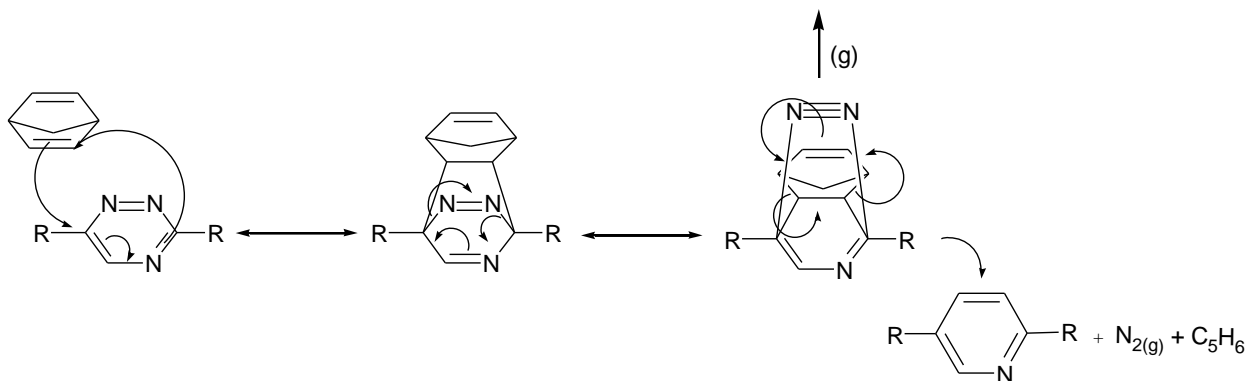
In the system proposed here, the presence of two 4-methoxyphenyl group on the triazine drastically reduces its reactivity. Thus, while the unsubstitued triazine reacts with 1-pyrrolidino-1-cyclopentane under mild conditions (CHCl₃, 25 °C, 1.5 h; 45 °C, 35 h)[8a] giving 74% of the desired product, in this work much stronger condition were used, being the reaction carried out for 20 h under reflux using 1,2-dichlorobenzene as solvent (boiling point 181 °C). Furthermore, because of the low boiling point of the dienophile, it was added several times in large excess during the reaction. The product was eventually obtained as a grey, fish scale, crystalline solid in 65% yield. No difference was found using morpholino instead than the more reactive pyrrolidino cyclopenetene, therefore the choice was determined by the lower cost of the former reagent. Scheme 3 shows the synthesis of the related ligand containing a fused C5 ring on the pyridine (Figure 11), using the same conditions.


2(n)

Figure 11-II 2,5-Di(4-alkoxyphenyl)cyclopentapyridine
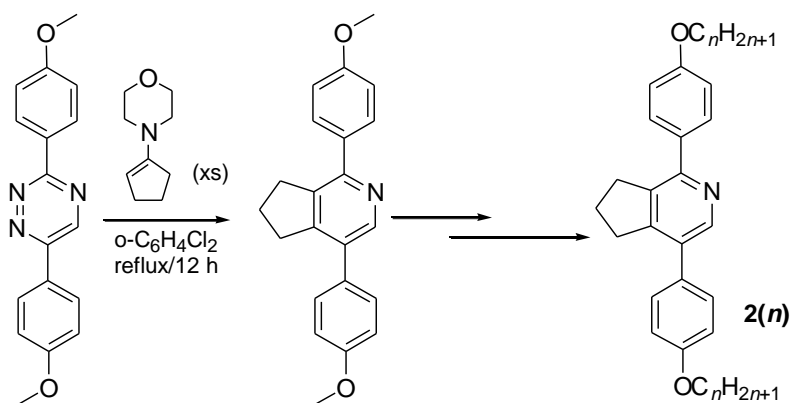
Scheme 3-II Synthetic route to the ligand **2(n)**; **n** =6,8,10 or 12 and represents the number of carbon atoms in the

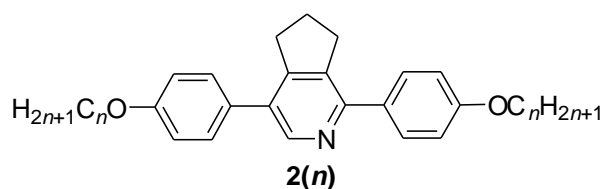The next step is a demethylation reaction, which was conducted in the melt using molten pyridinium chloride at 200 °C, protonating the two O-CH$_3$ groups; in this case the product is a green-brown solid (yield 57%). Finally, the diphenol product is doubly *O*-alkylated by reaction with the appropriate 1-bromoalkane in DMF, using Na$_2$CO$_3$ as a base at 90 °C to avoid DMF decomposition. The reaction yields a colourless, crystalline solid without any further purification.

In the synthesis of ligand **3(12)** (Figure 12) a further step was applied to produce the appropriate starting material, as described in Scheme 4. Thus, one equivalent of 3,4-dimethoxybenzophenone was reacted with 1.05 equivalents of Br$_2$ to yield the brominated acetophenone for the formation of the triazine. This three-chain ligand was only synthesised with a C$_{12}$ chain length as its platinum derivates complex did not show any liquid crystal properties and therefore neither would Pt complexes with shorter chains.
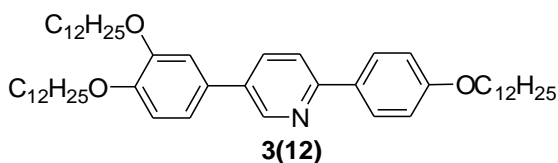
Figure 12-II 2-(4-alkoxyphenyl)-5-(3,4-dialkoxyphenyl)pyridine
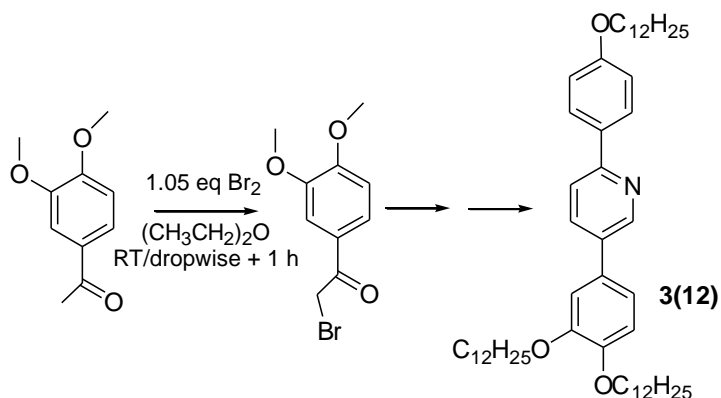
Scheme 4-II Synthetic route for the ligand **3(n)**. It has been synthesised only one derivate, with **n** = 12. The double arrows represent the same reaction condition shown in scheme 1

2.2.2 Ligands Liquid Crystal Properties

The mesomorphic properties of the ligands were investigated using polarised optical microscopy (POM) and differential scanning calorimetry (DSC); the thermal behaviour is collected in Table 1. Furthermore some comparisons between ligand **1(n)** and 3,6-di-(4-alkyloxyphenyl)pyridazines, shown in Figure 7 (**VII**), and between ligand **2(8)** and 2-cyano-3,6-di-(4-octyloxyphenyl)pyridine (Figure 19, **X**) are made to demonstrate the sensitivity of the liquid crystal properties to the molecular structure.

2.2.2.1 Ligand **1(n)**

All the ligands of series **1** were polymorphic and, consistent with their elongated structure of three rings connected only with σ-bonds, it is not surprising that in general they show quite high transition temperatures. Thus, their clearing points ranged from almost 240 °C for **1(6)** to 200 °C for **1(12)**, whereas the melting points ranged from 144 °C to 120 °C, respectively. Also, as expected, all these ligands show smectic phases as normal for their shape (rod-like). **1(6)** has the richest polymorphic sequence and the first phase seen was a SmA phase, clearly

identified by a focal conic fan texture and homeotropic regions. On further cooling this gave way to a SmC phase with a schlieren texture (Figure 13a) where the SmA phase had been homeotropic and broken fans in the planar areas. The SmC phase persisted for some 30 °C, until a transition was observed to a phase that also showed a schlieren texture, but this time the brushes were much broader and not very well defined. In general it was difficult to focus on the sample, phenomenon characteristic of the SmI phase (Figure 13b).[21]

Table 1-II Thermal behaviour of ligands **1(n)**, **2(n)** and **3(12)**. The ΔH and ΔS were determined by DSC.

Compound	n	Transition	T (°C)	ΔH (kJ mol^{-1})	ΔS (J K^{-1} mol^{-1})
1(6)	6	Cr-Cr′	68.8	2.2	60
		Cr′-G	144	1.4	4
		G-SmF	154	8.1	20
		SmF-SmI	166	5.6	13
		SmI-SmC	201.5	1.3	3
		SmC-SmA	231.5	0.3	1
		SmA-I	237.5	8.0	18
1(8)	8	Cr-Cr′[(1)]	107	10.9	28
		Cr′-J	121	13.4	34
		J-SmI	137	3.8	9
		SmI-SmC	187	2.8	6
		SmC-I	221	13.3	27
1(10)	10	Cr-J [(2)]	120.3	–	–
		J-SmI	121	41.2[(3)]	105[(3)]
		SmI-SmC	178.9	1.4	3
		SmC-I	210.6	14.4	30
1(12)	12	Cr-SmI	121.7	63.0	160
		SmI-SmC	171.6	2.4	5
		SmC-I	200.0	18.5	39
2(6)	6	Cr-N	81.4	29.8	84
		N-I	115.0	1.2	3
2(8)	8	Cr-N	84.8	29.3	82
		N-I	108.7	1.0	3
2(10)	10	Cr-N	99.2	47.8	129
		N-I	105.0	0.6	2
2(12)	12	Cr-SmA	94.8	59.2	161
		SmA-I	101.6	4.8	13

		Cr-Cr´[4]	84.8	9.0	25
3(12)	12	Cr-I	108.2	64.5	2
		(SmC-I)	(98.1)	(-8.6)	(-23)

(1) this phase is found only by DSC, (2) this phase is only found by microscopy, (3) values attributable to the sum of SmI-J and J-Cr, (4) this transition is found only in the first DSC cycle.

This phase showed a range of 35 °C before another transition occurred to a fluid phase. Two types of texture could be observed here. One was a classic broken fan texture (Figure 13c) while the other was a sort of mosaic texture (Figure 14); these are characteristic of a SmF phase. Below the SmF phase, a transition occurred to a crystal smectic phase whose texture (Figure 13d) was consistent with a crystal smectic G phase, which would also be the phase predicted to follow a SmF phase on cooling.[22] All of these transitions were identified by DSC analysis, which also showed two further transitions between crystal modifications at lower temperatures (Figure 15). The phases and transitions were also seen in the focal conic fan textures, but the transition between SmI and SmF phases is not really appreciable. The photomicrographs of the discussed transition are presented in Figure 16.

(a)

(b)

(c)

(d)
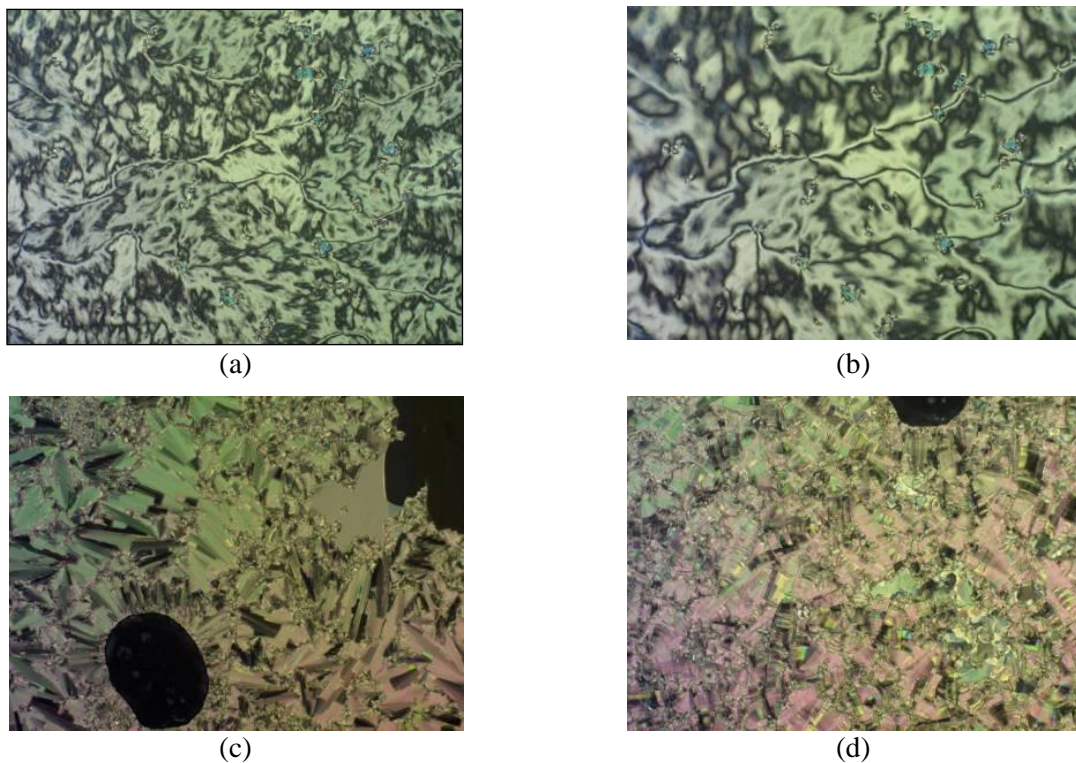
Figure 13-II Optical micrographs (on cooling) of **1(6)** (a) SmC phase at 203 °C; (b) the SmI phase at 198 °C; (c) SmF phase at 159 °C; (d) crystal smectic G phase at 152 °C

(a)

(b)

(c)
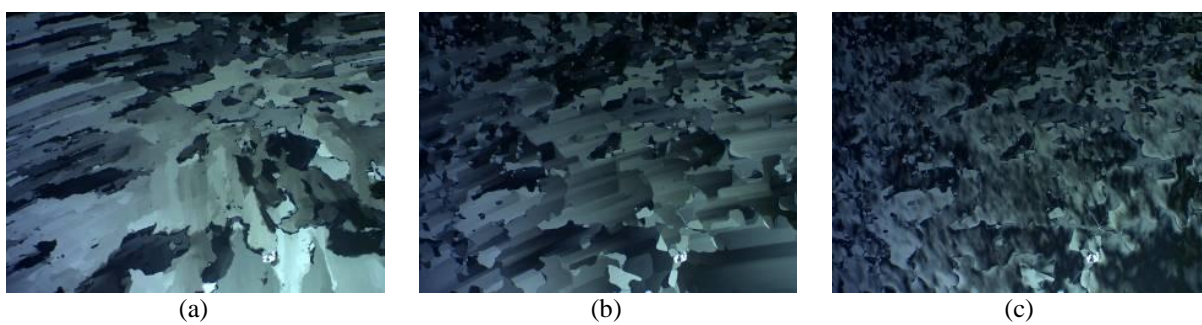
Figure 14-II Optical micrographs (on cooling) of **1(6)**: (a) Soft crystal G at 152°C; (b) SmF phase at 162 °C and (c) SmI phase at 170 °C
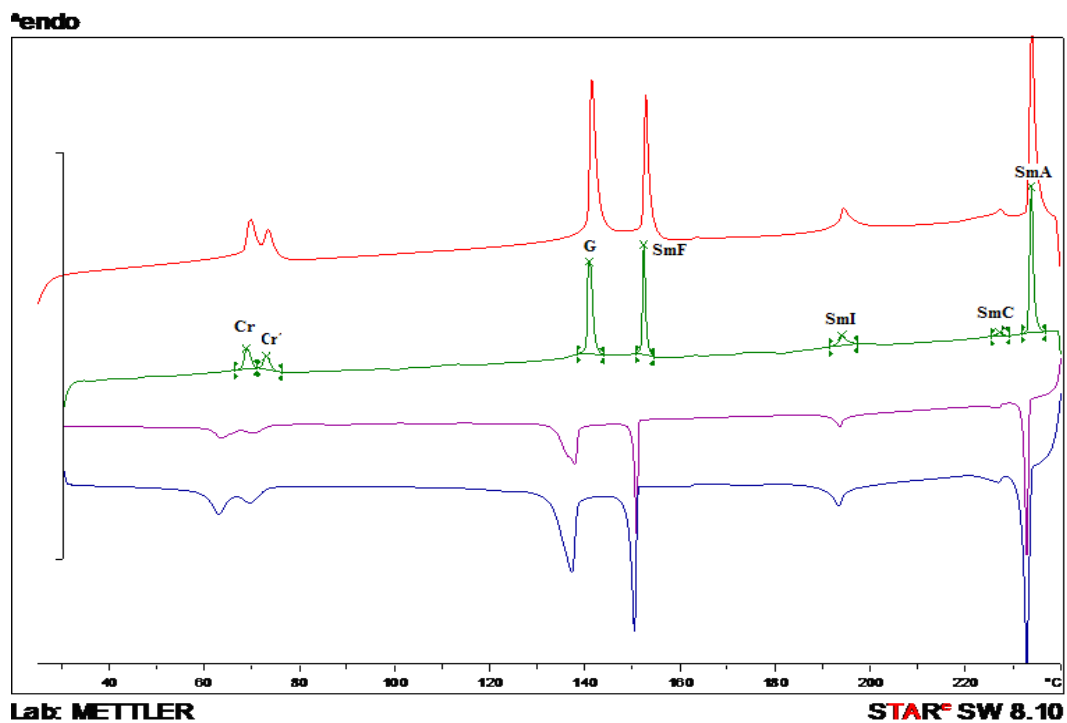
Figure 15-II DSC analyses of **1(6)** showing also the Cr-Cr´ transition

(a)   (b)

(c)   (d)
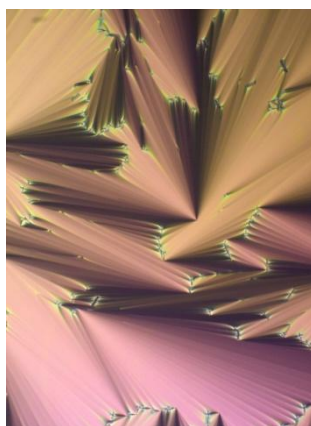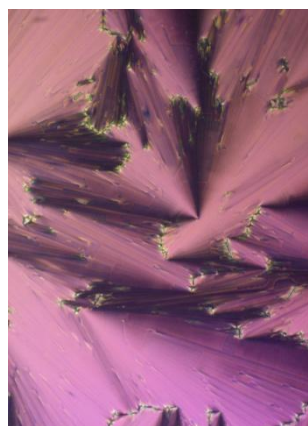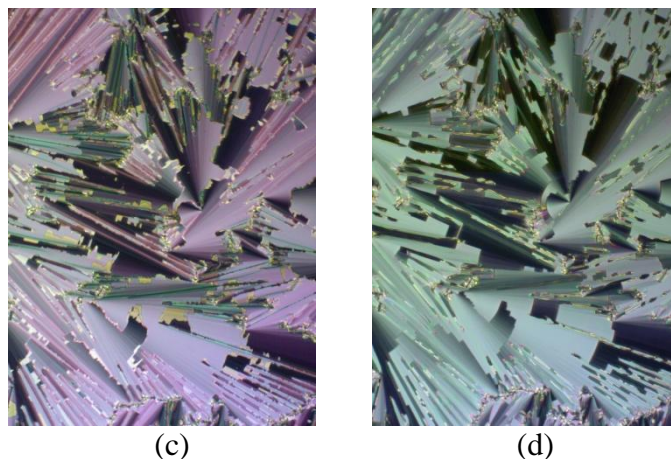
Figure 16-II Optical micrographs (on cooling) of the focal conic fan textures of **1(6)** in the same region: (a) SmA phase at 233 °C; (b) SmC phase at 227 °C; (c) SmI phase at 195 °C and (d) SmF phase at 155 °C.

For **1(8)**, **1(10)** and **1(12)**, the mesomorphism was almost the same, and indeed on cooling, a SmC phase is formed from the isotropic melt, identified through its characteristic schlieren texture. This was followed by a SmI phase, identified as it retained the defects of the SmC phase while the brushes became broad and sometime harder to focus on. In **1(8)**, a crystal-crystal transition was visible in the DSC trace, shown in Figure 17; moreover for **1(8)** and **1(10)**, a crystal smectic phase was seen on further cooling and, given that it was preceded by a SmI phase, it was assigned as a J phase; note that the crystal J phase has the same tilted hexagonal arrangement of the SmI phase and that, similarly, the SmF and crystal G phase are also so related so that assigning crystal smectic phases below these two fluid phases can be done with a degree of confidence assuming that the textures are not inconsistent with the phases proposed.[23]
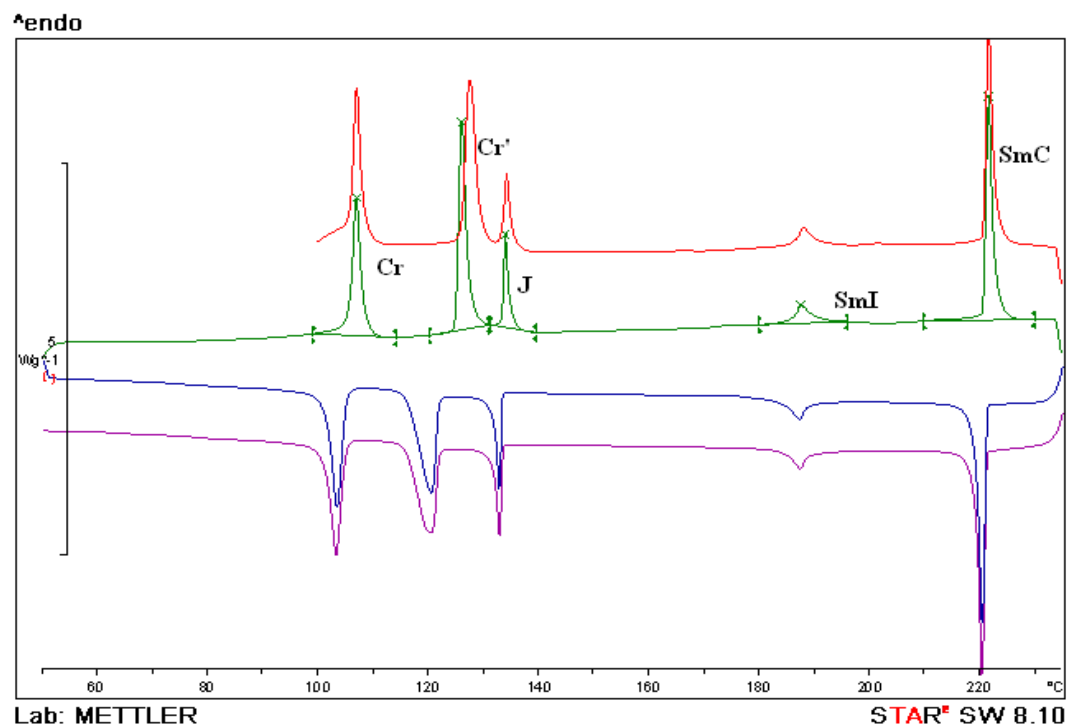
Figure 17-II DSC analyses of **1(8)** showing the Cr-Cr´ transition

Through the comparison of these pyridine systems **1(6)**, **1(8)** and **1(10)** with the pyridazine[15b] ligands of the systems **VII(6)**, **VII(8)** and **VII(10)**, shown in Figure 18, it is possible to determine some small differences in the liquid crystal behaviour (data in Table 2).

In general, the pyridazines ligands show higher clearing points (transition between liquid crystal state and isotropic liquid), but quite similar melting points (Figure 19). For example, the difference in clearing points between the two derivatives with the shortest chains is about 20 °C, for chains with eight carbon atoms it is almost 30 °C and for the longest chains this difference is hugely increased, reaching 60 °C. Strangely the differences do not concern only the temperature, indeed in the pyridazine ligands there is no indication of SmA or SmC phases, only SmF, SmI and a crystal smectic G phases are reported.[15b]
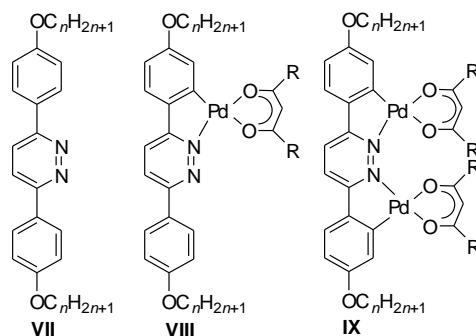
Figure 18-II Pyridazines ligands and their palladium β-diketonate complexes, n = 4, 5, 6, 7, 8 and 10
R = -CH_3 or -$CH_2(CH_2)_2CH_3$
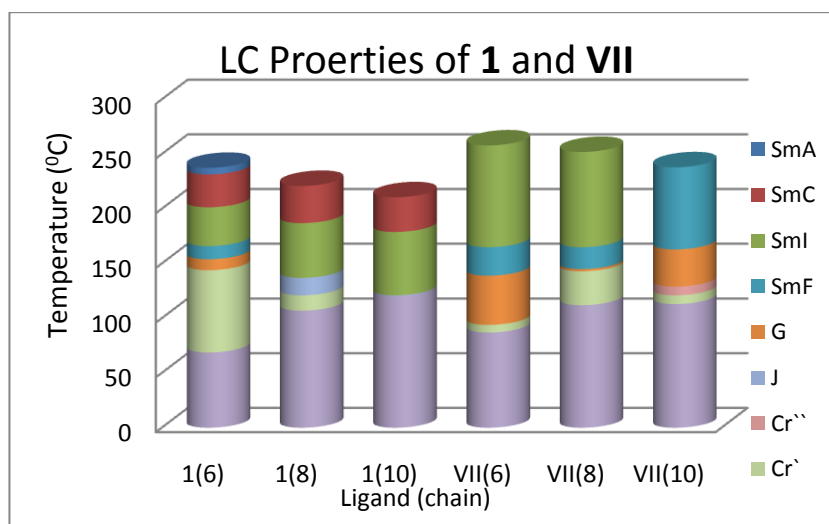
Figure 19-II Thermal behaviour of ligand **1**(*n*) on the left and **VII**(*n*) on the right.

This behaviour could be attributable to the more rigid structure that allows highly efficient intermolecular hexagonal packing interaction between the molecules in the liquid crystal phases. It is argued, indeed, that this rigidity is due essentially to the presence of an extra nitrogen atom in the pyridazine, because the lone pairs of the nitrogen interact with the vicinal hydrogen, forcing the ring in a planar structure (Figure 20),[4] but this computational speculation did not support the experimental observation. In fact, the distance between the interacting hydrogen and nitrogen atoms in the two structure shown in Figure 21 is not

dissimilar, 2.66 Å for **X** and 2.45 Å for **XI**, but, as shown in the single crystal X-ray analysis, they acquire two different conformation of the ring bearing the hydrogen interacting with nitrogen (full crystallographic data as appendix on CD). Moreover a third conformation is shown from the ligand **1(1)** herein used for which a single crystal structure was obtained. The images are shown in Figure 21 and they were obtained from the elaboration of X-ray data, after the removal of the disorder (the nitrogen was disordered overall four equivalent sites on the central ring). The distance of the interacting hydrogen and nitrogen atoms is not dissimilar from the two structures described above, with a value of 2.62 Å, but it is clearly visible that the phenyl rings in 2- and 5- position of the pyridine are not coplanar with the pyridine. These differences in mesomorphism are, therefore, due to other factors, one possibility being the different π-π interaction between the pyridazine ligands and pyridine ligands.
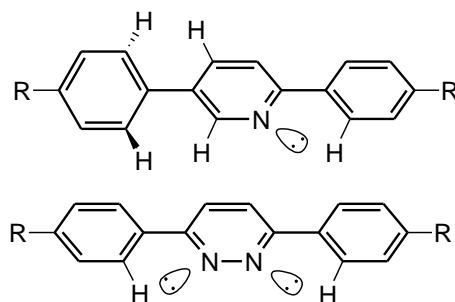
Figure 20-II Comparison of different structures of pyridine derivatives and pyridazines derivatives,from theoretical calculation the presence of two nitrogen atoms force, with their lone pairs, the molecule is assumed to have a completely flat structure, but this has not been confirmed from single crystal X-ray analysis.
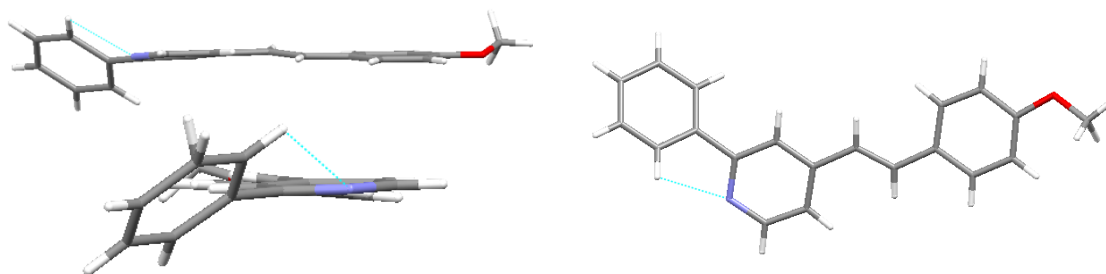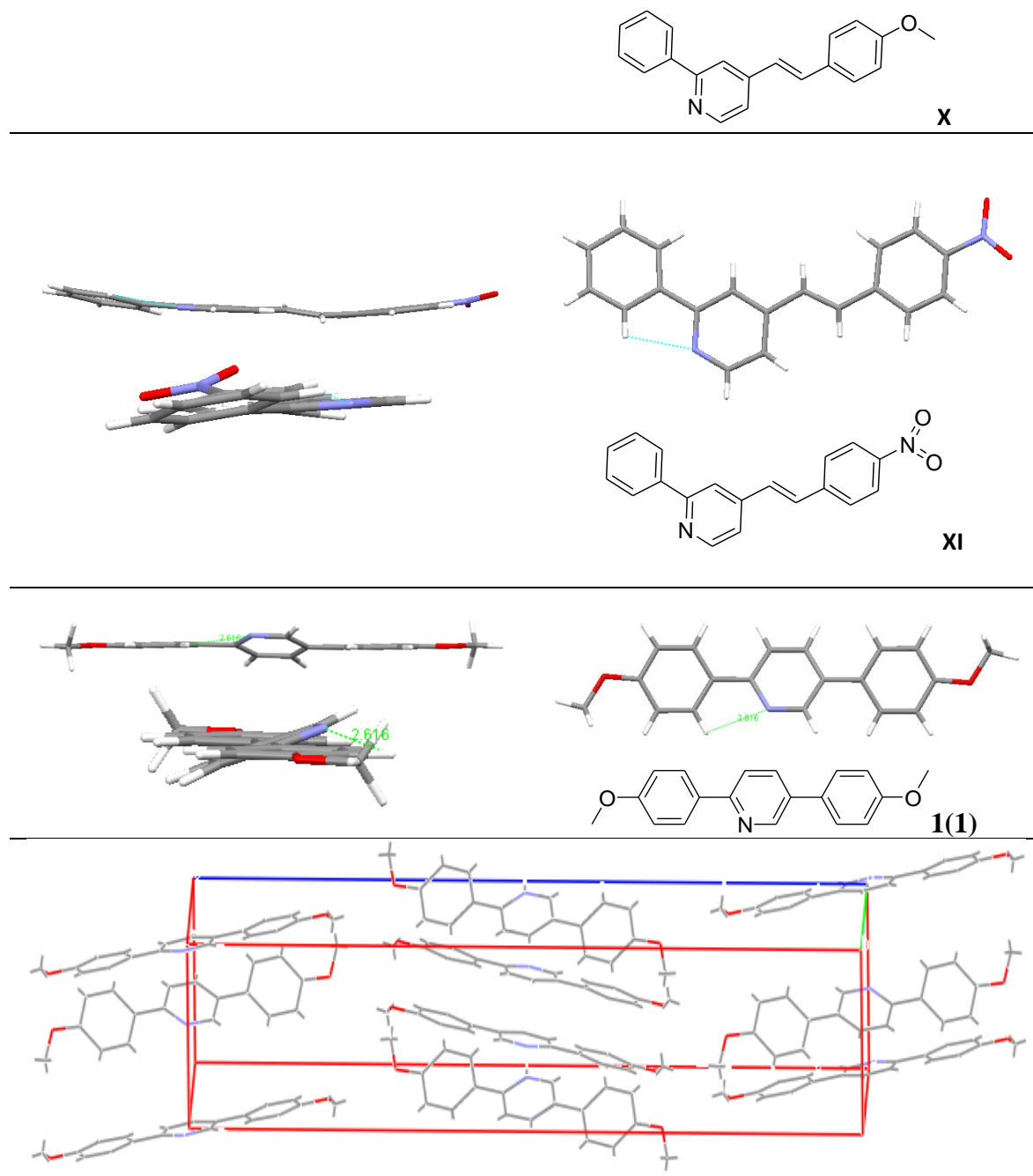
Figure 21-II Crystal structures of the 4-(*p*-methoxyphenyl-styryl)-2-phenylpyridines **X** on the top, 4-(*p*-nitrophenyl-styryl)-2-phenylpyridines **XI** in the centre and 2,5-dimethoxyphenylpyridine **1(1)** at the bottom.

Table 2-II Thermal behaviour of **VII(*n*)**. ΔH calculated by DSC.

Compound	*n*	Transition	T (°C)	ΔH (kJ mol^{-1})
VII(6)	6	Cr-Cr′	87	8.83
		Cr′-G	94	15.4

		G-SmF	139	0.17
		SmF-SmI	165	0.91
		SmI-I	258	11.2
VII(8)	8	Cr-Cr′	109	32.9
		Cr′-G	131	10.1
		G-SmF	142	0.1
		SmF-SmI	166	1.32
		SmI-I	249	13.3
VII(10)	10	Cr- Cr′	113	10.3
		Cr′- Cr′′	121	10
		Cr′′-G	129	10
		G-SmF	163	1.96
		SmF-I	238	15.7

There are only other two examples in the literature of 2,5-di(*alkyl(oxy)*-phenyl)pyridines (Figure 22).[4b,4c] One molecule possesses chiral chains, therefore SmA^* and SmC^* phases are seen, while the other bears photopolymerisable chains and shows a SmC phase. A comparison between these systems and **1(n)** would not be appropriate because of the huge difference in the lateral chains, but they are mentioned here for completeness.
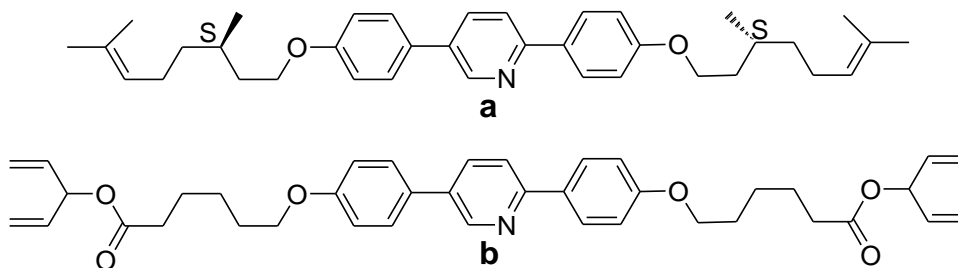
Figure 22-II Structure of 2,5-di(*alkyl(oxy)*-phenyl)pyridines. **a** Cr · 83 · SmC^* · 102 · SmA^* · 128 · I. **b** Cr · 87 · SmC · 126 · I.

2.2.2.2 Ligands **2(n)**

In ligands **2(n)**, the presence of the cyclopentene unit on the central ring destabilised the smectic phases, as the interactions between the molecules become disrupted by the presence of

the large, lateral substituent.[24] As such, the packing of the compounds into layers becomes inefficient and so the nematic phase becomes dominant. The only exception is **2(12)**, where the longer terminal chains appear able to overcome this destabilising influence and a SmA phase is found. The other important effect is that the cyclopentene ring destabilises both the crystal and the mesophases, resulting in a general reduction of the transition temperatures by about 100 °C; this is also not unexpected given the reduction in anisotropy. Figure 23 shows a classical picture of a nematic phase for **2(6)** at 107 °C, and a rather beautiful SmA texture for **2(12)** at 100 °C.

In a publication focused on triazine-based molecules, the presence of a lateral substituent has been investigated[5a] in a material similar to these, as shown in Figure 24. The presence of the cyano group give a stable SmC phase close to room temperature (26 °C) and then a N phase at 88 °C that clears at 101 °C. Comparing with ligand **1(8)**, the effect due to the introduction of the CN group is similar to that obtained with the introduction of cyclopentene described above, namely destabilisation of both the melting and the clearing points and disruption of the smectic phases. However it seems that the CN group has a greater tendency to stabilise the smectic phase than the cyclopentene group; this different behaviour could be due to the smaller size of the side group, but also, and more probably, to the stronger dipolar effect that gives rise to intermolecular dipole-dipole interactions between the CN groups.

(a)   (b)
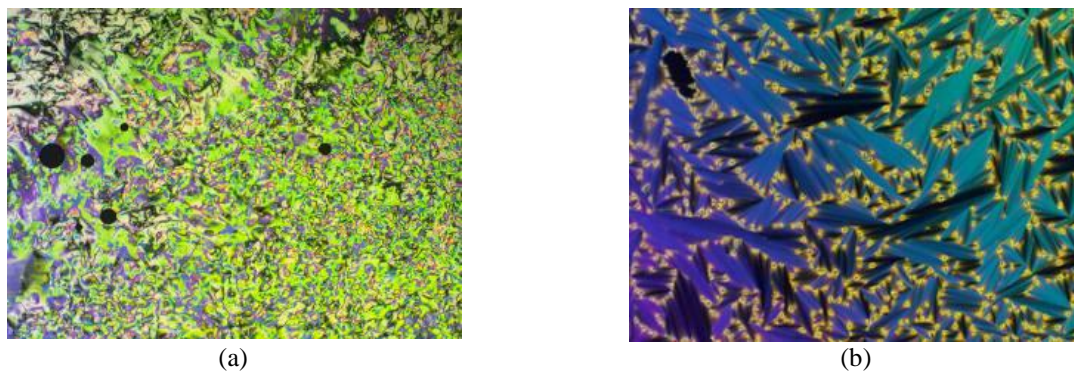
Figure 23-II Optical micrographs (on cooling) of the (a) N phase at 107 °C of **2(6)** and (b) the SmA phase at 100 °C of **2(12)**
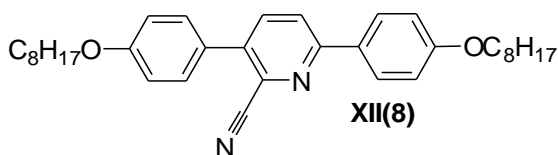
Figure 24-II 2-Cyano-3,6-di(octyloxyphenyl)pyridine **XII(8)**, Cr · 26 · SmC · 88 · N · 101 · I

It is interesting to note that the main information obtained by the two examples of comparison discussed above is that the liquid crystal properties are sensitive to any small change, as was shown for the introduction of an extra nitrogen atom.

2.2.2.3 Ligand **3(12)**

The introduction of a further chain in the *meta* position in system **3(12)**, drastically influenced the liquid crystal behaviour. *Multi-chain* systems are a well studied class of liquid crystals, called polycatenar compounds, which are molecules with a long, *rod-like* rigid core with some spacer usually made of double bonds or carboxylate groups, and ending with three or more alkyloxy chains grafted at each end of the molecules (Figure 25).[25] On the basis of the number of chains that the molecule possesses, it will be classified as: *hexacatenar* (6 chains), *pentacatenar* (5 chains), *tetracatenar* (4 chain) and, as in this case, *tricatenar* (3 chains). More

accurate identification can be given describing in the terminology the number and the relative position of each side chain using the letter *o*, *m*, and *p*. So, **3(12)**, Figure 9 and 12, would be classified as *tricatenar 2mp-1p*.
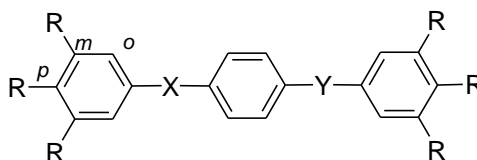
Figure 25-II General structure of polycatenar molecule

Many *tricatenar* compounds have been studied in the past,[26] with different chain combinations and usually these compounds behave principally as calamitic mesogen. In general they form only N and SmC phases; a SmA phase has never been observed for these *tricatenar* systems. This type of ligand falls within the classic liquid crystal behaviour for these *tricatenar* systems. Furthermore, if compared with **1(12)** it is possible to note a marked difference in the liquid crystal transitions temperature, indeed the clearing point is more than 100 °C lower, showing the destabilising effect of this additional chain. Nonetheless, a monothropic SmC phase is observed on cooling ($T_{(SmC-I)} = 98.1$ °C).

2.3 Platinum(II) Complexes

2.3.1 Synthesis

Platinum complexes were synthesised with ligands **1(*n*)**, **2(*n*)** and **3(12)**, and with a range of β-diketonates. Furthermore, complexes containing DMSO and Cl ligands, instead of acetyl acetonate, were also synthesised and characterised. The complexes are shown in Figure 26. Complexes **5(*n*)**, **6(*n*)**, **7(*n*)**, **9(*n*)**, **10(*n*)** and **11(*n*)** were prepared and characterised by Matthew Spencer as part of an undergraduate MChem project and he also conducted the isomerisation studies of **6(*n*)**, while *cis*-**15(*n*)** was prepared by Tabitha Petchey as part of her MChem project.

2.3.1.1 Platinum synthesis, first attempts.

Having obtained these phenylpyridine ligands, it was then necessary to establish optimum conditions for the reaction with platinum. There are several descriptions of suitable routes in the literature[9,13,15,27] but none of them gave the expected results. For example, the first attempt was made following a classic procedure,[13] reacting 2.5 molar equivalent of 2,5-di(4-methoxyphenyl)pyridine **1(1)** with $K_2[PtCl_4]$ in ethoxyethanol at reflux. The reaction was monitored every five hours but after four days, a highly insoluble green product was formed, which could not be identified by normal characterisation techniques, except for the presence of unreacted ligand.

Replacing ethoxyethanol with 1,2-dichlorobenzene (bp 181 °C) or acetic acid (bp 121 °C),

similarly did not lead to a characterisable product. Therefore it was decided to use a more reactive metal such as palladium in form of acetate salt to obtain more information on the reaction.
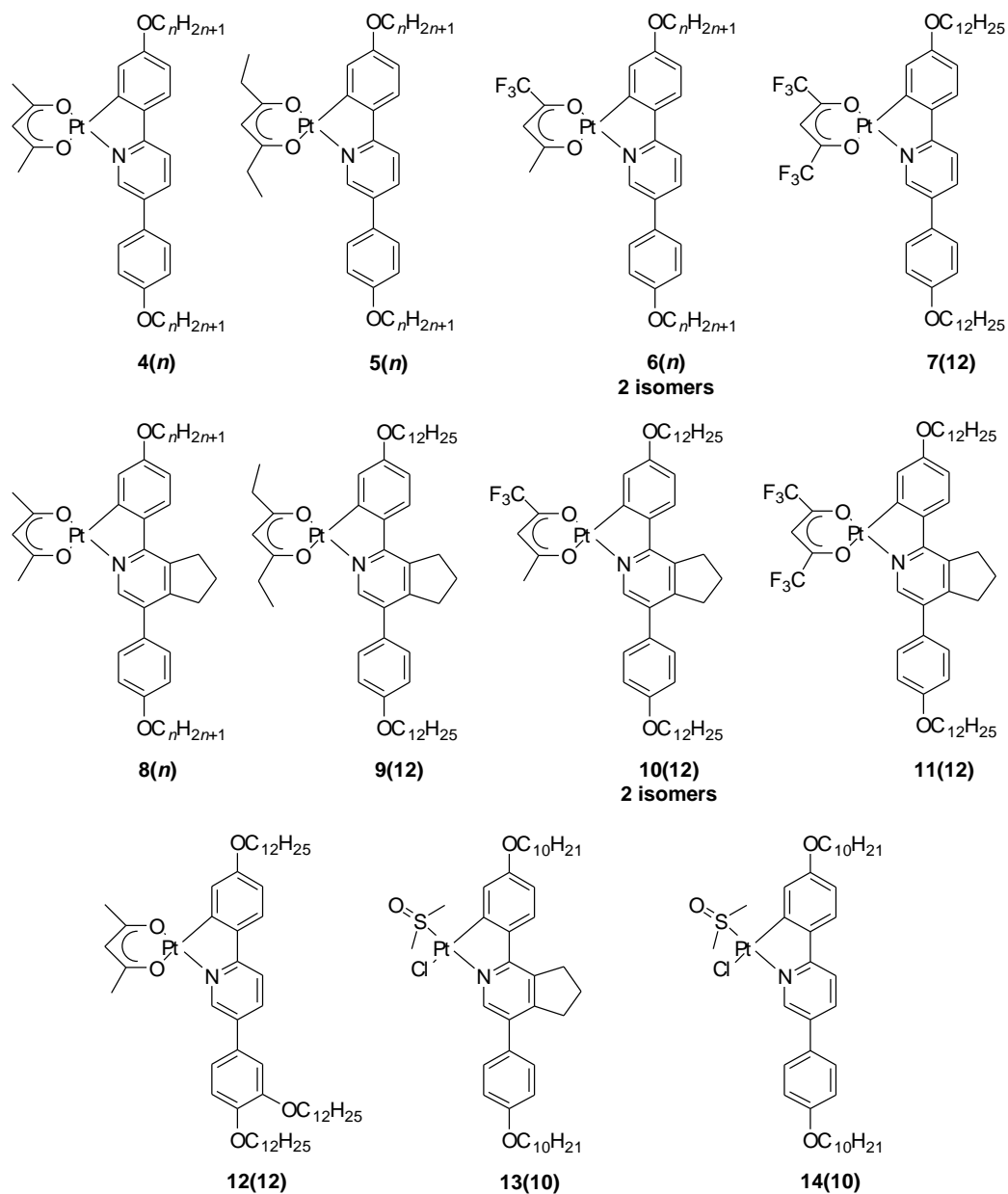
Figure 26-II The platinum complexes **8(*n*)**, **9(*n*)**, **10(*n*)** and **12(*n*)** have been synthesised with *n* = 6, 8, 10 and 12 carbon atom; **13(*n*)** and **14(*n*)** instead have been synthesised for all the complexes as intermediate but only the molecules with 6 and 10 carbon atom on the chains have been isolated and characterised. Some of these complexes, **6(*n*)** and **10(n)**, have been synthesised as two isomeric structures

Under the same conditions, this reaction gave the target compound easily going through the μ-acetato complex (Scheme 5). Thus, having found that the reaction worked well with palladium, it was hypothesised that the problem was connected with low solubility of the specific platinum salt used in the organic solvents, thus the solubility of the tetrachloroplatinate(II) anion was modified by preparing its salt with Bu_4N^+.[27]
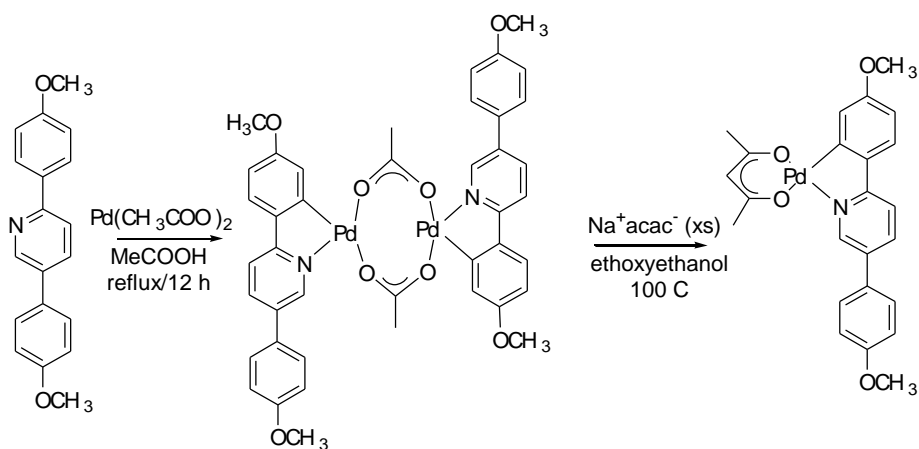
Scheme 5-II Reaction model to palladium complex. This compound was synthesised to collect information on the nature of the reaction. **n** = 1, no liquid crystal properties were found.

[Bu$_4$N]$_2$[PtCl$_4$] was much more soluble, but unfortunately, the reaction still did not give the expected results, again giving a green, insoluble powder, even when trying to use other solvents such as acetic acid and ethanol. Another attempt was made reacting this green solid directly with sodium acetyl acetonate in ethoxyethanol at reflux overnight. Unfortunately this procedure gave mixture of several products and some purification methodologies were tried without any appreciable success. Thus, a step back was taken, trying to find the solution for carrying out this reaction. It was decided to test the procedure with 2-phenylpyridine itself. Again a green powder was obtained and when the reaction was analysed, it was found that, in the adopted conditions, two products were formed.[26] With this information it was possible to

understand, or at least to have a better comprehension, of the green solid obtained. Figure 27 shows the complexes that have been found.
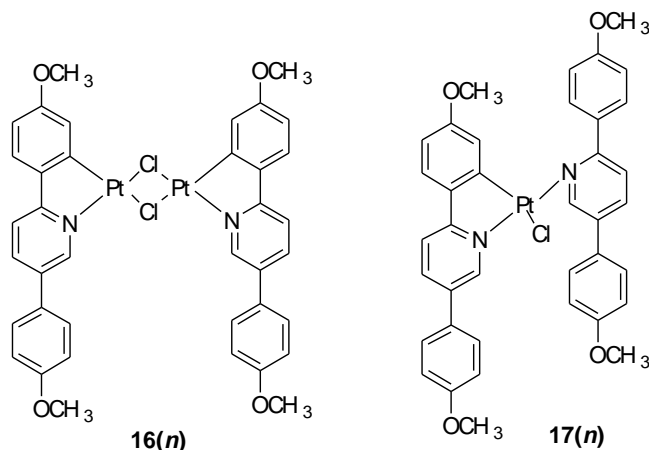
Figure 27-II Intermediate complexes to the formations of acac complex **4(*n*)**. For complexes **16(n)** is theoretically possible to obtain *cis* and *trans* like isomer.

The main reason for the formation of the unwanted compounds **17(*n*)** was the ligand excess and the mild condition applied. Thus, a perfect stoichiometric ratio and strong reflux were adopted. With this shrewdness was obtained mainly complex **16(*n*)** even if complex **17(*n*)** was still obtained in some occasions. Unfortunately purification was not possible because of the very low solubility of complex **16(*n*)**, even if long chains were used; complex **17(*n*)** was never isolated and was prevalently found when the conditions of the reaction were milder; its presence is easily detectable due to the presence of a peculiar set of ^{1}H-NMR signals, (Figure 28, the 2-phenylpyridine platinum(II) complex isolated during the test reaction.). In general, cyclometallation is recognised easily thorough the shifts of the hydrogen vicinal to nitrogen and its singlet proton signal with the typical $^{3}J_{Pt\text{-}H}$ coupling of about 20 Hz. In the complexes showed in the Figure 28 the presence of an extra ligand bonded with the N group to Pt results

in a slightly more complex spectrum where three doublet signals with Pt–coupling can be seen. The formation of the *trans* derivate is assigned from literature data.[15b]
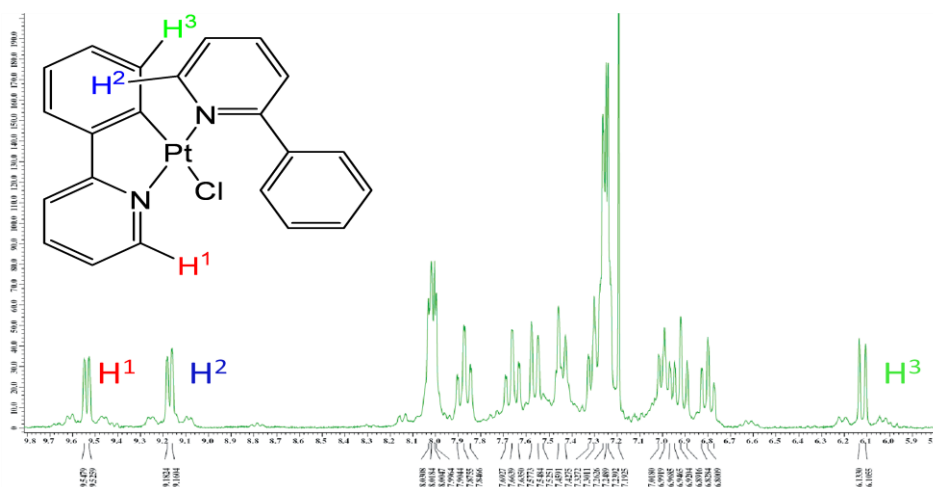
Figure 28-II Aromatic region of the ^{1}H-NMR spectrum of 2-phenylpyridine platinum(II)complex.

Having understood the nature of the green solid (**16(n)**), an attempt was made to obtain the target acetyl acetonate derivative direct from dimer **16(n)**. However due to the very low solubility of the reactant and also to the presence of impurities this approach led to a mixture of compounds that was impossible to purify. Therefore, an attempt was made to purify complex **16(n)** before the formation of the target compounds, by converting the dinuclear platinum complex into a complex that was easier to manage, and had higher solubility. Thus, reacting the green solid with DMSO[28] in the absence of other solvents a complex with S–bound DMSO *trans* to the nitrogen of the pyridine and with chlorine *trans* to the carbon-**14(n)** was yielded. The isomer has been identified by a single crystal analysis (Figure 29), and characterised through ^{1}H-NMR spectroscopy. The formation of complexes **14(n)** helped to simplify the methodology and to obtain the target compound in good yield, because, owing to

its greater solubility, it was possible to purify it and therefore utilise it in the next step.
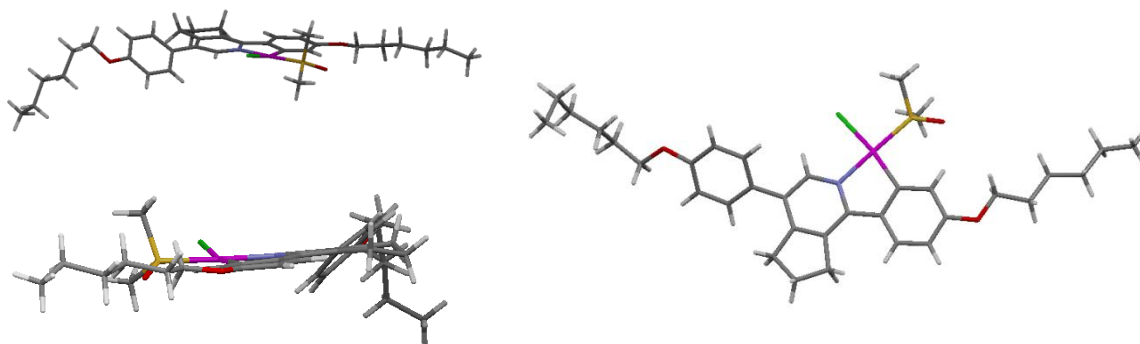
Figure 29-II Single crystal structure of **13(6)** shows the stereochemistry of the complex. Chlorine in green, oxygen in red, nitrogen in blue, platinum in violet, sulfur in yellow, carbon in black and hydrogen in grey.

In the Scheme 6 it is possible to see the methodology applied for the first complexes synthesised. The reported yields are calculated for **1(12)**, but even better yields are found for complexes of series **2(*n*)** compared with **1(*n*)**, owing to the greater solubility of the substituted ligands. The synthetic route will be described only for complex **4(*n*)** as same conditions are applied for the reactions with other ligands, any variations used will be shown and explained separately.
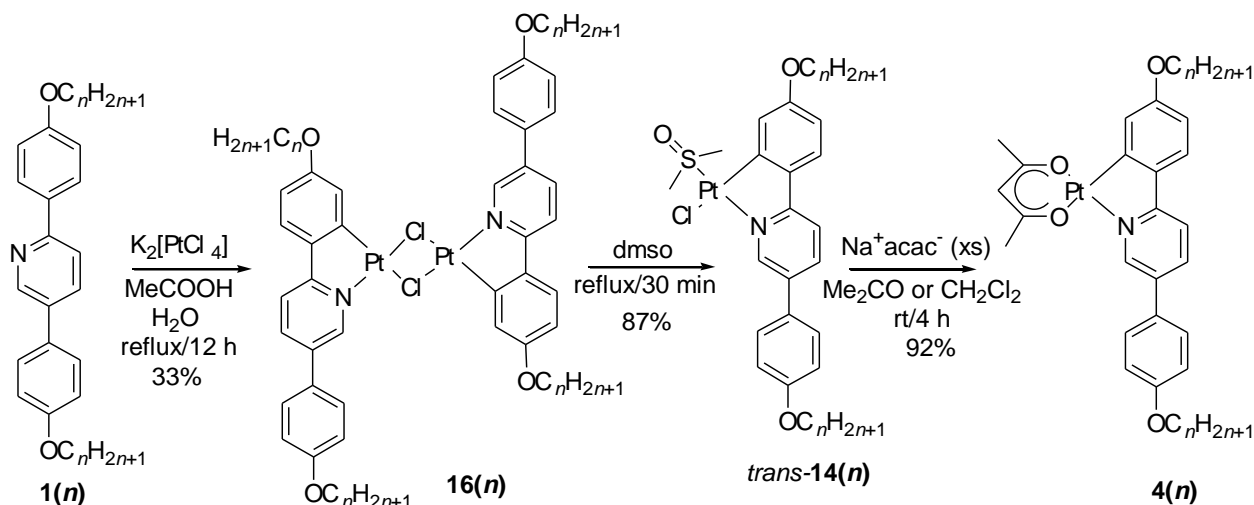
Scheme 6-II Synthetic route to the platinum complexes, yield shown for C12 derivatives. The same conditions were applied for **2(n)** and **3(12)**.
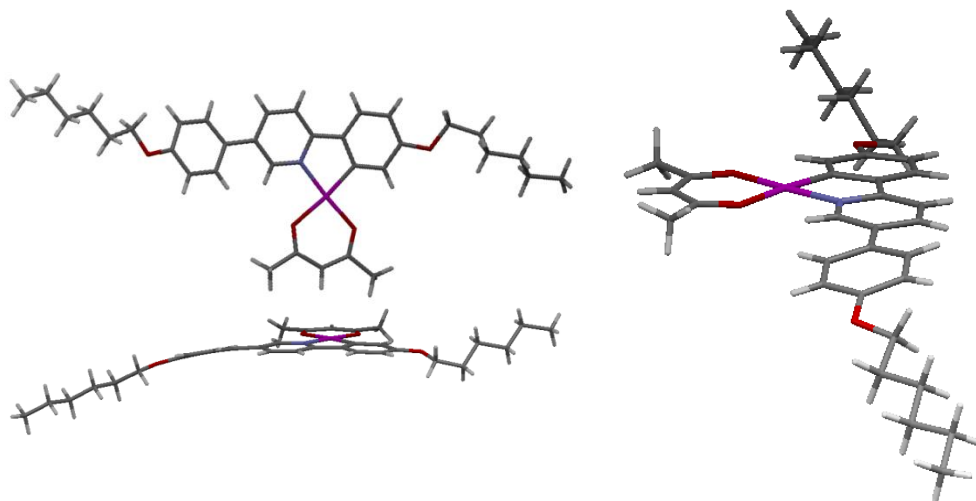
Figure 30-II Single crystal structure of **4(6)**. Oxygen in red, nitrogen in blue, platinum in violet, carbon in black and hydrogen in grey. The X-ray of complex **8(6)** is shown in the appendix X.

The first reaction foresees the presence of the ligands **1(n)**, potassium tetrachloroplatinate and acetic acid as protic solvent.[15b,15c] It was notice that is if a small amount of water is present (10% of total solvent), it helps the solubilisation of the platinum salt, and therefore the reaction proceeds more rapidly; indeed this step takes 12 h to be complete in the presence of

water and four days in its absence. The mixture is then filtered hot and washed first with hot acetic acid, trying to remove the maximum amount of unreacted ligand and then with water to remove the $K_2[PtCl_4]$ and at the end with acetone to dry. Unfortunately, in it is not possible to calculate the yield of the pure product because, as mentioned before, the extreme low solubility of the complex **16(*n*)** did not allow its purification and full characterisation, so that the reported yield is indicative and assumes that the material is pure. In the following step, complex **16(*n*)** is dissolved in DMSO and heated under reflux for 30 min, before filtering to remove any insoluble material and then drying. The complex is then purified on a column of silica gel using chloroform as eluent. Complex **14(*n*)** is afterwards reacted with a large excess of the appropriate sodium acetylacetonate in acetone or dichloromethane, which led to a solution containing only the desired product and the reagent (sodium acetylacetonate) in excess; therefore the product could be purified by washing with water. In some cases further purification is required, and can be done using dichloromethane as eluent on a silica gel column. Better yields are achieved in general when the reactions are carried out using ligand **2(*n*)**, because the presence of fused cyclopentene ring on the pyridine increase the solubility of the system improving thus, the reactivity. The yields using ligand **3(12)** are generally similar to those of ligand **1(*n*)**.

2.3.1.2 Recent methodology.

More recently, a different approach has been applied, trying to improve the overall yield (tested for ligand **1(12)**), for the production of complexes **4(*n*)** or other derivatives, trying to avoid the sparingly soluble di-*μ*-chloro dimer, **16**. Thus, instead of using potassium tetrachloroplatinate(II) as the starting material, the ligand was reacted directly with *cis-*

[PtCl$_2$(DMSO)$_2$].[29] This approach removes the step of the formation of dimer **16(*n*)** that is the weakest step in the described methodology, obtaining directly complex **14(*n*)**. This method gave unexpected and very interesting results. Thus, the formation of octahedral-liquid-crystalline di-platinum(III) complexes **18(*n*)** was observed, and, applying slightly different conditions, the formation of dimethylsulfide complexes **15(*n*)** was found too. The reactions are shown in the Scheme 7[30] and Scheme 8.

2.3.1.3 Formation of Complex **18(*n*)**

The first step was the reaction of potassium tetrachloroplatinate(II) to give *cis*-dichlorobis(dimethylsulfoxide)platinum(II), carried out in water at room temperature for 12 h using three equivalents of dimethylsulfoxide. The reaction yielded a creamy white precipitate ready to be used in the next step without further purification. After the formation of [PtCl$_2$(DMSO)$_2$] the logic consequence was to use it in the same conditions applied for the formation of complex **14(*n*)**. Therefore, one equivalent of ligand **1(12)** was added to one equivalent of [PtCl$_2$(DMSO)$_2$] in acetic acid with a small quantity of water and heated under reflux overnight. A deep-red, crystalline material was formed during the reaction (yield 45%) (Scheme 7). The ^{1}H-NMR spectrum showed clear evidence of a new product (see figure 32). The reaction was also carried out with **1(2)** and fortunately good crystals for single crystal X-ray analysis were obtained.[30]
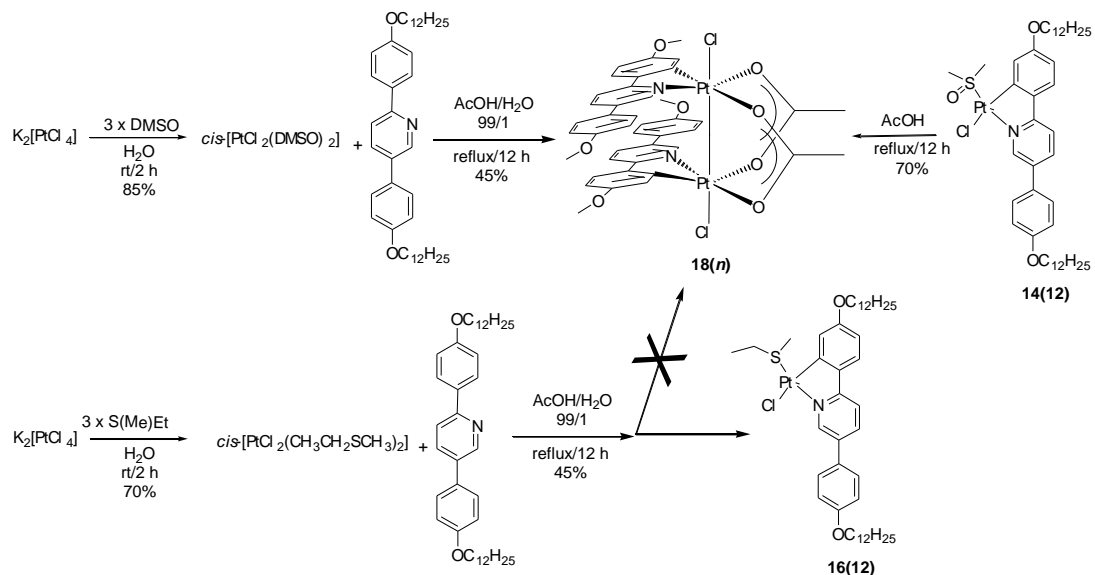
Scheme 7-II Reaction for the formation of complex **18**. Different conditions have been applied and they are discussed in the text.

In Figure 31 are shown different perspective of the complex obtained using the ligand with ethoxy chains, from which it can been seen that two ligands lie on the same side of the dimer, but the two five-membered cyclometallated rings are antiparallel. The Pt–Pt single bond is at distance of 2.5730(11) Å that is comparable to those in other Pt^{III}-Pt^{III} systems.[31] The two Pt centres are connected to each other by two μ^2-acetato ligands. The structure is unsymmetric in that there are two $d_{Pt–Cl}$ at 2.4648(11) and 2.4421(11) Å and the two planes passing through the square planes of the octahedral structure are not parallel, rather making an angle of about 16.71°. Moreover the two planes defined by the two cyclometallated five member rings (Pt-ligand) are not parallel, making an angle of 17.03°.

Dimeric Pt^{III} complexes are reasonably well-known in the literature and normally consist of a metal-metal bonded arrangement supported by four bridging ligands, for example OAc$^-$, SO$_4^{2-}$, pyrophosphites, and formamidinates.[32] Recently Sanford *et al.* reported a cationic metal-metal organoplatinum(III) dimer with two benzo[*h*]quinoline unit, two acetylacetonate

units and an acetate bridging the two metals,[31] with d_{Pt-Pt} at 2.5647(2). Also they reported a metal-metal platinum(III) dimer with four 2-phenylpyridine units, two for each platinum(III), and one chloride per Pt[III] without any bridging ligand.[33] Unfortunately, for this complex no X-ray analysis was given. These complexes, even if very interesting, are too different from the system herein showed and therefore, no comparison is made.
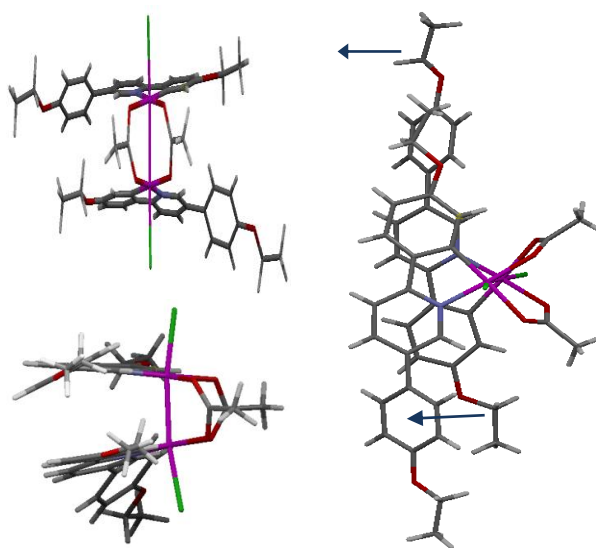
Figure 31-II Single crystal structure of **18(2)**. Chlorine in green, oxygen in red, nitrogen in blue, platinum in violet, carbon in black and hydrogen in grey.

In the ^{1}H-NMR spectrum of Pt[III] dimer with longer chains **18(12)**, shown in Figure 32, it is very interesting to see that the set of signals in the aromatic part, reflect the high symmetry of the molecule. Moreover in the X-ray structures showed in Figure 31, the two different –OCH$_2$ and CH$_3$ groups of each ligand have different environment, indeed one chain is under the centre of the unbound ring and the other is just facing empty space. They are highlighted by the arrow in the picture. This structural difference is present also in solution and from the NMR spectra is clearly evident, indeed four protons of the –OCH$_2$- of the unbounded rings

have the typical position at 3.9 ppm and they appear as a triplet, the other four hydrogens from $-OCH_2-$ of the bond phenyl rings, namely those that are facing the rings, present a different position in the ^{1}H-NMR spectra, with a multiplet at 3.3 ppm. This is due to the fact that the protons are pointing in the middle of the opposite pyridine rings, as is clearly evident in Figure 31, highlighted with the arrows. Therefore the ring current shields the protons which are present at higher field comparing with the normal $-OCH_2-$ groups. No difference is seen for the $-CH_3$ group because the NMR spectrum concerns a C12 derivatives therefore the $-CH_3$ groups are too far to be influenced by the rings. A similar effect should be present for the second $-CH_2-$ groups in the chains ($-OCH_2-CH_2-$) but the shift is covered by the large aliphatic signals.
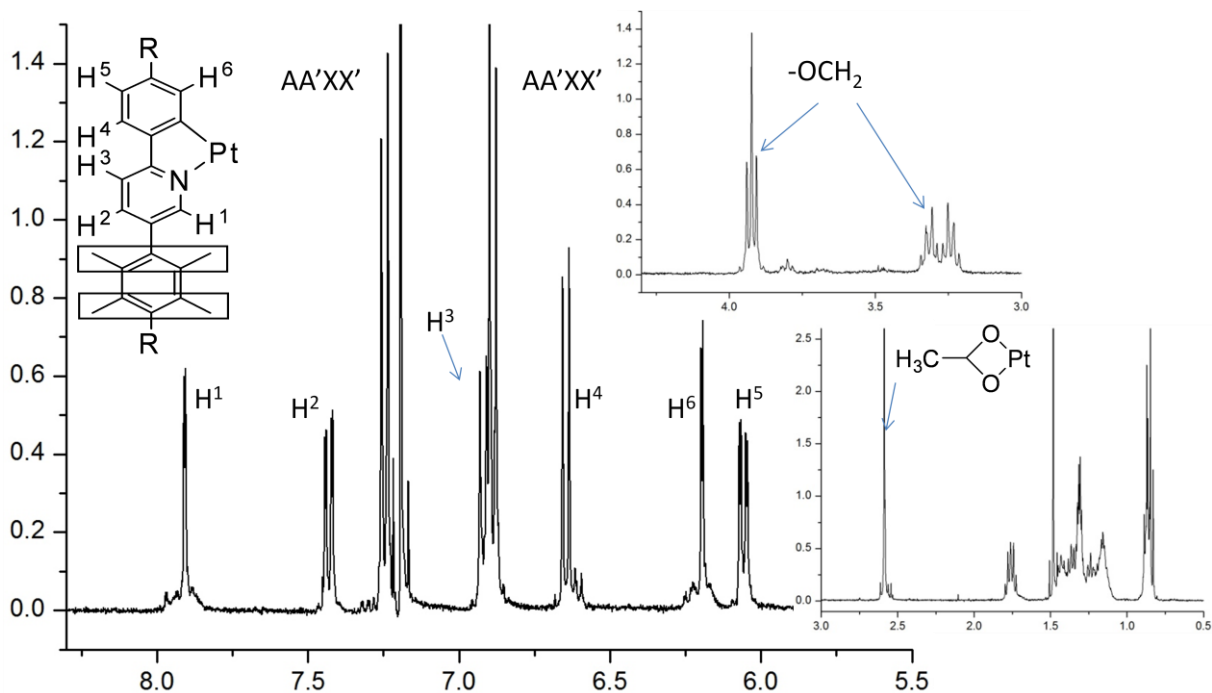
Figure 32-II ^{1}H-NMR of complexes **18(n)**, region from 5.5 ppm to 8.5 where is shown the position of the aromatic signals. In detail there are the $-OCH_2$ signals and the signals from the methyl groups of the acetate. R = $OC_{12}H_{25}$

This compound is of particular interest because there are relatively few examples of neutral, dimeric platinum(III) complexes, and all of them are obtained from Pt(II) using an external oxidant.[32] For example in Sanford *et al.* work[31] the oxidant was PhI(OAc)$_2$, and in general I^{III} reagents (PhICl2 or [R-I-R′]+) are common.[34]

However, several experiments were carried out to investigate the nature of the oxidant and the mechanism that plays a role in this reaction; some of them are reported in Scheme 7.[35]

The first attempts were focused on the identification of the oxidant, and so the reaction was carried out with rigorous exclusion of atmospheric oxygen. In these conditions the reaction still gave the complex **18**. Then the attention was turned to the coordinated DMSO. Thus, the reaction was repeated using *cis*-[PtCl$_2$(S(Me)Et)$_2$] as starting material and complex **16(n)** was formed without any trace of **18(n)**. Further evidence was obtained running the reaction under the same conditions using the DMSO complex **14(n)** as starting material; the reaction led smoothly to complex **18(n)** without further purification. Moreover, the oxidation of platinum(II) in this way is consistent with the published work where the oxidation of Pt^{II} to Pt^{IV} is reported using DMSO in acid conditions.[36]

2.3.1.4 Formation of Complex 15(n)

Changing the conditions slightly and using ethoxyethanol as solvent, a different complex was obtained (Scheme 8). A first suggestion was that the complex was the other geometric isomer of **14(n)**, in which the DMSO would be found *trans* to the metallated carbon. This identification (complex **15(12)**) was, however, complicated in the absence of X-ray information. Although this hypothesis turned out to be misleading, it was not necessarily inconsistent with the changes in the chemical shift (Figure 33) of the hydrogen *ortho* to the

pyridine nitrogen (δ 9.5 to 9.8) and of the hydrogen *ortho* to the metallated carbon (δ 7.9 to 7.1).
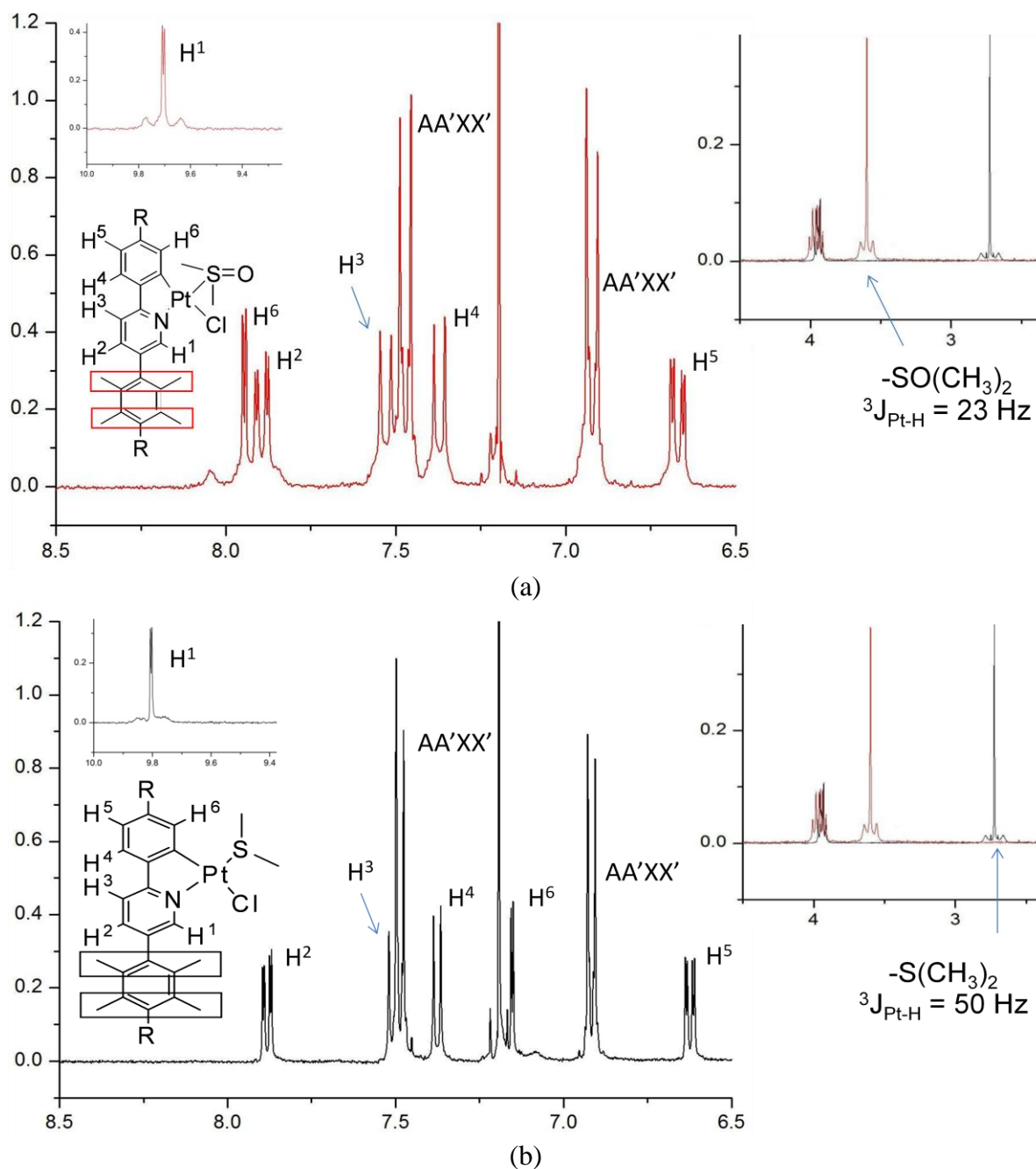
Figure 33-II ^{1}H-NMR of complexes **14** in red (a) and **15** in black (b), region from 6.5 ppm to 8.5 where is shown the different position of the aromatic signals, especially H[6]. In detail in every pictures there are the H[1] signals and the signals from the methyl groups of the bounded DMSO and DMS.

Further, the resonance of the DMSO hydrogens changes from δ 3.6 to δ 2.6. All these shifts suggested different rearrangement of the auxiliary ligands. Indeed, the DMSO *trans* to the C should shield the H^6 proton more, if compared with the Cl, and the change on the proton H^1 should be less evident because N is already a strong deshielding element and therefore the presence of Cl instead of DMSO does not give a bigger contribution. Also the upfield shift of the methyl groups of the DMSO was consistent with a *cis* conformation.

However, one datum that did not appear consistent was the coupling constant ($^3J_{\text{H-Pt}}$) of the methyl group of the sulfoxide ligand, which increased from 23 Hz in complex **14(10)** to 50.4 Hz in complex **15(12)**.

Another inconsistency came from a nOe experiment (Nuclear Overhauser Enhancement), undertaken trying to determine the structure of complex **15(12)**. Irradiation of S-Me at δ 2.72 caused a slight increase in intensity of the peak at δ 9.80, which corresponds to the proton vicinal to the nitrogen, and a much bigger increase in intensity for the peak at δ 7.50, which corresponds to the proton vicinal to the metallated carbon. Similarly, when the signal at δ 9.80 was irradiated, there was very little increase in the intensity of the S-Me peak, but a large increase in the AA′XX′ peak at δ 7.50, which corresponds to the two proton on the unbound phenyl group. When the signal at δ 7.20 was irradiated, this increased the intensity of the S-Me peak and the OCH_2 peak at δ 4.00 significantly. This suggests that the CH_3 groups of S-ligand are in fact close in space to the proton vicinal to the carbon bounded to Pt^{II}, which is indicative that **15(12)** has S-Me *trans* to nitrogen.[37]

Being then confident of the *trans* conformation, consideration was given to the possibility of DMSO bound through oxygen rather than sulfur. However Crosby *et al.*[38] have described the oxidation of cyclometallated Pt^{II} complexes of 2-(4-fluorophenyl)pyridines, with *S*-bound

DMSO ligands to give Pt^{IV} complexes that retain the *S*-bound DMSO ligands. They also reported an isomerisation reaction that results in a rearrangement of the ligands to give *O*-bound DMSO complexes. They reported a value of $^3J_{H-Pt}$ for Me-S(=O) in cyclometallated Pt^{II} complex of 23 Hz, while the value of $^3J_{H-Pt}$ for Me-S(=O) in Pt^{IV} complexes with *S*-bonded DMSO was 14.3 Hz. However, there was no evidence of coupling between Me-S(=O) and ^{195}Pt in the complex that was *O*-bonded. Therefore, now it is possible to exclude, with more confidence, the possibility of an *O*-bonded DMSO ligand because of the magnitude of the coupling constant for **15(12)**.
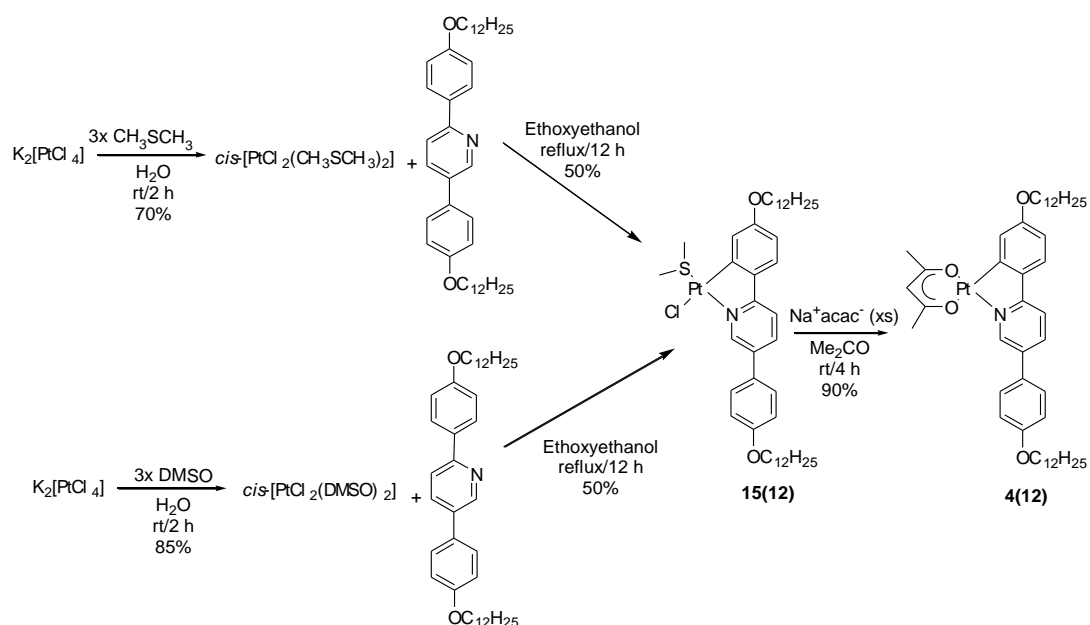
Scheme 8-II Different reaction for the formation of complex **15(12)**

An additional test suggested that complex **15(12)** was not a Pt^{IV} complex, as its reaction with sodium acetyl acetonate lead to complex **4(12)**. Two pieces of information thus, led to the identification of **15(12)**. Indeed, in determining the identity of the oxidant responsible for the

transformation of Pt^{II} to Pt^{III} in the formation of **18**, it had been shown[35] that reaction of *cis-*[PtCl$_2$(DMS)$_2$] with **1(12)**, Scheme 9, did not lead to **18**, rather forming a complex with NMR parameter identical to **15(12)**. Further, data where subsequently obtained for a DMS complex of Pt^{II} that showed chemical shift of $\sim \delta$ 2.5 and platinum-hydrogen coupling in excess of 50 Hz[39]

Therefore, **15(12)** is identified as Pt^{II} complex of DMS. Clearly, as sulfur is reduced from S^{IV} to S^{II}, there is a concomitant oxidation, but the identity of the oxidised species remains as yet unidentified.

2.3.1.5 Isomerisation

In considering complexes of the unsymmetric β-diketone, trifluoromethyl acetylacetone (tfacH), due account must be taken of the ability of the final complexes to exist as isomers, as shown in Figure 34.[40] Thus, it is possible that the –CF$_3$ group could lie *cis-* or *trans-* to the nitrogen on the pyridine ring.

6(n)
trans-like

6(n)
cis-like
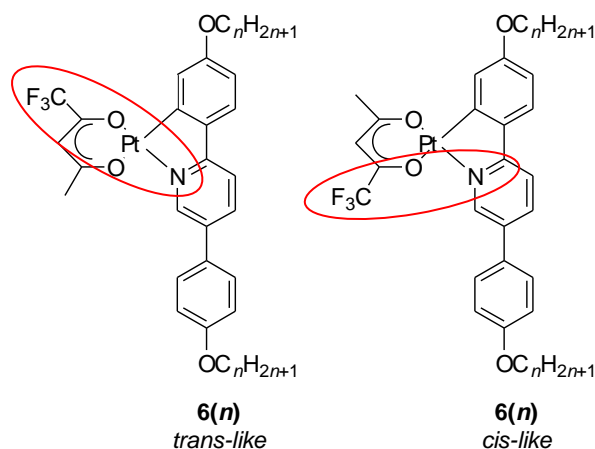
Figure 34-II Two isomers of complexes **6(n)**, these two compounds show a clearly different ^{1}H-NMR signal from the proton *ortho* to the nitrogen and the single proton on the β-diketonate.

Even if these two compounds showed a clearly different ^{1}H-NMR signal from the proton *ortho* to the ligand nitrogen and the methine proton of the β-diketonate, it was not possible to give a definitive assignment as to which peak corresponded to which isomer.

In order to try to isolate the two isomers, further studies were performed. Thus, in the first experiment, the reaction was carried out changing the temperature and the polarity of the solvent to understand if it was possible to have a control on the ratio formation. The results are reported in Table 3. It was found that the ratio appeared to be sensitive to the temperature at which the reaction was carried out, so that increasing the temperature to 40 °C the formation of what was the minor isomer increased to give a 1 : 1 ratio. However, running the reaction at 0 °C gave a 5 : 1 ratio. This shows that temperature affects the orientation of the β-diketonate on binding the platinum. Increasing the polarity of the reaction solvent to chloroform, at room temperature also appeared to increase the difference in isomeric ratio. Using acetone as a more polar solvent did not give any interesting results due to the insolubility of the *trans*-**14(*n*)**. Unfortunately none of the preparation methodologies used gave an isomerically pure complex, but for the shortest chain used, **6(6)**, fractional crystallisation method gave a 36 : 1 isomeric ratio. However with longer chains this method did not help to improve the purity of the isomer.

Table 3-II The effect of reaction conditions on the isomeric ratio

Solvent	Temperature (°C)	Ratio of Isomer (A:B)
CH_2Cl_2	0	5:1
CH_2Cl_2	r.t.	3:1
CH_2Cl_2	40	1:1
$CHCl_3$	r.t.	6:1
CH_3COCH_3	r.t.	No reaction

In order to check if an isomerisation takes place on the final complexes **6(*n*)**, some reactions were carried out, heating the solid samples at different temperatures and at reflux in

different solvents. The results are collect in Table 4. The mixture of isomers **6(8)** at 3 : 1 ratio were heated under reflux for 1 h in different solvents and the resulted ratio was determined by integration of the ^{1}H-NMR spectrum. No isomerisation occured, meaning that once the complexes are formed they are stable in solution. However while the isomeric ratio is stable in solution, the ratio does change on heating the solid. Thus, complex **6(8)** was heated between two cover slips on the hot stage of a polarised optical microscopy, under N_2. The sample was stable until reaching its melting points (135 °C and 147 °C; paragraph *3.2.2*) above which temperature the ratio changed progressively to 1 : 1. This shows that the trifluorinated β-diketonate ligand is a dynamic system and has the ability to disconnect from the platinum, rotate and then recombine forming the other isomer. At the best of our knowledge, this effect was not seen in any other complex reported in literature.

Table 4-II Thermal and in solution isomerisation of **10(8)** treated in both case for 1 h, melting point 147 °C

Solvent	Temperature (°C)	Ratio of Isomers by NMR (A:B)
CH_2Cl_2	40	3:1
$CHCl_3$	61	3:1
CH_3CN	82	3:1
no	25	3:1
no	100	3:1
no	140	3:1
no	160	1:1

Having obtained an almost isomerically pure complex, **6(6)**, an nOe experiment was undertaken to assign the correlation between structure and properties. When the methyl proton on the β-diketonate was irradiated, Figure 35, the irradiation did not increase significantly the signal coming from H[1] (8.89 ppm) but neither the signal coming from H[2] (6.94 ppm). This could be attributed to too great distance between the methyl group and the hydrogens (Figure

35). Similarly, irradiation of H^1 and H^2 did not lead to any significant enhancements in the intensity of the signals.
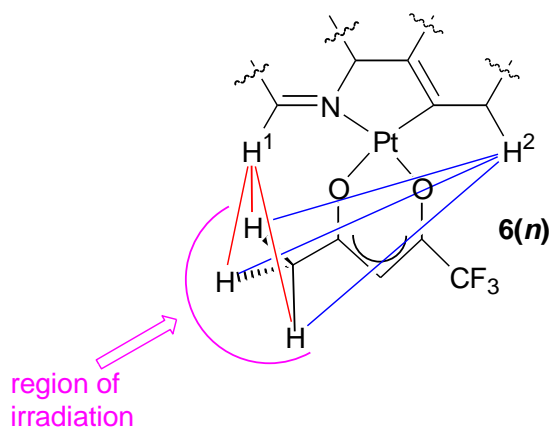
Figure 35-II One of the two possible isomers of **6(6)**. The red line represents the short interaction (between 3.575 and 4.872 Å) and the blue line represents the long interaction (between 7.366 and 7.445 Å). These data are obtained from the crystal structure of **4(6)**.

Despite the impossibility to assign the structure, it is possible to postulate which isomer is formed by considering the dipole moment of the two isomers. As nitrogen and fluorine have the highest dipole moments therefore when these groups are both on the same side, as in the *cis-like* isomer, the polarity of the molecule should be higher. If the *cis-like* isomer is the most polar then it is more likely to remain in solution with acetone a therefore the isomer that crystallise for first should be the *trans-like* isomer.

2.3.2 Liquid Crystal Properties of the Platinum(II) Complexes

The mesomorphic properties of the platinum complexes were investigated using polarised optical microscopy, and a full description is given in the following paragraph. Thermal data are collected in Table 5 for the acetylacetonato complexes **4(n)**, **8(n)** and **12(12)**, in Table 7 for the modified β-diketonato complexes **5(n)**, **6(n)**, **7(n)**, **9(12)**, **10(12)** and **11(12)**.and in Table 8 for the chloro(DMSO) Pt^{II} complexes and chloro(DMS) Pt^{II} complexes **13(n)** and **14(n)**. The transition temperatures reported between bracket are sign of the presence of a monotropic phases, where the liquid crystal behaviour is visible only on cooling the samples from isotropic phase.

2.3.2.1 Acetylacetonato Complexes, **4(n)**, **8 (n)** and **12(12)**

Through the comparison between complexes **4(n)** and the related ligands **1(n)**, it is possible to note different aspects of the liquid crystal behaviour. The first thing that is clearly visible is the drastic decrease in the number of phases.

Table 5-II Thermal behaviour of the platinum complexes **4(n)**, **8(n)** and **12(n)**. *n* = length of the alkoxy chains.

Compound	*n*	Transition	*T* (^{o}C)	Compound	*n*	Transition	*T* (^{o}C)
4(6)	6	Cr-SmA	200	**8(6)**	6	Cr-I	161
		SmA-I	258			(N-I)	(101)
4(8)	8	Cr-SmA	190	**8(8)**	8	Cr-I	141
		SmA-I^{dec}	250			(SmA-N)	(110)
4(10)	10	Cr-SmA	168			(N-I)	(115)
		SmA-I	244	**8(10)**	10	Cr-I	123
4(12)	12	Cr-SmA	170			(SmA-I)	(115)
		SmA-I	231	**8(12)**	12	Cr-I	121
12(12)	12	mp	135			(SmA-I)	(119)

Indeed all complexes **4(*n*)** show only a SmA phase while their ligands showed many smectic phases including SmA, SmC, SmF and SmI as well as crystal G and J phases. The SmA phase was identified through its typical focal-conical fan texture. This reduction in smectic polymorphism is consistent with much of the literature, in particular as there are no examples of tilted hexagonal phases in metallomesogens. Another interesting point is the general increase in transition temperatures in complexes **4(*n*)** in comparison with those of the ligands **1(*n*)**. One could expect that the presence of lateral Pt-(β-diketonate) moiety would decrease the anisotropy of the molecules, reduce their ability to pack and thus decrease the melting point. Instead, the melting points generally increase on average by 55 °C while the clearing points increase by about 30 °C, an effect ascribed to the larger molecular weight of the metal complexes. A general trend of decreasing transition temperature with the increase of the chain length was also observed. Note that for complex **4(8)**, it is difficult to determine the precise temperature of the SmA-I transition because decomposition started close to the clearing point.

Complexes **8(*n*)** show a completely different behaviour compared with their ligands, since as all ligands **2(*n*)**, with the exception of **2(12)**, show only a nematic phase, while the complexes (except **8(6)** which is nematic) show a smectic A phase. Also for these complexes, there is a large increase in melting point compared to the ligands, especially for **8(6)** and **8(8)** where the increase is 80 °C and about 56 °C respectively; for the other two complexes the increase is about 25 °C. However, the melting points of complexes **8(*n*)** are consistently lower than those of **4(*n*)**, due to the presence of the lateral substituent that suppresses intermolecular interactions. Regarding the temperatures of the clearing points in these complexes, they have similar values, indeed the increment is in each case only about 10 °C, so that stabilisation of

the crystal state is the reason for the observed monotropic behaviour. As for complexes **4(*n*)**, here the temperatures of the melting points again drop with chain length; but the temperatures of the clearing points in this case increase with the length of the chain, with a consequent stabilisation of the liquid crystal properties.
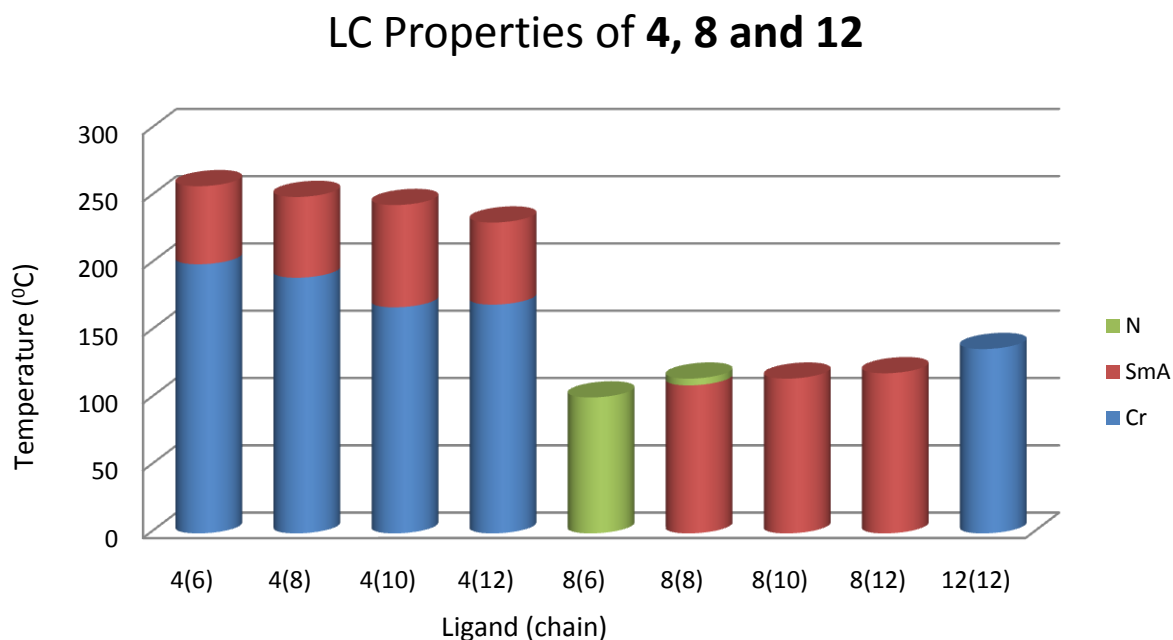
Figure 36-II Thermal behaviour of complexes **4(*n*)**, **8(*n*)** and **12(12)**. Complex **4(8)** decompose with the isotropic phase. The mp of complexes **8(*n*)** are reported in Table 5.
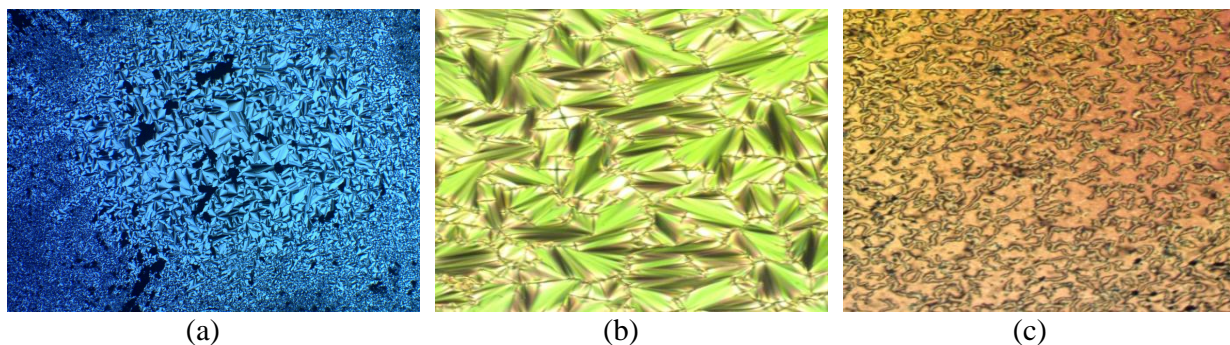
Figure 37-II Optical micrographs pictures (on cooling) of the (a) SmA phase at 113 °C of **4(6)**, (b) the SmA phase at 193 °C of **5(10)** and N phase at 144 °C of **6(6)** in 1 to 1 ratio.

Comparing system **4(*n*)** with **VIII(*n*)** (Figure 38, data collected in Table 6),[15b] it is possible to see that the general behaviour is very similar (Figure 39), with the exception of **VIII(10)** that is, inexplicably out of the general trend and on the reported publication[15b] no explanation was given. Complex **12(12)** does not show any liquid crystal phase, the reason is connected with the presence of the third chain that destroys lateral packing in the liquid crystal organisation.

Table 6-II Thermal behaviour of the Pt(II) complexes **VIII(*n*)** showed in Figure 7
and repeated here in Figure 38, obtained by POM

Compound	*n*	Transition	$T(^{o}C)$
VIII(6)	6	Cr-SmA	196
		SmA-I^{dec}	280
VIII(8)	8	Cr-SmA	162
		SmA-I^{dec}	264
VIII(10)	10	Cr-SmA	184
		SmA-I^{dec}	281
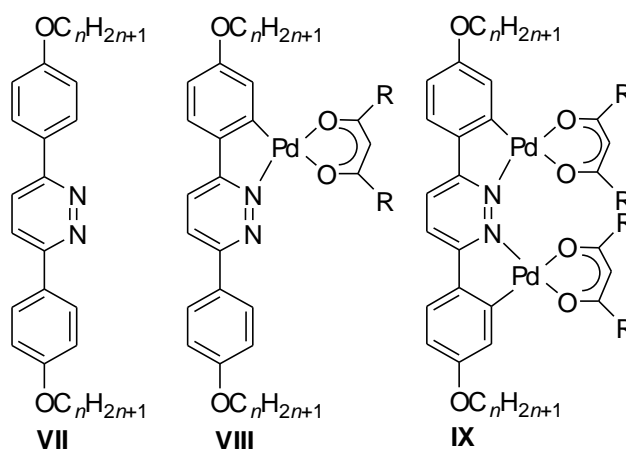
Figure 38-II Pyridazines ligands and their palladium β-diketonate complexes, *n* = 4,5,6,7,8 and 10
R = -CH$_3$ or -CH$_2$(CH$_2$)$_2$CH$_3$

LC Properties of 4 and VIII
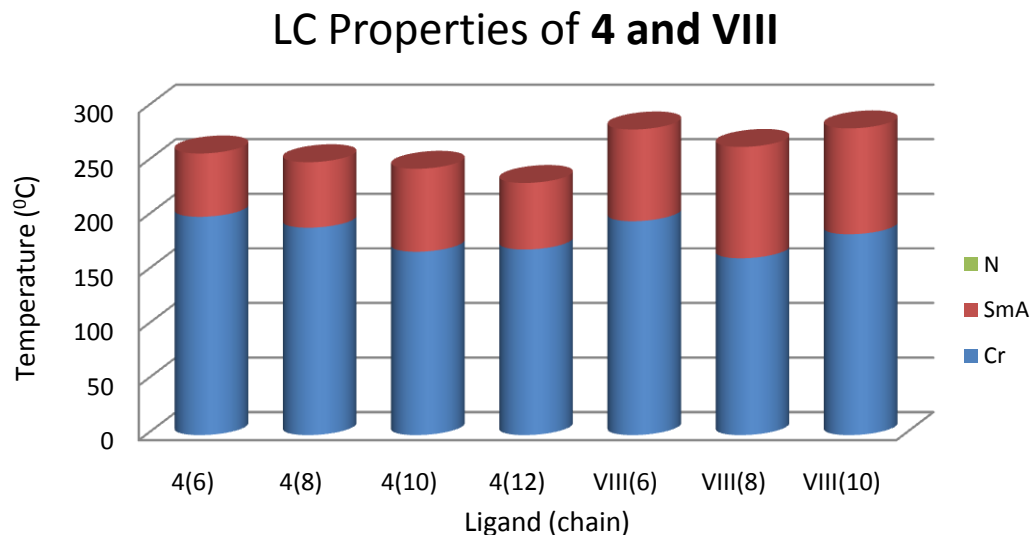
Figure 39-II Thermal behaviour of complexes **4(*n*)** on the left and **VIII(*n*)** on the right. Complex **4(8)** decompose with the isotropic phase, as well all the complexes **VIII**.

2.3.2.2 Modified β-diketonate Complexes, **5(*n*)**, **6(*n*)**, *and* **7(12)**; **9(12)**, **10(12)** *and* **11(12)**.

Table 7 shows the thermal properties of the complexes with different β-diketonate ligand. Complexes **7(12)** and **11(12)**, bearing the hexafluorinated acetyl acetonate, do not displays any liquid-crystalline phases and melt directly to the isotropic liquid at 151 ºC and 126 ºC respectevely. This is attributed to destabilisation caused by the introduction of six fluorine atoms, each 0.30 Å larger in radius than hydrogen.

Complexes **5(*n*)** all maintain a SmA phase, however the introduction of a two further CH_2 groups onto the β-diketonate lowered the transition temperatures. The melting and clearing points of these complexes relative to their related **4(*n*)** complexes are much lower as a reduction of the stabilisation. As the length of alkyl chain is increased, the melting point decreases as does the clearing point, exhibiting a very clear trend similar to that of the **4(*n*)** complexes.

Table 7-II Thermal behaviour of modified β-diketonate. Complexes **5(n)**, **6(n)**, **7(n)**, **9(12)**, **10(12)** and **11(12)**, obtained by POM

Complex	n	Transition	T (°C)	Complex	n	Transition	T (°C)
5(6)	6	Cr- SmA	169	**6(10)**	10	Cr-SmA	133
		SmA -I	228			SmA-SmA+I	144
5(8)	8	Cr- SmA	148			SmA+I-I	158
		SmA -I	225	**6(12)**	12	Cr-Cr+SmA	90
5(10)	10	Cr- SmA	116			Cr+SmA-SmA	114
		SmA -I	217			SmA-SmA+I	128
5(12)	12	Cr- SmA	100			SmA+I-I	164
		SmA -I	205	**7(12)**	12	Cr-I	151
6(6)	6	Cr-Cr+N	134	**9(12)**	12	Cr-I	108
		Cr+N-N	143			(SmA-I)	(87)
		N-N+I	145	**10(12)**	12	Cr-Cr+I	105
		N+I-I	150			Cr+I-I	115
6(8)	8	Cr-Cr+SmA	135	**11(12)**	12	Cr-I	126
		Cr+SmA-SmA	147				
		SmA-SmA+I	149				
		SmA+I-I	158				

Complexes **6(n)** present a more complicated picture as they contain a mixture of isomers. In order to ensure that the ratio of isomers did not change under heating on the microscope they were first isomerised to the 1:1 mixture. On examination it appears that the two isomers have different melting and clearing points and that they do not act as a eutectic mixture. For example, for complex **6(12)**, one isomer melts at 90 ºC forming a SmA phase while the other remains crystalline. Then at 114 ºC, the isomer which was still crystalline melted to form what appeared to be SmA phase. On further heating to 128 ºC, the first isomer cleared to leave the SmA phase of the first isomer dispersed within an isotropic fluid, then, finally at 164 ºC the second isomer cleared to give an isotropic fluid. All **6(n)** complexes exhibit only the SmA phase with the exception of **6(6)**, which, presumably due to its reduced anisotropy of the combination of a large lateral group and a short chain, gave a nematic phase (Figure 36). Overall these complexes show a general decrease in melting point and clearing point as chain

length increases, however this trend is not as well defined as with complexes **5(*n*)**, which could be attributed to the fact that these are a mixture of isomers. Unfortunately an analysis of the liquid crystal properties of the single isomer is not possible as the compound will isomerise to 1 to 1 ratio at the melting point temperature.

As shown also in Tables 1 and 5, the liquid crystal phases of the ligands and complexes are strongly destabilised by the introduction of the cyclopentene ring, which reduces anisotropy and interrupts intermolecular interactions; the liquid crystal data for platinum complexes bearing the ligand **2(12)** are collected on the right side of Table 7. The simultaneous presence of fluoro-substituted β-diketonate on platinum and cyclopentene on the ligand completely suppress the liquid crystal behaviour. Complex **11(12)**, with the presence of two, large, lateral components, further destabilises the complexes. Apart from the lost in liquid crystal properties it shows also a lower melting point (126 ºC) compared with its homologue without cyclopentane **7(12)**. Complex **10(12)**, with the unsymmetric trifluorinated β-diketonato, again like its analogous complex **6(12)**, displays two different melting points. The additional three fluorine groups in this case are also sufficient to inhibit the formation of liquid phases. Complex **9(12)** exhibits a monotropic SmA phase, however it is the only complex with a fused cyclopentene ligand, apart from **8(*n*)**, to display a liquid crystal phase, despite being similar in size to the other β-diketone ligands. This behaviour can again be attributed to the flexibility of the chain, causing it to disrupt intermolecular interactions to a lesser extent. Due to the larger destabilisation associated with these fused cyclopentene ligands it was decided not to synthesis ligands with a shorter chain and therefore reduced anisotropy, as this should further decrease the liquid-crystalline properties.

2.3.2.3 Chloro(DMSO) Pt Complexes 13(n) and 14(n).

As far as the DMSO complexes were concerned, only two homologues were prepared (n = 6 and 10) to gain an overview of the thermal behaviour.

Table 8-II Thermal behaviour of the platinum complexes **13(n)** and **14(n)**

Compound	n	Transition	T (^{o}C)
14(6)	6	Cr-SmA	200
		SmA-I	258
14(10)	10	Cr-SmA	190
		SmA-Dec	250
13(6)	6	mp	210
13(10)	10	Cr-I	141
		(SmA-N)	110

Table 8 shows that the behaviour of the DMSO complexes is very similar to that of complexes **4(n)** and to some extent **8(n)** (Table 5), revealing that in this case the co-ligands has relatively little influence on the mesomorphism. In fact, the only difference is in the phase transition temperatures which are lower than in the **4(n)** complexes, probably due to the more flexible behaviour, and slightly greater steric demands of DMSO. The exception is rapresented by complex **13(6)** where the reduced anisotropy due to the presence of shorter chains and the presence of a bigger substituent on platinum completely destabilise the liquid crystal properties.

2.4 Conclusion

This part of the thesis represents the central point, from where different topics were developed. The aim was to study a class of cyclometalated platinum(II) complexes that combine liquid crystal properties and luminescent properties. The interest in these structures is widely justified either from the liquid crystals point of view with the use of a *rod-like* ligands and a square planar metal complex, and from the luminescent point of view with the use of an elongated structure of 2-phenylpyridine type with a third row transition metal that give the possibility to achieve phospholuminescent emission.

In the ligand synthesis a Diels-Alder methodology was used to prepare two series of 2,5-diphenylpyridine-type ligands. Some of these exhibited a rich polymorphism, with different liquid crystal behaviour from the simplest nematic phase, to the less common SmF and SmI. Complexation to Pt^{II}, using a new synthetic methodology developed in this project,[28] let to square-planar materials with orthometallated ligands and acetylacetonate ligand. These were also liquid crystalline, but with a more limited mesomorphism. Furthermore, complexes of ligands bearing a fused cyclopentene showed a even more limited mesomorphism and generally reduced mesophase stability.

These complexes contain the [Pt(2-phenylpyridine)(acac)] emission chromosphere and, as mentioned above are liquid crystal in nature, providing thus, examples of multifunctional materials, whose photochemical properties will be described in Chapter 4.

References

1   (a) E. Holder, B. M. Langeveld and U. S. Schubert, *Adv. Mater.*, 2005, **17**, 1109; (b) H. Yersin, *Highly Efficient OLEDs with Phosphorescent Materials*, Wiley-VCH, Weinheim, Germany 2008.

2   J. A. G. Williams, *Top. Curr. Chem.* 2007, **281**, 205.

3   See: S. Takehara, M. Osawa, K. Nakamura, T. Shoji, H. Ogawa, N. Fujisawa and T. Kuriyama, Jpn Kokai Tokkyo Koho (1990), 43 pp. CODEN: JKXXAF JP 02292389 A 19901203 Heisei. Application: JP 89-109127 19890501. Priority:. CAN 115:123932 AN 1991:523932 CAPLUS. Y. Totani, T. Ochi, T. Muraishi, H. Hidetaka, M. Nakatsuka, Jpn Kokai Tokkyo Koho (2003), 28 pp. CODEN: JKXXAF JP 2003064366 A 20030305 Application: JP 2001-255590 20010827. Priority:. CAN 138:229336 AN 2003:167086 CAPLUS. H. Schlosser R. Wingen, J. Manero, Application number: DE19924236103 19921026 Priority number(s): DE19924236103 19921026.

4   (a) M. P. Aldred, M. Carrasco-Orozco, A. E. A. Contoret, D. Dong, S. R. Ferrar, S. M. Kelly, S. P. Kitney, D. Mathieson, M. O'Neill, W. C. Tsoi and P. Vlachos, *Liq. Cryst.*, 2006, **33**, 459; (b) M. P. Aldred, P. Vlachos, D. Dong, S. P. Kitney, W. C. Tsoi, M. O'Neill and S. M. Kelly, *Liq. Cryst.*, 2005, **32**, 951; (c) M. P. Aldred, A. J. Eastwod, S. P. Kitney, G. J. Richards, P. Vlachos, S. M. Kelly and M. O'Neill, *Liq. Cryst.*, 2005, **32**, 1251.

5   (a) V. N. Kozhevnikov, S. J. Cowling, P. B. Karadakov and D. W. Bruce, *J. Mater. Chem.*, 2008, **18**, 1703; (b) M. Xu, W. Li, Z. An, Q. Zhou and G. Wang, *Appl. Organometal. Chem.*, 2005, 19, 1225.

6   (a) N. Miyaure and A. Suzuki, *Chem. Rev.*, 1995, **95**, 2457; (b) T. Tagata and M. Nishida, *J. Org. Chem.*, 2003, **47**, 9412.

7   T. V. Saraswathi and V. R. Srinivasan, *Tetrahedron Lett.*, 1971, **12**, 2315.

8   Many application of organometallic complex of group 10 metals may be found as:

Compounds of Group 10, Ed. A. Canty in *Comprehensive Organometallic Chemistry III*, Ed R. H. Crabtree and D. M. P. Mingos, Elsevier, Oxford, 2007, vol 8.

9   J. Brooks, Y. Babayan, S. Lamansky, P.I. Djurovich, I. Tsyba, R. Bau and M.E. Thompson, *Inorg. Chem.*, 2002, **41**, 3055.

10   D W Bruce, R Deschenaux, B Donnio and D Guillon. in *Comprehensive Organometallic Chemistry III,* ed. R H Crabtree and D M P Mingos, Elsevier, Oxford, UK, 2006, Vol. 12. Chapter 12.05, pp 195.

11   M. Ghedini and D. Pucci, *J. Organomet. Chem.*, 1990, **395**, 105

12   (a) C. Damm, G. Israel, T. Hegmann and C. Tschierske, *J. Mater. Chem.*, 2006, **16**, 1808; (b) B. Bilgin-Eran, C. Tschierske, S. Diele and U. Baumeister, *J. Mater. Chem.,* 2006, **16**, 1145; (c) T. Hegmann, J. Kain, S. Diele, B. Schubert, H. Bögel and C. Tschierske, *J. Mater. Chem.,* 2003, **13**, 991; (d) T. Hegmann, J. Kain, S. Diele, G. Pelzl and C. Tschierske, *Angew. Chem. Int. Ed.,* 2001, **40**, 887; (d) K. Venkatesan, P. H. J. Kouwer, S. Yagi, P. Müller and T. M. Swager, *J. Mater. Chem.*, 2008, **18**, 400.

13   S. W. Thomas, S. Yagi and T. M. Swager, *J. Mater. Chem.*, 2005, **15**, 2829.

14   S. Lamansky, P. Djurovich, D. Murphy, F. Abdel-Razzaq, H. E. Lee, C. Adachi, P. E. Burrows, S. R. Forrest and M. E. Thompson, *J. Am. Chem. Soc.*, 2001, **123**, 4304.

15   (a) J. W. Slater and J. P. Rourke, *J. Organomet. Chem.*, 2003, **688**, 112; (b) J. W. Slater, D. P. Lydon and J. P. Rourke, *J. Organomet. Chem.,* 2002, **645**, 246; (c) J. W. Slater, D. P. Lydon, N. W. Alcock and J. P. Rourke, *Organometallics*, 2001, **20**, 4418.

16   V. N. Kozhevnikov, B. Donnio and D. W. Bruce, *Angew. Chem. Inter. Ed.*, 2008, **47**, 6286.

17   R. A. Carboni and R. V. Lindsey, *J. Am. Chem. Soc.*, 1959, **81**, 4342.

18   H. Neunhoeffer and P. F. Wiley, *Chem. Heterocycl. Compd.*, 1978, **33**, 18.

19   (a) D. L. Boger and J. S. Panek, *J. Org. Chem.,* 1981, **46**, 2179; (b) D. L. Boger, J. S. Panek and M. M. Meier, *J. Org. Chem.,* 1982, **47**, 895.

20   (a) V. N. Kozhevnikov, D. N. Kozhevnikov, O. V. Shabunina, V. L. Rusinov and O. N. Chupakhin, *Tetrahedron. Lett.*, 2005, **46**, 1521; (b) V. N. Kozhevnikov, D. N. Kozhevnikov, O. V. Shabunina, V. L. Rusinov and O. N. Chupakhin, *Tetrahedron. Lett.*,

2005, **46**, 1791.

21 G. W. Gray and J. W. Goodby, *Smectic Liquid Crystals: Textures and Structures*, Leonard Hill, Glasgow, 1984.

22 K. J. Toyne, in *Thermotropic Liquid Crystal*, Ed. G. W. Gray, Wiley, Chichester, 1987.

23 X. –H. Liu, B. Heinrich, I. Manners, D. Guillon and D. W. Bruce, *J. Mater. Chem.*, 2000, **10**, 637.

24 W. Weissflog, in *Handbook of Liquid Crystals*, eds. D. Demus, J. Goodby, G. W. Gray, H. –W. Spiess, V. Wiley-VCH, Weinheim, 1998, Vol 2B, Chapter XI

25 H. T. Nguyen, C. Destrade and J. Malthête, *Adv. Mater.*, 1997, **9**, 375

26 M. Gharbia, A. Gharbi, H. T. Nguyen and J. Malthetec, *J. Curr. Opin. Colloid. Interface. Sci.*, 2002, **7**, 312

27 M. M. Mdleleni, J. S. Bridgewater, R. J. Watts and P. C. Ford, *Inorg. Chem.*, 1995, **34**, 2334.

28 (a) A. Santoro, A. C. Whitwood, J. A. G. Williams, V. K. Kozhevnikov and D. W. Bruce, *Chem. Mater.* 2009, **21**, 3871; (b) V. N. Kozhevnikov, M. M. Ustinova, P. A. Slepukhin, A. Santoro, D. W. Bruce and D. N. Kozhevnikov, *Tetrahedron Lett*., 2008, **49**, 4096; (c) D. N. Kozhevnikov, V. N. Kozhevnikov, M. M. Ustinova, A. Santoro, D. W. Bruce, B. Koenig, R. Czerwieniec, T. Fischer, M. Zabel and H. Yersin, *Inorg. Chem.*, 2009, **48**, 4179; (d) G. W. V. Cave, F. P. Fanizzi, R. J. Deeth, W. Errington and J. P. Rourke, *Organometallics*, 2000, **19**, 1355.

29 (a) J. H. Price, A. N. Williamson, R. F. Schramm and B. B. Wayland, *Inorg. Chem.*, 1972, **11**, 1280; (b) R. Melanson and F. D. Rochon, *Can. J. Chem.*, 1975, **53**, 2371.

30 A. Santoro, M. Wegrzyn, A. C. Whitwood, B. Donnio and D. W. Bruce, *J. Am. Chem. Soc.*, 2010, **132**, 10689.

31 A. R. Dick, J. W. Kampf and M. S. Sanford, *Organometallics*, 2005, **24**, 482.

32 (a) T. G. Appleton, K. A. Byriel, J. M. Garrett, J. R. Hall, C. H. L. Kennard, M. T. Mathieson and R. Stranger, *Inorg. Chem.*, 1995, **34**, 5646; (b) F. A. Cotton, L. R. Falvello and S. Han, *Inorg. Chem.*, 1982, **21**, 2889; (c) D. M. Roundhill, H. B. Gray and C.-M. Che, *Acc. Chem. Res.*, 1989, **22**, 55; (d) F. A. Cotton, J. H. Matonic and C. A.

Murillo, *Inorg. Chem. Sacta*, 1997, **264**, 61.

33   S. R. Whitfield and M. S. Sanford, *Organometallics*, 2008, **27**, 1683.

34   (a) D. C. Powers and T. Ritter,. *Nat. Chem.*, 2009, **1**, 302; (b) N. R. Deprez and M. S. Sanford, *J. Am. Chem. Soc.*, 2009, **131**, 11234.

35   M. Wegrzyn, *MSc Project*, University of York, 2010

36   (a) Yu. N. Kukushkin, *Coord. Chem. Rev.*, 1995, 139, 375; (b) A. D. Ryabov, G. M. Kazankov, I. M. Panyashkina, O. V. Grozovsky, O. G. Dyachenko, V. A. Polyakov and L. G. Kuzmina, *J. Chem. Soc*., *Dalton Trans*., 1997, 4385; (c) L. Alexandrova, O. G. Dyachenko, G. M. Kazankov, V. A. Polyakov, P. V. Samuleev, E. Sansores and A. D. Ryabov, *J. Am. Chem. Soc.*, 2000, **122**, 5189.

37   T. Petchey, *MChem Report*, University of York, 2010.

38   S. H. Crosby, G. J. Clarkson, R. J. Deeth and J. P. Rourke, *Organomet.*, 2010, **29**, 1966.

39   L. Alexandrova, O. G. D'yachenko, G. M. Kazankov, V. A. Polyakov, P. V. Samuleev, E. Sansores and A. D. Ryabov, *J. Am. Chem. Soc*., 2000, **122**, 5189.

40   M. Spencer, A. Santoro, J. A. G. Williams and D. W. Bruce, in preparation.

Chapter 3: Preparation and Liquid Crystal Properties of Iridium(III) Complexes

3.1 Background

3.1.1 Introduction

In the last 10 years, OLEDs have received enormous interest from the scientific community and from the industrial sector; as such, the materials connected with these devices have also received a good deal of attention. One of the primary aims of new technologies is the reduction in power consumption, which is important from the environmental point of view, but more important for the industries is the achievement of portable displays that last longer. This is the example of the Sony wireless, battery-powered version of the XEL-1 shown in chapter 1 (paragraph § 1.2).

Therefore, the use of specific transition metals with luminescent properties, specifically phosphorescent emission, has received great attention in current research.[1] Indeed as mentioned in the introduction chapter (§1.2.1), in chapter 2 (§2.1.1) for platinum(II) complexes and as will be described in detail in chapter 4, the application of third-row transition metals gives the theoretical possibility to achieve a quantum yields up to 100% as they allow access to the triplet mainfold,[2] increasing therefore, the external light yield of the devices.

There are four different excited states from which the emission could be obtained; of these, three give a resultant spin of one, the triplet state, and one gives zero, the singlet state. Unfortunately, in the case of pure organic luminescent materials, only emission from singlet state is permitted. Because of the working system of the OLEDs, this is a great limitation. Indeed in these devices there is the creation of all the excited states included the formation of spin-forbidden state through the introduction of electrons from the cathode in the LUMO of the emitting material and holes from the anode in the HOMO of the emitting material.[3] Thus, if fluorescent materials (emitter compound only from singlet state) are used, this limitation appears to be clear. Therefore the use of organometallic compounds containing heavy atoms as dopant is of primary interest and benefit in these displays. Indeed the efficient spin-orbit coupling (SOC) allows rapid singlet-triplet conversion, facilitating thus the intersystem crossing leading to an enhanced triplet formation; SOC also allows relatively rapid decay (μs region) of the triplet states. As such and as outlined in previous chapters, cyclometallated complexes of Ir^{III} are of significant current interest.

The relevant advantages of cyclometalated iridium complexes, with respect to complexes from other metals, have made them the most studied complexes for OLED application in the last five years. Indeed, an impressive expansion of the literature on luminescent Ir^{III} complexes is visible from the diagram in Figure 1 where it is evident that, in less than ten years, the number of publications has increased by a factor of 30. The most outstanding characteristics that make these complexes highly appealing as emitters in light-emitting diode devices are the tunability of the electro-optical properties.[4] Their metal-ligand-based luminescence provides the opportunity to change the emission energy,[5] tuning the colour in the visible range within electrophosphorescent devices.[6] They also typically exhibit high quantum yields ($\Phi_P = 0.1$ -

0.9) with an excited state lifetime generally in the microsecond region.[7] Other remarkable advantages are related to the fact that neutral species can be obtained and they are more amenable to OLED fabrication processes than charged analogues.[8] Nowadays organometallic complexes of *tris*-(phenylpyridine)iridium(III) (also available commercially, £137 per 250 mg 99% purity http://www.sigmaaldrich.com) or acetylacetonatobis(2-phenylpyridine)iridium(III) are also applied in several highly efficient green devices as emitting materials with external quantum efficiencies reaching 19% (Figure 2).[9]
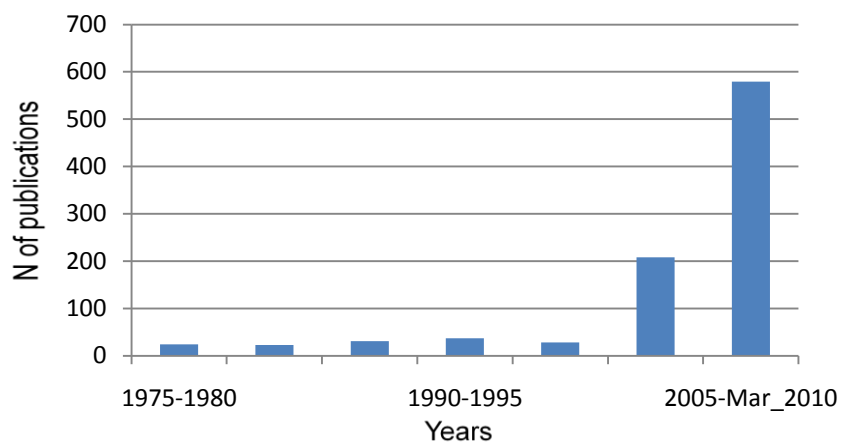
Figure 1-III Representative number of papers dealing with the iridium luminescent complexes in the 25 years to March 2010 (data from web of science on www.isiknowledge.com 15/03/2010)

Several different Ir^{III} complexes of ligands such as 2,2´-bipyridine, terpyridine, 2-phenylpyridine and including their modified structures, have been studied and characterised, resulting in an incredible amount of literature, as mentioned above. There is an exhaustive study of the luminescent properties of the Ir^{III} complexes with bidentate, monoanionic cyclometalated ligands, especially those derived from 2-phenylpyridine, exploring their visible emission, (examples in Figure 2).[7,9c,10] These materials represent some of the best materials

106

developed so far. They respect some of the most important parameters such as high quantum yield, colour purity, and stability. As mentioned above, only green (G) emitters have been applied successfully in commercially available devices. The luminescent properties of the Ir^{III} complexes, paying particular attention to 2-phenylpyridine derivatives, will be discussed in more details in Chapter 4
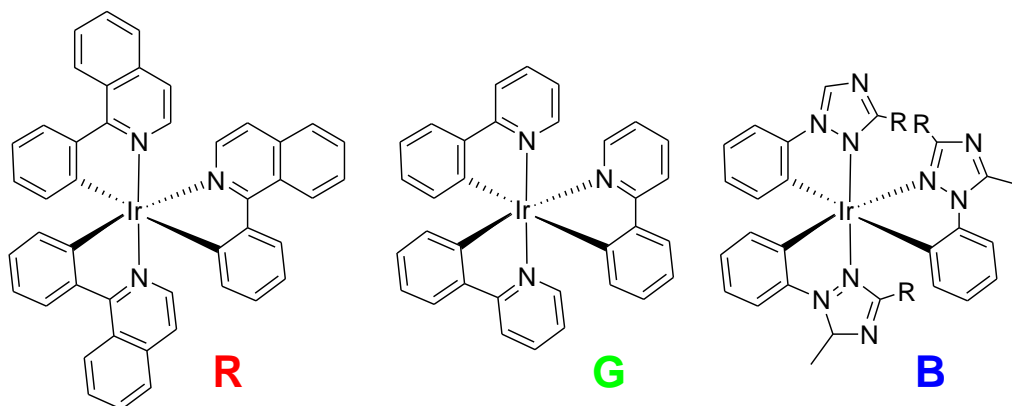
Figure 2-III R: Tris(2-phenylquinoline)iridium(III), λ_{max} = 620 nm, Φ = 0.26; **G**: Tris(2-phenypyridine)iridium(III), λ_{max} = 514 nm, Φ = 0.40; **B**: Tris(1-Phenyl-1-(3-propyl-2-methyl-1,2,4-triazolyl))iridium(III) λ_{max} = 449 nm, Φ = 0.66.

Therefore, in this part of the project, the challenge was no longer the luminescent properties of the complexes, as there are several excellent examples from this point of view.[1,2,4] Rather the challenge was more related to obtaining liquid crystal properties from these luminescent compounds.

Liquid crystal behaviour from iridium(I) complexes is well known,[11] indeed its square-planar structure, as described for platinum(II) (§2.1), is consistent with the required anisotropy, as shown in Figure 3. Thus, these complexes can be designed to obtain *rod-like* system and also *disk-like* system.
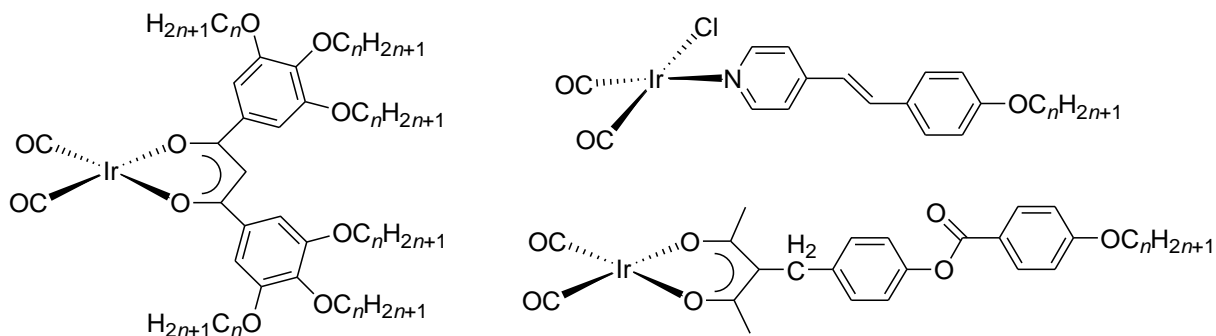
Figure 3-III Three examples of liquid crystal Ir^I complexes.

Iridium(III) has a $5d^6$ electronic configuration and, therefore, prefers an octahedral geometry (Figure 4). Thus, the degenerate d orbitals are split in an octahedral ligand field, by an amount Δ_o. The value of Δ_o is characteristic of the metal and also it depends on the field strength exerted by the ligands;[12] this is an important parameter, as will be discussed in Chapter 4 where a detailed description of the luminescent properties will be made.
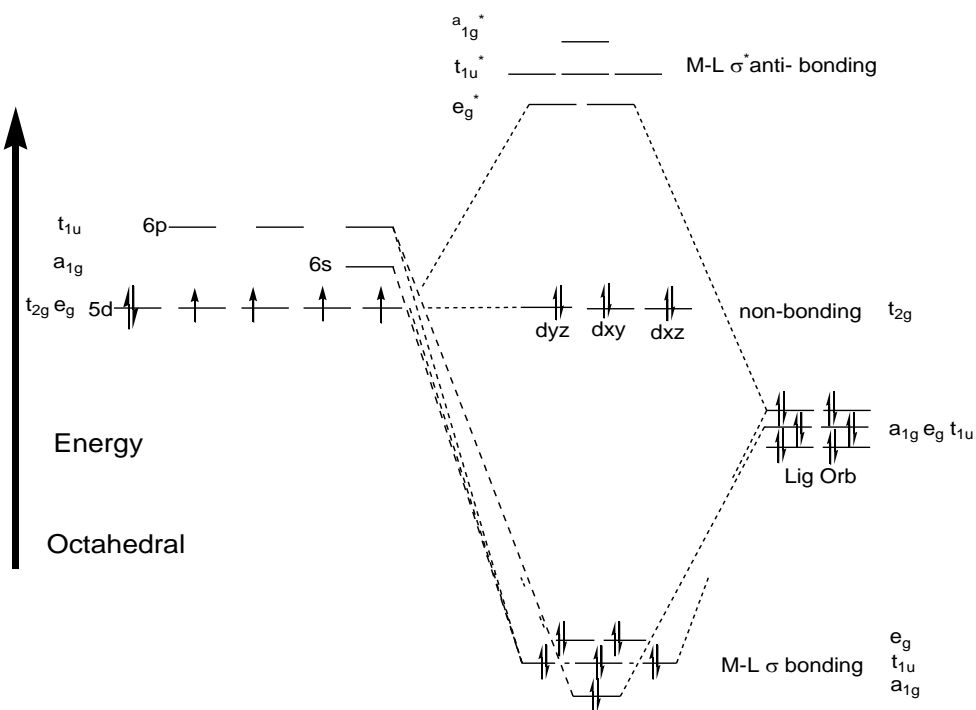

Figure 4-III Simple ligand field-splitting diagram for metals d-orbital in an octahedral geometry.

However the major issue, in the case of Ir^{III} is trying to construct an anisotropic motif around a six-coordinated, octahedral centre. This is difficult because it is not immediately obvious how a suitable disposition of the ligands may be constructed to give a target shape. Furthermore, it is also difficult to control the location of the substituents on the six free positions of the iridium metal centre, thus, it could be very difficult, for example, to obtain the complex shown in Figure 5, where the two ligands are in the square-planar plane of the octahedral.
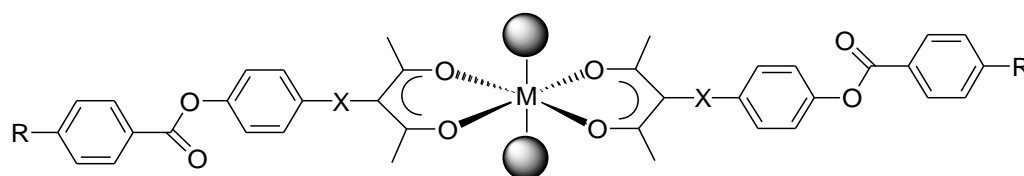

Figure 5-III The anisotropy of the molecules decreases when an octahedral geometry is present. R represent the aliphatic chains.

Figure 6 shows an approach to this problem, using highly anisotropic ligands to overcome the structural perturbation of the octahedral centre.[13] Indeed, the presence of an axial substituent has a great effect on the liquid crystal properties, so that the free ligand of the last complex **C** in Figure 6 with n = 12, shows a clearing point temperature (N-I transition) of 307 °C, while the related complex with Re^{I} has a clearing point (N-I) of 145 °C. This element is clear evidence of the destabilisation effect due to the presence of an octahedral metal centre.
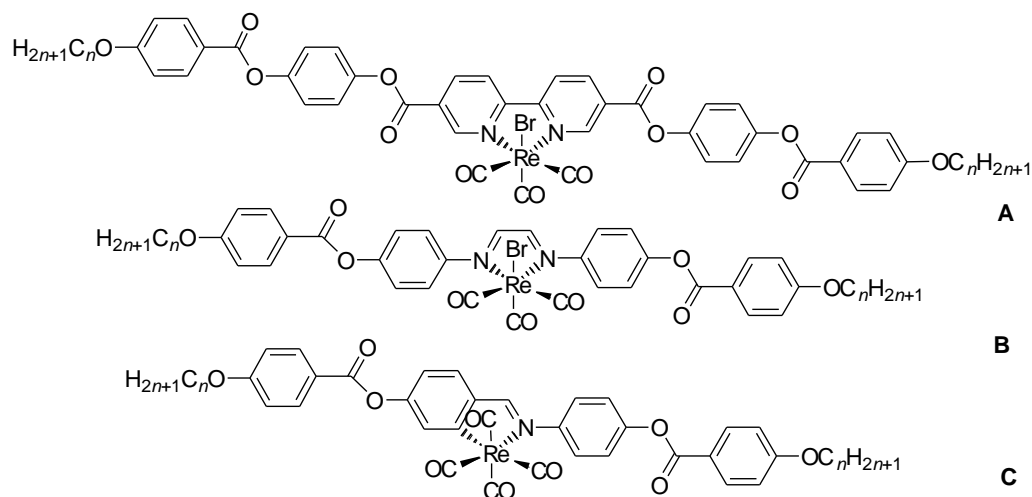
Figure 6-III Three rhenium complexes that show liquid crystal properties, *n* can be 4, 8 or 12.

Another approach, which is less immediately obvious, is reported in initial work by Giroud-Godquin *et al*[14] on heavily alkylated tris(β-diketonato)iron(III) complexes, in which they postulated the formation of a mesophase. These complexes were later investigated in more detail by Swager and co-workers[15] who showed that this organisation is promoted by the interactions between the pendant aromatic rings and the chains and that it depends on the chiral configuration (Δ or Λ) of the nearest neighbours (Figure 7).
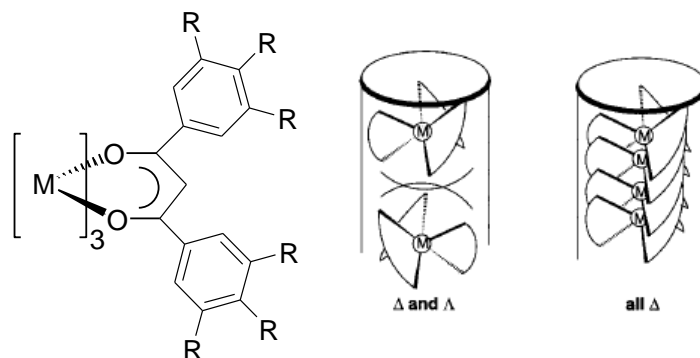

Figure 7-III General structure of an octahedral complex with liquid crystal properties. R = $O(CH_2)_{11}CH_3$. On the right there are the proposed organisations of the complexes shown in a column.

When the closest complexes have the same absolute configuration, an efficient packing and a helical columnar structures are formed. A mismatched structure will concurrently limit the dipolar interactions between mesogens. Therefore it was demonstrated that octahedral metallomesogen based liquid crystals can spontaneously resolve into microdomains with net chirality (Δ or Λ).

3.1.2 Target Compounds

Based on the above background, different complexes were identified to try to overcome the problem of the octahedral geometry. Some examples are shown in Figure 8, which reflect the discussion on the different approaches mentioned above.

The two structures at the top represent the 'multichain approach', while the structure on the bottom is the 'anisotropic approach', obtained increasing length of the ligand. The first complex to be investigated was 2,5-di(4-dodecyloxyphenyl)pyridine and using one containing the acetylacetonate as co-ligand which, as described in detail in Chapter 4 and also mentioned in the Chapter 2, should assure an improved quantum yield in comparison with other β-diketones such as diphenyl-1,3-diketone.[16] Therefore, to become familiar with iridium chemistry and in general to find the optimal condition for the complexation of this class of ligands, it was decided to synthesise complex **21(12)** shown in Figure 9. Thus, the Ir complexes were prepared and characterised, using the same ligands applied in the platinum project.
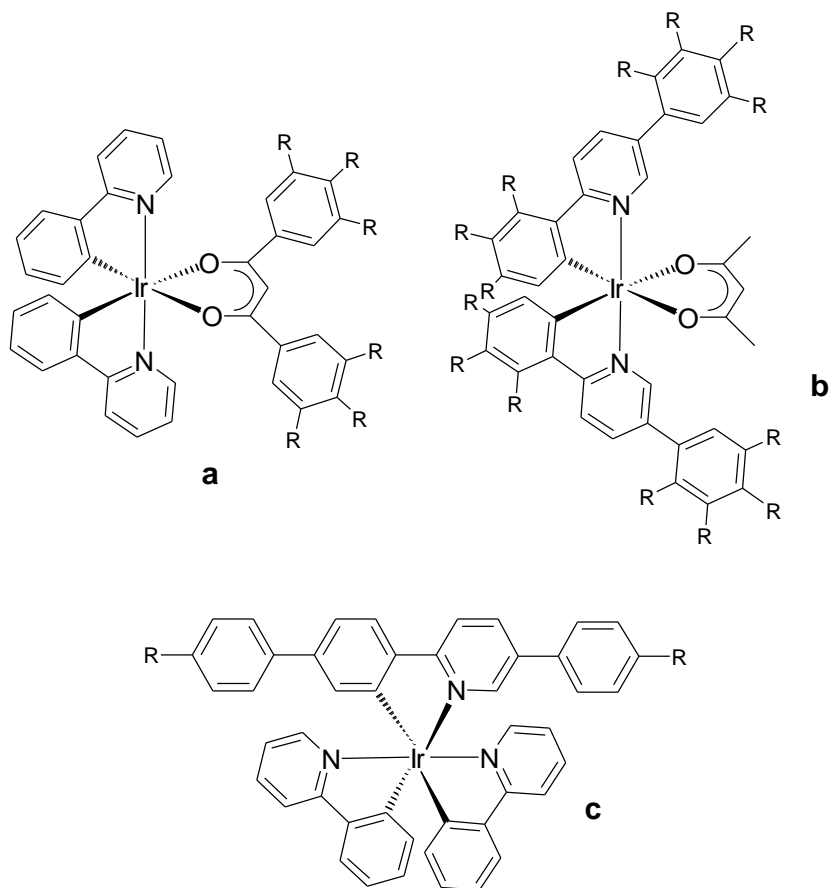
Figure 8-III Designed structure for Ir^{III} complexes to obtain liquid crystal properties. R could be H or alkoxy chain. **a** and **b** two polycatenar designee, R can be H or alkoxy chain. **c** anisotropic designee, R are alkoxy chains.
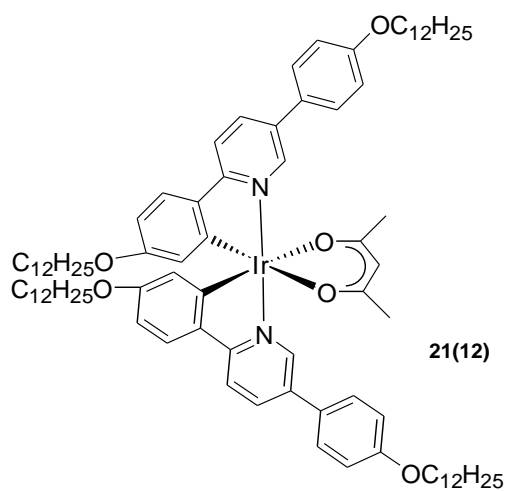

Figure 9-III Structure of the first synthesised Ir^{III} complex.

112

3.2 Iridium(III) Complexes

3.2.1 Synthesis

There are several different approaches to the synthesis of iridium complexes,[17] but for 2-phenylpyridine ligands one of the most used methods is that developed by Nonoyama in 1974.[18] This methodology describes the reaction of 2.5 molar equivalent of the ligand with one molar equivalent of hydrated $IrCl_3$ in a 3:1 mixture of ethoxyethanol and water. In this project, a small modification of this established route was developed to adapt it to the ligands used; all the reactions were carried out under a nitrogen atmosphere. Iridium complexes were synthesised using ligands **1(12)** and **3(12)** (Figure 11), and with a range of different auxiliary ligands that will be discussed later.
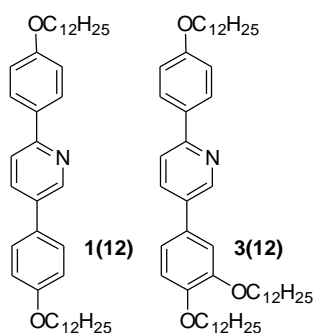

Figure 10-III Ligand used in the formation of the Ir[III] complexes.

3.2.1.1 Synthesis of Iridium Complex *21(12)*

As mentioned before, Nonoyama's conditions were modified to increase the solubility of the ligand, and a 5:1 ratio of ethoxyethanol to water was used. Interestingly, the reduced

amount of water decreased the reaction time from 25 h to overnight, and a smaller excess of ligand (0.2 molar equiv.) was necessary.
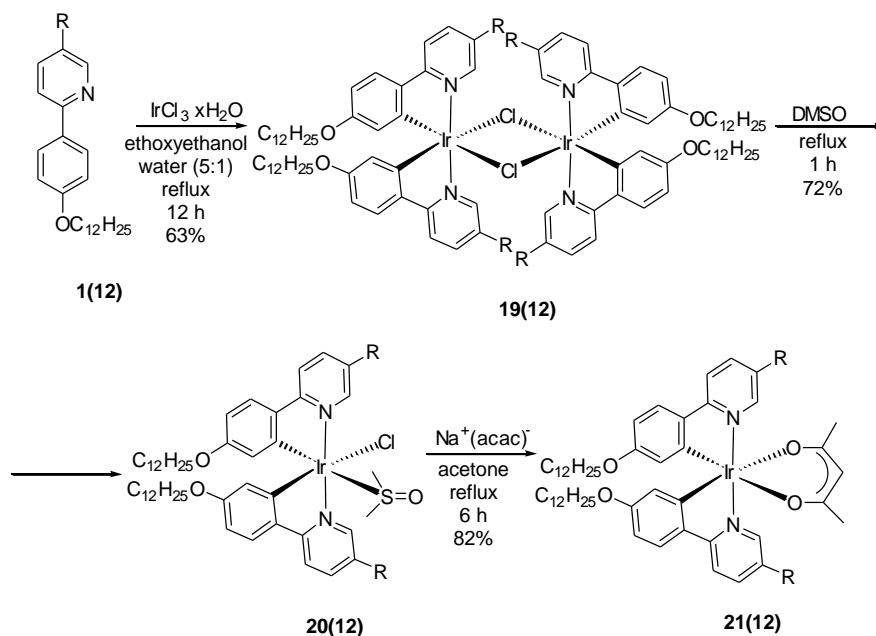
Scheme 1-III Synthesis of **21(12)**; R = 4-dodecyloxyphenyl.

Complex **19(12)** was obtained *via* purification on a chromatography column on silica gel using dichloromethane as eluent, yielding a yellow-red crystalline material (yield 63%). Once the di-μ-chloro complex (**19(12)**) was prepared, rather than react it directly with Na(acac) as reported in other publications,[6,8c] the dichloro bridge was cleaved using DMSO to give **20(12)**, which was then reacted with Na(acac). This approach has been developed to improve the overall yield of the reaction and to have a more reliable method to the synthesis of different complexes, as the DMSO derivative proved to be easily convertible in other complexes. Thus, complex **19(12)** was reacted in pure and dry DMSO under nitrogen for 1 h at reflux and, after cooling to room temperature, complex **20(12)** was obtain by filtration without further purification. Complex **20(12)** was then reacted for 6 hours with Na(acac) in acetone under

reflux. The reaction yielded complex **21(12)** in a very good yield (82%) often without the need for further purification. Complex **21(12)** was not liquid crystalline and melted straight to the isotropic liquid at 76 °C. However, on evaluating the behaviour of **20(12)**, it was surprisingly found that it showed well-defined liquid crystal behaviour, with a transition from the crystal to a lamellar phase at 86 °C, followed by a transition between a lamellar and columnar rectangular phase at 100 °C, and finally a transition from columnar rectangular to the isotropic phase at 130 °C. There is only one very recent example that shows an iridium(III) complex with liquid crystal properties.[19] This compound fall within the category of the polycatenar system discussed above (Figure 11).
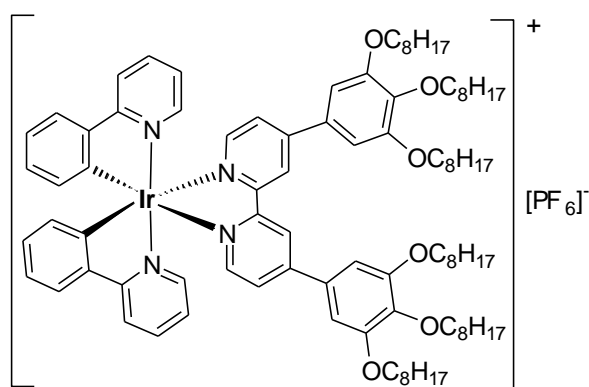

Figure 11-III Complex synthesised by Ghedini *et al.* in 2010 that shows monotropic liquid crystal properties. Cr · 184 · I (Col$_h$ · 130 · I).

The liquid crystal properties of our system arise from completely different system, indeed our two ligands are off of the square plane of the octahedral and they point in different region of the space.

Using a short-chain ligand, needle-like single crystals of **20(1)** were obtained using vapour diffusion technique with CHCl$_3$ and CH$_3$COCH$_3$ as solvents. In Figure 12 are shown some

115

projection of the structure of complex **20(1)**, the crystallisation solvent has been removed for clarity. The pictures show a complex with a distorted octahedral coordination geometry around the iridium(III) and the two phenylpyridines show the two nitrogens *trans* to one another, and the two carbons *cis*, as reported in all the literature data and as reported for the analogous complex **21** without long alkoxy chains.[20]
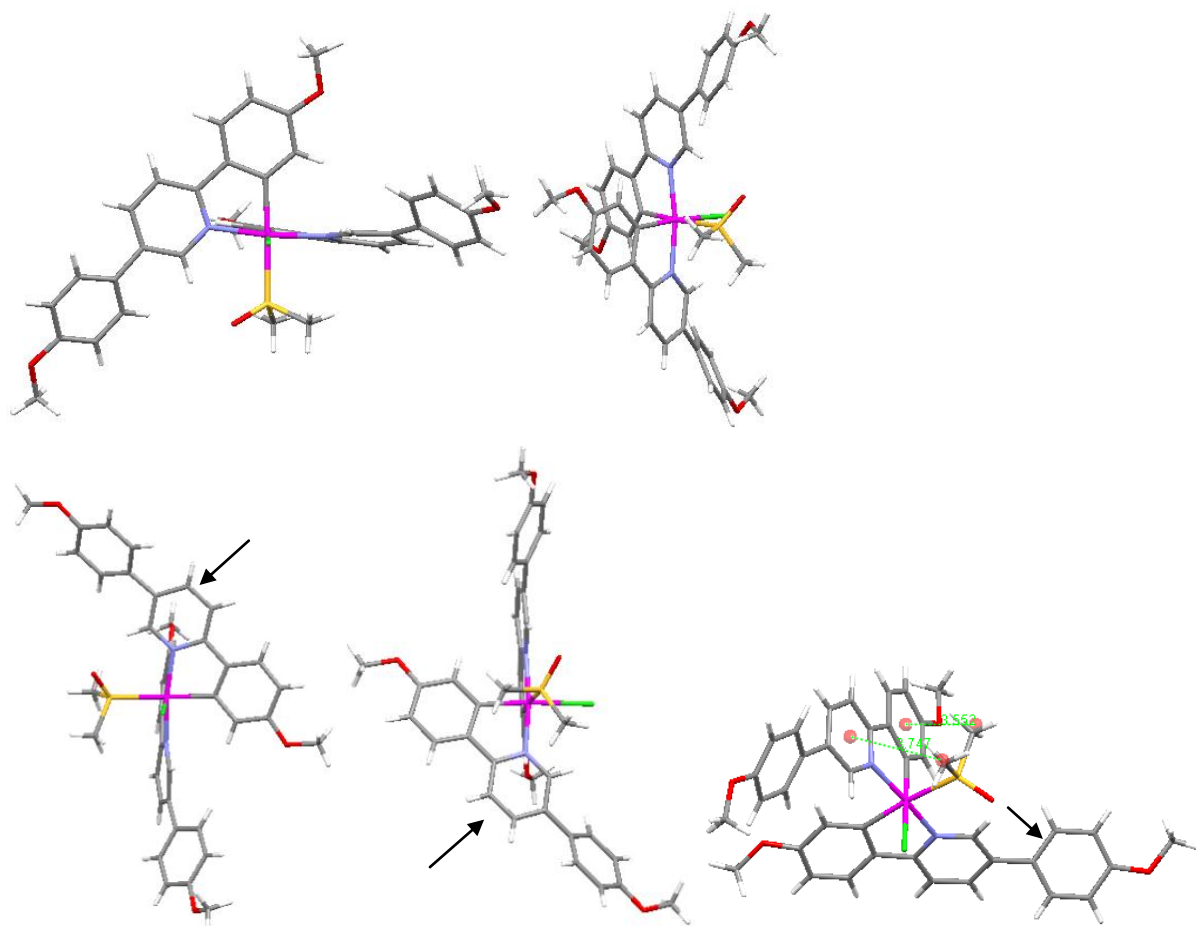
Figure 12-III Different perspectives of the crystal structure of **20(12)**

The Ir-N bond length are equivalent at 2.071(3) Å and 2.070(3) Å, respectively, they prove to be in general longer than the acetylacetonatobis(2-phenylpyridine)iridium(III),[21] 2.010(9) Å and also longer than the acetylacetonatobis(2,5-diphenylpyridinato)iridium(III),[20] 2.034(3) Å.

The Ir-C bonds were found to be 2.027(3) Å (S-Ir-C) and 2.016(3) Å (Cl-Ir-C), which are longer than in the acetylacetonatobis(2,5-diphenylpyridinato)iridium(III) (Ir-C 1.989(4) Å) and comparable with those acetylacetonatobis(2-phenylpyridine)iridium(III) (Ir-C 2.003(9) Å).

In each ligand, the two bound rings are not co-planar and there is a small torsion angle between them (8.28° in one case and 10.4° in the other). Greater torsion angles were between the unbound rings and the bound pyridine, indeed the angle between the plane obtained from the cyclometallated ring and the unbound ring is 32.02° in one case, while in the other ligand the angle is slightly higher at 41.71°. The difference could be due to the position of the oxygen of the DMSO group that points in the direction of the unbound ring forcing it to have a smaller torsion to minimise the electronic repulsion between the lone pairs of the oxygen and the delocalised electronic density of the ring. As is highlighted with the arrows in Figure 13, two of the four $-OCH_3$ point in the middle of the opposite unbound ring (7.412 Å and 8.372 Å) and, as described below, this has an effect on the ^{1}H-NMR spectrum of the complex, even if in the NMR spectroscopic analysis the group is $-OCH_2$ because of the longer chains.

Thus, the ^{1}H-NMR spectrum of compound **20(12)** shows a doubling of the signals due to the reduction in symmetry attributable to the presence of the DMSO and chloride substituents, (Figure 13) as the two carbons of the phenyl ring bound to Ir are no longer equivalent. Unfortunately it was impossible to assign the signals for each ligand and so assignments were done without distinguishing between the two substituents. The protons vicinal to the metal-bound carbon (H^6) gave two different signals and the difference of about 0.6 ppm is clearly visible in Figure 13. This difference in chemical environment for the two carbons is also reflected in the proton signal *ortho* to the nitrogen (H^1) of the pyridine; in this case the

difference is smaller, being only 0.3 ppm. It is very interesting to observe that the signals of the four $-OCH_2-$ are different. The signals of the $-OCH_2-$ on the unbound rings have the typical chemical shift of 3.9 ppm and appear as a triplet. The other two sets of protons from $-OCH_2-$ of the bound phenyl rings present a different chemical shift in the ^{1}H-NMR spectrum, indeed they are at 3.5 ppm and appear as a broad multiplet. This is due to the fact that the protons are pointing in the middle of the opposite pyridine rings and, as mentioned above, they present different distance from the rings (Figure 13, highlighted with the arrows). Therefore the ring current shields the protons which resonate at higher field comparing with the normal $-OCH_2-$ groups. A similar effect was observed for dimeric Pt^{III} complexes in § 2.3.1.3.

Furthermore, there are two singlets at 3.1 and 2.0 ppm. From the integration, these two signals represent three protons each and they are the signals of the $-S-CH_3$ hydrogens. They show to be clearly different in chemical shift, this could be attributed to the rigidity of the Ir-S bond that does not allow free rotation, indeed also in this case the $-CH_3$ groups point in the centre of the rings. However this behaviour could be also be explained with the chirality of the Ir^{III} centre. As proved by single crystal analysis, there are two diastereoisomers and therefore, two DMSO groups with two methyl groups that are diastereotopic, accounting for the two different signals.
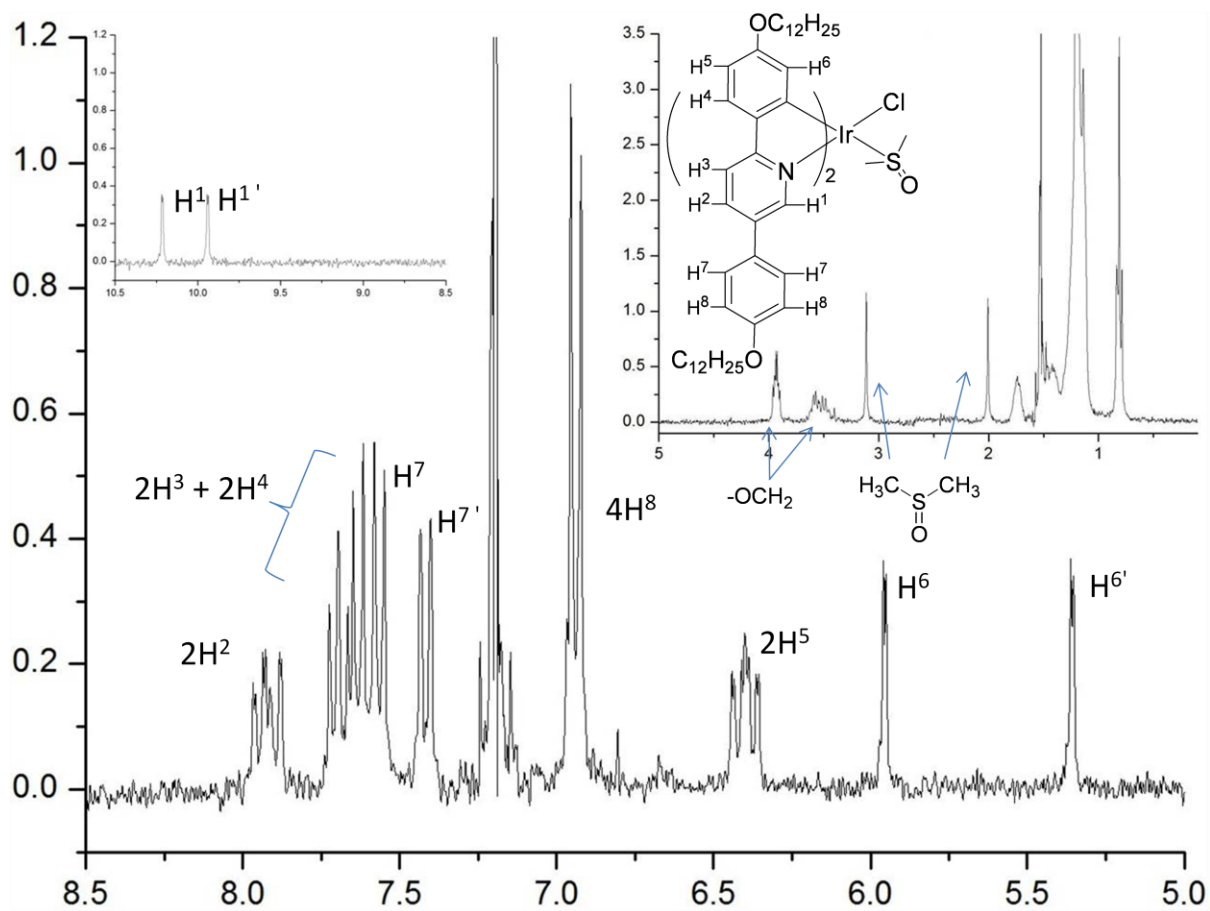
Figure 13-III ^{1}H-NMR spectrum of complex **20(12)** in CDCl$_3$. H^6/H$^{6'}$ and H^7/H$^{7'}$ represent the protons of the two different ligands

3.2.1.2 Lability of Complex 20(12).

Purification of complex **20(12)** was impossible because during all such procedures it changed to form an unknown complex designated **29(12)**. The only purification methodology that gave any significant yield of **20(12)** was crystallisation from DMSO, but this was often accompanied by the formation of complex **29(12)**. The reason for the formation of complex **29(12)** is not yet clear and its identity is also still a mystery. The first hypothesis was that the lability was due to the relatively labile nature of the Ir-S bond, and so it was decided to use a strong-field ligand such as CO **22(12)** to try to realise an inert complex. (Scheme 2).
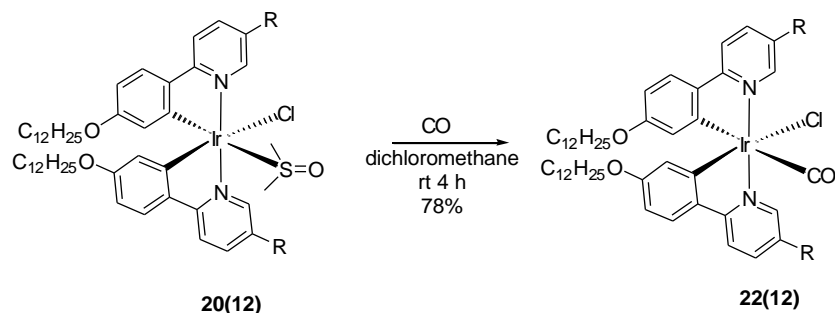
Scheme 2-III Synthesis of carbon monoxide derivate **22(12)**.

Complex **22(12)** was synthesised by reacting DMSO complex **20(12)** with carbon monoxide in dichloromethane for 5 h under an atmosphere of CO, Scheme 2. This complex was also liquid crystalline (Cr · 91 · LC · 130 · I), but the phases have not been characterised as yet. Unfortunately, this complex showed the same lability as DMSO complex **20(12)** forming the same identical product, **29(12)**. Because the synthesis of complex **22(12)** demonstrated a lability similar to **20(12)**, complex **I(12)** was identify as a target to counteract the possibility of a labile Cl ion, but despite repeated attempts, it was not possible to obtain the complex.

Interestingly, in the reaction to form acetylacetonate derivate **21(12)**, no lability, neither side product formation was observed. Indeed complex **21(12)**, where the remaining coordination sites are occupied by a bidentate ligand, seemed to confer greater inertness to the complex.[20]

As the acac complex **21(12)** was rather inert, yet failed to show mesomorphism, two other complexes with a monoanionic, bidentate ancillary ligand were identify, namely **25(12)** and **I(12)** (Figure 14).

25(12) **I(12)**
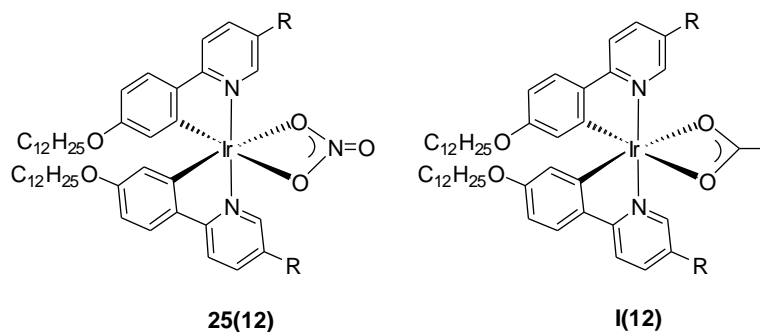
Figure 14-III Left: Target complex **25(12)**. Right: Target complex **I(12)** no suitable synthesis was found.

Complex **25(12)** derived from ligand **1(12)** was obtained using the method[22] shown in Scheme 3, using AgNO$_3$ to remove the chlorine atoms of the chloro-bridge complex **19(12)**. The reaction was carried out at room temperature for 7 h in acetonitrile, giving the intermediate complex **24(12)** in good yield. Without any purification, complex **24(12)** was then heated under reflux in the same solvent for 3 h. The reaction was then cooled to room temperature and the solvent was removed under reduced pressure yielding complex **25(12)** in 74% yield.
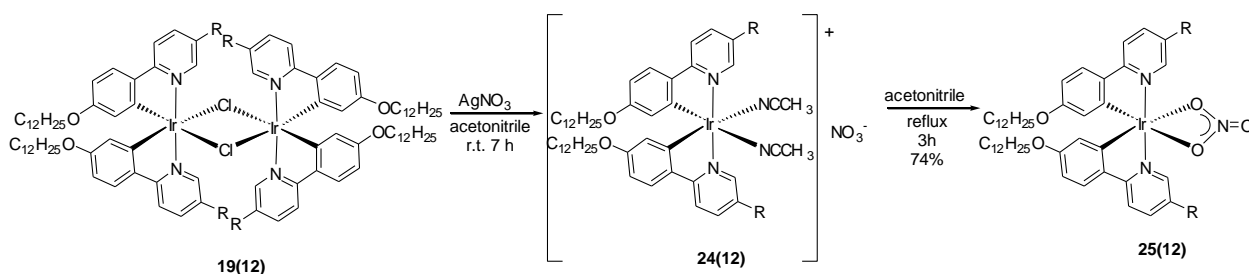
Scheme 3-III Synthesis of Ir^{III} complexes **25(12)**, same method has been applied for the synthesis of **23(12)**. R = dodecyloxyphenyl group.

Complex **23(12)** (Figure 15) was synthesised with the same methodology only that instead of using AgNO$_3$, AgO$_3$SCF$_3$ was used instead. This complex proved to be stable and there was no evidence of complex **29(12)** during the reaction and/or storage. Complex **25(12)**, similarly

121

to acac complex **21(12)**, does not show any lability and proved to be rather inert with a melting point of 77 ºC very similar to **21(12)** (76 ºC).

Unfortunately, even after numerous attempts, it was impossible to obtain complex **I(12)**, and the various conditions used are reported in Table 1. Also in these cases the formation of complex **29** was found.

Table 1-III Experimental condition for the synthesis of **I(12).**

Starting Material	Solvent	Condition	Result
19(12) CH_3COOH, K_2CO_3	2-methoxyethanol	reflux 16 h	Dec
20(12) CH_3COONa	acetic acid	reflux 10 h	**29(12)**
20(12) CH_3COOH, Et_3N	toluene	reflux 8 h	**29(12)**
19(12) CH_3COOAg	acetonitrile	room temp/ reflux	no react

Other complexes were synthesised using the three-chains ligand **3(12)** (Figure 15), mainly to investigate if any liquid-crystalline behaviour was obtained for the acac derivate **27(12)**. During the synthesis of complex **27(12)**, its precursors were also prepared, therefore, complex **26(12)** and **28(12)** were obtained. All these complexes showed exactly the same behaviour of their two-chains homologues, thus lability for **26(12)** and **28(12)**, and the absence of any liquid crystal property for **27(12)**. More polycatenar ligands are planned to be synthesised and used to complex Ir[III] but this is part of another project that will be developed in future.
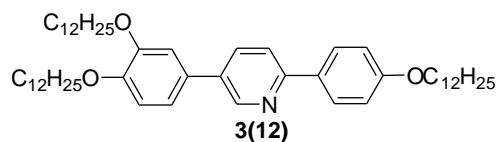
Figure 15-III Three-catenar ligand, **3(12)**
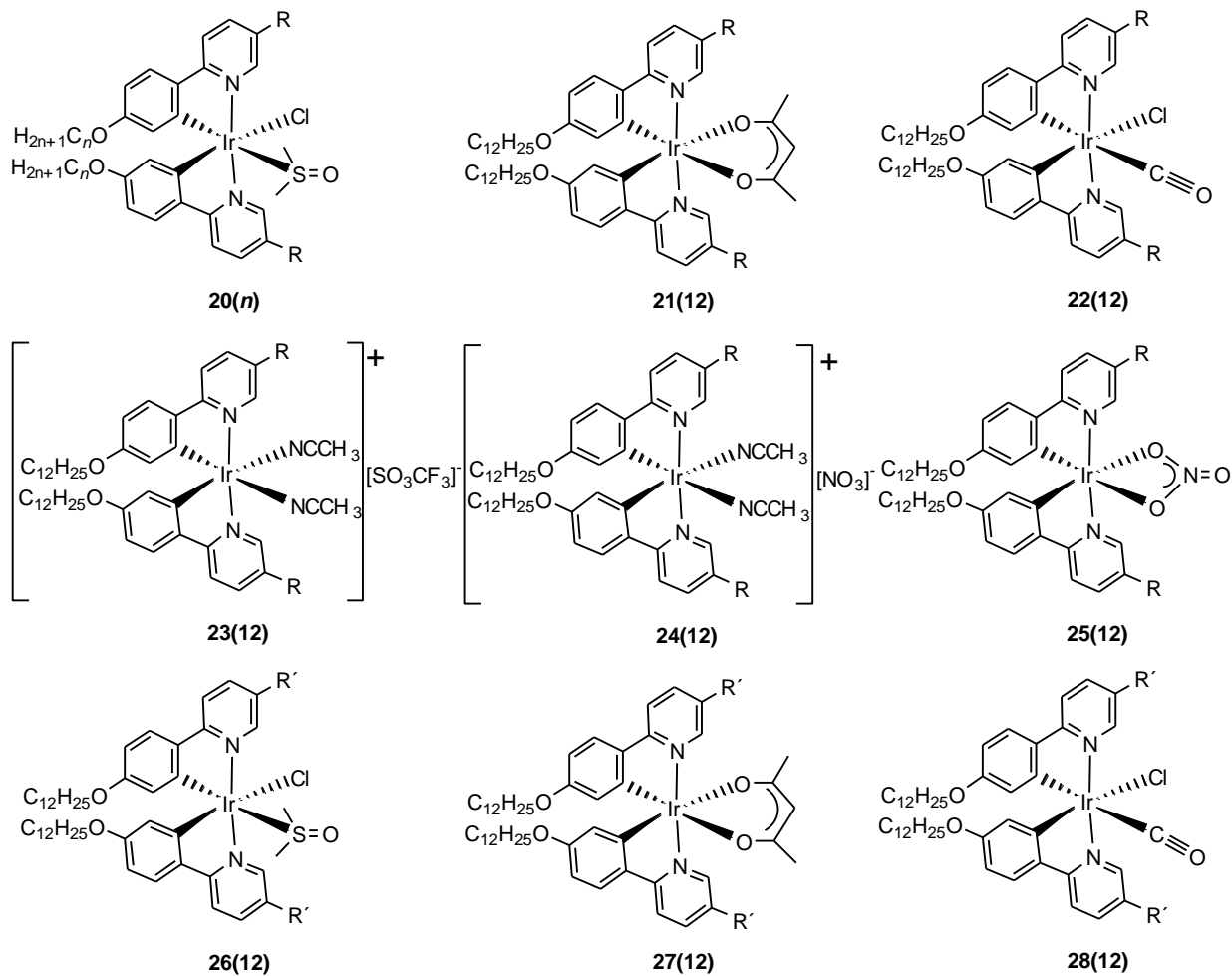
Figure 16-III Complex **20(n)** was synthesised with 12 and 8 carbon atoms on the chains. Iridium complexes from **21(12)** to **25(12)** have been synthesised only with 12 carbon atoms on the chains; **26(12)**, **27(12)** and **28(12)** instead have been synthesised with ligand **3(12)**, and also in this case only with 12 carbon atoms. R is 4-dodecyloxyphenyl group, R´ is 3,4-didodecyloxyphenyl group.

3.2.2 Liquid-Crystalline Properties of the Iridium Complexes.

The mesomorphic properties of the iridium complexes were investigated using polarised optical microscopy and X-ray diffraction. Unfortunately the production of good materials for the characterisation has been extremely difficult because of the unsolved problem of the lability of many of the complexes. All the reported liquid crystal transition temperatures were obtained from pure samples, and the samples were also checked after thermal treatment to assure the reliability of the analysis. The thermal behaviour of the complexes is collected in Table 2.

Table 2-III Thermal behaviour of the iridium complexes. Complex **29(T12)** is obtained using ligand **3(12)**

Compound	n	Transition	T (^{o}C)
19(12)	12	m.p.	235
20(12)	12	Cr-Lam	86
		Lam-Colr[1]	100
		Colr-I	122
21(12)	12	m.p.	76
29(12)	12	m.p.	36
29(T12)	12	m.p.	55
22(12)	12	Cr-LC	91
		LC-I	130
23(12)	12	Cr-LC	151
		LC-I	165
25(12)	12	m.p.	77
26(12)	12	Cr-LC	119
		LC-I	103
27(12)	12	m.p.	54
28(12)	12	Cr-LC	85
		LC-I	96

1 this transition was seen only in the XRD

In general the identification of the liquid crystal phases is very difficult with polarised

microscopy because the high viscosity of the samples does not allow well-defined textures to form; therefore, in this case the use of X-ray diffraction is of absolute importance to identify the liquid crystal phases.

Thus, DMSO complex **20(12)**, was sent to the Institut de Physique et Chimie des Matériaux de Strasbourg for X-ray diffraction in the liquid crystal phase; the results are shown in Figure 18. There are two liquid crystal phases, one, a lamellar phase (86-100 °C), and another one, a columnar rectangular or ribbon phase (100-120 °C). In the lamellar phase with a reduced symmetry, the assignment of the symmetry of the mesophase is based on the analysis of the *d*-spacing from those data. In the small-angle region ($0 < 2\theta < 10°$), four different reflections were observed corresponding to the fundamental orders of diffraction indicative of the lamellar phase, indeed periodic signals at (001) 35.6 Å, (002) 17.54 Å, (003) 11.63 Å and (004) 8.82 Å ($d_{theor.}$: 35.44, 17.72, 11.81, and 8.86) are clear evidence of this lamellar organisation. Furthermore, in Figure 17a at high angles ($2\theta \sim 20°$) a broad, diffuse scattering peak is present, corresponding to the liquid-like order of the molten aliphatic chains.

At higher temperature, the assignment of the two-dimensional rectangular symmetry of the column rectangular mesophase is also a result of the analysis of the *d*-spacings from those data. In the small-angle region ($0 < 2\theta < 5°$), three different reflections were observed corresponding to the fundamental orders of diffraction indicative of the two-dimensional lattice, which could be either columnar rectangular or a ribbon phase with *c2mm* planar symmetry ($a = 60.92$ Å, $b = 43.1$ Å, $S = 2651$ Å^2). Indeed refection corresponding to (01), (22), and (40) are clear evidence of a rectangular organisation. Also in this case, in Figure 17b a broad high-angle ($2\theta \sim 20°$), diffuse scattering peak is seen. This, as well, corresponds to the liquid-like order of the aliphatic chains. In the absence of a refection corresponding to a

stacking period it is impossible to distinguish between a columnar rectangular phase and a ribbon phase.
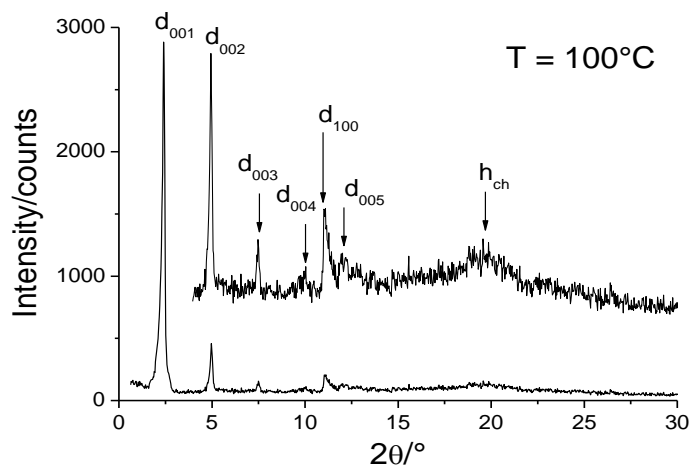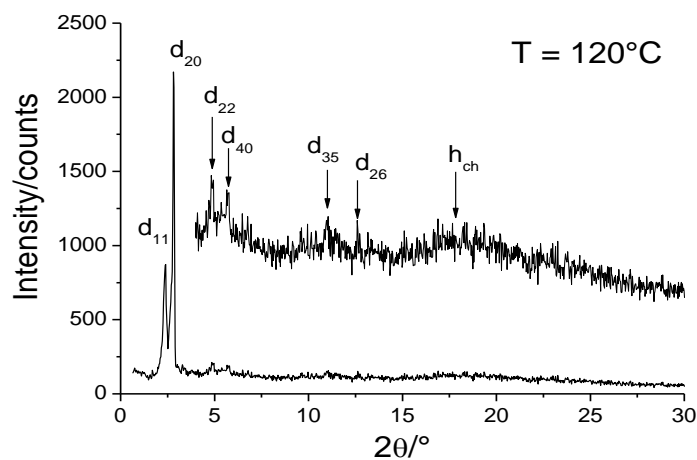
Figure 17-III X-ray diffraction powder analysis of complex **20(12)**. **a** lamellar phase, **b** columnar rectangular/ribbon phase

The reason why these complexes show this unexpected liquid crystal behaviour is not clear yet. At the moment there is no information of the organisation of the complexes in the liquid crystal phases. One possibility is that they could organise themselves into columns (Figure 18)

with each iridium(III) complex inside the column interacting with another iridium(III) complex through their ligands. The two interacting Ir^{III} complexes would be twisted of an angle of ~ 30°, therefore the DMSO groups are organised alternatively. The chains of each column of molecules point in an alternated fashion, indeed one set of chains points all "up" and the other from the other column points all "down". It is assumed that, by analogy with the work of Swager's group,[15] each column would be homochiral.

However what is still not clear is why the complexes with acetylacetonate or with nitrate do not show any liquid crystal behaviour. One of the possible explanations could be the higher flexibility of the monodentate system allowing the molecules to arrange in a different manner and this different organisation facilitates the appearance of the liquid crystal properties.
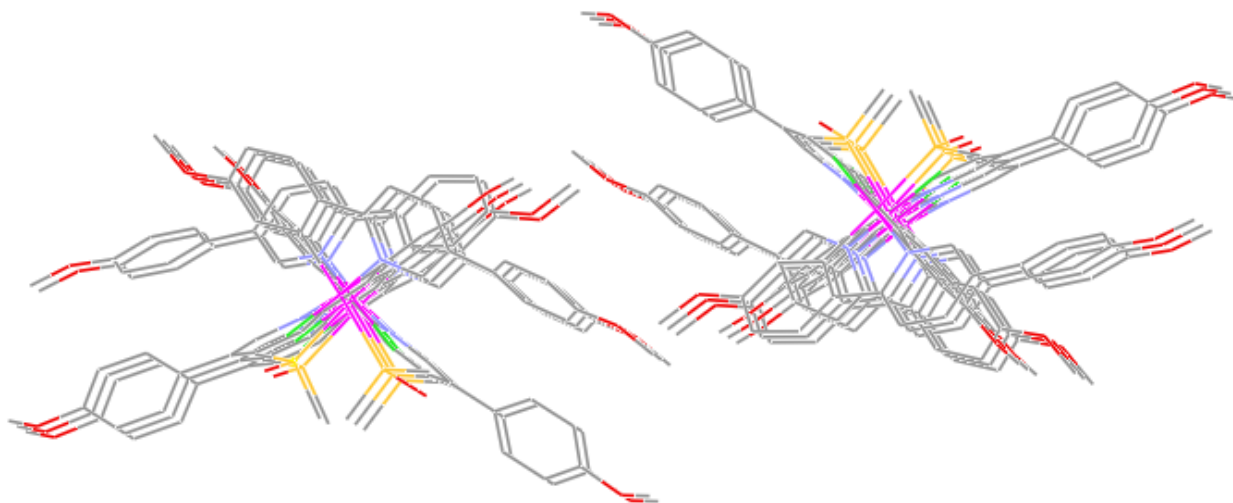
Figure 18-III Possible conformation in the liquid crystal column rectangular mesophase. Determinate by close interaction in Mercury. The iridium(III) complexes are organised in alternated fashion in each column and the column have the chains that point in alternate directions.

3.2.3 Complex 29, the "Impurity".

It has been already mentioned that DMSO complex **20(12)**, along with all monodentate complexes, showed lability with the production of an unidentified complex, **29(12)**. Indeed, in some cases complete conversion from complex **20(12)** to **29(12)** was observed. This section has the intention of clarifying the bases for the hypothesised structure of complex **29(12)** and to explain what has been done to try to identify this complex.

3.2.3.1 Observations and Occurrences

Before starting with hypothesis and speculation on the nature of this material (**29**), a clear report of all the observations and occurrences should be made. Complex **29(12)** was observed in the reactions for the formation of μ-chloro bridge complex **19(12)** from ligand **1(12)** and $IrCl_3 \cdot xH_2O$ in 2-ethoxyethanol-water 5:1, and almost always in the formation of all the monodentate complexes, but never in the synthesis of the acetylacetonate derivatives, or in general complexes with a third bidentate complexes. In Table 3, a resumé of every compound synthesised along with the formation of complex **29(12)** is reported. Complex **29(12)**, was found especially when DMSO complex **20(12)** was used, while when μ-chloro bridge complex **19(12)** was used the formation of complex **29(12)** was observed only at reflux in 1,2-dichlorobenzene solution. Therefore, it seems that complex **19(12)** could be more stable than complex **20(12)**. Similar behaviour was showed in Table 1 for the synthesis of the acetate complex **I(12)**.

Table 3-III Formation of complex 29

Synthesised Complex	Formation Complex 29	Possible Purification
19(12)	Yes	Column on silica gel
20(12)	Yes	no
21(12)	No	any
22(12)	Yes	no
23(12)	No	any
25(12)	No	any
26(12)	Yes	no
27(12)	No	any
28(12)	Yes	no
30(12)	Yes	Column on silica gel

In the case of complex **19(12)**, its stability allowed its purification and storage as a dry solid, and no formation of complex **29(12)** was found ever since. In the case of the purification of DMSO complex **20(12)** and CO complex **22(12)**, different purification techniques were applied such as flash and gravity chromatography, crystallisation and sublimation, but all attempts to obtain an analytically pure materials were unsuccessful. Table 4 contains all the information on the stability of almost all the synthesised iridium(III) complexes; at this stage, no long-term stability tests have been carried out.

Table 4-III Stability of the Iridium Complexes.

Compounds	Conditions	Stable
19(12)	any	YES
20(12)	AIR, N_2, DARK, COLD	NO
21(12)	any	YES
22(12)	AIR, N_2, DARK, COLD	NO
25(12)	any	YES
29(12)	any	YES

In one experiment the preparation of acetylacetonate complex **21(12)** was carried out using a mixture of DMSO complex **20(12)** and complex **29(12)** in a 4:1 ratio in acetone under reflux for six hours. Under these conditions complex **29(12)** was partially consumed in the reaction. To then prove that complex **29(12)** reacted with Na(acac) to give complex **21(12)**, the same reaction was tried using pure complex **29(12)** in ethoxyethanol under reflux for five hours, the solvent was changed to increase the temperature of the reflux to increase the yield. It reacted smoothly, and gave **21(12)** in a good yield (72%). giving exactly the same compound that it was obtained starting from DMSO complex **20(12)**.
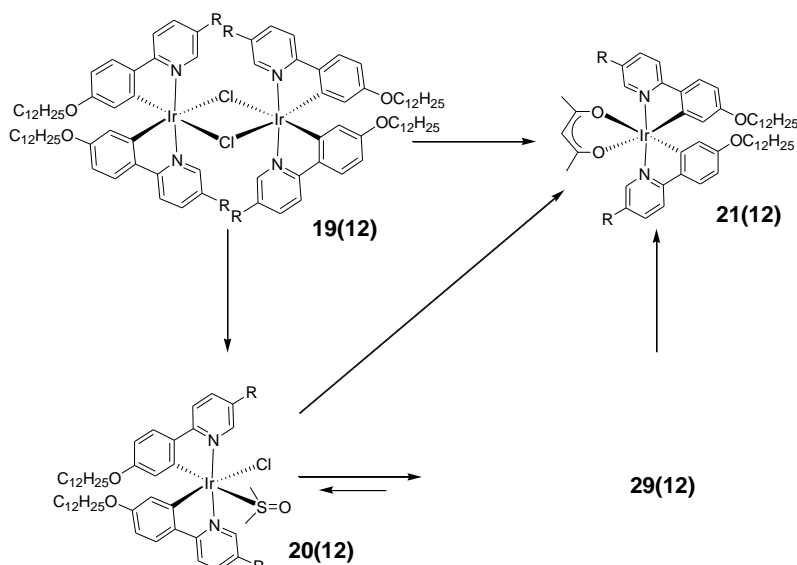
Scheme 4-III Equilibrium berween Ir^{III} complexes. R = dodecyloxyphenyl.

During the synthesis of these complexes, it was discovered also that an equilibrium exists between the complexes **20(12)** and **29(12)**, more precisely if pure complex **29(12)** is solubilised in DMSO and heated there will be the formation of complex **20(12)**. However the reaction does not go beyond certain limits (Scheme 4). In general by the relative intensity of

the ^{1}H-NMR signals of the proton *ortho* to the nitrogen, it is possible to estimate that the reaction does not proceed beyond 20% conversion.
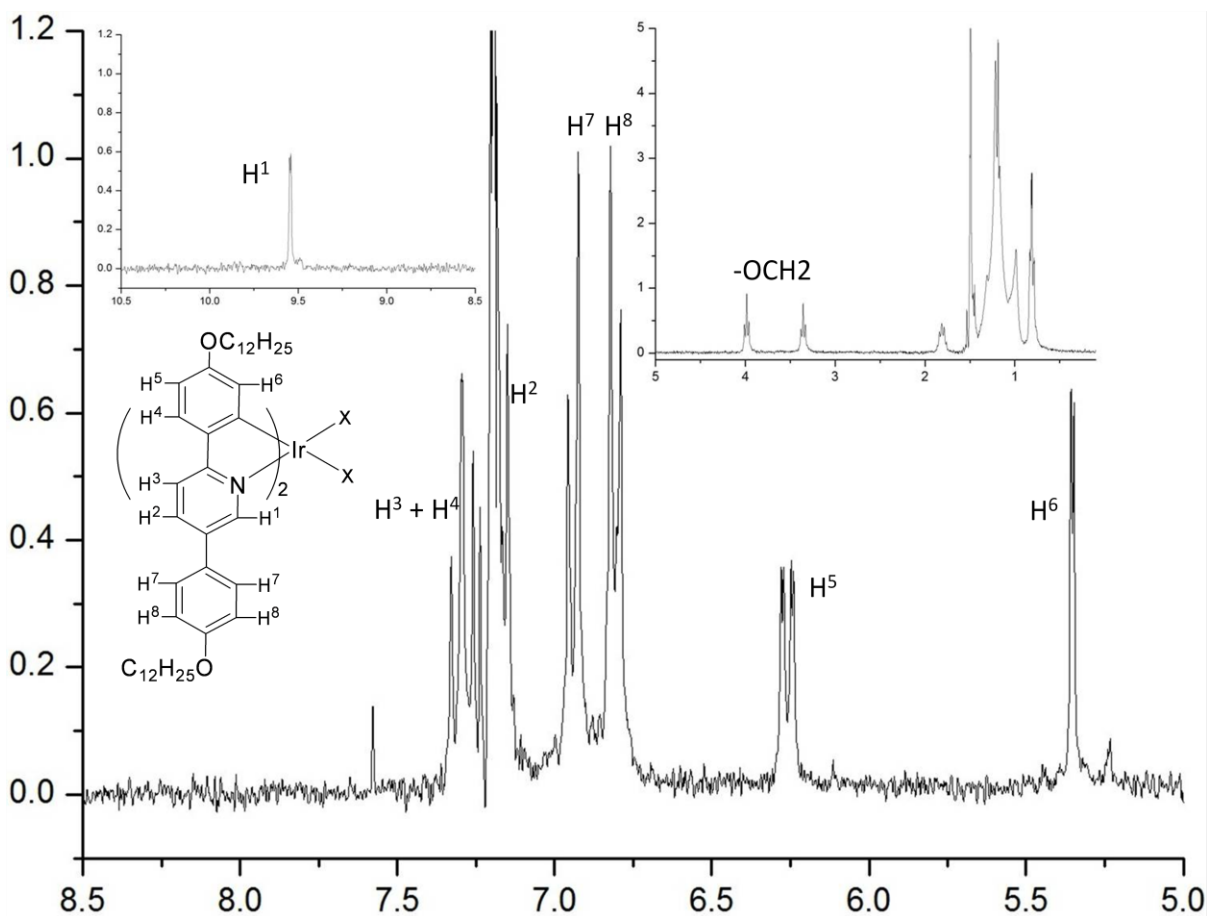

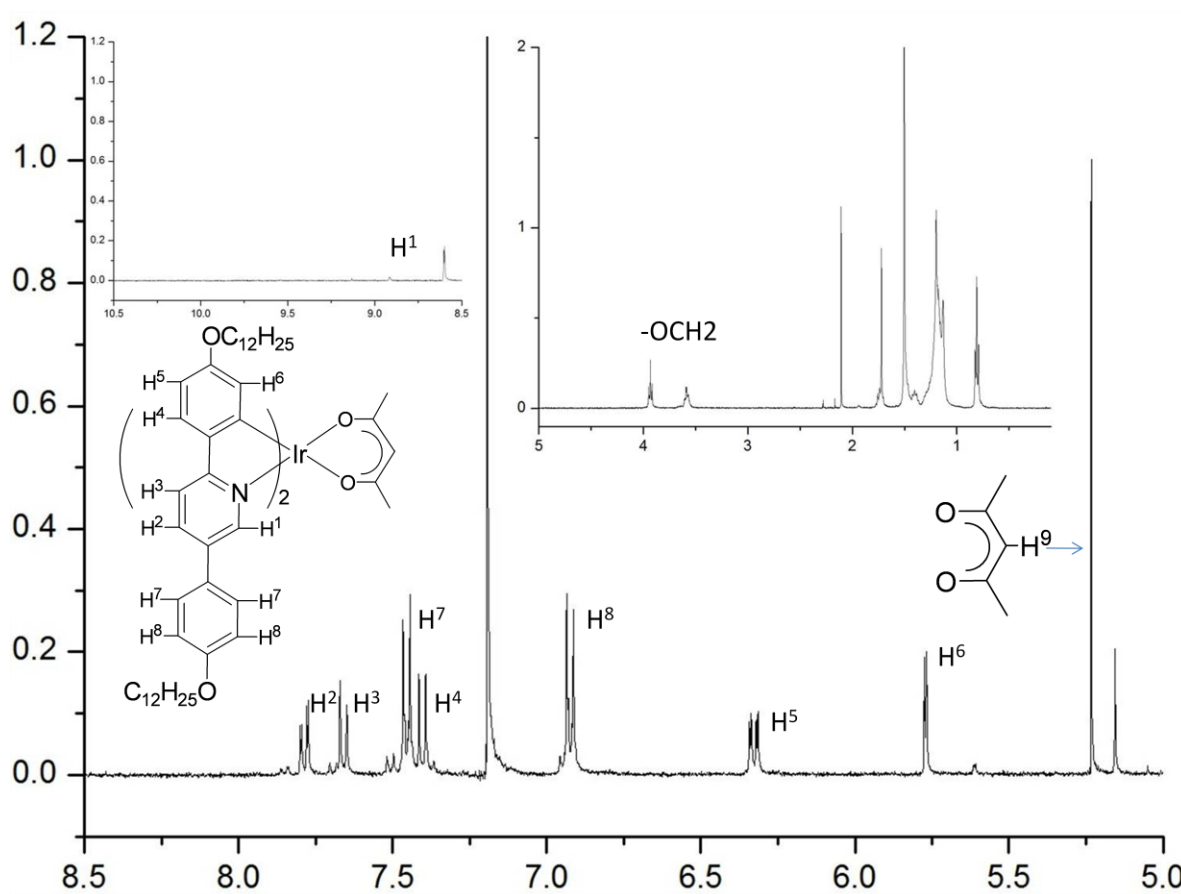**Figure 19-III** ^{1}H-NMR spectrum of complex **29(12)** in CDCl$_3$ at 270 MHz.

Unfortunately, despite many attempts, no single crystals for X-ray analysis were obtained. The only few structural information come from the ^{1}H-NMR spectrum. It showed only one set of signals, implying that the complex **29(12)** is symmetric; indeed there was only one signal from the hydrogen ortho to the pyridine nitrogen. Furthermore the integration showed no protons, apart from the one of the phenylpyridine ligands, (Figure 20).

Further results were obtained from the work of postdoctoral fellow Dr Anton Prokhorov. It

was found that complex **29(12)** gave a positive result in a 'quick and dirty' Beilstein test for the identification of chloride where A copper wire is cleaned and heated in a bunsen burner flame to form a coating of copper(II) oxide. It is then dipped in the sample to be tested and once again heated in a flame. A positive test is indicated by a green flame caused by the formation of a copper halide.[23] A more important result was obtained by the elemental analysis, that showed the complex to be consistent with μ-chloro derivative with respect to its C, H and N values.

In Figure 21 the ^{1}H-NMR spectrum of acetyl acetonate complex **21(12)** is shown. As it is possible to see there is only one set of signals and the clear presence of the methine proton of the acetylacetonate group. Unfortunately this ^{1}H-NMR spectrum is not consistent with the spectrum found in the literature, indeed in the published work of Xu *et al.* they reported for iridium(III)bis[2,5-di(4-ethoxyphenyl)pyridine]acetylacetonate a different sequence of signals[20] (8.57 (s, 2H), 8.18 (m, 4H), 7.67 (m, 6H), 7.11 (d, 4H), 6.42 (d, 2H), 5.57 (s, 2H), 5.32 (s, 1H), 4.10 (m, 4H), 3.75 (m, 4H), 1.75 (s, 6H), 1.37 (t, 6H), 1.11 (t, 6H)). Even if they did not assign the signals, it is still evident that those two complexes are different. The most evident dissimilarity, apart from the small difference in δ, is the absence of two signals in the region between 7.3 and 8.2 ppm. Indeed, they reported the presence of two multiplets at 7.67 (6H) and 8.18 (4H), while complex **21(12)** showed the presence of four signals, doublet at 7.39 (2H), AA'XX' at 7.49 (4H), doublet at 7.65 (2H) and double of doublet at 7.80 (2H). This element influenced strongly the hypothesis on the complex **29(12)**. Indeed, if the acetyl acetonate complex **21** is different from the one reported in the literature but it is still an iridium(III)bis[2,5-di(4-dodecyloxyphenyl)pyridine]acetylacetonate, then the possibility of a different conformation is not absurd, and thus, also complex **29(12)** could be a different
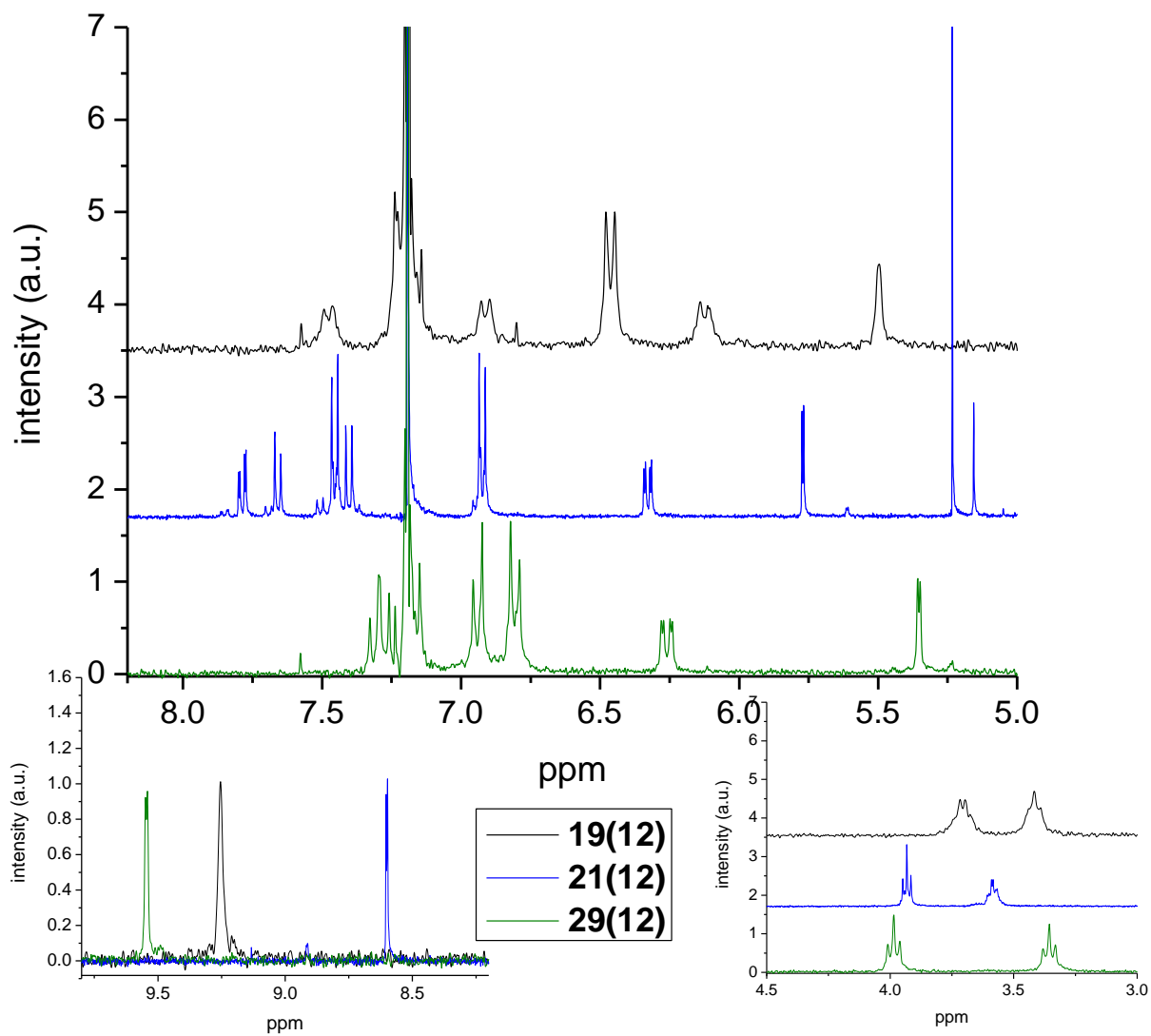
conformation of μ-chloro bridge **19(12)** (Figure 22). In Figure 24 is shown a comparison between the ^{1}H-NMRs of μ-chloro bridge complex **19(12)**, acac complex **21(12)** and unknown complex **29(12)**.

Figure 20-III ^{1}H-NMR spectrum of complex **21(12)** in CDCl$_3$ at 270 MHz
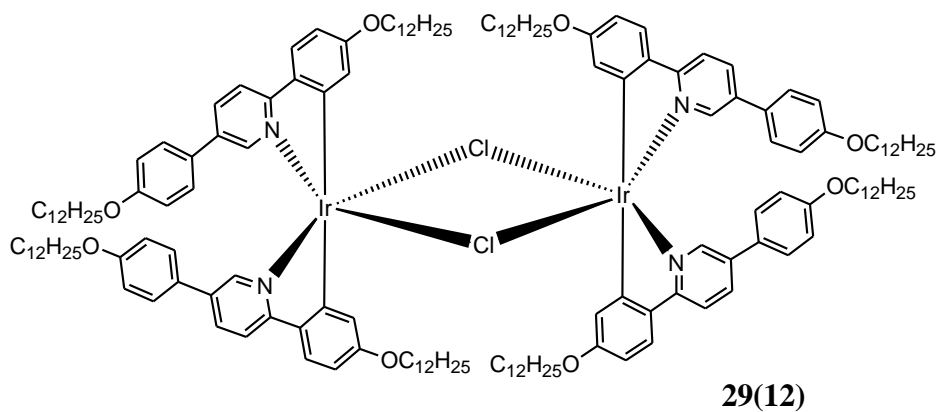
Figure 21-III Proposed structure for complex **29(12)**

Figure 22-III ^{1}H-NMR comparison in CDCl$_3$ at 270 MHz of **19(12)** (black), **21(12)** (blue) and **29(12)** (green).

A recapitulation is needed to clarify the suggested structure. Complex **29** is:

- Formed in the synthesis of μ-chloro bridge **19(12)**.

- Formed in the synthesis of all the monodentate complexes.

- Not formed in the synthesis of the bidentate complexes.

- Formed under several different reaction conditions.

- Formed in different conditions, during the storage of all the monodentate complexes,

but not for bidentate complexes and not for **19(12)**.

- In equilibrium with DMSO complex **20(12)**.

- React with Na(acac) to yield the different acetyl acetonate complex **21(12)**.

- Symmetric.

- Positive Beilstein test.

- In agreement with the CHN analysis.

One hypothesis that could take into account all these information is the formation of a

different μ-chloro bridge, (Figure 23), with the two carbon atoms *trans* instead of the two

nitrogens. This hypothesis is based also on the different luminescent properties of the μ-chloro

bridge, indeed **19(12)** is not luminescent while complex **29(12)** shows a weak luminescence.

This symmetric structure will deal perfectly with the observed reactivity, and will give

positive answers to Beilstein test and CHN analysis. The above structure will also help to

explain the difference in ^{1}H-NMR spectrum between the acetyl acetonate complex **21(12)** and

the one reported in literature. In fact if this rearrangement is considered favourable it is clearly

possible that in the synthesis of complex **21** a conversion takes place with the formation of a

different complex from the one reported by Xu *et al.* However, at this stage it is not yet

possible to exclude other possibilities. For example, because the Beilstein test is not a reliable

analysis, there is another structure that could deal with almost all the information above, and it is shown in Figure 24. Without a doubt this structure provides to be symmetric, and its CHN theoretical values are consistent with the one obtained for μ-chloro bridge complex **29**. The only problem is that several tests were carried out with rigorously absence of atmospheric air and water, but the complex **29** was still formed.
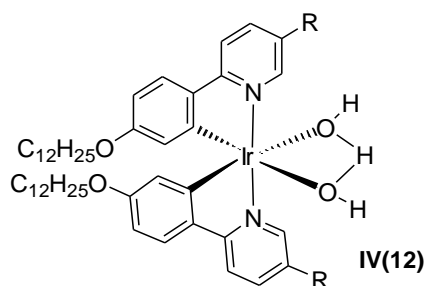
Figure 23-III Alternative structure for complex **29(12)**. R = 4-dodecyloxyphenyl.

At present, efforts are underway to obtain single crystals of complex **21**and **29**, since all the information so far obtained are not unequivocally interpretable. One experiment that could be set to identify the complex in absence of X-ray data is to synthesise another Ir[III] complex using an unsymmetric ligand like the one showed in Figure 25. The idea is to use the different position of the $-OCH_2-$ signals, showed in the ^{1}H-NMR of all the Ir[III] complexes as hint for the structure determination. If the $-OCH_2-$ groups shift that means that in complex **29** the two nitrogens are *trans*, on the other hand if the two $-CH_2-$ groups are those to be shifted that means that the two carbon atoms have to be *trans*.
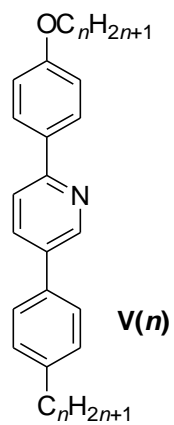
Figure 24-III Structure of asymmetric ligand, for structural identification of complex **29**.

3.3 Conclusion

This part of the work has shown the potential of some iridium(III) complexes, where very interesting liquid crystal properties were discovered. Indeed a completely new class of liquid crystal materials was discovered, namely a structure that does not present a large or a polycatenar ligand to overcome the perturbation due to the presence of octahedral shape but rather two ligands that are not co-planar in the octahedral metal complex. It was found also that monodentate complexes showed lability with the formation of an unknown complex **29(12)**. On the basis of different experiments and observations a structure for complex **29(12)** has been proposed, but the proposal cannot be supported unequivocally. Thus, there are still several aspects that need more attention. The most important is the structure of complex **29(12)**, and thus, more analysis can be carried out such as Chlorine elemental analysis, LiFDI mass spectroscopy, or some specific IR at 200 cm^{-1} for the determination of Cl bonds. If the identification is still unsuccessful the follow strategy could be to attempt to impose the liquid crystal properties from acetylacetonate complex **21(12)** or **25(12)**, the two stable complexes, maybe using some polycatenar system. If the identification will be successful the opportune precautions have to be taken to avoid its formation and to have pure complexes to carry out all the characterisation on the synthesised compounds. After the disclosure of the structure of complex **29(12)** several other complexes can be synthesised having a better understanding of the bases for their liquid crystal properties.

References

1   (a) E. Holder, B. M. Langeveld, U. S. Schubert, *Adv. Mater.*, 2005, **17**, 1109; (b) *Highly Efficient OLEDs with Phosphorescent Materials*, (Ed: H. Yersin) Wiley-VCH, Weinheim, Germany 2008.

2   (a) Y. Kawamura, K. Goushi, J. Brooks, J. J. Brown, H. Sasabe, C. Adachi, *Appl. Phys. Lett.*, 2005, **86**, 071104-1; (b) H. Yersin, *Top Curr. Chem.*, 2004, **241**, 1 (c) A. Adachi, M. A. Baldo, S. R. Forrest, M. E. Thompson, *Appl. Phys. Lett.*, 2000, **77**, 904.

3   A. I. Burshtein, A. A. Neufeld and K. L. Ivanov, *J. Chem. Phys.*, 2001, **115**, 10464.

4   C. Ulbricht, B. Beyer, C. Friebe, A. Winter and U. S. Schubert, *Adv. Mater.*, 2009, **21**, 4418.

5   K. Dedeian, P. I. Djurovich, F. O. Garces, G. Carlson, R. J. Watts, *Inorg. Chem.*, 1991, **30**, 1685;

6   Adachi, M. A. Baldo, S. R. Forrest, S. Lamansky, M. E. Thompson, R. C. Kwong, *Appl. Phys. Lett.*, 2001, **78**, 1622.

7   R.C. Evans, P. Dougles and C. J. Winscom, *Coord. Chem. Rev.*, 2006, **250**, 2093.

8   L. Flamigni, A. Barbieri, C. Sabatini, B. Ventura and F. Barigelletti, *Top Curr. Chem.*, 2007, **281**, 143.

9   (a) M. Ikai, S. Tokito, Y. Sakamoto, T. Suzuki, and Y. Taga, *Appl. Phys. Lett.*, 2001, **79**, 156; (b) C. Adachi, M. A. Baldo, M. E. Thompson, and S. R. Forrest, *J. Appl. Phys.*, 2001, **90**, 5048; (c) S. Lamansky, P. Djurovich, D. Murphy, F. Abdel-Razzaq, H.-E. Lee, C. Adachi, P. E. Burrows, S. R. Forrest, and M. E. Thompson, *J. Am. Chem. Soc.*, 2001, **123**, 4304.

10   (a) A. Tsuboyama, H. Iwawaki, M. Furugori, T. Mukaide, J. Kamatani, S. Igawa, T. Moriyama, S. Miura, T. Takiguchi, S. Okada, M. Hoshino, and K. Ueno, *J. Am. Chem. Soc.*, 2003, **125**, 12971; (b) T. Sajoto, P. I. Djurovich, A. Tamayo, M. Yousufuddin, R. Bau, M. E. Thompson, R. J. Holmes, and S. R. Forrest, *Inorg. Chem.*, 2005, **44**, 7992; (c) S. Lamansky, P. Djurovich, D. Murphy, F. Abdel-Razzaq, R. Kwong, I. Tsyba, M.

Bortz, B. Mui, R. Bau, and M. E. Thompson, *Inorg. Chem.*, 2001, **40**, 1704.

11 (a) J. Barbera, A. Elduque, R. Gimenez, F. J. Lahoz, J. A. Lopez, L. A. Oro, J. L. Serrano, B. Villacampa, and J. Villalba, *Inorg. Chem.*, 1999, **38**, 3085; (b) S. T. Trzaska, and T. M. Swager, *Chem. Mater.*, 1998, **10**, 438; (c) D. W. Bruce, *Adv. Muter.* 1994, **6**, 699. (d) D W Bruce, R Deschenaux, B Donnio and D Guillon. in *Comprehensive Organometallic Chemistry III,* ed. R H Crabtree and D M P Mingos, Elsevier, Oxford, UK, 2006, Vol. 12. Chapter 12.05, pp 195.

12 D. M. Roundhill,in *Photochemistry and Photophysics of Metal Complexes*. Plenum Press, New York, 1994.

13 (a) D. W. Bruce, and X.-H. Liu, *Liq. Cryst.*, 1995, **18**, 165; (b) D. W. Bruce, and X.-H. Liu, *J. Chem. Soc., Chem. Commun.,* 1994, **6**, 729; (c) R. W. Date, E. Fernandez Iglesias, K. E. Rowe, J. M. Elliott and D. W. Bruce, *Dalton Trans.*, 2003, **10**, 1914; (d) K. E. Rowe and D. W. Bruce, *J. Chem. Soc., Dalton Trans.*, 1996, **20**, 3913.

14 A.M. Giroud-Godquin, A. Rassat, and C. R. Seances *Acad. Sci. Ser. 2* 1982, **294**, 241.

15 (a) H. Zheng, and T. M. Swager, *J. Am. Chem. Soc.*, 1994, **116**, 671; (b) S. T. Trzaska, H-. F. Hsu, and T. M. Swager, *J. Am. Chem. Soc.*, 1999, **121**, 4518.

16 S. W. Thomas, S. Yagi, and T. M. Swager, *J. Mater. Chem.*, 2005, **15**, 2829.

17 P. I. Djurovic and M. E. Thompson, in *Highly Efficient OLEDs with Phosphorescent Materials*, (Ed: H. Yersin) Wiley-VCH, Weinheim, Germany 2008, pp 131-161

18 M. Nonoyama, *Bull. Chem. Soc. Jpn.*, 1974, **47**, 767.

19 E. I. Szerb, A. M. Talarico, I. Aiello, A. Crispini, N. Godbert, D. Pucci, T. Pugliese, and M. Ghedini, *Eur. J. Inorg. Chem.*, DOI: 10.1002/ejic.201000462.

20 M. Xu, W. Li, Z. An, Q. Zhou, and G. Wang, *Appl. Organometal. Chem.*, 2005, **19**, 1225.

21 S. Lamansky, P. Djurovich, D. Murphy, F. Abdel-Razzaq, H. Lee, C. Adachi, P. E. Burrows, S. R. Forrest, and M. E. Thompson. *Inorg. Chem.* 2001, **40**: 1704.

22 (a) B. Schmid, F. O. Garces and R. J. Watts, *Inorg. Chem.*, 1993, **33**, 9; (b) W.-S. Sie, J.-Y. Jian, T.-C. Su, G.-H. Lee, H.M. Lee, and K.-B. Shiu, *J. Organomet. Chem.*, 2008, **693**, 1510.

23   F. Beilstein, *Ber. Dtsch. Chem. Ges.,* 1872, **5**, 620.

Chapter 4 Luminescent Properties of Platinum and Iridium Complexes.

4.1 Platinum(II) Complexes

4.1.1 Introduction

4.1.1.1 General Information

During an electronic transition different process can take place, all of them are reported in

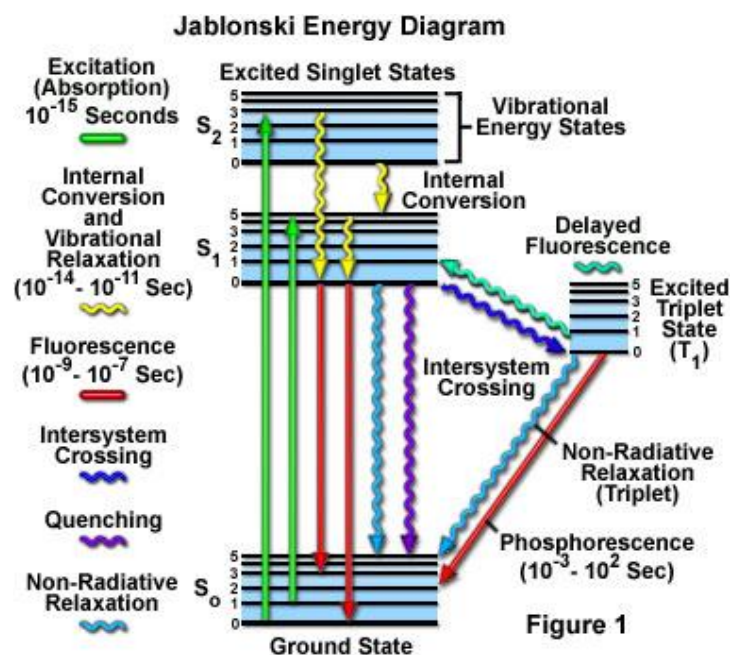the Jablonski diagram in Figure 1 where radiative and non-radiative process are shown.

Figure 1-IV Jablonski diagram of the different electronic and vibrational transition.

Platinum is the third-row element of Group 10 in the transition block of the periodic table. Nickel and palladium belong to the same group, and they are characterised by the fact that the number of electrons on the valence shell can fully fill the d-orbital.

However, in the gas phase, they usually acquire different configurations, such $4s^2\ 3d^8$ nickel(0), $5s^0\ 4d^{10}$ palladium(0) and $6s^1\ 5d^9$ platinum(0). The difference in filling the external shells is essentially due to the size of the atom and to the difference in energy of the orbital levels.

The most common oxidation state for these metals is the +2, with electronic configuration d^8. The simple ligand-field splitting diagram reveals that these metal ions show thermodynamic preference to form square-planar complexes in presence of strong crystal-field, (Figure 2). With this geometry the single unoccupied orbital ($d_{x^2-y^2}$) is pushed to high energy, whilst three of the occupied orbitals are substantially stabilised. For the Ni^{II} though, the most common geometries are octahedral, or tetrahedral when the ligands are sterically demanding, and can be square-planar only when a strong field ligand like CN^- is used. In the case of Pt^{II} and Pd^{II} the ligand field induced by the metal is almost always sufficiently large to ensure their complexes are square-planar.[1] As described in the Chapter 2 (paragraph *2.1.1*) and Chapter 3 (paragraph *3.1.1*) the geometry of Pt^{II} is very important especially having a dramatic influence on the liquid crystalline characteristics of its complexes. Pt^{II} complexes can be also found in a five-coordinate geometry and this property is the reasons in some cases for its peculiar luminescent properties, indeed in a square-planar geometry some time the "vacant" position may be occupied by weakly bound solvent molecules in solution and/or another Pt^{II} metal complex, this aspect will be described in more detail later in this paragraph.
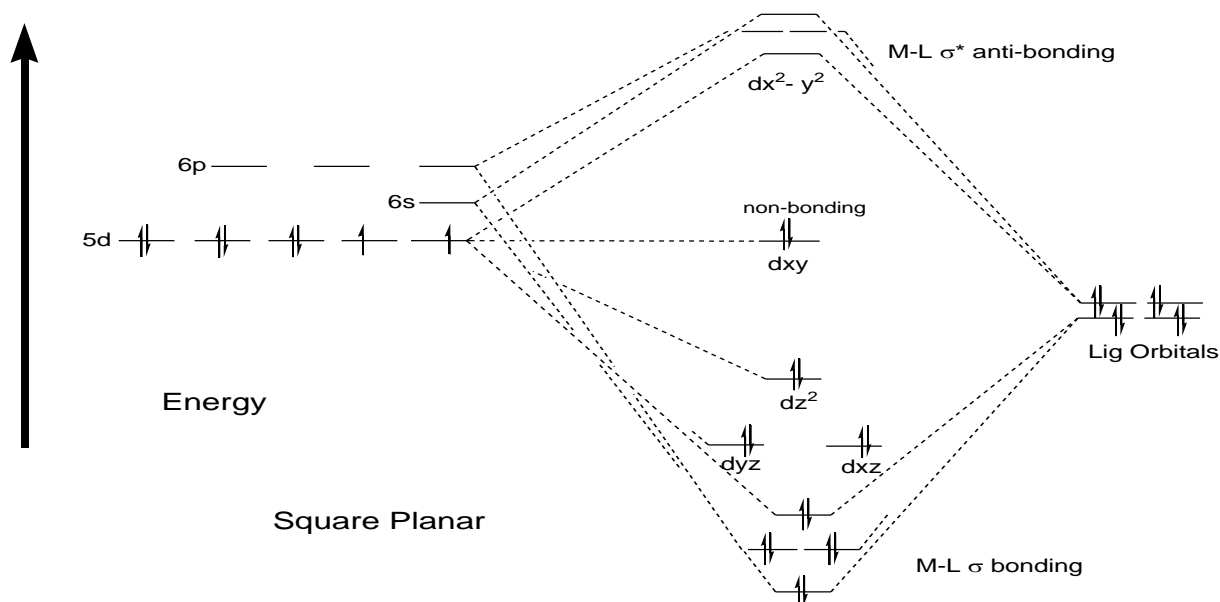
Figure 2-IV Partial molecular-orbital energy level diagram for metal *d*-orbitals in a square-planar geometry with a d^8 configuration. The order of the lower energy levels depends on the ligand set (*e.g.*, relative importance of σ− and π− effect) but the $d_{x^2-y^2}$ is always the highest in energy.

As mentioned above the square-planar geometry is also responsible for many of the photochemical properties of the platinum(II) complexes, making them very different from the other luminescent complexes such as those of Ir[III], Os[II], Rh[III] *etc.*, because most of them are octahedral and in the case of lathanides, they often present an even higher coordination number.

When the complexes are excited, the strongly antibonding orbitals $d_{x^2-y^2}$ can be populated; in this case the molecules could suffer significant distortion with the Pt-L bond lengths increased. This effect can be represented in an simplified diagram in term of *d-d* excited state potential energy that is markedly displaced compared to the ground state potential energy (Figure 3a). This distortion could represent an unfavourable scenario for the emission from the excited state, because it could provide a thermally accessible pathway for an non-radiative emission in the role of an isoenergetic crossing point where an internal conversion or an

intersystem crossing to the ground state can occur.[2]
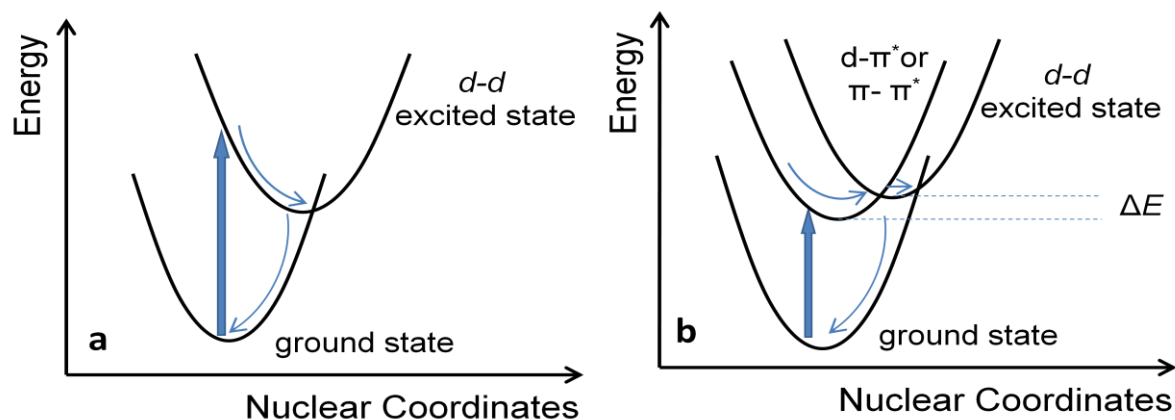
Figure 3-IV (**a**) The distortion due to population of the $d_{x^2-y^2}$ is illustrated by the displacement of the potential energy surface of the excited state compared to the ground state. (**b**) Even if other excited states may lie at lower energies (d-π^* or π-π^*) there is still a concrete possibility of termically accessible non-radiative decay. The blue thick arrow represent the excitation and the thin blue arrows represent the non-radiative decay

One of the consequences of this thermally accessible, non-radiative pathway is that simple platinum(II) complexes, such as $[Pt(NH_3)_4]^{2+}$ or $[PtCl_4]^{2-}$, are unlikely to be luminescent in solution or are, at best, only weakly so. This is also due to the small radiative decay rate of the forbidden d-d transition by Laporte rule. In some cases if the distortion is inhibited, analysing for example the samples at low temperature, an emission may be observed. This is due to the fact that at low temperature the two potential curves are less shifted with respect to one another and the isoenergetic crossing point will be at higher energy, thus, the non radiative decay is partially inhibited and emission could be seen.

The introduction of conjugated aromatic ligands around the metal centre slightly complicates the scenario, introducing also other transitions such as ligand-centered (LC) (π - π^* or n - π^*) and charge-transfer (metal to ligand charge transfer, MLCT, d - π^*) (Figure 3b). A very important parameter in these complexes is the difference in energy, ΔE, between the

transition states. Indeed, if this difference is comparable with kT, the d-d transition can still provide a concrete pathway for a non-radiative emission. Even if other excited states may lie at lower energies (d-π^* or π-π^*) there is still a possibility of a thermally accessible, non-radiative decay. Therefore, the most emissive platinum(II) complexes are generally those where ΔE is large, and this could be obtained either when the emissive state is lower in energy than the d-d what or when the d-d state has been raised to inaccessible energies state. In these cases, ΔE will be too large compared with the kinetic energies of the molecules and the presence of non-radiative decay is less probable.

The square-planar nature of the platinum(II) complexes, as mentioned above, is also the key factor for some of its peculiar luminescent properties. In fact, if ligands with high steric hindrance are avoid, the complexes are essentially flat and this allows the possibility of close metal-metal interactions with the overlaying of their dz^2 orbitals in an end-on manner. This interaction can bring to the formation of weakly bound, $d\sigma$, and anti-bonded, $d\sigma^*$ states, as shown in Figure 4. Thus, formation of dimers in the ground state or excimers in the excited state are possible. One of the implications in the formation of these interactions is that the highest occupied molecular orbital (HOMO) could increase in energy compared to that of the monomer so that the lowest-energy transition will be red shifted. Additionally, a switch of the HOMO level can occur, with a consequent change in the nature of the possible transitions, for example a $d\sigma^*$-π^* (MLCT) instead of a π-π^* (LC) (Figure 4). Similar effect can be obtained also when planar, conjugated aromatic ligands give rise to π-π intermolecular interactions.
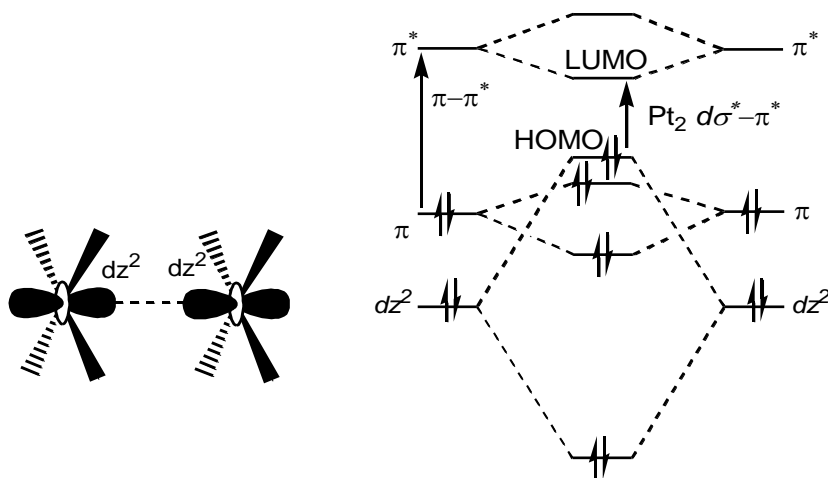
Figure 4-IV Simplified diagram of the possible face-face interaction of the square-planar platinum(II) complexes.

A further and very important property is the large spin-orbit coupling constant, ξ, possessed by platinum ions and shared with other third-row and many second-row transition metal ions. The spin-orbit coupling promotes rapid intersystem crossing (ISC) between the singlet excited state and the triplet excited state.

For excited states with significant contributions of metal orbitals, ISC is normally thought to occur at a rate constant of the order of 10^{12} s^{-1} which is much greater than the rate constant for radiative emission from singlet state (fluorescence, ~ 10^8 s^{-1}). Therefore, emission from platinum(II) complexes is anticipated to emanate from the triplet state (phosphorescence), unless the excited state is localised on a remote part on the ligand with little or no interaction with the metal centre. Emission from triplet states, is formally a forbidden process in pure organic system, since it is too slow (τ ≤ 10^3 s^{-1}) to allow phosphorescence to compete with non-radiative decay at room temperature. However in the case of platinum(II) ions this constant rate is increased to $10^5 – 10^7$ s^{-1}, high enough to compete with the other non-radiative processes. Thus, provided that non-radiative decay pathways do not increase the rate of non-

radiative proceses, phosphorescent emission can be seen on a microsecond timescale.

Although only a few d^8 metal complexes are known to be emissive in fluid solution at room temperature, compared to the d^6 metal ions that will be described later, the phosphorescence of platinum(II) complexes has been well documented only in recent years.[3] Indeed the triplet emissions from Pt[II] complexes at room temperature in solution were reported for the first time in late 1980s.[4] A different scenario belongs to the other two metals of the group. Ni[II] does not show any ability to facilitate intersystem crossing due to the very weak spin-orbit coupling. This is also true for Pd[II], thus phosphorescent palladium(II) complexes are rare compared with platinum(II), and palladium(II) complexes mostly display very weak triplet emission but only at low temperature.[5] Several different platinum complexes have been reported,[3] and some of them have been tested in prototype devices with good results.[6]

As mentioned before, the presence of low-lying, metal-centred excited states provides a facile radiationless deactivation pathway *via* the intermolecular distortion. This problem can be reduced by increasing ΔE, either utilising ligands with lower-lying excited-state orbitals and/or using ligands with a strong ligand field effect to increase the energy of the metal *d-d* states. In the next part of the chapter, attention will be focused on derivatives of 2-phenylpyridine ligands in complexes with platinum(II) and iridium(III).

4.1.1.2 Cyclometallated Complexes of Platinum(II)

*Cyclometallation* is defined as the phenomenon occuring when a polydentate ligand is bound to a metal *via* a covalent metal-carbon bond while the remaining bonds are normally with heteroatoms such as nitrogen. A classic cyclometallated ligand is the 2-phenylpyridine and its derivatives. Their strong ligand-field raises the energy of the non-radiative *d-d*

transition so that the LUMO is a mix of metal-ligand orbitals and, therefore, there will be a higher probability of a MLCT transition with extensive spin-orbit coupling, facilitating therefore emission from the triplet state. These properties are based on the fact that the anionic carbon is a strong σ-donor and the nitrogen a good π-acceptor.[6b,7] Thus, these molecules act as anionic, bidentate or polydentate ligands whose coordination sites are the nitrogen atom of the pyridine ring and the *ortho*-carbon atom of the phenyl ring. As such they can complex a variety of second- and third-row transition metal ions, and the complexes so formed are rather inert due to the chelate effect and the good ligating ability of both atoms.

4.1.1.3 Cyclometallated Platinum(II) Complexes

One of the most studied classes of ligands with square-planar Pt^{II} is tridenate systems. In the obtained complexes the origin of the emission depends strongly on the substituent on the cyclometallated ligands and also on the coordination mode of the ligand (N^N^C, C^N^C, N^C^N).[8] Interesting results were obtained by Williams *et al.*[9] using N^C^N-coordinating dipyridylbenzene ligand. These complexes show intense green emission with an exceptional high phosphorescent quantum yield (Φ_P = 0.58-0.68). Another important work, using the same ligand system, was reported by Kozhevnikov *et al.*[10] In this case the importance arises from the control of the luminescent emission on the basis of liquid crystal properties. This complex (Figure 5) in the liquid crystal phase (Col$_r$) shows an intense emission at 575 and 624 nm while in the isotropic state it shows an excimer broad emission at 660 nm. Unfortunately no solid-state quantum yield was reported and the quantum yield in solution appeared to be very poor (Φ_P = 0.07). The reasons of this different luminescent behavior can be attributed to the

formation of an excimer in the isotropic phase as the spectra are broad and largely red-shifted.
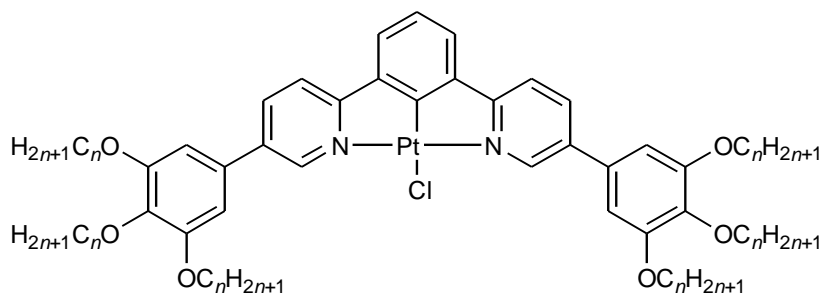
Figure 5-IV Pt^{II} complex of 1,3-di(2-pyridyl)benzenes. With R = OC$_6$H$_{13}$ Cr · 126 · Col$_r$ · 187 · I.

The luminescent properties, as mentioned above, are influenced from several different aspects such as structure and coordination mode of the ligands, substituents on the emitting unit with their relative positions and also structure and nature of the auxiliary ligands. All these parameters make it difficult to generalise and foresee the emission properties of a particular complex.

4.1.1.4 Ancillary ligands on 2-phenypyridine platinum(II) complexes.

There are almost an infinite number of ligands and combination thereof that can be used in the structure shown in Figure 6. For example L and L´ can be the same monodentate atoms such as [Pt(2-phenylpyridine)Cl$_2$]$^-$,[11] or the same atoms of a bidentate ligand such as [Pt(2-phenylpyridine)ethylenediamine]$^+$,[11] and [Pt(2-phenylpyridine)bipyridine]$^{+11}$ or [Pt(2-phenylpyridine)(acac)],[12] and [Pt(2-phenylpyridine)(diphenylpropandionate)].[13] As mentioned above, the presence of different auxiliary ligands can influence the luminescent properties of the complexes, since their electron-donating or electron-withdrawing character can increase or
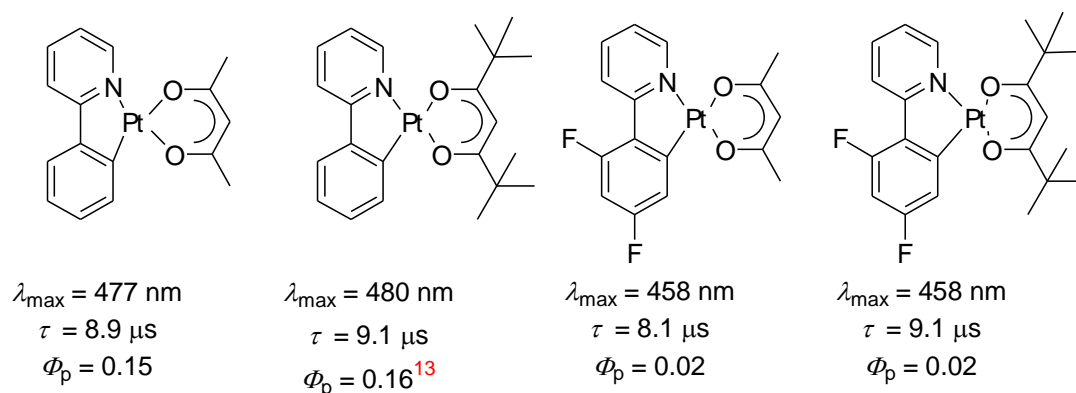
decrease the amount of electronic density on the metal and thus, modify the amount of MLCT character mixed with the lowest-energy transition, altering the wavelength emission and the lifetime.[12] In this respect a interesting work was made by Kvam and co-worker[11] investigating the absorption and the emission properties of the complexes **a-d** in Figure 6 two chlorine atoms, 1,2-ethylendiammine, 2,2′-bipyridine and 1,10-phenanthroline.

a L = L′ = Cl
b L-L′ = 1,2-ethylendiamine
c L-L′ = 2,2′-bipyridine
d L-L′ = 1,10-phenanthroline
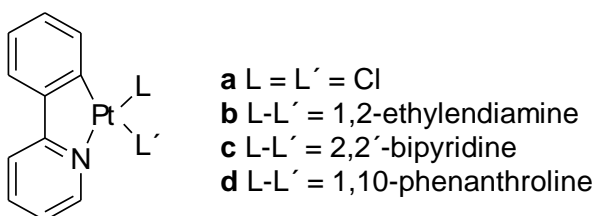
Figure 6-IV 2-Phenylpyridine platinum(II) complex.

The presence of weak-field chlorine ligands switches off the luminescence at room temperature, indeed [Pt(phpy)Cl$_2$]$^-$ complexes provide to be luminescent only at 77 K. This strong temperature dependence was due to the decreased energy gap between the ^{3}MLCT and the deactivating *d-d* state, therefore, as described in above, a non-radiative deactivating pathway is accessible at room temperature. A different situation was described for the stronger-field derivatives (1,2-ethylendiammine, 2,2′-bipyridine and 1,10-phenathroline), and all of them provided to be luminescent in DMF solution at room temperature with $\lambda_{max} \sim 486$ nm and microsecond lifetimes. For all the complexes, the emission wavelength was reported to be very similar even if, with the assistance of electrochemical data, they reported triplet emissions of a different nature. For the 1,2-ethylendiamine complex **b**, $d_{Pt} \rightarrow \pi^*_{(N^\wedge C)}$ was observed, while the 2,2′-bipyridine **c** and 1,10-phenathroline **d** complexes presented a $d_{Pt} \rightarrow \pi^*_{(N^\wedge N)}$ transition.
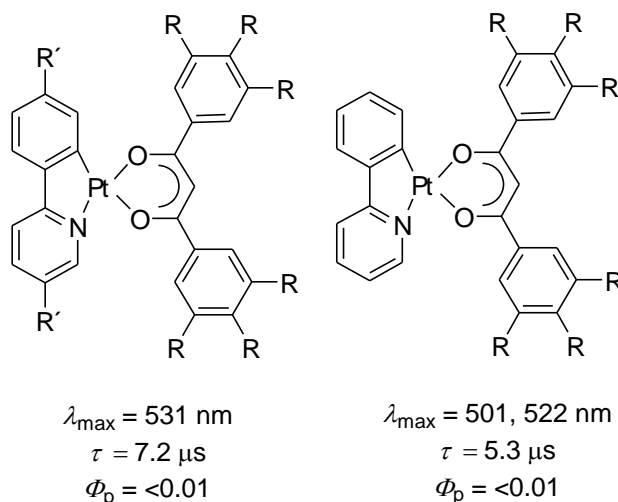
Further information was reported by Brooks *et al.*,[12] one of the pioneering groups in the research of triplet emitter for OLEDs application. They analysed more than twenty different complexes based on the N^C chelating system, including several containing substituent on the 2-phenylpyridine ligand. They also investigated two different ancillary group such as acetylacetonate (acac) and dipivaloylmethane (dpm) with the motivation of solubility problems, reporting no significant effect on the luminescent properties. DFT (density functional theory) calculations on [Pt(phpy)(acac)] suggest that the HOMO consists of a mixture of phenyl, Pt^{II} and acac orbitals while the LUMO is predominantly dominated by 2-phenylpyridine character. No real difference was observed for complexes bearing different ancillary ligands (Figure 7).

λ_{max} = 477 nm
τ = 8.9 µs
Φ_p = 0.15

λ_{max} = 480 nm
τ = 9.1 µs
Φ_p = 0.16[13]

λ_{max} = 458 nm
τ = 8.1 µs
Φ_p = 0.02

λ_{max} = 458 nm
τ = 9.1 µs
Φ_p = 0.02

Figure 7-IV Different platinum(II) complexes that show similar luminescent properties. The wavelengths and the lifetimes are obtained at 77 K in 2-methyltetrahydrofuran. Φ_p was taken at 298 K. Data from reference.[12]

Thomas and co-workers[13] reported a different behaviour for square-planar complexes of platinum(II) containing 2-phenylpyridine and the 1,3-diphenyl-1,3-propandionato ligands. Thus, in general the emission wavelengths were shifted bathochromically (24 nm) if compared with the model compound [Pt(phpy)acac], due to the extended conjugation of the auxiliary

group. More importantly in these compounds, the presence of diphenyl β-diketonate drastically decreased the quantum yield and lifetime of the phosphorescence in THF (Figure 8).


$$\lambda_{max} = 531 \text{ nm}$$
$$\tau = 7.2 \text{ } \mu s$$
$$\Phi_p = <0.01$$

$$\lambda_{max} = 501, 522 \text{ nm}$$
$$\tau = 5.3 \text{ } \mu s$$
$$\Phi_p = <0.01$$

Figure 8-IV [Pt(phpy)diphpropandione], R = -OC$_{10}$H$_{21}$ and R′ = -C$_{12}$H$_{25}$. The wavelengths and the lifetimes are obtained at 77 K in tetrahydrofuran. Φ_p was taken at 298 K

Thomas *et al.*[13] proposed that the reduction in efficiency is due to stabilisation of a MO localised on the acac to a level close to yet above the LUMO centred on the 2-phpy ligand. They argue that the diPhacac-based MO is in thermal equilibrium with the LUMO so reducing emission efficiency. They claim further support for this from the observation that in cyclohexane solution at room temperature, complexes with the diphenylacac ligand show good emission efficiency (25-30%) and long excited-state lifetimes ($\approx$2 μs), whereas in THF, efficiencies are less than 1% and lifetimes are in the ns time regime. They hold that the Pt-diketone CT states are more polar and therefore perturbed by the polar THF.

An alternative explanation is that this could be due to the stabilisation of a molecular orbital largely localised on the acac ligand so that it actually becomes the LUMO, changing the nature
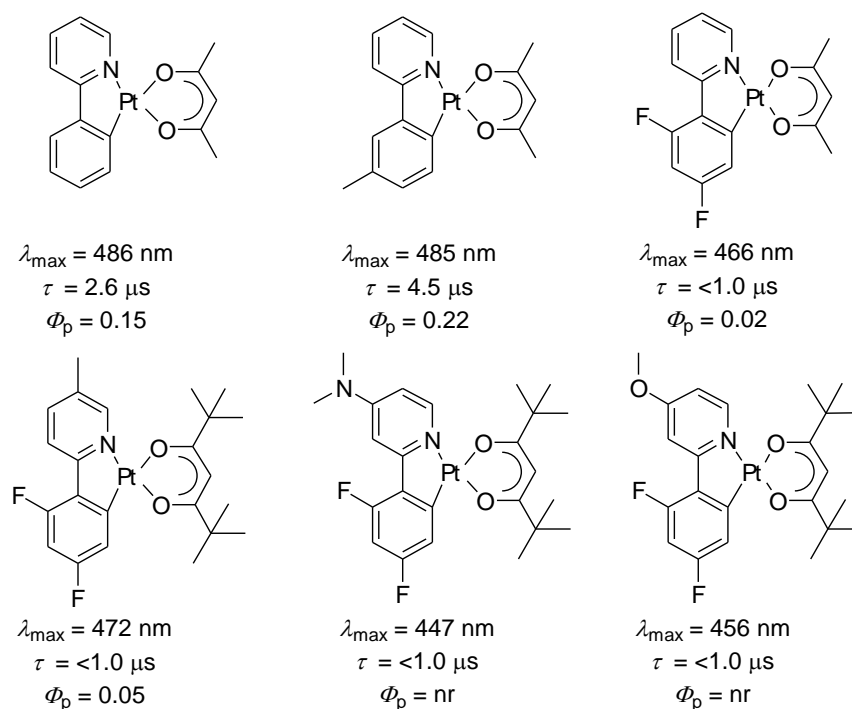
of the transition and reducing emission efficiency. Support for this comes from DFT calculations reported by Ghedini *et al.*[14] who showed that the LUMO + 1 of the [Pt(2-phpy)(acac)] is basically acac in character, and the LUMO is univocally 2-phenylpyridine and metal in character. Replacing acac by hfac stabilised LUMO + 1 so that it became the LUMO, so switching off luminescence. Thus, it could also be the case that replacing acac by diPhacac similarly stabilises LUMO + 1, once more compromising luminescence efficiency. Directly analogous arguments are used by Lamansky *et al.*[15] to account for the switching off of the luminescence properties of [Ir(2-phpy)₂(L-L)] complexes when L-L = acac is replaced by L-L = diPhacac.

LUMO + 1
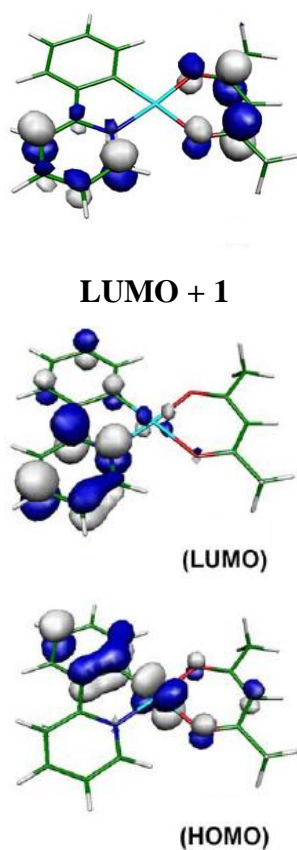
(LUMO)

(HOMO)

Figure 9-IV TD-DFT computational model of HOMO and LUMO orbitals of [Pt(2-phpy)(acac)].[14] Printed with the authorisation of the corresponding authors.

4.1.1.5 Effect of substituents on 2-phenylpyridine platinum(II) complexes.

Almost all the compounds mentioned above are intensely luminescent at 77 K, and several are also quite strongly luminescent at in solution room temperature. The emission can be associated to a predominant [3]MLCT character. Thus, the introduction of an electron-withdrawing group on the ligand such as –F or –CF_3 in 4´ and 6´ position of the phenyl ring induces an hypsochromic shift as the HOMO is stabilised and therefore its reduced energy increase the energy gap (Figure 10). A similar effect was obtained with the introduction of electro-donating group such as –OCH_3 or –$N(CH_3)_2$ on the pyridyl ring, inducing an increase in the energy of the LUMO, obtaining thus the same hypsochromic shift (Figure 10).[12] The two variations can be combined and, since the effects are qualitatively additive, the result would be a quite substantial blue shift.[1]

λ_{max} = 486 nm
τ = 2.6 µs
Φ_p = 0.15

λ_{max} = 485 nm
τ = 4.5 µs
Φ_p = 0.22

λ_{max} = 466 nm
τ = <1.0 µs
Φ_p = 0.02

λ_{max} = 472 nm
τ = <1.0 µs
Φ_p = 0.05

λ_{max} = 447 nm
τ = <1.0 µs
Φ_p = nr

λ_{max} = 456 nm
τ = <1.0 µs
Φ_p = nr

Figure 10-IV Substituent effect on the luminescent properties of 2-phenylpyridine platinum(II) complexes. Wavelengths, lifetimes and quantum yields are obtained at 298 K in 2-methyltetrahydrofuran. nr = not reported

Despite the high energy emission, these blue-shifted complexes scarcely emit at room temperature. Presumably the high-lying LUMO could match the high-lying MC, therefore generating a non-radiative process.

On the other hand, bathochromic shift (red shift) can be achieved by extending the π-systems or introducing more polarisable atoms in the aromatic ring. In general more extended electronic delocalisation causes a lowering of the ligand-centred LUMO, in turn resulting in the lower-lying of both of ^{3}MLCT and ^{3}LC nature.[1] Also in this case, several complexes were investigated by Thompson's group[12] highlighting the different emission characteristics (Figure 11). The longer lifetime, especially for benzoquinoline derivate, can be indicative of a greater ^{3}LC character in the excited state due to both the decreased energy of the ^{3}LC and the weaker metal-ligand interaction.[16]

$\lambda_{max} = 550$ nm
$\tau = 20.4$ μs
$\Phi_p = 0.11$

$\lambda_{max} = 493$ nm
$\tau = 122$ μs
$\Phi_p = $ nr

$\lambda_{max} = 555$ nm
$\tau = 10.3$ μs
$\Phi_p = $ nr
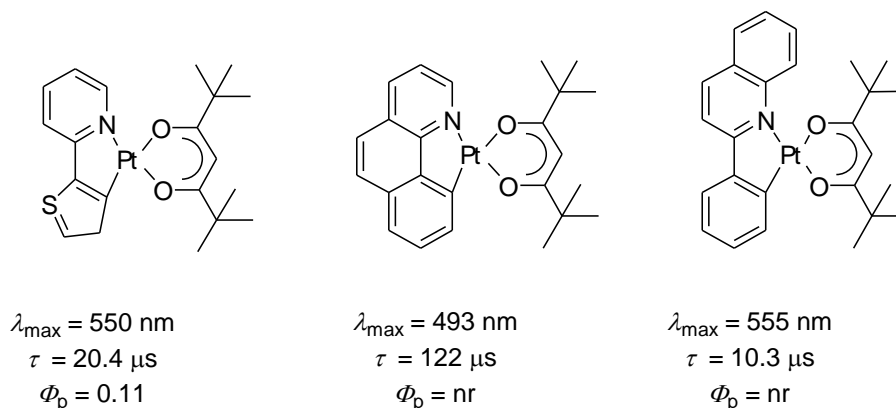
Figure 11-IV More polarisable atoms or an elongated π-system affect the luminescent properties of the platinum(II) complexes. The wavelengths and the lifetimes are obtained at 77 K in 2-methyltetrahydrofuran. Φ_p was taken at 298 K

4.1.2 Luminescent Properties of the Synthesised Platinum(II) Complexes
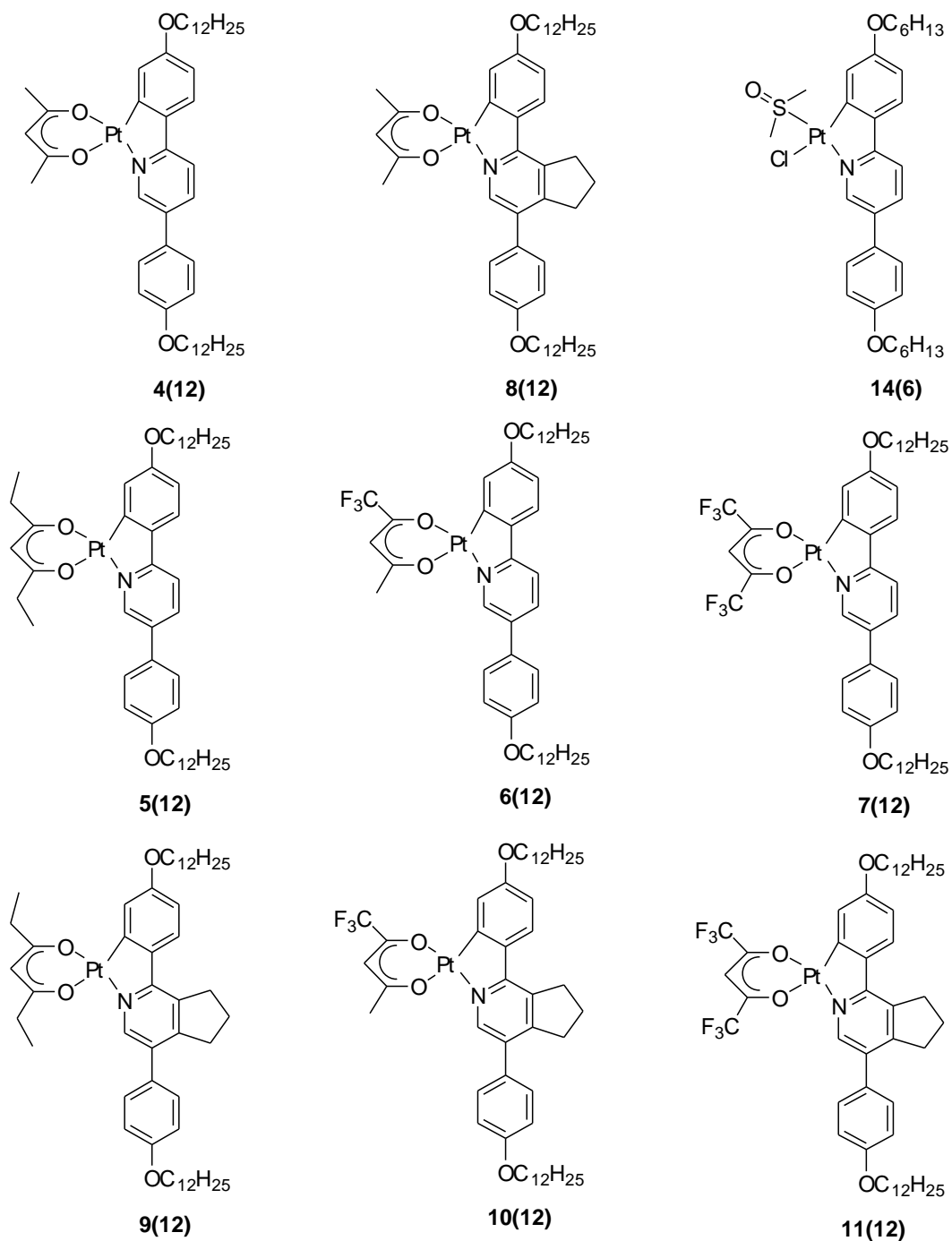
Figure 12-IV 2,5-dialkoxyphenyl-pyridine platinum(II) complexes.

All the complexes herein described were analysed at the Department of Chemistry in the University of Durham by Dr Gareth Williams. The samples were analysed in CH_2Cl_2 solution with an approximate concentration of 10^{-4} M. They were degassed applying three freeze-pump-thaw cycles. All the quantum yields were calculated using $[Ru(bpy)_3]Cl_2$ in air-equilibrated aqueous solution as standard; furthermore, the spectra were corrected for the wavelength dependence of the detector. On the other hand, the lifetime at room temperature and 77 K was measured in air-equilibrated ethanol-isopentane-ether (2:2:1) glass.

The luminescence properties of the complexes (Figure 12) in dichloromethane solution are discussed first, followed by the behaviour of **4(12)** and **8(12)** in solid and liquid crystal phases and in films. Apart from complexes **7(12)** and **11(12)**, all the other complexes are emissive in solution at room temperature.

The chain length was found to have no influence on the solution luminescence wavelength (Figure 13), but as will be describe later it may have an influence on the quantum yield. Emission quenching under the interaction with O_2 also occurs readily in air-equilibrated samples, so degassing with argon or with freeze-vacuum cycle is necessary; Figure 14 shows the reduction in luminescence of an air-equilibrated sample.

The compounds with twelve carbon atoms in the chain were selected to undergo more detailed studies, for which the solution data are summarised in Tables 1 and 2. Corresponding data for the known complex [Pt(2-phenylpyridine)(acetylacetonate)] (**M**) are also included for comparison. Representative spectra for **8(12)** are shown in Figure 15.
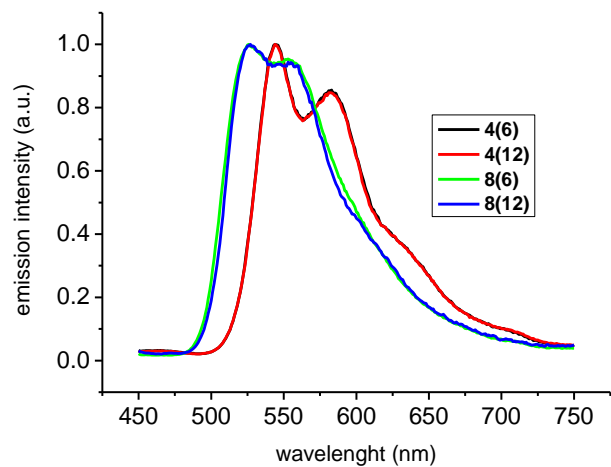
Figure 13-IV Emission spectra of Pt^{II} complexes with different chains length. **4(6)** and **4(12)**; **8(6)** and **8(12)**. (Conc. ca. $1 \cdot 10^{-5}$)
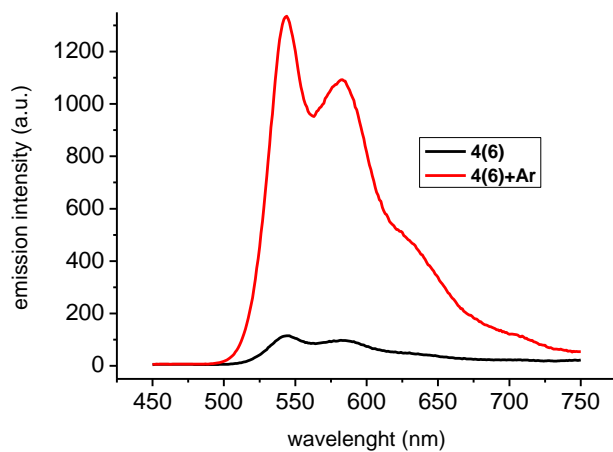
Figure 14-IV The effect of air equilibration (O_2 quenching) on emission spectra of **4(6)** in CH_2Cl_2 solution at 298 K. (Conc. ca. $1 \cdot 10^{-5}$)
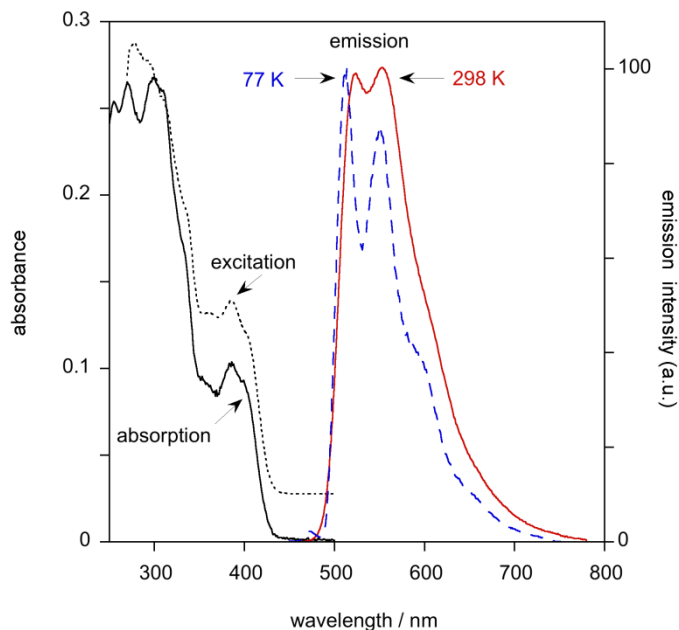
Figure 15-IV Absorption, excitation (λ_{em} = 545 nm) and emission (λ_{ex} = 400 nm) spectra of **8(12)** in CH$_2$Cl$_2$ solution at 298 K, and the emission spectrum at 77 K in an ethanol-isopentane-ether glass (2:2:1).

4.1.2.1 Complexes **4(12)**, **8(12)** and **14(6)**

The absorption spectra of the complexes **4(12)**, **8(12)** and **M** in CH$_2$Cl$_2$ show three distinct absorption peaks and one shoulder at about 400 nm. In particular, the high energy (λ <350 nm), more intense absorption bands may be attributed to allowed $\pi \rightarrow \pi^*$ (240-300 nm) and the corresponding $n \rightarrow \pi^*$ transitions (300-350 nm) of the platinum(II) complexes. As a consequence of the cyclometallation, and thus of the mixing of the metals and ligands orbitals, these transition bands result to be red-shift with respect to free ligand. The absorption bands in the range of 340-450 nm may be assigned to metal-ligand charge transfer (MLCT) transitions (Figure 16).[17] The lowest-energy absorption maximum is red-shifted compared to that of **M**, sign of a lower-lying MLCT. A more pronounced red-shift is observed in emission, but the effect is smaller for the fused-ring complex **8(12)** than for **4(12)**, being the emission maxima at

298 K 523 and 541 nm respectively, compared to 485 nm for **M** (Figure 16). The lowering in energy of the emissive state upon introduction of electron-donating alkoxy substituents into the phenyl ring of the 2-phenylpyridine is anticipated from the destabilization of the HOMO, which is typically localised on the metal, and from the cyclometallating phenyl ring. A similar effect was previously observed for the 5-methoxy-substituted complex prepared by Brooks *et al.*[12].

In the present case, the simultaneous introduction of the aryl group into position-5 of the pyridyl ring has no effect on the HOMO and probably does not have large effect on the LUMO either, such that there is a net decrease in the energy gap between the excited state and the ground state, leading to a red-shift. The higher energy of the emissive state of **8(12)** is likely to be due to the steric influence of the *ortho*-CH_2 groups of the cyclopentene ring which reduces the planar structure that would maximise conjugation between the rings, as it is shown in the crystal structure.
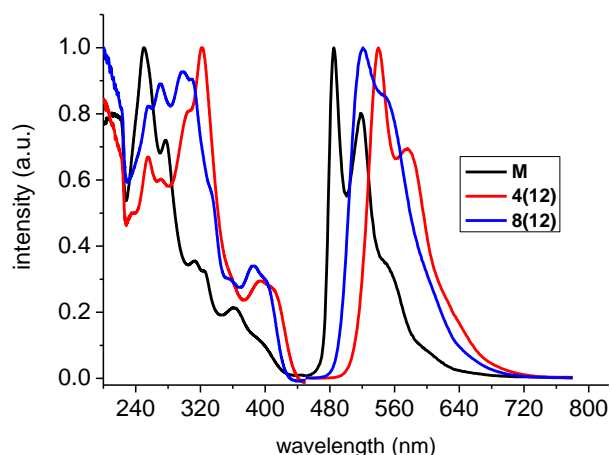
Figure 16-IV Absorption and emission spectra of **4(12)** and **8(12)** in CH_2Cl_2 solution at 298 K ($\lambda_{ex} = 400$ nm), together with that of [Pt(ppy)(acac)] (**M**) for comparison. (Conc. ca. $1 \cdot 10^{-5}$)

Complexes **4(12)** and **8(12)** are very brightly luminescent, with emission lifetimes at room temperature of 27 μs. [18] The quantum yields at room temperature are around 0.5, considerably superior to those of **I**. Indeed, the values are competitive with the brightest Pt-based emitters, and appear to be the highest hitherto reported with 2-phenylpyridine-type ligands.[1]

The observation that the luminescence lifetimes are essentially the same at 77 K as at 298 K is poof of the absence of any significant thermally activated non-radiative decay pathways at ambient temperature.[19]The intermediates formed by cleavage of the μ-chloro bridge dimer with dimethylsulfoxide **14(6)** are also luminescent, although of an order of magnitude weaker than the acac derivatives **4(12)** and **8(12)**. The lower efficiency at room temperature and the exceptionally long lifetime of 78 μs recorded at 77 K could be due primarily to a lower radiative decay rate constant, rather than to elevated non-radiative decay pathways. Possibly the metal orbitals are energetically less well placed for mixing with the π-orbitals of the cyclometallating ligand in the DMSO adducts, owing to a more weakly donating set of ancillary ligands, so that the excited state has greater ^{3}LC character.

Table 1-IV Absorption and emission data for Pt complexes and the model [Pt(ppy)(acac)], in CH_2Cl_2 at 298 ($\pm$3)

	4(12)	**8(12)**	**M**	**14(6)**
Absorption – λ_{max}/nm	400, 322, 305, 272, 255	400(sh), 386, 298, 271, 356	393(sh), 362, 325, 312, 278, 248	397, 317, 260
$\Sigma/10^4$ M^{-1} cm^{-1} (λ/nm)	3.05 (322)	2.82 (298)	2.72 (248)	2.89 (317)
Emission – λ_{max} / nm	541, 582, 628(sh)	523, 553, 608(sh)	485, 520, 551	550, 588
τ degassed (aerated)/μs	27 (0.55)	27 (0.38)	2.6 (0.45)	23 (0.80)
Φ_{lum}	0.49	0.57	0.16	0.08
Emission 77 K [a] λ_{max} / nm	526, 562	512, 552, 594	480 [b]	532, 574, 616
τ 77 K / μs [a]	31	25	9.0 [b]	78

(a) In ether–isopentane–ethanol (2:2:1). *(b)* In 2-methyltetrahydrofuran; data from reference.[12]

4.1.2.2 Complexes 5(12), 6(12) and 7(12), 9(12), 10(12) and 11(12)

Also these complexes are brightly luminescent (with the exception of **7(12)** and **11(12)**), their quantum yields are in fact all above 0.5 (Table 2). In general the measurements of quantum yields have an error of ±10%, making a comparison of the quantum yields of the complexes difficult. What is clear is that this complexes are as luminescent or perhaps more luminescent than the acetylacetonate complexes **4(12)** and **8(12)**. Lifetimes of the complexes at room temperature follow in the range from 26-30 µs, comparable with those described above, with the exception of **10(12)**, which has a shorter lifetime of 13 µs. The reasons for this shorter lifetime are not clear yet, particularly as homologues **6(12)** and **8(12)** do not show any different behaviour in lifetime value. It is possible that the combined effects of cyclopentene and trifluorinated acetylacetonate decrease the amount of ^{3}LC character favouring the ^{3}MLCT character in the emitting state.

Table 2-IV Absorption and emission data for Pt complexes in CH_2Cl_2 at 298 (±3)

	5(12)	6(12)	7(12)	9(12)	10(12)	11(12)
Absorption λ_{max}/nm	397, 323	392, 318)	391, 314	386, 360	379, 307	379, 304
	306, 270	303, 266	262, 241	309, 298	265, 252	332, 293
	256, 235	250		271, 256		263, 244
				241		
Σ/10^4 M^{-1} cm^{-1} (λ/nm)	323 (3.01)	318 (3.45)	314 (3.25)	309 (2.86)	307 (2.81)	304 (2.82)
Emission λ_{max} / nm	545, 583	544, 581	-	526, 554	525, 555	-
τ degassed (aerated) µs	30 (0.50)	26 (0.56)	-	26 (0.37)	13 (0.35)	-
Φ_{lum}	0.62	0.70	-	0.61	0.53	-

Figure 17 shows an overlay of the emission spectra of all the complexes and a comparison

of the two acetylacetonate complexes, **4(12)** and **8(12)** described above.

4.1.2.3 Platinum(II) hexafluoroacetylacetonate complexes

As described by Brooks and co-workers[12] for [Pt(phpy)(acac)], the HOMO is only partially localised on the *β*-diketone, and the LUMO is predominantly 2-phenylpyridine in character (Figure 18, left), thus, it is not surprising that the presence of a single –CF$_3$ group does not influence the emission characteristics of the complexes. However, what is surprising is the fact the hexafluorinated complexes **7(12)** and **11(12)** are not luminescent at all.
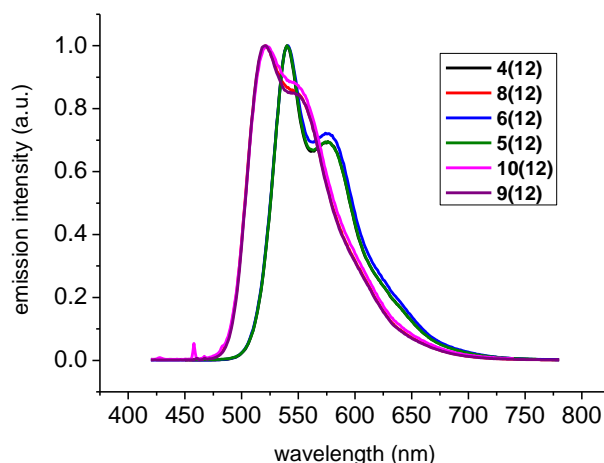
Figure 17-IV Emission spectra of Pt[II] complexes, bearing acetylacetonate **4(12)** and **8(12)**; trifluoroacetylacetonate **6(12)** and **10(12)**; and heptandionate **5(12)** and **9(12)**.

Ghedini *et al.*[14] in 2008 reported that the introduction of six electron-withdrawing fluorine atoms using hexafluoroacetylacetonate, affects the HOMO of [Pt(phpy)(hfacac)], but more importantly it affects the LUMO to such an extent that no luminescence occurs at all (Figure 18, right). What was reported was that although generally the LUMO is characterised by the

contribution of phenyl, metal and acetylacetonate character, there is a LUMO+1 at higher energy with a predominant, almost exclusive β-diketone character. When six fluorine atoms are introduced on the ancillary substituent, they stabilise LUMO+1 to the extent that a switch between the two different molecular orbitals takes place so that the LUMO is now the orbitals localise on the hfac. It is this new organisation of the emitting state that compromises the luminescent properties.
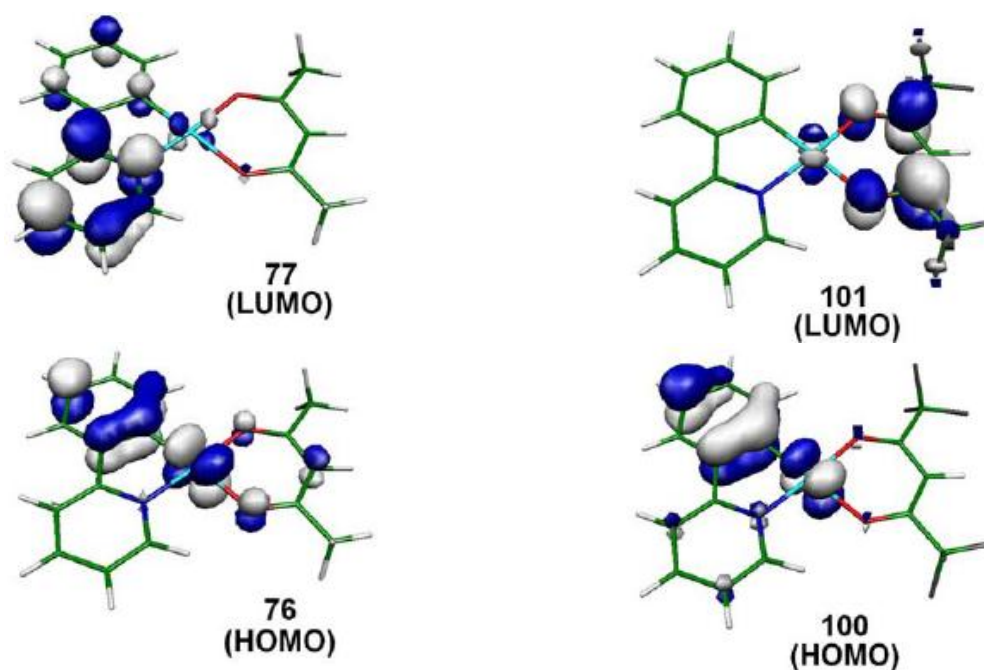

Figure 18-IV TD-DFT computational model of HOMO and LUMO orbitals of [Pt(phpy)(acac)] (left) and [Pt(phpy)(hfacac)] (right).[14] Printed with the authorisation of the corresponding authors.
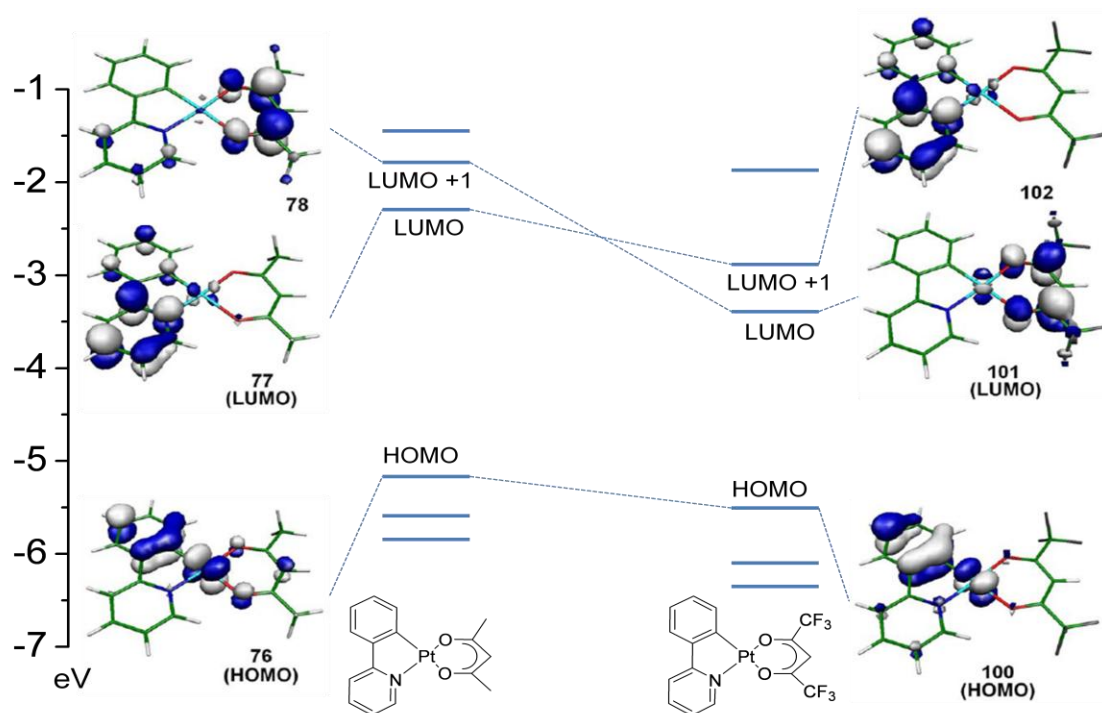
Figure 19-IV Energetic diagram of HOMO and LUMO orbitals with the exchange with LUMO+1.[14] Printed with the authorisation of the corresponding authors.

In this context it is also possible to give an explanation of the unchanged luminescent properties of trifluorinated (tfac) complexes **6(12)** and **9(12)**. Perhaps the presence of only three fluorinated atoms gives a reduced stabilisation of the LUMO+1, at the extent that there is no switch in the emitting state. Therefore, as the presence of different β-diketone has also a very little influence on the HOMO, the emission will remain unchanged.
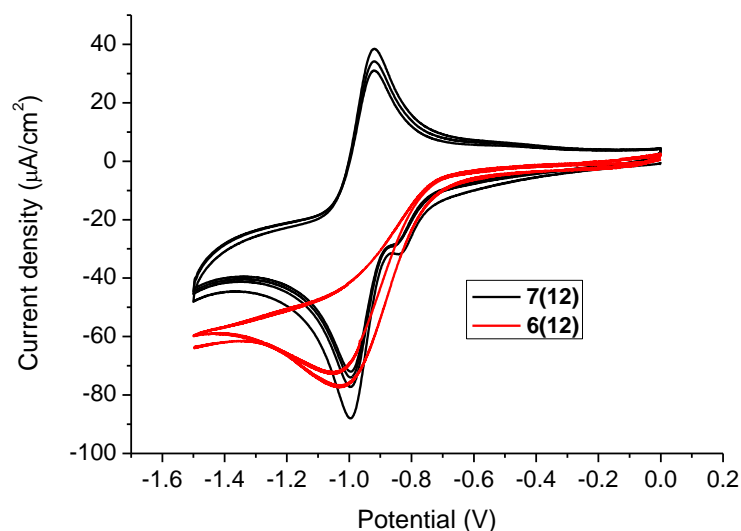
Figure 20-IV Cyclic voltammetry of hexafluoroacetylacetonate platinum(II) complex **7(12)** and trifluor. The potential are measured in DMF and using $(Cp_2Fe/Cp_2Fe^+, 0.64 \text{ V})$ as internal reference.

The finding reported by Ghedini *et al.*[14] are consistent with our finds that tfac complex **6(12)** are still luminescent while hfac complex **7(12)** are not. Indeed, further evidence that the LUMO has changed comes from cyclic voltammetry. Thus, complexes of acac and tfac show an irreversible reduction at ~ -1.0 V, while the hfac complex shows a reversible reduction at a similar potential (Figure 20).

4.1.2.4 Luminescence Properties of the Single isomer of 6(6)

Trifluorinated complexes **6(*n*)** and **9(*n*)** were obtained from their synthesis as a 3:1 mixture (*§ 2.3.1.5*). The isomeric purity was improved by fractional crystallisation, indeed a 36:1 mixture was achieved. The luminescence of this *single-isomer* (36:1) of **6(6)** was investigated and the results are reported in Figure 21. As expected the spectrum of single-isomer at 77 K is more structurated and is also hypsochromically shifted due to the rigidity of the frozen-glass

system compared to the spectrum of the single isomer[20] at 298 K.
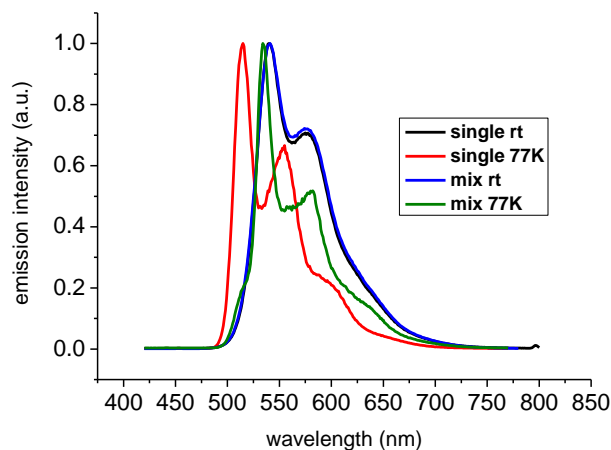
Figure 21-IV Comparison of the emission spectra of **6(6)** in 1:1 isomeric ratio at 77 K (λ_{max} 534 nm) and 298 K (λ_{max} 541 nm), single isomer at 77 K (λ_{max} 515 nm) and 298 K (λ_{max} 541 nm)

On the other hand the two spectra of the mixture at 1:1 ratio (77 k and 298 K) do show structure at lower temperature, but no blue-shift was show on the base of the stiffening of the molecules at 77 K. Thus, the comparison of the spectra of single isomer at 77 K and 298 K shows blue-shift and structure while the comparison of the mixture shows only structure. What is even more peculiar is that the spectrum of the mixture at 298 K closely resembles the single isomers at 298 K, and they present the same maximum wavelength emission of the mixture at 77 K (544 nm). Therefore the one that seems to behave differently is the single isomer at 77 K. Unfortunately there are no examples of this effect in the literature, Adamovich *et al.*, who report similar phenylpyridine platinium(II) complexes with an unsymmetric acetylacetonate ligand, report no difference in luminescent properties.[21] What could be very useful at this stage would be to obtain the luminescent properties of the other isomer. Unfortunately as mentioned in *§ 2.3.1.5*, it has been impossible to recover the other isomer isomerically pure, and no clear

168

assignments have been possible to correlate the structure with the properties so far. Thus, this odd behaviour of the single isomer of complex **6(6)** does not have an explanation at present and more data are needed.

*4.1.2.5 Luminescence properties in films of **4(12)** and **8(12)***

The luminescence of complexes **4(12)** and **8(12)** was studied at different concentrations in a polycarbonate (PC) matrix, as thin films prepared by spin coating. In the case of **4(12)**, the emission spectrum is unchanged on increasing the concentration from 1% to 50%, but higher concentrations result in a small increase in the relative intensity of the red component of the emission. Normalised spectra are shown in Figure 21. This low-energy emission may be due to the formation of aggregates or excimers, a feature frequently encountered for square-planar platinum(II) complexes, which as mentioned before can arrange to give intermolecular face-to-face interactions. A similar effect is observed for the cyclopentene-modified complex **8(12)** at high doping levels in PC (Figure 22).
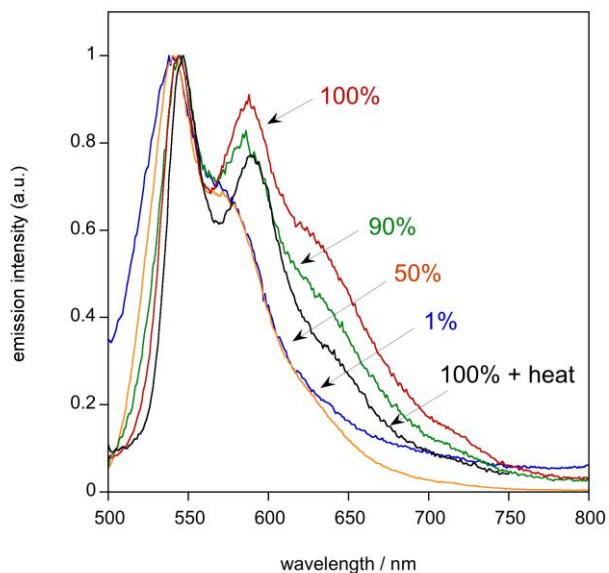
Figure 22-IV Normalised emission spectra of thin films of **4(12)** in polycarbonate at the proportions by mass indicated. The spectrum of the neat film after heating to 110 ℃ is also shown.
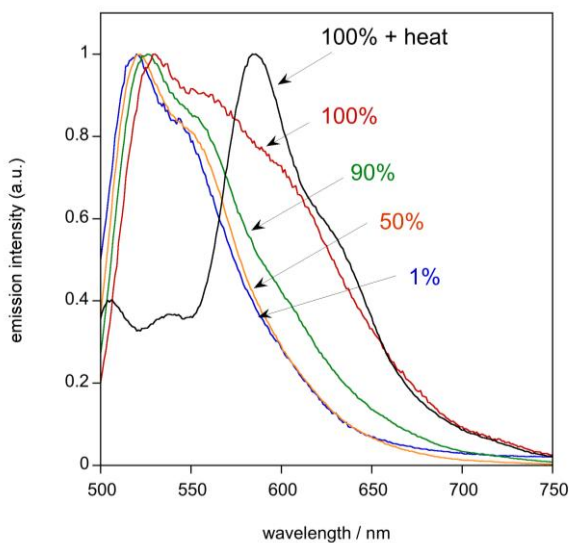
Figure 23-IV Normalised emission spectra of thin films of **8(12)** in polycarbonate at the proportions by mass indicated, together with the spectrum of the neat film after heating to 110 ˚C.

Interestingly, however, a impressive difference emerges heating the pure (100%) films to 110˚C, just below the melting point of the samples. Sample **8(12)** displays an intense new band at 600 nm at the expense of the emission bands in the 525–550 nm region, whereas the

spectrum of **4(12)** is virtually unchanged. Apparently, heating **8(12)** results in the formation of a new emitting species. The lifetime of the emission registered at 600 nm is around 17 ± 3 µs. The dramatic effect of heating is observed only for the 100% film; for example, the spectrum of the 90% sample in PC is unchanged after heating. This observation suggests that the formation of the new species must be associated with specific intermolecular interactions, as may be the case for aggregation *via* orbital overlap.
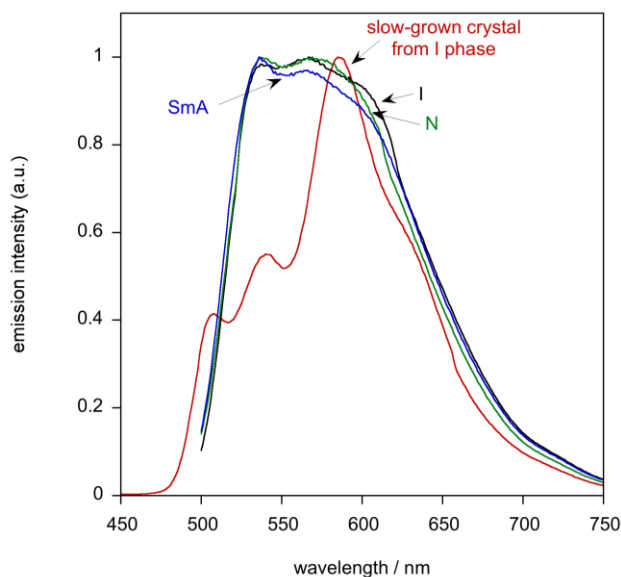
Figure 25-IV Emission spectra of **8(8)** in different crystalline and liquid-crystalline phases. Note that the emission spectrum of the crystal grown from the isotropic phase resembles that of the heat-treated film of **8(12)** in Figure 17.

The change in the spectrum could be indicative of the formation of a more crystalline structure. In support of this hypothesis the luminescence was investigated in different liquid crystal phases. The samples were prepared putting the complex **8(8)** between two cover slices and heating at the appropriate phase temperature, paying particular attention at growing large and well defined liquid crystal domain. When the liquid crystal phase was fully developed the

sample was rapidly cooled at room temperature, harnessing thus, the sample in a glassy state. The integrity of the domain was then checked before analysing the luminescent properties. It is clear that the emission from the film after heating treatment closely resembles the emission from crystal grown slowly from isotropic phase. Meanwhile the emission profiles of the LC and isotropic phases present a broad emission (Figure 24).

Therefore, the liquid crystal nature of these compounds it seems to have an influence on the intermolecular organization and the different states of such organization have an effect on the emission characteristics. This is not a novelty indeed, as mentioned before, it has been reported a related effect in disc-like complexes of platinum(II),[10] while Sagara and Kato have made similar observations in non-metal systems.[22]

4.2 Iridium(III) Complexes

4.2.1 Introduction

4.2.1.1 General Information

Iridium is the third-row transition element of Group 9 in the periodic table along with rhodium and cobalt.

For cobalt, the most common oxidation state is +2 (d^7) with a tetrahedral geometry, while the d^6 +3 oxidation state is also well known, usually with strong-field ligands it shows on octahedral geometry. The principal oxidation states for Rh and Ir are +1 and +3. In the state +1 they are predominantly found as square-planar (or occasionally trigonal bipyramid) complex, while in the state +3 the most common geometry is octahedral. In Chapter 3 the recent impressive expansion of the literature on the luminescent Ir^{III} complexes, mostly from cyclometallating ligands, has been mentioned.[23] One of the relevant reasons for this trend is related to the use of organometallic complexes as triplet emitters for OLEDs devices.[24] However between all the second- and third-row transition metals showing a large spin-orbit coupling constant, therefore leading to a phosphorescent behaviour, attention has been mainly focused on Ir^{III} complexes essentially because of their tunability of the electro-optical properties.[25] Indeed their metal-ligand-based luminescence provides the opportunity to change the emission energy more easily.[26] A further great contribution to the tunability is given by the rich coordination chemistry of Ir^{III} that covers a wide range of complexes including mono-, bis-, and tris-cyclometallated species.[27] Thus the colour can be tuned in the visible range within electrophosphorescent devices.[28] Moreover, the Ir^{III} complexes typically exhibit high quantum yields (Φ_P = 0.1 - 0.9) with an excited-state lifetime generally in the microsecond

region.[29] Other remarkable advantages are related to the fact that neutral species can be obtained and they are more amenable to OLED fabrication processes than charged analogues.[30]

Iridium(III) has a $5d^6$ electronic configuration and, as shown in Figure 25, the degenerate d-orbitals of the cation are split in an octahedral ligand field, by an amount Δ_o. The value of Δ_o depends on the field strength exerted by the ligands.[31]
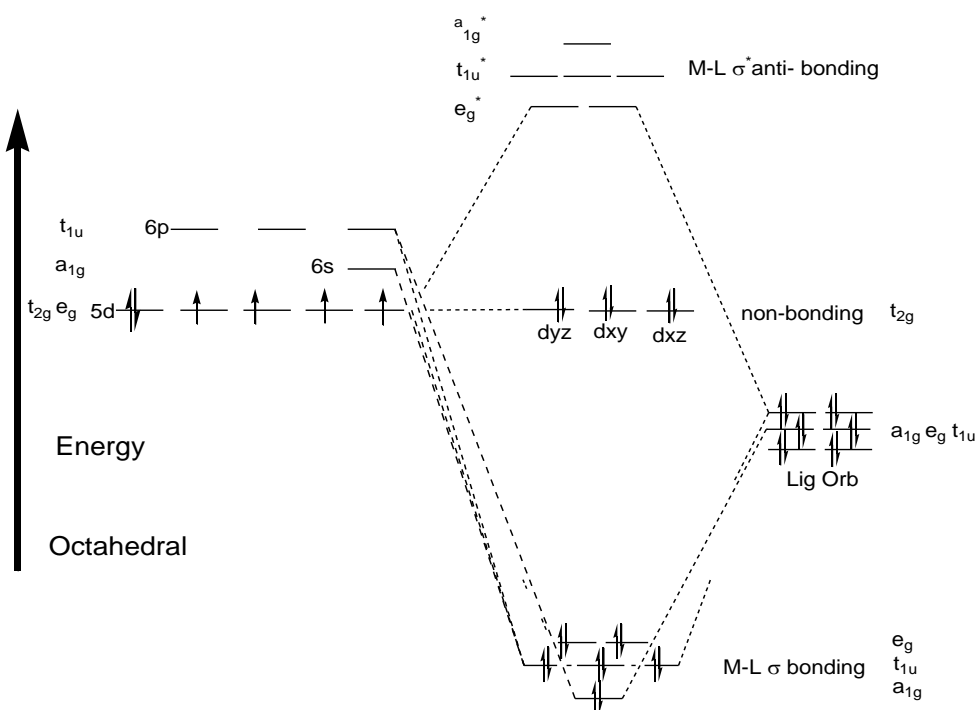
Figure 25-IV Simple ligand field-splitting diagram for Ir d-orbitals in an octahedral geometry assuming no π-bonding

In Figure 26, a simplified potential energy diagram of the states that may be involved in the emission process is reported. It should be noted that usually in these cyclometallated complexes, light absorption (thick blue arrow) is associated with an electronic transition from the ground state to mostly singlet states of various natures and energies similarly to the Pt^{II}.

174

There is a ligand-centred state (^{1}LC) that involves $\pi \rightarrow \pi^*$ or $n \rightarrow \pi^*$ transitions; or metal-to-ligand charge-transfer state (^{1}MLCT) that involves $d \rightarrow \pi^*$ transition; and/or also a metal-centred state (^{1}MC) that involves a $d \rightarrow d$ transition. Generally, the emissions are almost always from triplet levels as a consequence of the high spin-orbit coupling constant of the metal centre; thus, emission from ^{3}LC or ^{3}MLCT states occur.[32] However, if an excited state of the type ^{3}MC is involved as mentioned before for Pt^{II}, it could provide a facile, radiationless deactivation pathway. This problem can be reduced by increasing the ΔE, either utilising a ligand with lower-lying excited state orbitals and/or using ligands with a strong ligand field effect to increase the energy of the metal d-d states. The properties of the 2-phenylpyridine-type ligands prove to have the same effects on Ir^{III} as those described in § *4.1.1.2*.
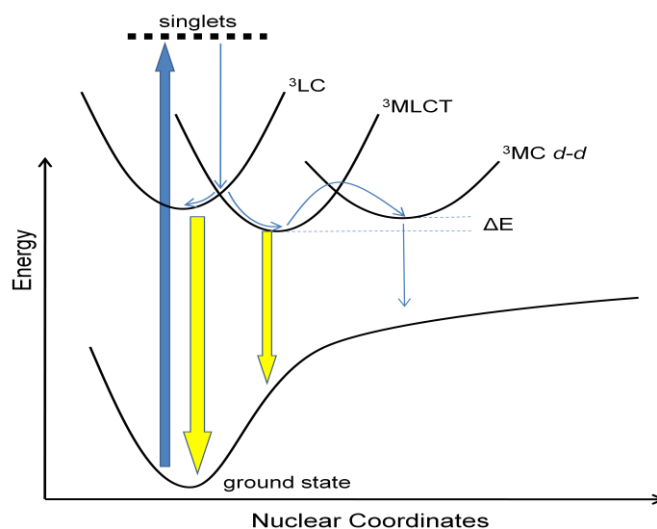
Figure 26-IV Electronic transition diagram involving essentially triplet states. The blue thick arrow represent the excitation, the yellow thick arrows represent the emission and the thin blue arrows represent the non-radiative processes.

Due to their desirable photophysical properties, Ir^{III}-based triplet emitters have attracted substantial interest for OLED technology,[3] with the major development originated by the

collaboration between the groups of Thompson and Forrest. Nowadays, organometallic complexes of [Ir(2-phenylpyridine)$_3$] or [Ir(2-phenylpyridine)$_2$(acac)] are also applied in several highly efficient green devices as emitting materials, with external quantum efficiencies reaching 19% (Figure 27).[33] Devices emitting in other regions of the visible spectrum have also been prepared. A yellow OLED based on [Ir(2-phenylbenzothiozoline)$_2$(acac)] and a red device based on [Ir(2-(2′-benzothienyl)pyrinine)$_2$(acac)] were reported by the Thompson group with maximum external quantum efficiencies of 9.5 and 11.6%, respectively.[15,34]

There have also been limited reports of blue Ir(III)-based OLEDs and in 2003 Nazeeruddin *et al.* reported a series of blue-emitting mixed-ligand Ir^{III} complexes containing electron-rich ancillary ligands such as CN, NCS, NCO, with astonishingly high room-temperature quantum yields ($\Phi_P = 0.9$).[35]

More recently, Tokito *et al.* reported a blue OLED incorporating [Ir(3′,5′-difluoro-2-phenylpyridine)$_2$(picolinate)] in the emissive layer exhibiting a maximum external quantum efficiency of 10.4%, and also a very interesting white device incorporating two emissive layers, a blue–green one using [Ir(3′,5′-difluoromethyl-2-phenylpyridine)$_2$(picolinate)] and a red one based on [Ir(2-(2′-benzothienyl)pyrinine)$_2$(picolinate)], with a maximum external quantum efficiency of 12%.[36]

In general, iridium(III) complexes respond to stimuli, such as the use of different ancillary ligands and/or the use of substituted 2-phenylpyridine derivatives, in very similar way to platinum(II) complexes. Thus, in this part of the chapter only different properties or effects, will be mentioned. Furthermore, to simplify the discussion of the Ir^{III} complexes and their luminescent properties this paragraph, will focus mainly on neutral bis-cyclometallated complexes with 2-phenylpyridine derivatives.

4.2.1.2 Tris-Cyclometallated Ir[III] Comlexes.

The first time the neutral *fac*-[Ir(phpy)$_3$] species appeared was as side-product of the formation of dichloro-bridge dimers complex of the type [Ir(phpy)$_2$Cl]$_2$ by King *et al.* in the 1985.[37] Since then, numerous complexes of this kind [Ir(bidentate)$_3$],[38] but also a large number of variations of the basic [Ir(phpy)$_3$] structure, such as the introduction of electro-withdrawing or electro-donating groups,[39] or extensions of the π-conjugated system,[40] have been reported. The outstanding properties and characteristic of these tris-cyclometallated complexes based on phenylpyridine type ligands are highlighted by the tremendous number of publications and patents dealing with the synthesis and/or the application of the respective complexes.[28] Tris-cyclometallated Ir[III] complexes can be formed in two configurational isomers (Figure 27) and notably they present different photophysical properties. Almost always the *fac*-isomers have a lifetime an order of magnitude longer and higher quantum efficiencies than their meridional counterparts.[41]

$$fac\text{-}[\text{Ir(C}^\wedge\text{N)}_3] \qquad mer\text{-}[\text{Ir(C}^\wedge\text{N)}_3]$$
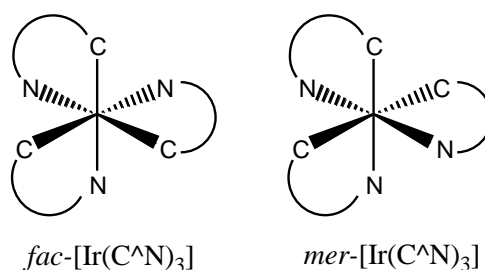
Figure 27-IV Different configuration of the tris-cyclometallate complexes of iridium(III)

Nowadays, the control of the emission wavelength and the colour purity are of the most important parameters along with quantum efficiency and lifetime; therefore, combination of different ligands can be really helpful for tuning the emission wavelengths. In 2001,

Lamansky *et al.*[36] proved the high similarity of the wavelengths emission of the complexes shown in Figure 28 with their homologues tris-cyclometallated complexes. The quantum yields and lifetimes for the two classes of complexes are also the same. The similarity of the two classes of complexes is consistent with emissions predominantly from the "C^N$_2$Ir" fragment in [Ir(C^N)$_2$(acac)] complexes. It has been shown that emission from [Ir(C^N)$_3$], comes, in general, from ^{3}MLCT and ^{3}LC transitions.[42]

[Ir(phpy)$_2$(acac)]
λ_{max} = 516 nm
τ = 3.2 μs
Φ_p = 0.34

[Ir(bezq)$_2$(acac)]
λ_{max} = 548 nm
τ = 23.3 μs
Φ_p = 0.27

[Ir(mephpy)$_2$(acac)]
λ_{max} = 512 nm
τ = 4.5 μs
Φ_p = 0.31
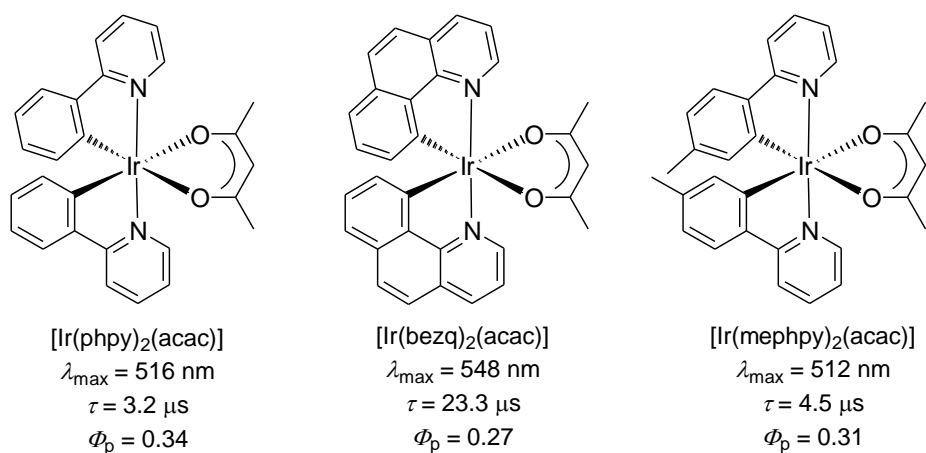
Figure 28-IV Iridium(III) complexes that show similar luminescent properties of their tris-cyclometallated homologues. The wavelengths and the lifetimes are obtained at 77 K in 2-methyltetrahydrofuran. Φ_p was taken at 298 K

Considering that the absorption spectra of the 2-phenylpyridine, 7,8-benzoquinoline and 4′-methyl-2phenylpyridine acac complexes are very similar to their [Ir(C^N)$_3$] analogues, it is not surprising that the emission spectra of [Ir(C^N)$_2$(acac)] and [Ir(C^N)$_3$] complexes are similar, since all the complexes presumably emit from MLCT states of the same energy. For all the acetylacetonate complexes mentioned above, the triplet levels of the ancillary ligand (acac) lie well above the energies of the LC and MLCT excited states. Thus, the luminescence is not influenced by the presence of a diverse ancillary ligand, being dominated by ^{3}LC and

[3]MLCT transitions. On the other hand, the presence of different substituents on the 2-phenylpyridine ligand influences the emission wavelength. The extended π-conjugation of the 7,8-benzoquinoline has in fact the same effect shown for Pt[II], shifting the emission bathocromically and increasing the lifetime enormously due to an increased [3]LC character, while the presence of an electro-donating group in 4 position does not influence the emission properties much.

4.2.1.3 Bis-Cyclometallated Ir[III] Complexes.

Changing the nature of the cyclometallated ligands through the introduction of different substituents typically has a marked effect on the luminescent properties of the complexes, while changing the ancillary ligands often leads to a relative minor effect, although as shown before (*§ 4.1.1.3*), in some cases the luminescence can be compromised. Indeed, Lamansky *et al.* demonstrated the drastic effect of using diphenyl *β*-diketone also on Ir[III] complexes, and the results were very similar to those described for Pt[II] complexes.[15]

λ_{max} = 562 nm
τ = 5.3 µs
Φ_p = 0.12

λ_{max} = 597 nm
τ = 2 µs
Φ_p = 0.1
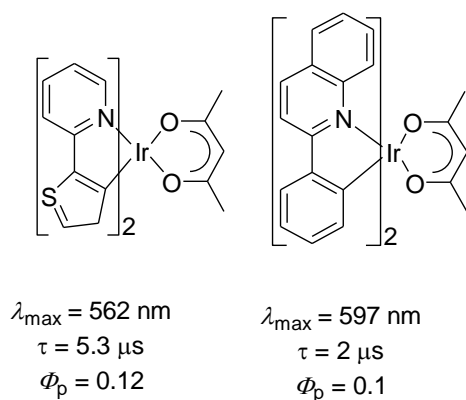
Figure 29-IV Iridium(III) complexes. The wavelengths and the lifetimes are obtained at 77 K in 2-methyltetrahydrofuran. Φ_p was taken at 298 K

As seen above, and as demonstrated for Pt^{II} complexes, the approaches to realise green-red emission from Ir^{III} complexes are mainly based on the extension and/or manipulation of the π-conjugation of the pyridine-type system.

More difficult and less obvious are the approaches chosen to obtain blue Ir^{III} emitters. Different strategies have been revised and discussed by Thompson, Forrest and co-workers[43] and are discussed here.

(a) As mentioned also for Pt^{II}, the use of electro-withdrawing substituents (–F or –CF_3) on the cyclometallated ligands. This has the effect of lowering the energy of the HOMO, stabilising it without influencing much the LUMO. As a consequence, the energy gap between the ^{3}LC and/or ^{3}MLCT and the HOMO, is increased and thus, the emission will be shifted hypsochromically (Figure 30).[43a]

λ_{max} = 514 nm λ_{max} = 468 nm λ_{max} = 465 nm λ_{max} = 458 nm
τ = 2.0 μs τ = 1.6 μs τ = 0.68 μs τ = 1.6 μs
Φ_p = 0.40 Φ_p = nr Φ_p = 0.15 Φ_p = 0.30
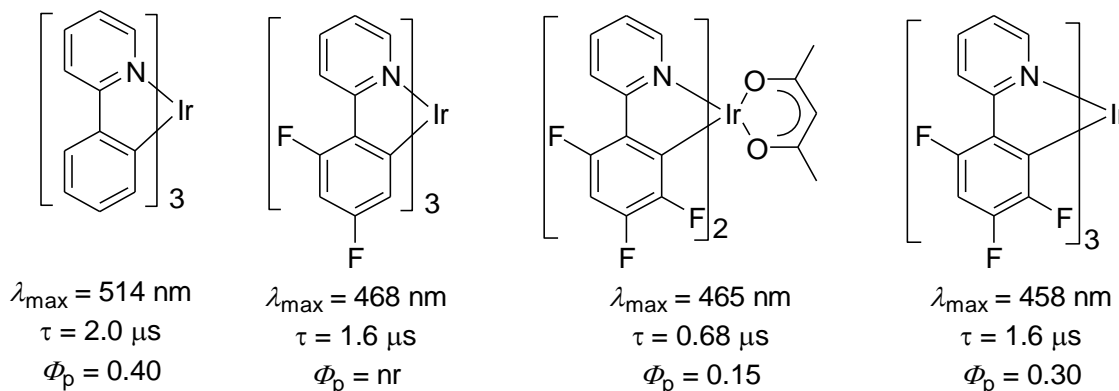
Figure 30-IV Iridium(III) complexes. The wavelengths the lifetimes and quantum yield are obtained from Flamigni *et al.* review.[25] Solvent not reported. nr = not reported.

(b) Similar perturbation of the HOMO-LUMO energy gap by influencing the energy of the HOMO can be obtained also using different ancillary ligands that tune the HOMO energy of the [Ir(bidentate)$_2$LL] (Figure 31).[43b] Indeed as shown above in these chapter the LUMO of

these complexes is mainly characterise by the contribution of phenylpyridine, while the HOMO in general is made from a contribution of metal centre, phenylpyridine-type ligand and also auxiliary ligand, thus, if an auxiliary ligand that can stabilise the HOMO is used the energy gap between the emitting state and the HOMO is increased, resulting in a hypsochromic shift.

λ_{max} = 512 nm
τ = 1.4 μs
Φ_p = 0.38

λ_{max} = 480 nm
τ = 3.5 μs
Φ_p = 0.52

λ_{max} = 468 nm
τ = 4.7 μs
Φ_p = 0.04
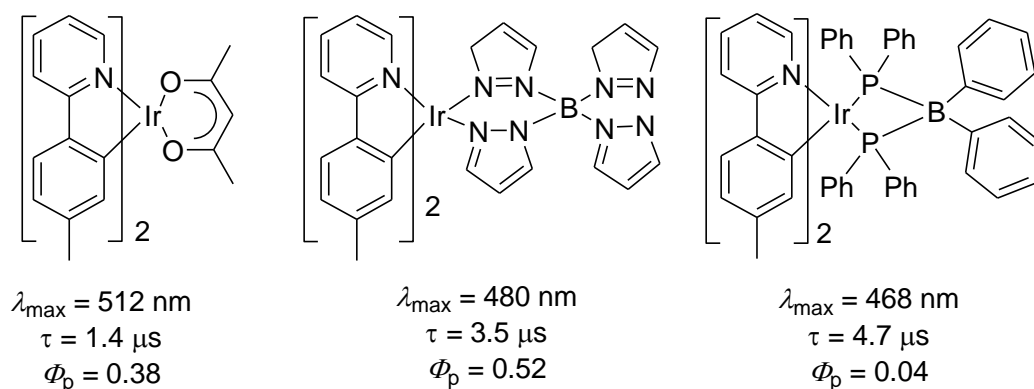
Figure 31-IV Iridium(III) complexes. The wavelengths the lifetimes and quantum yield are obtained from Flamigni *et al.* review.[25] Solvent not reported.

(c) The last approach can be to use ligands no longer based on 2-phenylpyridine but replacing the heterocyclic fragment with a higher-lying LUMO fragment, with the effect to raising the energy of the MLCT and LC transition. The problem with these system is that sometimes the high energy of the LUMO induces a matching between the high-lying MC and the emitting state MLCT and LC supplying a deactivation pathway that reduces the quantum yield drastically (Figure 32).[43a]
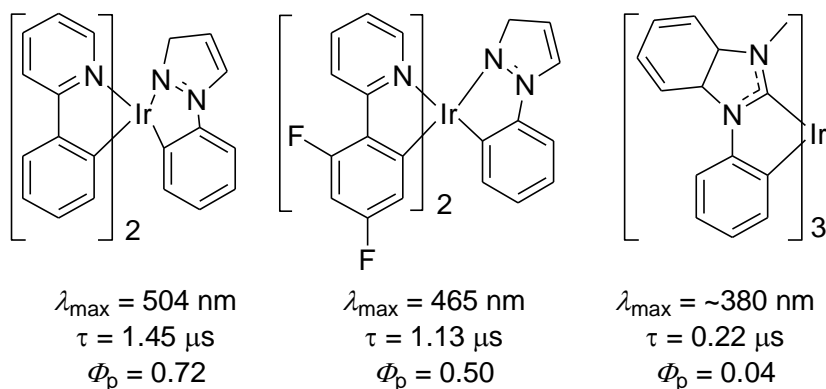
Figure 32-IV Iridium(III) complexes. The wavelengths the lifetimes and quantum yield are obtained from reference 25.

4.2.2 Luminescent Properties of the Synthesised Iridium(III) Complexes

Unfortunately because of the lability of the iridium(III) complexes herein synthesised, few analysis were carried out. The complexes analysed are shown in Figure 33. For the DMSO complex, **20(12)**, the lifetime and the quantum yield were determinate by Dr Williams in Durham. For acac complexes **21(12)** and acetonitrile complex **23(12)** only the emission wavelengths were investigated. Thus, deeper luminescent studies are required to characterise these complexes fully.
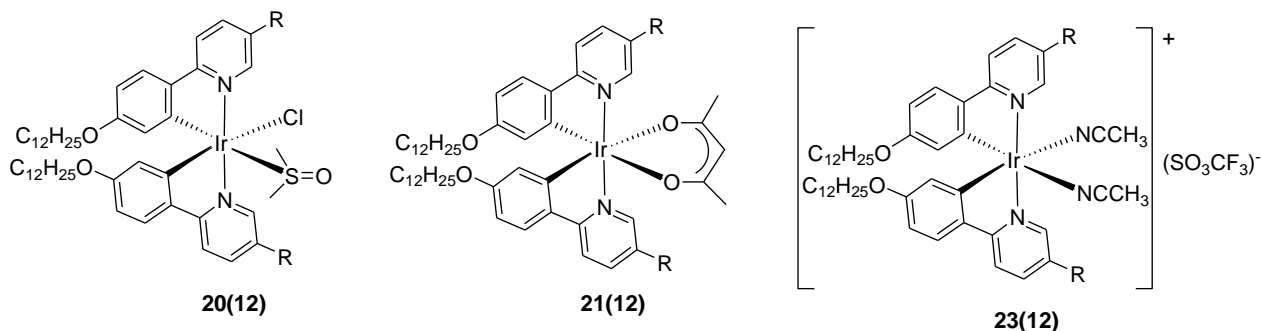
Figure 33-IV 2,5-dialkoxyphenyl-pyridine iridium(III) complexes.
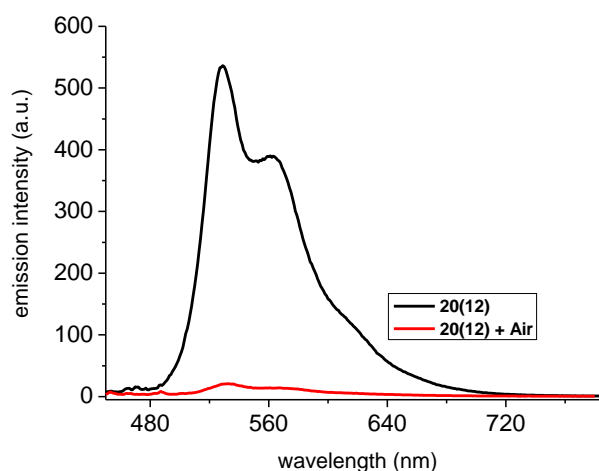
Figure 34=IV The effect of air equilibration on emission spectra of **20(12)** in CH_2Cl_2 (Conc. *ca.* $1 \cdot 10^{-5}$) solution at 298 K.

As was seen for platinum(II) complexes and also for Ir^{III}, emission quenching occurs readily in air-equilibrated samples, so the freeze-vacuum cycle is necessary; Figure 34 shows the reduction in luminescence of an air-equilibrated sample. The emission spectra of the DMSO complex **20(12)**, acac complex **21(12)** and acetonitrile complex **23(12)** are shown in Figure 35 along with their absorption spectra. The intense absorption bands at high energy (λ <350 nm), may be attributed to allowed singlet $\pi \rightarrow \pi^*$ (250-350 nm) and the bands in the range 350–440 nm corresponded to spin allowed metal-ligand charge transfer band (^{1}MLCT). Weak absorption at 440–500 nm was assigned to the formally spin-forbidden ^{3}MLCT transition, similar to reported value of $[Ir(phpy)_2(acac)]$.[36] All the wavelengths and the other data are reported in Table 3.
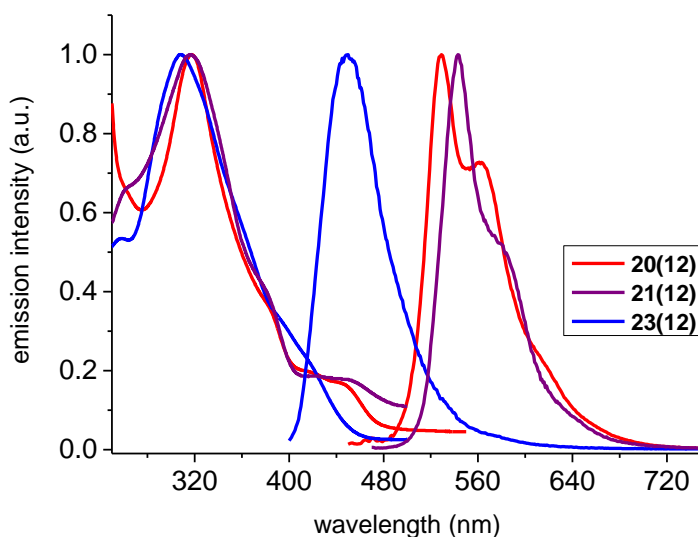
Figure 35-IV Absorpition and emission spectra of **20(12)**, **21(12)** and **23(12)** in CH$_2$Cl$_2$ solution at 298 K. λ_{ex} = 400 nm for **20(12)**, λ_{ex} = 450 nm for **21(12)** and λ_{ex} = 380 nm for **23(12)**.

In this case, the bathochromic shift in comparison with [Ir(phpy)$_2$(acac)] has been explain by Xu *et al.*[44] to be due principally to the introduction of the electron-withdrawing phenyl group in the 5-position of the pyridyl ring, lowering the LUMO level and resulting in a decreased energy gap between the excited state and the ground state. Furthermore the introduction of alkoxy group in the 4-position of the phenyl ring of the 2-phenyppyridine seems to increase the energy of both the HOMO and LUMO, resulting in a no-change situation in the emission wavelength. On the other hand, introduction of the alkoxy group on the 4-position of the other phenyl group results in a small increase in the LUMO energy and thus in a blue-shift. Complexes **21(12)** shows a 27 nm red-shift according with the description above. The problem is that Xu *et al.* synthesised the same Ir^{III} acac complex **21(2)** and they reported an emission wavelength of 534 nm, slightly different from the one reported here (543 nm). As was shown before, this cannot be attributable to the difference in chain length. This

could be due to the different conformation suggested in the Chapter 3 (two carbon atoms *trans* instead than two nitrogen) even if it would be expected a larger difference from a such different geometry. However it could be also possible, seen the small difference, that this is due to instrumentation differences.

Table 3-IV Absorption and emission data for Ir^{III} complexes in CH_2Cl_2 at 298K ($\pm$3) nr = not reported

	$[Ir(phpy)_2(acac)]^a$	21(2)[b]	20(12)	21(12)	23(12)
Absorption[c] λ_{max}/nm	260, 345,	260, 318,	318, 380	318, 390	310, 355
	412, 460,	381, 443	435	450	410
	497				
Emission λ_{max} / nm	516	534	529, 563	543, ~580	450
τ degassed (aerated) µs	1.6(nr)	nr	80 (nr)	nr	nr
Φ_{lum}	0.34	nr	<0.01	nr	nr

(a) In 2-methyltetrahydrofuran; data from reference.[35] *(b)* data from reference.[45] *(c)* molar extinction coefficients not calculated

In the case of complex **20(12)**, there is a small hypsochromic shift of about 14 nm; but if compared with **21(2)** the difference is only about 5 nm thus, no comments are useful in this contest until a clear definition on the nature of complex **21** is acheived. However, the presence of a longer lifetime and very low phosphorescent efficiency as in the case platinum(II) DMSO complex **14(6)**, is probably due to the lower decay rate constant.

A completely different situation was found for complex **23(12)**. This complex shows an unpredictable, broad blue emission at 450 nm. Because of the absence of ^{3}MLCT peacks in the absorption (350-440 nm), but especially because of the small value of the Stokes shift, it is assumed that in this case no phosphorescence is seen but rather an intense fluorescence emission, so that the emission is ligand centred. The emission wavelengths of complexes

19(12) and **29(12)** were also checked and the *μ*-dichloro bridge **19(12)** was not luminescent and **29(12)** was only weakly so (Figure 36). As mentioned before more analysis is needed to have a clear characterisation of these complexes.
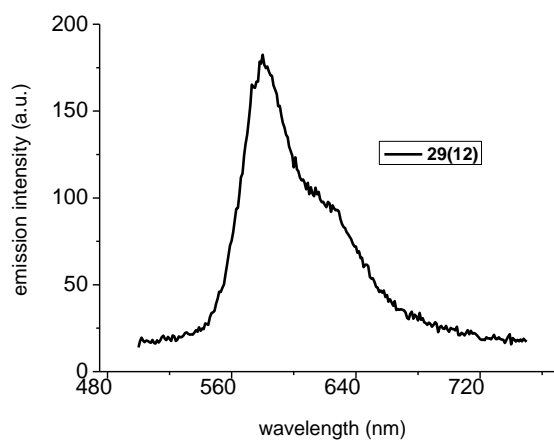
Figure 36-IV Emission spectrum of complex **29(12)** at 298 K (λ_{ex} = 480 nm)

4.3 Conclusion

The luminescence of the platinum(II) complexes herein synthesises have been fully characterised. Apart from complexes **7(12)** and **11(12)** all the complexes show a high quantum yield in the range of 0.49 to 0.70 (0.08 for **14(6)**), lifetimes were also good, with all complexes giving times between 26 and 30 μs except **10(12)** which has a lifetime of 13 μs. All show triplet emission with yellow phosphorescence (500-550 nm). Comparing these complexes with the model compound [Pt(2-phpy)(acac)], the luminescence analysis demonstrated a bathochromic shift between 38 to 65 nm due to the insertion of a 4-methoxyphenyl and 4-alkoxy group on the frame of 2-phenylpyridine. For complexes of the cyclopentene substituted ligand **2(n)**, the red-shift is limited by reduced π-conjugation due to the induced torsion in the unbound rings. Moreover, the presence of different class of acetylacetonate ligand was investigated, and it was found that there was no change in the luminescent properties of the complexes bearing acetylacetonate, trifluoroacetylacetonate or heptanedionate. However, a very interesting switch-off effect was found for the complexes bearing the hexafluoroacetylacetonate **7(12)** and **11(12)**.

A similar effect was reported by by Ghedini *et al.*[14] in platinum(II) complexes bearing 2-phenylpyridine and 2-phenylpyridine-type ligands. Their explanation has been reinforced with a cyclic voltammetry analysis of complexes **7(12)**, **6(12)** and **5(12)** where the different nature of the LUMO of complexes **7(12)** has been highlighted by its reversible reduction potential, while the other complexes show an irreversible one.

Moreover, complexes **4(12)** and **8(12)** were analysed in a thin-film state at different concentration in polycarbonate and in pure film, and complexes **8(8)** has been analysed also in different liquid crystal phases. No emission changes were notice for complex **4(12)**. While for

complex **8** a significant change in emission of the pure film was found after thermal treatment (λ_{em} changes from 520 nm to 600 nm). On the base of the analysis made on solid sample (**8(8)**) in different phases, it has been found that this diverse emission belong to a crystal phase grown slowly from isotropic phase.

Thus, it has been shown that the combination of emitter and liquid crystal properties could offers control over the nature of the emission *via* the molecular organisation. This combination of properties is then expected to lead to highly efficient, polarised emission which, if realised, would have very significant technological applications. Furthermore, the lifetimes of all the platinum compounds are within the desired range making this type of compounds suitable for their intended application. Some specific tests are necessary to investigate the possibility of polarised emission and this will be the main topic of the Proof of Concept White Rose fellowship assigned to our research group.

Unfortunately, as mentioned above, the luminescent properties of the iridium(III) complexes have not been fully characterised yet. The preliminary results show an orange luminescence (520-600 nm) with very poor quantum yield and long lifetime for complex **20(12)**. More analysis are required to fully comprehend the trend of the new class of liquid crystal iridium(III) complexes. It will be also very interesting to investigate the influence of the liquid crystal phases on the luminescence for these materials.

References

1   J. A. G. Williams, *Top. Curr. Chem.*, 2007, **281**, 205.

2   Q. –Z. Yang, L. –Z. Wu, Z. –X. Wu, L. –P. Zhang, and C. –H. Tung, *Inorg. Chem. Comm.*, 2002, **41**, 5653.

3   R. C. Evans, P. Douglas, and C. J. Winscom, *Coord. Chem. Rew.*, 2006, **250**, 2093.

4   (a) M. Maestri, D. Sandrini, V. Balzani, U. Maeder, and A. von Zelewsky, *Inorg. Chem.*, 1987, **26**, 1323; (b) D. Sandrini, M. Maestri, V. Balzani, L. Chassot, and A. von Zelewsky, *J. Am. Chem. Soc.*, 1987, **109**, 7720; (c) R. Ballardini, G. Varani, M. T. Indelli, and F. Scandola, *Inorg. Chem.*, 1986, **25**, 3858; (d) F. Barigelletti, D. Sandrini, M. Maestri, V. Balzani, A. von Zelewsky, L. Chassot, P. Jolliet, and U. Maeder, *Inorg. Chem.*, 1988, **27**, 3644.

5   (a) F. Neve, A. Crispini, C. D. Pietro, and S. Campagna, *Organometallics*, 2002, **15**, 223; (b) P. D. Harvey, and H. B. Gray, *J. Am. Chem. Soc.*, 1988, **110**, 2145.

6   (a) M. A. Baldo, D. F. O'Brien, Y. You, A. Shoustikov, S. Sibley, M. E. Thompson, and S. R. Forrest, *Nature*, 1998, **395**, 151; (b) W. Lu, B. –X. Mi, M. C. W. Chan, Z. Hui, C. –M. Che, N. Zhu, S. and –T. Lee, *J. Am. Chem. Soc.*, 2004, **126**, 5653; (c) V. Adamovich, J. Brooks, A. B. Tamayo, A. M. Alexander, P. I. Djuorovich, B. W. D'Andrade, C. Adachi, S. R. Forrest and M. E. Thompson, *New J. Chem.*, 2002, **26**, 1171.

7   (a) J. A. G. Williams, A. Beeby, S. Davies, J. A. Weinstein, and C. Wilson, *Inorg. Chem.*, 2003, **42**, 7720; (b) S. J. Lee, S. Kang, S. H. Lee, K. J. Hwang, N. K. Park, and Y. S. Kim, *Mater. Sci. Eng. C*, 2002, **24**, 221.

8   (a) V. W. –W. Yam, R. P. L. Tang, K. M. –C. Wong, X. –X. Lu, and K. –K. Cheung, *Chem. Eur. J.*, 2002, **8**¸ 4066; (b) S. –W. Lai, M. C. W. Chan, T. –C. Cheung, S. –M. Peng, and C. –M. Che, *Inorg. Chem.*, 1999, **38**, 4046.

9   J. A. G. Williams, A. Beeby, S. Davies, J. A. Weinstein, and C. Wilson, *Inorg. Chem.*, 2003, **42**, 8609.

10   V. N. Kozhevnikov, B. Donnio, and D. W. Bruce, *Ang. Chem. Int. Ed.*, 2008, **46**, 6286.

11   P. –I. Kvam, M. V. Puzyk, K. P. Balashev, and J. Songstad, *Acta Chem. Scand.*, 1995,

49, 335.

12   J. Brooks, Y. Babayan, S. Lamansky, P. I. Djurovich, I. Tsyba, R. Bau, and M. E. Thompson, *Inorg. Chem.*, 2002, **41**, 3055.

13   (a) S. W. Thomas III, S. Yagi, and T. M. Swager, *J. Mater. Chem.*, 2005, **15**¸ 2829; (b) K. Venkatesan, P. H. J. Kouwer, S. Yagi, P. Muller, and T. M. Swager, *J. Mater. Chem.*, 2008, **18**, 400.

14   M. Ghedini, T. Puglise, M. La Deda, N. Godbert, I. Aiello, M. Amati, S. Belviso, F. Leji, G. Accorsi, and F. Barigeletti, *Dalton Trans.*, 2008, **32**, 4303.

15   S. Lamansky, P. Djurovich, D. Murphy, F. Abdel-Razzaq, H. E. Lee, C. Adachi, P. E. Burrows, S. R. Forrest, and M. E. Thompson, *J. Am. Chem. Soc.*, 2001, **123**, 4304.

16   M. V. Kulikova, K. P. Balashev, and P. –I. Songstad, *J. Russ. J. Gen. Chem.*, 2000, **70**, 173.

17   (a) V. M. Miskowski, and V. H. Houlding, *Inorg. Chem.*, 1989, **28**, 159; (b) D. Steinborn, M. Gerisch, T. Hoffmann, C. Bruhn, G. Israel, and F. W. Muller, *J. Organomet. Chem.*, 2000, **598**, 286.

18   A. Santoro, A. C. Whitwood, J. A. G. Williams, V. N. Kohevnikov and D. W. Bruce, *Chem. Mater.*, 2009, **21**, 3871.

19   J. A. G.Williams, S. Develay, D. L. Rochester, and L. Murphy, *Coord. Chem. Rev.*, 2008, **252**, 2596.

20   M. Spencer, A. Santoro, and D. W. Bruce, *in preparation.*

21   V. Adamovich, J. Brooks, A. Tamayo, A. M. Alexander, P. I. Djurovich, B. W. D'Andrade, C. Adachi, S. R. Forrest and M. E. Thompson, *New J. Chem.*, 2002, **26**, 1171.

22   Y. Sagara, and T. Kato, *Angew. Chem., Int. Ed.*, 2008, **47**¸ 5175.

23   L. Flamigni, A. Barbieri, C. Sabatini, B. Ventura and F. Barigelletti, *Top. Curr. Chem.*, 2007, **281**, 143.

24   (a) E. Holder, B. M. Langeveld, and U. S. Schubert, *Adv. Mater.*, 2005, **17**, 1109; (b) *Highly Efficient OLEDs with Phosphorescent Materials*, (Ed: H. Yersin) Wiley-VCH, Weinheim, Germany 2008.

25 C. Ulbricht, B. Beyer, C. Friebe, A. Winter and U. S. Schubert, *Adv. Mater.*, 2009, **21**, 4418.

26 K. Dedeian, P. I. Djurovich, F. O. Garces, G. Carlson, and R. J. Watts, *Inorg. Chem.*, 1991, **30**, 1685.

27 I. M. Dixson, J. –P. Collin, J. –P. Sauvage, L. Flamigni, S. Encinas, and F. Barigeletti, *Chem. Soc. Rev.*, 2000, **29**, 385.

28 Adachi, M. A. Baldo, S. R. Forrest, S. Lamansky, M. E. Thompson, and R. C. Kwong, *Appl. Phys. Lett.*, 2001, **78**, 1622.

29 R.C. Evans, P. Dougles and C. J. Winscom, *Coord. Chem. Rev.*, 2006, **250**, 2093.

30 L. Flamigni, A. Barbieri, C. Sabatini, B. Ventura and F. Barigelletti, *Top Curr. Chem.*, 2007, **281**, 143.

31 D. M. Roundhill, *Photochemistry and Photophysics of Metal Complexes*. Plenum Press, New York, 1994.

32 H. Yersin, *Top. Curr. Chem.*, 2004, **241**, 1.

33 (a) M. Ikai, S. Tokito, Y. Sakamoto, T. Suzuki, and Y. Taga, *Appl. Phys. Lett.*, 2001, **79**, 156; (b) C. Adachi, M. A. Baldo, M. E. Thompson, and S. R. Forrest, *J. Appl. Phys.*, 2001, **90**, 5048; (c) S. Lamansky, P. Djurovich, D. Murphy, F. Abdel-Razzaq, H.-E. Lee, C. Adachi, P. E. Burrows, S. R. Forrest, and M. E. Thompson, *J. Am. Chem. Soc.*, 2001, **123**, 4304.

34 S. Lamansky, P. Djurovich, D. Murphy, F. Abdel-Razzaq, R. Kwong, I. Tsyba, M. Bortz, B. Mui, R. Bau, and M. E. Thompson, *Inorg. Chem.*, 2001, **40**, 1704.

35 M. K. Nazeeruddin, R. Humphrey-Baker, D. Berner, S. Rivier, L. Zuppiroli, and M. Graetzel, *J. Am. Chem. Soc.*, 2003, **125**, 8790.

36 S. Tokito, T. Tsuzuki, F. Sato, and T. Iijima, *Curr. Appl. Phys.*, 2005, **5**, 331

37 K. A. King, P. J. Spellane, and R. J. Watts, *J. Am. Chem. Soc.*, 1985, **107**, 1431.

38 (a) K. Dedeian, J. Shi, N. Shepherd, E. Forsythe, and D. C. Morton, *Inorg. Chem.*, 2005, **44**, 4445; (b) L. Chen, C. Yang, J. Qin, J. Gao, H. You, and D. Ma, *J. Organomet. Chem.*, 2006, **691**, 3591.

39 (a) R. Ragni, E. A. Plummer, K. Brunner, J. W. Hofstraat, F. Babudri, G. F. Farinola, F. Naso, and L. De Cola, *J. Mater. Chem.*, 2006, **16**, 1161; (b) Y. J. Su, H. L. Huang, C. L.

Li, C. H. Chien, Y. T. Tao, P. T. Chou, S. Datta, and R. S. Liu, *Adv. Mater.*, 2003, **15**, 884; (c) G. Y. Park, Y. Kim, and Y. Ha, *Mol. Cryst. Liq. Cryst.*, 2007, **462**, 179; (d) J. Otsuki, T. Tokimoto, Y. Noda, H. Tomohiro, C. Takeshi, X. Chen, and Y. Okamoto, *Chem. Eur. J.* 2007, **13**, 2311; (e) K. Ono, M. Joho, K. Saito, M. Tomura, Y. Matsushita, S. Naka, H. Okada, and H. Onnagawa, *Eur. J. Inorg. Chem.*, 2006, 3676; (f) H. C. Bottcher, M. Graf, H. Kruger, and C. Wagner, *Inorg. Chem. Comm.*, 2005, **8**, 278.

40   (a) G. Zhou, W.-Y. Wong, B. Yao, Z. Xie, and L. Wang, *Angew. Chem., Int. Ed.* 2007, **46**, 1149; (b) Y. You, C.-G. An, D.-S. Lee, J.-J. Park, and S. Y. Park, *J. Mater. Chem.*, 2006, **46**, 4706; (c) S. Bettington, M. Tavasli, M. R. Bryce, A. Beeby, H. Al-Attar, and A. P. Monkman, *Chem. Eur. J.*, 2007, **13**, 1423; (d) M. Tavasli, S. Bettington, M. R. Bryce, A. S. Batsanov, and A. P. Monkman, *Synthesis*, 2005, 1619; (e) S. Okada, K. Okinaka, H. Iwawaki, M. Furugori, M. Hashimoto, T. Mukaide, J. Kamatani, S. Igawa, A. Tsuboyama, T. Takiguchi, and K. Uneo, *Dalton Trans.*, 2005, 1583; (f) N. Cumpstey, R. N. Bera, P. L. Burn, and I. D. W. Samuel, *Macromolecules*, 2005, **38**, 9564; (g) S. C. Lo, G. J. Gary, J. P. J. Markham, E. B. Ebinazar, S. Sharma, P. L. Burn, and I. D. W. Samuel, *Adv. Funct. Mater.*, 2005, **15**, 1451.

41   A. B. Tamayo, B. D. Alleyne, P. I. Djurovic, S. Lamansky, I. Tysba, N. N. Ho, R. Bau, and M. E. Thompson, *J. Am. Chem. Soc.*, 2003, **125**, 7377.

42   (a) M. G. Colombo, A. Hauser, and H. U. Gudel, *Inorg. Chem.*, 1993, **32**, 3088; (b) M. G. Colombo, T. C. Burmold, T. Riedener, and H. U. Gudel, *Inorg. Chem.*, 1994, **33**, 545.

43   (a) T. Sojoto, P. I. Djurovich, A. Tamayo, M. Yousufuddin, R. Bau, and M. E. Thompson, *Inorg. Chem.*, 2005, **44**, 7992; (b) J. Li, P. I. Djurovich, B. D. Alleyne, M. Yousufuddin, N. N. Ho, J. C. Thomas, J. C. Peters, R. Bau, and M. E. Thompson, *Inorg. Chem.*, 2005, **44**, 1713.

44   M. Xu, W. Li, Z. An, Q Zhou and G. Wang, *Appl. Organometal. Chem.*, 2005, **19**, 1225.

Chapter 5: Conclusions

Molecular materials with optoelectronic characteristics occupy a special place in materials chemistry research as several examples of real, and highly profitable, applications exist. Improvements in device performances can always be linked to, among other things, the tuning of bulk properties *via* molecular design, so that an intimate knowledge of structure/function relationships is a key factor in determining advances. Thus, combining liquid crystals characteristics with one or more other desirable properties leads to multifunctional materials where, for example, light emission may be found in a mesomorphic material. It has been mentioned that liquid-crystalline order, namely an organised, supramolecular structure, could be expected to improve charge mobility due to the cooperativity of physical properties in these self-organised materials and could be of significance in polarised emission, and it has also been proved that the liquid crystal phases can influence the luminescent emission.

Based on this background, attention was focused on a material that can deal with both phosphorescent emission and liquid crystal properties at the same time. Therefore, a metal with high spin-orbit coupling to deal with the triplet emission and with an appropriate geometry to deal with the liquid crystal properties was required and, as explained in the first part of this thesis, the platinum(II) seemed to be the perfect combination of these characteristics. The choice of the 2-phenylpyridines as ligands is well documented being, its superb characteristic as a strong-field ligand with orbitals of appropriate energy. Thus, the idea came to modify the structure of 2-phenylpyridine inserting another phenyl ring in 5-position of

the pyridine and inserting two alkoxy chains in 4-position of the two phenyl groups, so that the increased anisotropy of the ligand could compensate for the lateral distortion due to the presence introduction of the square-planar platinum group (Pt and acetylacetonate).

4(*n*) **8(*n*)**
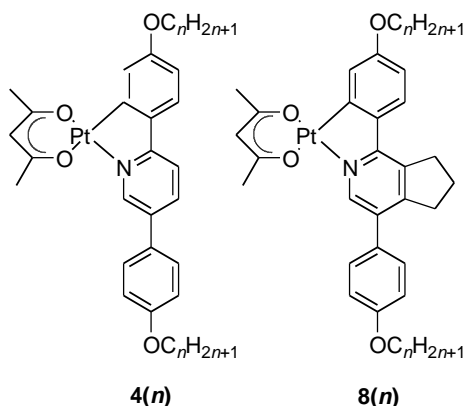
Figure 1-V Pt complexes of the 2-phenylpyridine derivatives

Thus, the preparation of the 2,5-di(4-alkoxyphenyl)pyridine ligands used in this project was obtained by means of a very flexible chemistry for *N*-heterocycle synthesis, which first involved the formation of a triazine and then an inverse-electron-demand Diels-Alder reaction to substitute two nitrogens with two carbons or with a fused cyclopentene. The introduction of a fused cyclopentene ring was designed to lower the transition temperature of the ligands, which weas expected to be quite high for a three rings connected with a σ-bond.

The use of the fused cyclopentene works very well, indeed the melting points for ligands **1(*n*)** show high clearing points that vary from 240 ºC for **1(6)** to 200 ºC for **1(12)**, but when the fused ring is present, **2(*n*),** the transition temperatures are much lower, in fact the clearing points vary from 115 ºC for **2(6)** to 100 ºC for **1(12)**. Interestingly, as expected, the introduction of a lateral substituent, apart from lowering the transition temperature, also affects greatly the number of liquid crystal phases. For example ligand **1(*n*)** is characterised by

194

the presence of several different smectic phases, while ligand **2(*n*)** is characterised predominantly by the less ordered nematic phase, and only in the case of the longer chains (C12) is a SmA phase seen.
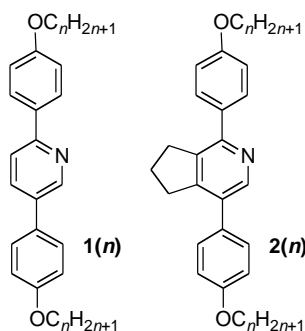
Figure 2-V Ligands synthesised in this project.

Not without any difficulty, these ligands were then complexed to platinum(II) in a cyclometallated fashion. Indeed, because of the lack of solubility of the μ-chloro bridge intermediate **16(*n*)** and because of the lack of reference in the literature, in the beginning the synthesis proved to be a tough challenge, then with the nice touch of converting these insoluble complexes to the more soluble and easy-handling DMSO derivatives, everything became easier and the target complexes **4(*n*)** and **8(*n*)** were obtained in a good yield and with a simple methodology. Remarkably almost all the platinum complexes are liquid crystalline and, as expected, the transition temperatures of the series **4(*n*)** are very high (clearing points from 260 ºC for **4(6)** to 230 ºC for **4(12)**) making them less interesting for the devices. Unfortunately the presence of the fused cyclopentene ring, although lowering the clearing points (from 160ºC for **8(6)** to 121 ºC for **8(12)**), destabilised the liquid crystal phases, making them monotropic. Thus, in order to obtain lower transition temperature but at the same time keeping stable liquid crystal phases, attention focused on the use of different β-diketones.

195

Better results were obtained using 3,5-heptanedione as an auxiliary ligand in the presence of ligand **1(n)**, indeed these complexes proved to have lower clearing points (228 ºC for **5(6)** to 205 ºC for **5(12)**). This is due to the more steric demanding auxiliary ligand that induce a partial reduction between of the molecular interaction lowering thus the melting points. However, complexes containing the cyclopentene- functional ligand were not mesomorphic in conjunction with the heptandione ligand; a similar effect was also found with other *β*-diketonates (tfac and hfac). The transition temperatures of complex **6(n)** are still very high and some modifications are required to lower them.
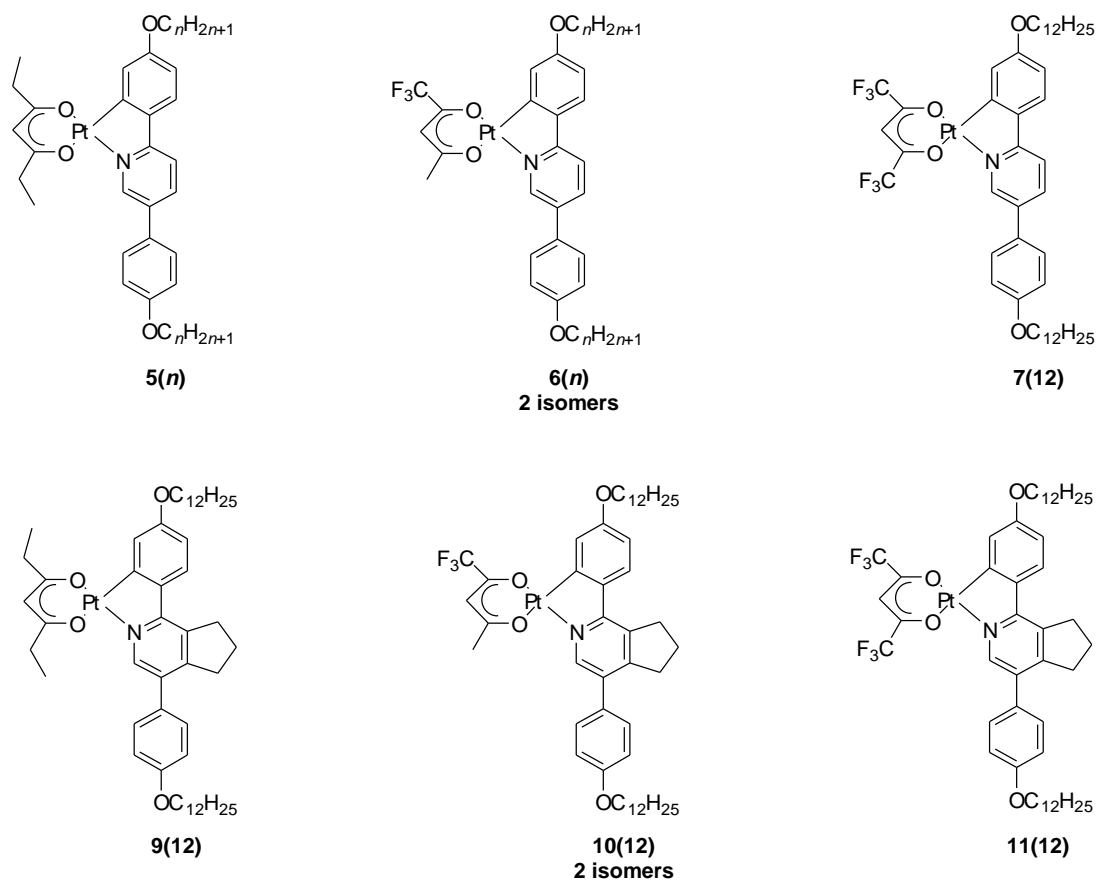
Figure 3-V Structure of platinum complexes bearing a series of *β*-diketone.

When using tfac, it was found that the reaction with this unsymmetric diketone yields a 3:1

mixture of isomers and it is possible to change the relative ratio, both during and after the reaction. The maximum isomeric purity achievable is 36:1 by fractional crystallisation. However, the important discovery resides in the dynamic behaviour of the β-diketonates which, at appropriate temperature, are able to disconnect from the platinum and reconnect in a different orientation. Moreover, isomers of these complexes (**6(*n*)**) exhibit different melting and clearing points and do not act as a eutectic mixture.

The analysis of the luminescent properties show remarkable quantum yields that range from 0.49 for **4(12)** to 0.70 for **6(12)**, the best ever reported for this kind of complex; lifetimes were also good, with almost all complexes giving times between 26 and 30 μs. Further, it was found that the different isomers of the tfac complexes gave different emission characteristics at 77 K. However, when using hfac it was found that the presence of the six strongly electron-withdrawing fluorine atoms on the β-diketonate switches off the luminescence. This is almost certainly because the MO on the hfac is stabilised to the extent that it drops in energy and becomes the LUMO, so changing the nature of the excited state leading to a non-radiative pathway that deactivates the luminescence.

It was discovered that all the samples of series **8(*n*)** in a thin-film preparation and under a thermal treatment at 110 ºC, show a shift in the emission wavelength, from 520 to 600 nm. In trying to control and to interpret this behaviour, an analysis of the luminescence typical of the different liquid crystal phase was undertaken, bu heating the solid samples **8(8)** into the liquid crystal phase and then cooling rapidly to form a glassy mesophase. It was found that there was an emission-structure correlation which could be controlled. Indeed, the emission from liquid crystal phases shows a weak broad peak at 520 nm, while in the crystal phase, grown from a liquid crystal state, the emission shows an intense and sharp red-shifted peak at 600 nm. This

could be due to the formation of new interaction, such as Pt-Pt for example in the closer crystal packing, while in the more fluid liquid or liquid crystal phase these interaction are inhibited.

Thus, these samples prove to be liquid crystalline and phosphorescent respecting the aims of this project. Furthermore they show to have very good luminescent properties, although, unfortunately, the liquid crystal transition temperatures are still a bit too high. However this combination of properties is expected to lead to highly efficient, polarised emission which, if realised, would have very significant technological applications. Some specific tests are necessary to establish whether polarised emission occurs and to what extent it does occur, and therefore if the complexes are suitable for their intended purpose. This will be the main topic of the White Rose Proof-of-Concept fellowship assigned to our research group on the base of this project.

Future research continuing on this project may investigate the effect of changing the substituent on the ligands, with the aim of lowering the transition temperatures and tuning the emission wavelength for example using ligand fluorination

During the study of these Pt^{II} complexes and under the effort to improve the yield of the reactions, different, and very interesting complexes, were discovered. For example, a dimeric platinum(III) complex was found when potassium tetrachloroplatinate(II) was changed for the more soluble *cis*-bis(dimethylsulfoxide)dichloroplatinum(II), conducting the reaction in acetic acid. The combination of ligated DMSO and acid were responsible for the oxidation.[1] This complex **18(12)** is the first example of Pt^{III} dimeric complex showing liquid crystal properties and proving also to be stable at high temperature. Analogous complexes of Pd^{III} reported by Powers and Ritter[2] containing an *ortho*-metallated benzoquinone ligand, are, in fact, stable

only below -30 °C in the solid state. Complexes of this type could be relevant to mechanistic studies of catalysis by palladium and platinum.[3]

By contrast if the above reaction is carried out in ethoxy ethanol instead of acetic acid, a dimethylsulfide complex of Pt^{II} is formed instead. Clearly, DMSO (S^{IV}) has been reduced to (S^{II}), but the identity of the oxidised product is not as yet clear.

Having prepared liquid-crystalline complexes of a well-known Pt^{II} chromophore, attention then turned to the best-known organometallic chromophore system, namely 2-phenylpyridine complexes of Ir^{III}. These are a different challenge as Ir^{III} shows octahedral geometry and generating the aniotropic structures necessary for liquid crystallinity is not so easy with such high coordination numbers. Here there was good luck as in learning how to make and handle such complexes, 2,5-di(4-dodecyloxyphenyl)pyridine ligand, **1(12)** used with Pt^{II} was selected and, while the acac complex **21(12)** was not liquid crystalline, the intermediate dmso complex **20(12)** was and showed both a lamellar and a rectangular mesophase, showing their mesomorphism between 100 and 122 °C. That such a complex was liquid crystalline is quite remarkable and entirely without precedent for the reasons discussed in Chapter 3. Some related complexes were also prepared that were liquid crystals: **22(12), 23(12)**.

The photophysical properties of these first complexes were slightly disappointing, showing rather low quantum yields and excited-state lifetimes of *ca* 80 μs.
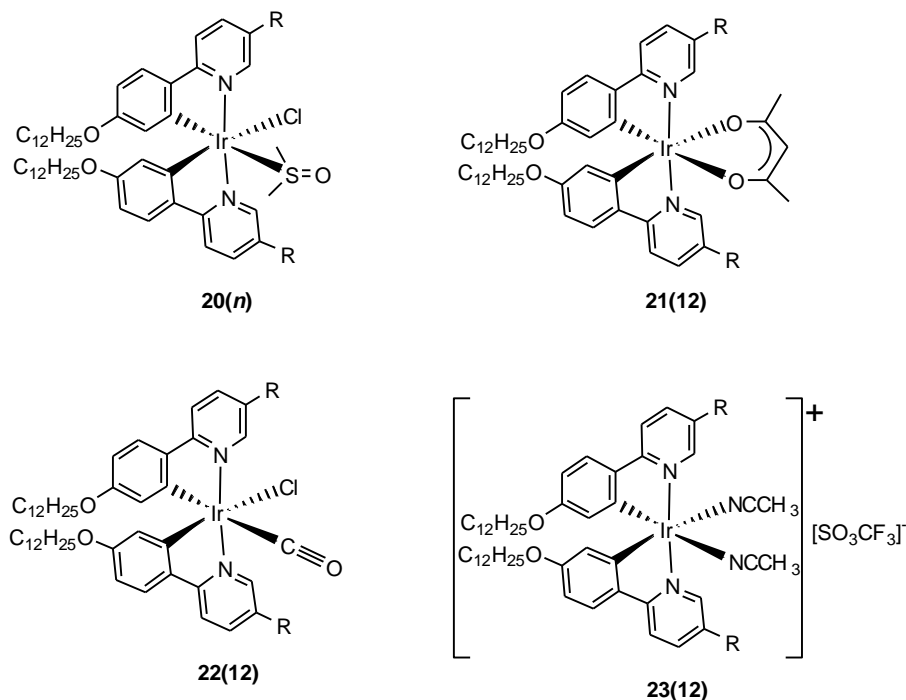
Figure 4-V Structure of the mentioned iridium complexes.

However, while it was exciting to generate these new complexes, it became apparent that all complexes containing monodentate ligands (**20(12)**, **22(12)** and **23(12)**) were unstable and converted more or less rapidly into a new complex of unknown structure (**29**). Despite many attempts, **29** remains uncharacterised and the only thing that is certain about its structure is that the two diphenylpyridine ligands are disposed symmetrically as there is a single set of resonances. In contrast, the iridium complexes containing bidentate ligands appeared stable and did not convert to **29** and so the next challenge is to find a strategy that will allow the incorporation of such bidentate ligands while retaining liquid crystal properties. Such strategies may draw on previous successes in generating liquid crystals from octahedral metal centres, such as used of polycatenar ligands or of highly anisotropic ligands.

As the literature contains only two reports of amphiphilic iridium complexes and one (very

recent) example of a liquid-crystalline complex of iridium(III), then it is clear that this work is at the forefront of the subject. And, given the importance of iridium(III) in OLED technology, they remain attractive synthetic targets despite the challenges posed.

In all of this work, the true test is of course not the photophysical parameters determined in solution, rather the data obtained from these materials in prototype devices; this work will form part of the White Rose project.

References

1   A. Santoro, M. Wegrzyn, A. C. Whitwood, B. Donnio, and D. W. Bruce, *J. Am. Chem. Soc.*, 2010, **132**, 10689.

2   D. C. Powers, and T. Ritter, *Nat. Chem.* 2009, **1**, 302.

3   (a) N. R. Deprez,and M. S. Sanford, *J. Am. Chem. Soc.* **2009**, *131*, 11234; (b) W. R. Dick, J. W. Kampf,and M. S. Sanford, *Organometallics* **2005**, *24*, 482.

Chapter 6: Experimental

6.1 General Information

6.1.1 Instrumentation

6.1.1.1 UV-Vis and Luminescence Spectroscopy

Absorption spectra in solution were measured on a Biotek Instruments XS spectrometer, using quartz cuvettes of 1 cm path length. Steady-state luminescence spectra were measured using a Jobin Yvon FluoroMax-2 spectrofluorimeter, fitted with a red-sensitive Hamamatsu R928 photomultiplier tube; the spectra shown are corrected for the wavelength dependence of the detector, and the quoted emission maxima refer to the values after correction. Samples for emission measurements were contained within quartz cuvettes of 1 cm path length modified with appropriate glassware to allow connection to a high-vacuum line. Degassing was achieved *via* a minimum of three freeze-pump-thaw cycles whilst connected to the vacuum manifold; final vapour pressure at 77 K was $< 5 \times 10^{-2}$ mbar, as monitored using a Pirani gauge. Luminescence quantum yields were determined using [Ru(bpy)$_3$]Cl$_2$ in air-equilibrated aqueous solution ($\phi = 0.028$[1]) as the standard; estimated uncertainty in ϕ is $\pm$ 20% or better. The emission spectra of the films were measured using a Hitachi F-4500 spectrophotometer, and the samples were prepared using a Chemat Technology Spin-Coater KW-4A.

The luminescence lifetimes of the complexes in degassed solution were measured by multichannel-scaling following excitation using a μs-pulsed xenon lamp at 400 nm. The emitted light was detected at 90° using a Peltier-cooled R928 PMT after passage through a monochromator. The estimated uncertainty in the quoted lifetimes is ±10% or better. The shorter lifetimes of the model complex [Pt(phpy)(acac)] and those of the new complexes in aerated solution, were measured using the same detector operating in time-correlated single-photon-counting mode, by excitation with a laser diode at 374 nm. Bimolecular rate constants for quenching by molecular oxygen, k_Q, were determined from the lifetimes in degassed and air-equilibrated solution, taking the concentration of oxygen in CH_2Cl_2 at 0.21 atm O_2 to be 2.2 mmol dm^{-3}.[2] The luminescence lifetimes of the films were measured using the same system.

6.1.1.2 ^{1}H- and ^{13}C-NMR Spectroscopy

The ^{1}H- and ^{13}C-NMR spectra were recorded using a Jeol ex270 running Delta software (270 MHz ^{1}H; 67.5 MHz ^{13}C), a Jeol ECX400 or ECS400 both running Delta (400 MHz ^{1}H; 100 MHz ^{13}C). Data are expressed in parts per million downfield shift from tetramethylsilane as an internal standard or relative to $CDCl_3$. All J values are given in Hertz. Assignments are made with the calculation of the constant coupling.

6.1.1.3 Small-Angle X-ray Scattering

The XRD patterns were obtained with two different experimental set-ups. In all cases, a linear monochromatic Cu-Kα$_1$ beam (λ = 1.5405 Å) was obtained using a sealed-tube

generator (900 W) equipped with a bent quartz monochromator. In the first set, the transmission Guinier geometry was used, whereas a Debye-Scherrer-like geometry was used in the second experimental set-up. In all cases, the crude powder was filled in Lindemann capillaries of 1 mm diameter and 10 μm wall thickness. An initial set of diffraction patterns was recorded on an image plate; periodicities up to 80 Å can be measured, and the sample temperature controlled to within ± 0.3 °C from 20 to 350 °C. The second set of diffraction patterns was recorded with a curved Inel CPS 120 counter gas-filled detector linked to a data acquisition computer; periodicities up to 60 Å can be measured, and the sample temperature controlled to within ± 0.05 °C from 20 to 200 °C. In each case, exposure times were varied from 1 to 4 h.

6.1.1.4 Single-Crystal X-ray

Diffraction data were collected typically at 110 K (see CIF files for any variation), on a Bruker Smart Apex diffractometer with Mo-K_α radiation ($\lambda = 0.71073$ Å) using a SMART CCD camera. Diffractometer control, data collection and initial unit cell determination was performed using 'SMART'.[3] Frame integration and unit-cell refinement was carried out with 'SAINT+'.[4] Absorption corrections were applied by SADABS.[5] Structures were solved by either direct methods or Patterson map (see CIF file for *solution_primary*) using SHELXS-97[6] (Sheldrick, 1997) and refined by full-matrix least squares using SHELXL-97[7] (Sheldrick, 1997). All non-hydrogen atoms were refined anisotropically. Hydrogen atoms were placed using a 'riding model' and included in the refinement at calculated positions.

6.1.1.5 Mass Spectroscopy

Mass spectra were recorded using a Fisons Analytical VG Autospec spectrometer operating in chemical ionization (CI), electron ionisation (EI) or fast atom bombardment (FAB) mode or on a Bruker Daltronics microTOF spectrometer operating in electrospray ionisation (ESI) mode.

6.1.1.6 CHN Instrument

Values were obtained on a Exeter Analytical Inc., CE-440 Elemental Analyser. Calibration performed against acetanilide standards and checked by the use of *S*-benzyl thiouronium chloride as internal standard (both analytical grade, supplied by Exeter Analytical). Carrier gas is CP-grade Helium and combustion gas is N5.5 grade Oxygen, both from BOC.

6.1.1.7 Differential Scanning Calorimetry and Optical Micreoscopy

Enthalpies of liquid crystal transitions were measured using a Mettler Toledo DSC822e differential scanning calorimeter, equipped with Mettler Toledo TS0801RO Sample Robot and calibrated against pure indium metal. Heating and cooling rates were 5 or 10 ^{o}C min^{-1}. Optical textures were recorded using an Olympus BX50 polarizing microscope equipped with a Linkam scientific LTS350 heating stage, Linkam LNP2 cooling pump, and Linkam TMS92 controller.

Voltalab 50, PST050, produced by Radiometer Analytical. The reference electrode is a Ag/AgCl and the working electrode is platinum. The voltammogram were recordered in DMF using (cpFe/cpFe$^+$ 0.64 V) as internal standard.

6.2 Synthesis

All chemicals and solvents were used as supplied, unless noted otherwise. The synthesis is given for one example of each series of molecules with C12 chains, while the elemental analysis data are detailed in paragraph 6.3, for all ligands and complexes. All the ligands and platinum complexes are already published.[8] All unpublished compounds are noted in the text below.

6.2.1 Ligands

*6.2.1.1 Ligand **1(n)***

(i) **2,5-Di(4-methoxyphenyl)-1,2,4-triazine**:
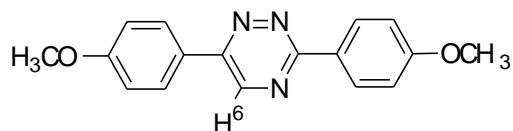
Structure of triazine.

4-Methoxybenzohydrazide (8.74 mmol, 1.45 g), 2-bromo-4'-methoxyacetophenone (4.37

mmol, 1.00 g) and sodium acetate (4.81 mmol, 0.39 g) were added to a solution of ethanol and acetic acid (20 cm^3, 7:3). The mixture was stirred and heated under reflux for 16 h, after which it was cooled slowly. The crystalline precipitate was filtered off and washed with ethanol (10 cm^3) and diethyl ether (10 cm^3) to give a yellow, crystalline solid. Yield 0.97 g (3.32 mmol, 76%).

^{1}H-NMR δ_H (270 MHz, CDCl$_3$): 8.94 (1H, s, H^6), 8.50 (2H, d, J = 8.9 Hz, AA'XX') 8.09 (8H, d, J = 8.8 Hz, AA'XX'), 7.07 (2H, d, J = 8.8 Hz, AA'XX'), 7.04 (2H, d, J = 8.9 Hz, AA'XX'), 3.89 (3H, s, OCH$_3$), 3.88 (3H, s, OCH$_3$).

(ii) **2,5-Di(4-methoxyphenyl)pyridine**:
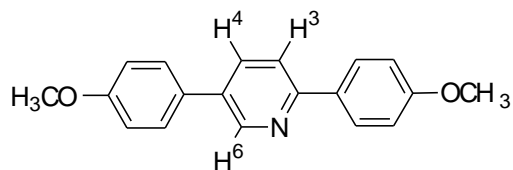
Structure of 2,5-Di(4-methoxyphenyl)pyridine.

2,5-Di(4-methoxyphenyl)-1,2,4-triazine (8.52 mmol, 2.50 g) was added to a solution of bicyclo[2.2.1]hepta-2,5-diene (86.3 mmol, 7.95 g) in 1,2-dichlorobenzene (20 cm^3). The mixture was stirred and heated under reflux for 5 h. During the reaction more bicyclo[2.2.1]hepta-2,5-diene (88.45 mmol, 8.15 g) was added and the solution was left under reflux overnight, after which it was cooled, the solvent was removed by filtration and the solid washed with ethanol (50 cm^3) and ethoxyethane (50 cm^3) to give a grey, crystalline solid. Yield 1.61g (5.54 mmol, 65%).

^{1}H-NMR δ_H (270 MHz, CDCl$_3$): 8.79 (1H, d, $^4J_{HH}$ = 2.7 Hz, H^6), 7.79 (2H, d, J = 8.9 Hz, AA'XX'), 7.86 (1H, dd, $^3J_{HH}$ = 8.3 Hz, $^4J_{HH}$ = 2.7 Hz, H^4), 7.71 (1H, d, $^3J_{HH}$ = 8.2 Hz, H^3),

7.55 (2H, d, $^3J_{HH}$ = 8.8 Hz, AA'XX'), 6.95 (2H, d, J = 8.9 Hz, AA'XX'), 6.94 (2H, d, J = 8.8 Hz, AA'XX'), 3.85 (3H, s, OCH_3), 3.86 (3H, s, OCH_3).
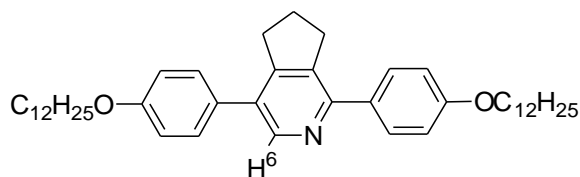
(iii) **2,5-Di(4-hydroxyphenyl)pyridine**:
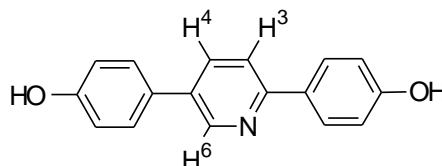
Structure of 2,5-Di(4-hydroxyphenyl)pyridine.

2,5-Di(4-methoxyphenyl)pyridine (3.60 mmol, 1.05 g) was added to molten pyridinium chloride (45.43 mmol, 5.25 g) at 200 °C and stirred for 16 h. After some cooling, the still warm mixture was added to water (50 cm^3) and stirred for 15 minutes. The resulting solid was recovered by filtration and washed with water (100 cm^3) and propanone (100 cm^3), to give a green solid. Yield 0.56 g (2.14 mmol, 59%).

^{1}H-NMR δ_H (270 MHz, dmso): 10.11 (1, broad s, OH), 9.87 (1H, broad s, OH), 8.86 (1H, d, $^4J_{HH}$ = 1.9 Hz, H^6), 8.53 (1H, dd, $^3J_{HH}$ = 8.7 Hz, $^4J_{HH}$ = 1.9 Hz, H^4), 8.19 (1H, d, $^3J_{HH}$ = 8.7 Hz, H^3), 7.98 (2H, d, $^3J_{HH}$ = 8.7 Hz, Ar), 7.70 (2H, d, $^3J_{HH}$ = 8.6 Hz, Ar), 6.98 (2H, d, $^3J_{HH}$ = 8.7 Hz, Ar), 6.94 (2H, d, $^3J_{HH}$ = 8.6 Hz, Ar).

(iv) **Ligand 1(12)**:
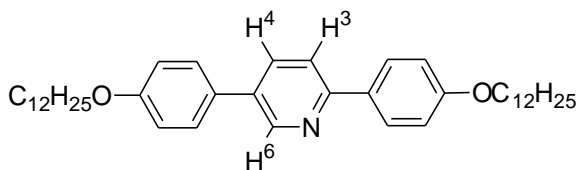
Structure of ligand **1(12)**.

2,5-Di(4-hydroxyphenyl)pyridine (1.90 mmol, 0.50 g) was added to a solution of 1-bromododecane (4.73 mmol, 1.18 g) and potassium carbonate (5.50 mmol, 0.76 g) in DMF (20 cm^3). The solution was stirred and heated under reflux for 12 h. Following cooling, the solid was recovered by filtration and washed with water (70 cm^3), propanone (50 cm^3) and chloroform (10 cm^3), to give a colourless, crystalline solid. Yield 0.51 g (0.85 mmol, 45%).

^{1}H-NMR δ_H (270 MHz, CDCl$_3$): 8.79 (1H, d, $^4J_{HH}$ = 2.3 Hz, H^6), 7.90 (2H, d, J = 8.9 Hz, AA'XX'), 7.80 (1H, dd, $^3J_{HH}$ = 8.3 Hz, $^4J_{HH}$ = 2.3 Hz, H^4), 7.64 (1H, d, $^3J_{HH}$ = 8.3 Hz, H^3), 7.48 (2H, d, J = 8.7 Hz, AA'XX'), 6.94 (2H, d, J = 8.9 Hz, AA'XX'), 6.93 (2H, d, J = 8.8 Hz, AA'XX'), 3.94 (4H, m, OCH$_2$), 1.74 (4H, m, CH$_2$), 1.41 (4H, m, CH$_2$), 1.19 (32H, broad m, CH$_2$), 0.81 (6H, t, Me). ^{13}C-NMR δ_C (400 MHz, CDCl$_3$): 147.61, 134.45, 133.9, 130.14, 128.03, 127.96, 119.48, 115.29, 114.87, 68.32, 68.27, 31.95, 29.69, 29.66, 29.63, 29.61, 29.44, 29.36, 26.11, 22.69, 14.07. HRMS-ESI (m/z): [MH$^+$], for C$_{41}$H$_{62}$NO$_2$ found (expected) 600.4775 (600.9365).

*6.2.1.2 Ligand **2(n)***

(i) **2,5-Di(4-methoxyphenyl)cyclopentenepyridine**:
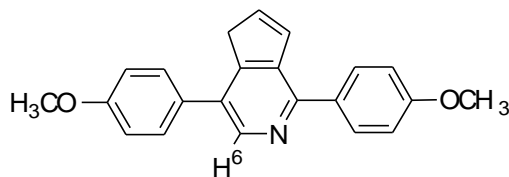
Structure of ligand 2,5-Di(4-methoxyphenyl)cyclopentenepyridine. .

3,6-Di(4-methoxyphenyl)-1,2,4-triazine (4.00 mmol, 1.17 g) was added to 1-(*N*-morpholino)cyclopentene (18.8 mmol, 2.88 g). The mixture was stirred and heated under an

argon atmosphere, at 190 °C for 2 h. During the reaction more 1-(*N*-morpholino)cyclopentene (6.30 mmol, 0.97 g) was added, and the solution was left for an additional 1 h at 190 °C. After the mixture was cooled, ethanol (10 cm^3) was added. The precipitate was recovered by filtration and the solid washed with ethanol (15 cm^3) to give a colourless, crystalline solid. Yield 0.88 g (2.68 mmol, 67%).

^{1}H-NMR δ_H (270 MHz, CDCl$_3$): 8.49 (1H, s, H[6]), 7.74 (2H, d, J = 2.27 Hz, AA'XX'), 7.41 (2H, d, J = 2.10 Hz, AA'XX'), 6.99 (4H, d, J = 8.8 Hz, AA'XX'), 3.85 (H, s, OCH$_3$), 3.14 (2H, t, CH$_2$ cyclopentene), 3.01 (2H, t, CH$_2$ cyclopentene), 2.04 (2H, m, CH$_2$ cyclopentene).

(ii) **2,5-Di(4-hydroxyphenyl)cyclopentenepyridine**:
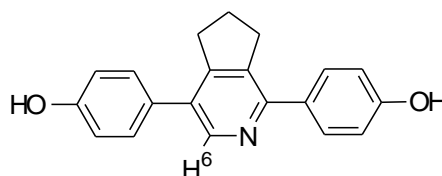
Structure of 2,5-Di(4-hydroxyphenyl)cyclopentenepyridine.

2,5-Di(4-methoxyphenyl)- cyclopentenepyridine (3.59 mmol, 1,19 g) was added to molten pyridinium chloride (45.43 mmol, 5.25 g) at 200 °C and stirred for 12 h. When the mixture was still warm, water (50 cm^3) was added and the mixture stirred for 15 minutes. The solid was recovered by filtration and washed with water (100 cm^3) and propanone (100 cm^3), to give a dark solid. Yield 0.98 g (3.23 mmol, 90%).

^{1}H-NMR δ_H (270 MHz, dmso): 10.47 (1H, broad s, OH), 10.05 (1H, broad s, OH), 8.51 (1H, s, H[6]), 7.66 (2H, d, $^3J_{HH}$ = 8.7 Hz, Ar), 7.47 (2H, d, $^3J_{HH}$ = 8.6 Hz, Ar), 6.98 (4H, m, Ar), 3.15 (4H, m, CH$_2$ cyclopentene), 2.09 (2H, m, CH$_2$ cyclopentene).

(iii) **Ligand 2(12)**:

Structure of ligand **2(12)**.

2,5-Di(4-hydroxyphenyl)cyclopentenepyridine (1.90 mmol, 0.581 g) was added to a solution of 1-bromododecane (4.73 mmol, 1.18 g) and potassium carbonate (5.50 mmol, 0.762 g) in DMF (20 cm³). The solution was stirred and heated under reflux for 12 hours. After the mixture was cooled, it was dissolved in water (150 cm³), filtered off the precipitate and washed with ethanol (50 cm³) and propanone (25 cm³). The crude product was purified by column chromatography (silica gel 10:1 CHCl₃: ethyl acetate), the fractions were collected and the solvent was removed by rotary evaporator to give a brown pale solid. Yield 0.68 g (0.85 mmol, 55%).

¹H-NMR δ_H (270 MHz, CDCl₃): 8.49 (1H, s, H⁶), 7.73 (2H, d, J = 8.7 Hz, AA'XX'), 7.39 (2H, d, J = 8.7 Hz, AA'XX'), 6.98 (4H, d, J = 8.7 Hz, AA'XX'), 3.94 (4H, m, OCH₂), 3,14 (2H, t, CH₂ cyclopentene), 3.02 (2H, t, CH₂ cyclopentene), 2.04 (2H, m, CH₂ cyclopentene), 1.80 (4H, m, CH₂), 1.47 (4H, m, CH₂), 1.28 (32H, broad m, CH₂), 0.88 (6H, t, Me). ¹³C-NMR δ_C (400 MHz, CDCl₃): 225.03, 129.88, 114.75, 114.41, 68.21, 33.29, 31.99, 29.68, 29.65, 29.49, 29.41, 29.36, 26.15, 22.77, 14.21. HRMS-ESI (*m/z*): [MH⁺], for C₄₄H₆₆NO₂ found (expected) 640.5088 (641.0003).

6.2.1.3 Ligand 3(12)

(iv) **2-Bromo-3',4'-dimethoxyacetophenone:**
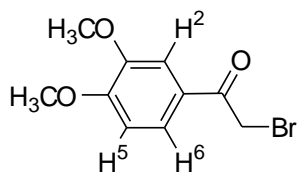
Structure of 2-Bromo-3',4'-dimethoxyacetophenone.

Bromine (8.74 mmol, 1.40 g) was added drop by drop to a solution of 3,4-dimethoxybenzophenone (8.32 mmol, 1.50 g) in diethyl ether (100 cm^3) at room temperature. After complete addition the reaction was left to stir for 1 h. The diethyl ether solution was then washed with aqueous NaHCO$_3$ saturated and then brine. The organic fractions were collected, dried over anhydrous MgSO$_4$ and the solvent was removed by rotary-evaporation giving a white solid. Yield 1.08 g (4.16 mmol, 50%).

^{1}H-NMR δ_H (270 MHz, CDCl$_3$): 7.60 (1H, dd, $^3J_{HH}$ = 8.5 Hz, $^4J_{HH}$ = 2.0 Hz, H^6), 8.50 (1H, d, $^4J_{HH}$ = 1.9 Hz, H^2) 6.89 (1H, d, $^3J_{HH}$ = 8.8 Hz, H^5), 4.40 (2H,s, -CH$_2$Br), 3.95 (3H, s, OCH$_3$), 3.92 (3H, s, OCH$_3$).

(v) **2-(4-Methoxyphenyl)-5-(3,4-dimethoxyphenyl)-1,2,4-triazine**:
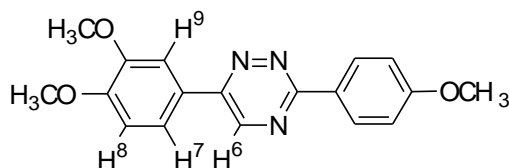
Structure of 2-(4-Methoxyphenyl)-5-(3,4-dimethoxyphenyl)-1,2,4-triazine.

4-Methoxy-benzo-hydrazide (7.72 mmol, 1.28 g), 2-bromo-3',4'-dimethoxy-acetophenone (3.86 mmol, 1.00 g) and sodium acetate (4.00 mmol, 0.32 g) were added to a solution of ethanol and acetic acid (20 cm^3, 7:3). The mixture was stirred and heated under reflux for 16

h, after which it was cooled slowly. The crystalline precipitate was filtered off and washed with ethanol (10 cm^3) and diethyl ether (10 cm^3) to give a yellow, crystalline solid. Yield 0.80 g (2.47 mmol, 64.1%).

^{1}H-NMR δ_H (270 MHz, CDCl$_3$): 8.98 (1H, s, H^6), 8.51 (2H, d, J = 8.9 Hz, AA'XX') 7.90 (1H, d, $^4J_{HH}$ = 2.0 Hz, H^9), 7.57 (1H, dd, $^3J_{HH}$ = 8.5 Hz, ^4J = 2.1 Hz, H^7), 7.03 (3H, m, AA'XX' + H^8) 4.00 (3H, s, OCH$_3$), 3.96 (3H, s, OCH$_3$), 3.90 (3H, s, OCH$_3$).

(vi) **2-(4-Methoxyphenyl)-5-(3,4-methoxyphenyl)pyridine**:
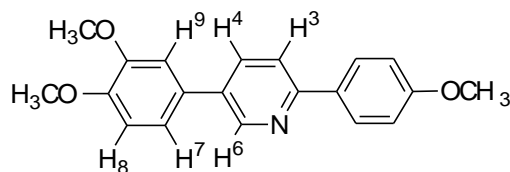
Structure of 2-(4-Methoxyphenyl)-5-(3,4-methoxyphanyl)pyridine.

2-(4-mMethoxyphenyl)5-(3,4-dimethoxyphenyl)-1,2,4-triazine (8.73 mmol, 2.50 g) was added to a solution of bicyclo[2.2.1]hepta-2,5-diene (86.3 mmol, 7.95 g) in 1,2-dichlorobenzene (20 cm^3). The mixture was stirred and heated under reflux for 5 h. During the reaction more bicyclo[2.2.1]hepta-2,5-diene (88.5 mmol, 8.15 g) was added and the solution was left under reflux overnight, after which it was cooled, the solvent was removed by filtration and the solid washed with ethanol (50 cm^3) and ethoxyethane (50 cm^3) to give a grey, crystalline solid. Yield 1.50g (5.15 mmol, 59%).

^{1}H-NMR δ_H (270 MHz, CDCl$_3$): 8.85 (1H, d, $^4J_{HH}$ = 2.6 Hz, H^6), 7.99 (2H, d, J = 8.9 Hz, AA'XX'), 7.89 (1H, dd, $^3J_{HH}$ = 8.1 Hz, $^4J_{HH}$ = 2.2 Hz, H^4), 7.71 (1H, d, $^3J_{HH}$ = 8.5 Hz, H^3), 7.18 (1H, dd, $^3J_{HH}$ = 8.2 Hz, $^4J_{HH}$ = 2.2 Hz, H^7), 6.11 (1H, d, $^4J_{HH}$ = 1.8 Hz, H^9), 7.02 (3H, m, AA'XX' + H^8), 3.96 (3H, s, OCH$_3$), 3.93 (3H, s, OCH$_3$), 3.87 (3H, s, OCH$_3$).

(vii) **2-(4-Hydroxyphenyl)-5-(3,4-dihydroxyphenyl)pyridine**:
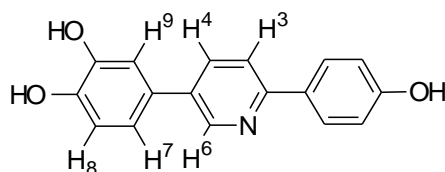
Structure of 2-(4-hHydroxyphenyl)-5-(3,4-hydroxyphenyl)pyridine.

2-(4-Methoxyphenyl)-5-(3,4-dimethoxyphenyl)pyridine (3.11 mmol, 1.00 g) was added to molten pyridinium chloride (45.43 mmol, 5.25 g) at 200 °C and stirred for 16 h. After some cooling, the still warm mixture was added to water (50 cm^3) and stirred for 15 minutes. The resulting solid was recovered by filtration and washed with water (100 cm^3) and propanone (100 cm^3), to give a green solid. Yield 0.43 g (1.56 mmol, 50%).

^{1}H-NMR δ_H (270 MHz, dmso): 10.11 (not integrable, broad s, OH), 9.87 (not integrable, broad s, OH), 8.76 (1H, d, $^4J_{HH}$ = 2.1 Hz, H^6), 8.53 (1H, dd, $^3J_{HH}$ = 8.5 Hz, H^4), 8.16 (1H, d, $^3J_{HH}$ = 8.3 Hz, H^3), 7.95 (2H, d, J = 9.1 Hz, AA'XX'), 7.20 (1H, d, $^4J_{HH}$ = 2,1 Hz, H^9), 7.13 (1H, dd, $^3J_{HH}$ = 8.2 Hz, $^4J_{HH}$ = 2.1 Hz H^7), 6.96 (2H, d, J = 8.9 Hz, AA'XX') 6.88 (1H, d, $^3J_{HH}$ = 8.3, H^8).

(viii) **Ligand 3(12)**:
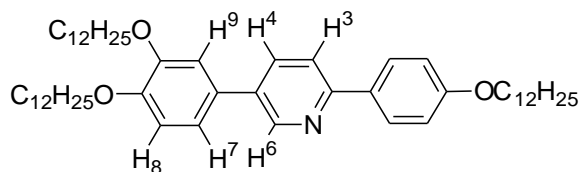
Structure of ligand **3(12**.**)**

2-(4-Hydroxyphenyl)-5-(3,4-dihydroxyphenyl)pyridine (3.58 mmol, 1.00 g) was added to a

solution of 1-bromododecane (12.5 mmol, 3.13 g) and potassium carbonate (8.25 mmol, 1.14 g) in DMF (20 cm^3). The solution was stirred and heated under reflux for 12 h. Following cooling, the solid was recovered by filtration and washed with water (70 cm^3), propanone (50 cm^3) and chloroform (10 cm^3), to give a colourless, crystalline solid. Yield 1.09 g (1.40 mmol, 39%).

^{1}H-NMR δ_H (270 MHz, CDCl$_3$): 8.81 (1H, d, $^4J_{HH}$ = 1.9 Hz, H^6), 7.98 (2H, d, J = 8.2 Hz, AA'XX'), 7.86 (1H, dd, $^3J_{HH}$ = 8.5 Hz, $^4J_{HH}$ = 1.9 Hz, H^4), 7.72 (1H, d, $^3J_{HH}$ = 8.5 Hz, H^3), 7.19 (1H, d, ^4J = 1.8 Hz, H^9), 6.99 (4H, m, AA'XX' + H^7 + H^8), 4.03 (6H, m, OCH$_2$), 1.81 (6H, m, CH$_2$), 1.49 (6H, m, CH$_2$), 1.25 (48H, broad m, CH$_2$), 0.86 (9H, m, Me). HRMS-ESI (*m/z*): [MH$^+$], for C$_{41}$H$_{62}$NO$_2$ found (expected) 783.1529 (783.6529).

6.2.1 Platinum(II) Complexes

In some cases it was not possible to observe the Pt satellite for H[7]. I those cases, the data were simply omitted.

6.2.1.1 Platinum complexes of 1(12)

(i) **Complex 16(12)**:
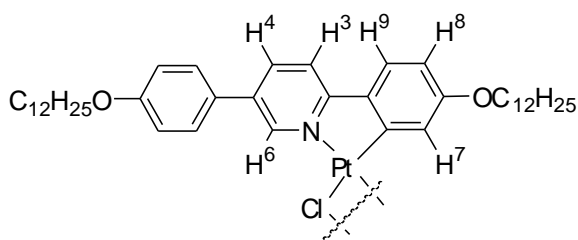
Structure of platinum complex **16(12)**.

Potassium tetrachloroplatinate(II) (0.241 mmol, 0.100 g), solubilised in the minimum amount of hot water (1.0 cm^3), was added to a solution of **1(12)** (0.242 mmol, 0.145 g) in acetic acid (50 cm^3). The mixture was stirred and heated under vigorous reflux overnight. The precipitate was recovered by filtration, washed successively with hot acetic acid (30 cm^3), water (60 cm^3), chloroform (50 cm^3) and diethyl ether (30 cm^3). The product was insoluble in the most common NMR solvents and was used in the next step without further purification. Yield 0.094 g (0.057 mmol, 33%).

(ii) **Complex 14(12)**:
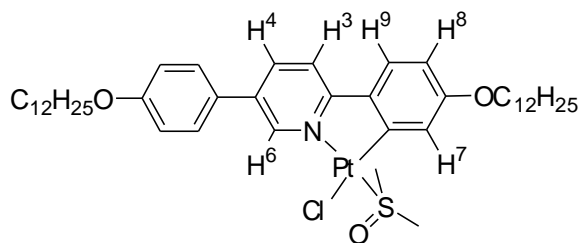
Structure of complex **14(12)**

μ-Chloro (0.060 mmol, 0.100 g) was dissolved in dmso (10 cm^3) and heated under reflux with stirring for 30 min. The solvent was removed by rotary evaporator and the resulting compound purified on a short chromatography column on silica, using chloroform as eluent. Yield 0.095 g (0.105 mmol, 87%).

^{1}H-NMR δ_H (270 MHz, CDCl$_3$): 9.70 (1H, d, $^4J_{HH}$ = 2.0 Hz, $^3J_{HPt}$ = 36.8 H^6), 7.94 (1H, d, $^4J_{HH}$ = 2.3 Hz, H^7), 7.87 (1H, dd, $^3J_{HH}$ = 8.5 Hz $^4J_{HH}$ = 2.0 Hz, H^4), 7.51 (1H, d, $^3J_{HH}$ = 8.8 Hz, H^3), 7.46 (2H, d, J = 8.7 Hz, AA'XX'), 7.36 (1H, d, $^3J_{HH}$ = 8.6 Hz, H^9), 6.91 (2H, d, J = 8.7 Hz, AA'XX'), 6.66 (1H, dd, $^3J_{HH}$ = 8.7 Hz, $^4J_{HH}$ = 2.3 Hz, H^8) 3.95 (4H, m, OCH$_2$), 3.59 (6H, s, $^3J_{HPt}$ = 21.2 Hz, SMe), 1.72 (4H, m, CH$_2$), 1.39 (4H, m, CH$_2$), 1.20 (32H, broad m, CH$_2$), 0.81 (6H, t, Me).

(iii) **Complex 4(12)**:

4(12) R = R' = CH$_3$
5(12) R = R' = CH$_2$CH$_3$
6(12) R = CF$_3$ R' = CH$_3$
7(12) R = R' = CF$_3$
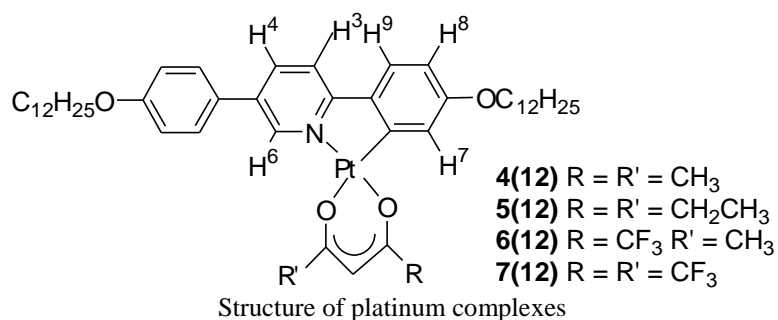
Structure of platinum complexes

Complex **14(12)** (0.111 mmol, 0.100 g) was added to a solution of sodium acetylacetonate monohydrate (1.16 mmol, 0.163 g) in propanone (60 cm^3), and stirred at room temperature for 4 h. After the reaction, the solvent was removed by rotary evaporation, washed with water (50 cm^3), and crystallised from propanone. Yield 0.091 g (0.102 mmol, 92%).

^{1}H-NMR δ_H (270 MHz, CDCl$_3$): 9.04 (1H, d, $^4J_{HH}$ = 2.1 Hz, $^3J_{HPt}$ = 36.6 H^6), 7.82 (1H, dd, $^3J_{HH}$ = 8.5 Hz, $^4J_{HH}$ = 2.1 Hz, H^4), 7.45 (2H, d, J = 8.8 Hz, AA'XX') 7.42 (1H, d, $^3J_{HH}$ = 8.6 Hz, H^3), 7.39 (1H, d, $^3J_{HH}$ = 8.6 Hz, H^9), 7.05 (1H, d, $^4J_{HH}$ = 2.5 Hz, H^7), 6.94 (2H, d, J = 8.8 Hz, AA'XX'), 6.60 (1H, dd, $^3J_{HH}$ = 8.5 Hz, $^4J_{HH}$ = 2.5 Hz, H^8), 5.41 (1H, s, CO-CH-CO), 4,00 (2H, t, OCH$_2$), 3.94 (2H, t, OCH$_2$), 1.94 (3H, s, -CO-CH$_3$), 1.93 (3H, s, -CO-CH$_3$), 1.74 (4H, m, CH$_2$), 1.40 (4H, m, CH$_2$), 1.20 (32H, broad m, CH$_2$), 0.81 (6H, t, Me). ^{13}C-NMR δ_C (400 MHz, CDCl$_3$): 135.81, 127.78, 124.44, 117.48, 115.31, 110.79, 31.00, 29.72, 29.43, 28.44, 26.19, 26.12, 22.77, 14.19. MS-FAB (*m/z*): [M$^+$], for C$_{46}$H$_{67}$NO$_4$Pt found (expected) 892.47 (892.47).

(iv) **Complex 7(12)** not published**:** Complex **14(12)** (0.166 mmol, 0.150 g) was solubilised in dichloromethane (20 cm^3); to this solution sodium hexafluoroacetylacetonate (0.332 mmol, 0.076 g) was added. The solution was stirred at room temperature for 24 hours, after which time the solvent was removed and the product purified by silica column chromatography on silica using a chloroform eluent. Yield 0.090 g (0.090 mmol, 54.3%).

^{1}H-NMR δ_H (400 MHz, CDCl$_3$): 8.71 (1H, s, $^4J_{HH}$ = 2.2 Hz, $^4J_{HPt}$ = 32.9 Hz ^{6}H), 7.86 (1H, dd, $^3J_{HH}$ = 8.5 Hz, $^4J_{HH}$ = 2.2 Hz, ^{4}H), 7.42 (3H, d, J = 8.6 Hz, H^3 and AA'XX'), 7.26 (1H, d, $^3J_{HH}$ = 8.8 Hz, H^9), 6.95 (2H, d, J = 8.6 Hz, AA'XX'), 6.76 (1H, d, $^4J_{HH}$ = 2.7 Hz, H^7), 6.60 (1H, dd, $^3J_{HH}$ = 8.8 Hz, $^4J_{HH}$ = 2.7 Hz, H^8), 6.16 (1H, s, CO-CH-CO), 3.95 (4H, t, OCH$_2$), 1.74 (4H, m, CH$_2$), 1.39 (4H, m, OCH$_2$), 1.20 (32H, broad m, CH$_2$), 0.81 (6H, t, CH$_3$). Anal. For C$_{46}$H$_{61}$F$_6$NO$_4$Pt found (expected): C 54.97 (55.19), H 6.08 (6.14), N 1.26 (1.40).

(v) **Complex 6(12)** not published: Complex **14(12)** (0.166 mmol, 0.150 g) was solubilised in

dichloromethane (20 cm^3), to this solution sodium 1,1,1-trifluoro-2,4-pentanedionate (0.332 mmol, 0.058 g) was added. The solution was stirred at room temperature overnight, after which time the solvent was removed and the product purified by silica column chromatography using a chloroform eluent. Yield 0.101 g (0.106 mmol, 64%).

^{1}H-NMR δ_H (400 MHz, CDCl$_3$): 8.89 (1H, d, $^4J_{HH}$ = 2.0 Hz, $^3J_{HPt}$ = 37.5 Hz, H^6), 7.85 (1H, dd, $^3J_{HH}$ = 8.6 Hz, $^4J_{HH}$ = 2.0 Hz, H^4), 7.43 (2H, d, J = 8.5 Hz, AA'XX'), 7.43 (1H, d, $^3J_{HH}$ = 8.6 Hz, ^{3}H), 7.30 (1H, d, $^3J_{HH}$ = 8.4 Hz, H^9), 6.94 (2H, d, J = 8.5 Hz, AA'XX'), 6.94 (1H, d, $^4J_{HH}$ = 2.4 Hz, H^7), 6.61 (1H, dd, $^3J_{HH}$ = 8.4 Hz, $^4J_{HH}$ = 2.4 Hz, H^8), 5.79 (1H, s, CO-CH-CO), 3.99 (2H, t, OCH$_2$), 3.99 (2H, t, OCH$_2$), 2.02 (3H, -CO-CH$_3$), 1.75 (4H, m, CH$_2$), 1.41 (4H, m, CH$_2$), 1.20 (32H, broad m, CH$_2$), 0.80 (6H, t, Me). Anal. For C$_{46}$H$_{64}$F$_3$NO$_4$Pt found (expected): C 58.29 (58.21), H 6.78 (7.01), N 1.45 (1.48).

(vi) **Complex 5(12)** not published: Complex **14(12)** (0.166 mmol, 0.150 g) was solubilised in dichloromethane (20 cm^3), to this solution sodium 3,5-heptanedionate (0.403 mmol, 0.061 g) was added. The solution was stirred at room temperature overnight, after which time the solvent was removed and the product purified by silica column chromatography using a chloroform eluent before crystallisation from hot acetone. Yield: 0.090 g (0.098 mmol, 59 %).

^{1}H-NMR δ_H (270 MHz, CDCl$_3$): 9.12 (1H, d, $^4J_{HH}$ = 2.00 Hz, $^3J_{HPt}$ = 39.0 Hz, H^6), 7.82 (1H, dd, $^3J_{HH}$ = 8.5 Hz, $^4J_{HH}$ = 2.00 Hz, H^4), 7.46 (2H, d, J = 8.8 Hz, AA'XX'), 7.42 (1H, d, $^3J_{HH}$ = 8.5 Hz, ^{3}H), 7.30 (1H, d, $^3J_{HH}$ = 8.6 Hz, H^9), 7.1 (1H, d, $^4J_{HH}$ = 2.5 Hz, H^7), 6.94 (2H, d, J = 8.8 Hz, AA'XX'), 6.60 (1H, dd, $^3J_{HH}$ = 8.6 Hz, $^4J_{HH}$ = 2.5 Hz, H^8), 5.41 (1H, s, CO-CH-CO), 4.01 (2H, t, OCH$_2$), 3.94 (2H, t, OCH$_2$), 2.20 (4H, m, CO-CH$_2$), 1.75 (4H, m, CH$_2$), 1.40 (4H, m, CH$_2$), 1.20 (32H, broad m, CH$_2$), 1.18 (6H, t, O-CH$_2$- CH$_3$), 0.81 (6H, t, CH$_3$). Anal. For C$_{48}$H$_{71}$NO$_4$Pt found (expected): C 62.03 (62.45), H 7.73 (7.97), N 1.47 (1.52)

(vii) **Complex *cis*-[PtCl$_2$(DMSO)$_2$]^9**: Potassium tetrachloroplatinate(II) (2,41 mmol, 1,00 g), was solubilised in water (50 cm^3), to this solution was added dimethylsulfoxide (7.23 mmol,

0.565 g). The mixture was stirred at room temperature for 30 min and then left to precipitate for 2 h. The white precipitate was recovered by filtration, washed successively with water (10 cm^3), and acetone (30 cm^3). The product was used in the next step without further purification. Yield 0.865 g (2.05 mmol, 85%).

^{1}H-NMR δH (400 MHz, CDCl$_3$): 3.52 (12H, s, $^3J_{HPt}$ = 27.9 Hz from referecne)

(viii) **Complex *cis*-[PtCl$_2$(DMS)$_2$]**: The synthesis of *cis*-[PtCl$_2$(DMS)$_2$] was achieved by the same method applied for cic-[PtCl$_2$(DMSO)$_2$].

^{1}H-NMR $δ_H$ (400 MHz, CDCl$_3$): 2.52 (6H, s, $^3J_{HPt}$ = 49.2 Hz), 2.41 (6H, s, $^3J_{HPt}$ = 41.0 Hz)

(ix) **Complex 18(2)**:
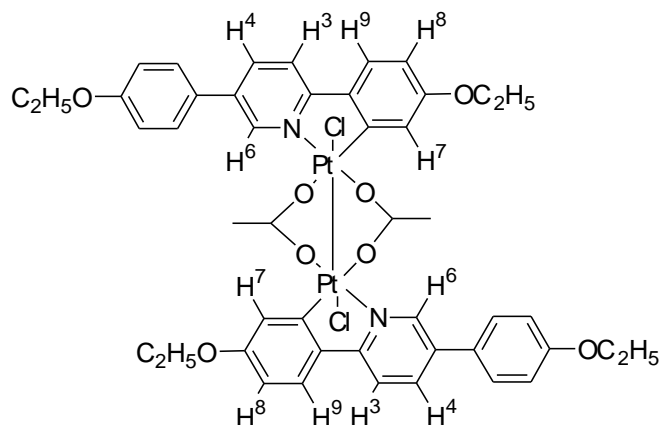
Structure of complex **18(2)**, The structure is not representative of the real geometry of the molecule.

cis-[PtCl$_2$(DMSO)$_2$] (1.18 mmol, 0.500 g) was solubilised in acetic acid (50 cm^3), to this solution **1(12)** (1.18 mmol, 0.377 g) was added. The mixture was heated under reflux for 12 h. Then the reaction was cooled and the product was recovered by filtration. The filtrate was

washed with water (10 cm^3), and propanone (30 cm^3). Finally the product was crystallised from propanone. Yield 0.547 g (0.531 mmol, 45%).

^{1}H-NMR δ_H (270 MHz, CDCl$_3$): 7.96 (2H, d, $^4J_{HH}$ = 1.8 Hz, $^3J_{HPt}$ = 32.2 Hz, H^6), 7.51 (2H, dd, $^3J_{HH}$ = 8.4 Hz, $^4J_{HH}$ = 1.8 Hz, H^4), 7.31 (4H, d, J = 8.8 Hz, AA'XX'), 6.99 (2H, d, $^3J_{HH}$ = 8.4 Hz, ^{3}H), 6.95 (4H, d, J = 8.8 Hz, AA'XX'), 6.72 (2H, d, $^3J_{HH}$ = 8,5 Hz, H^9), 6.27 (2H, d, $^4J_{HH}$ = 2.2 Hz, $^3J_{HPt}$ = 27.1 Hz, H^7), 6.12 (2H, dd, $^3J_{HH}$ = 8.4 Hz, $^4J_{HH}$ = 2.2 Hz, H^8), 4.08 (4H, t, OCH$_2$), 3.45 (2H, m, OCH$_2$), 2.65 (6H, m, CO-CH$_3$), 1.18 (6H, m, -CH$_3$), 1.11 (6H, m, -CH$_3$).

(x) **Complex 15(12)** not published
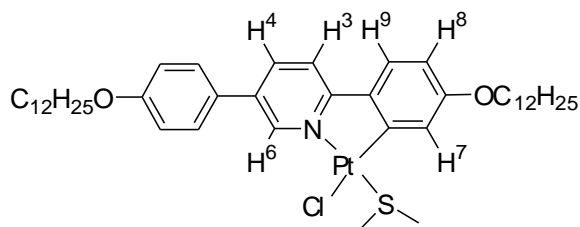
Structure of complex **15(12)**.

Preparation 1: *cis*-[PtCl$_2$(DMSO)$_2$] (1.67 mmol, 0.70 g) and **1(12)** (1.67 mmol, 1.00 g) were solubilised in ethoxyethanol (60 cm^3). The mixture was heated under reflux for 20 h under an atmosphere of nitrogen. The solution was left to cool forming a creamy yellow precipitate. This was filtered then washed with water (20 cm^3), ethanol (20 cm^3) and propanone (30 cm^3). The product was purified on silica-gel column using chloroform as eluent. Yield: 0.49 g (0.544 mmol, 32.6%)

^{1}H-NMR δ_H (400 MHz, CDCl$_3$): 9.80 (1H, d, $^4J_{HH}$ = 2.1 Hz, $^3J_{HPt}$ = 37.6 Hz, H^6), 7.88 (1H, dd, $^3J_{HH}$ = 8.4 Hz, $^4J_{HH}$ = 2.2 Hz, H^4), 7.50 (3H, m, AA'XX'+ H^5), 7.37 (1H, d, $^3J_{HH}$ = 8.6 Hz, H^9), 7.15 (1H, d, $^4J_{HH}$ = 2.5 Hz, $^3J_{HPt}$ = 57.6 Hz, H^7), 6.91 (2H, d, J = 8.6 Hz, AA'XX'), 6.62

(1H, dd, $^3J_{HH}$ = 8.5 Hz, $^4J_{HH}$ = 2.4 Hz, H^8), 3.94 (4H, m, OCH$_2$), 2.72 (6H, s, $^3J_{HPt}$ = 50.4 Hz, DMS), 1.74 (4H, m, -CH$_2$), 1.40 (4H, m, -CH$_2$), 1.20 (32H, m, -CH$_2$), 0.81 (6H, t, 7.1 Hz, -CH$_3$).

Preparation 2: *cis*-[PtCl$_2$(DMS)$_2$] (1.18 mmol, 0.46 g) and **1(12)** (1.18 mmol, 0.71 g) were solubilised in ethoxyethanol (40 cm^3). The solution was heated under reflux for 20 h under an atmosphere of nitrogen. The yellow precipitate that formed was filtered and then washed with water (20 cm^3), ethanol (20 cm^3) and propanone (30 cm^3). The product was crystallised from propanone. Yield: 0.20 g (0.354 mmol, 19.7%).

^{1}H-NMR δ_H (400 MHz, CDCl$_3$): 9.81 (1H, d, $^4J_{HH}$ = 2.2 Hz, $^3J_{HPt}$ = 36.8 Hz, H^6), 7.87 (1H, dd, $^3J_{HH}$ = 8.5 Hz, $^4J_{HH}$ = 2.2 Hz, H^4), 7.49 (3H, m, AA'XX'+ H^5), 7.37 (1H, d, $^3J_{HH}$ = 8.7 Hz, H^9)), 7.15 (1H, d, $^4J_{HH}$ = 2.5 Hz, $^3J_{HPt}$ = 55.4 Hz, H^7), 6.91 (2H, d, J = 8.6 Hz, AA'XX'), 6.62 (1H, dd, $^3J_{HH}$ = 8.6 Hz, $^4J_{HH}$ = 2.5 Hz, H^8), 3.94 (4H, m, OCH$_2$), 2.72 (6H, s, $^3J_{HPt}$ = 50.4 Hz, DMS), 1.74 (4H, m, -CH$_2$), 1.40 (4H, m, -CH$_2$), 1.20 (32H, m, -CH$_2$), 0.81 (6H, m, -CH$_3$).
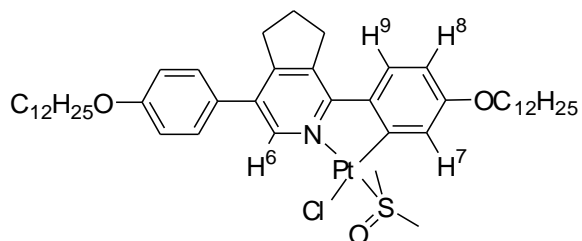
6.2.1.2 Platinum Complexes of 2(12)

(i) **Complex 16(12)cp**:
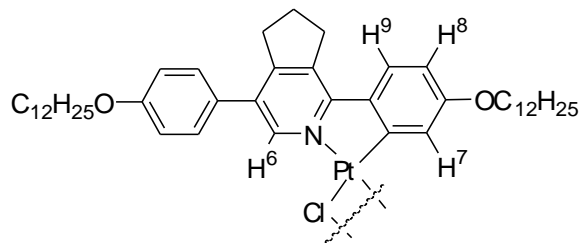
Structure of platinum complex **16(12)cp**.
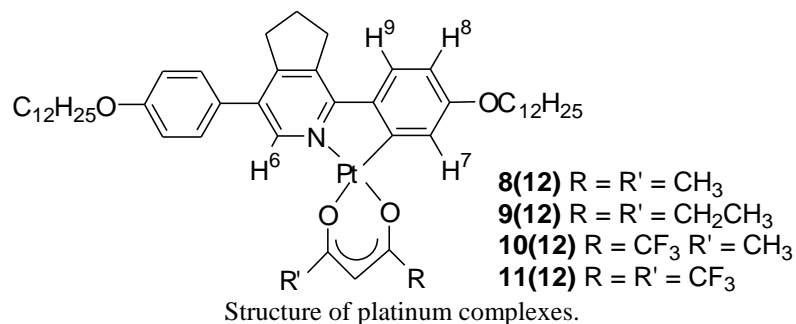
(ii) **Complex 13(12)**:

Structure of complex **13(12)**.

Complex **16(12)cp** (0.0575 mmol, 0.100 g) was dissolved in dmso (10 cm^3) and heated under reflux with stirring for 30 min. The solvent was removed by rotary evaporator and the resulting compound purified by column chromatography on silica, using chloroform as eluent. Yield 0.101 g (0.105 mmol, 95%).

^{1}H-NMR δ_H (270 MHz, CDCl$_3$): 9.45 (1H, s, $^3J_{HPt}$ = 36.7 Hz, H^6), 8.04 (1H, d, $^4J_{HH}$ = 2.6 Hz, $^3J_{HPt}$ = 55.3 Hz, H^7), 7.52 (1H, d, $^3J_{HH}$ = 8.8 Hz, H^9) 7.31 (2H, d, *J* = 8.7 Hz, AA'XX'), 6.90 (2H, d, *J* = 8.7 Hz, AA'XX'), 6.67 (1H, dd, $^3J_{HH}$ = 8.6 Hz, $^4J_{HH}$ = 2.5 Hz, H^8), 3.99 (2H, t, OCH$_2$), 3.93 (2H, t, OCH$_2$), 3,59 (6H, s, $^3J_{HPt}$ = 21.2 Hz, SMe), 3.29 (2H, t, CH$_2$ cyclopentene), 3.01 (2H, t, CH$_2$ cyclopentene), 2.12 (2H, m, CH$_2$ cyclopentene), 1.74 (4H, m, CH$_2$), 1,40 (4H, m, CH$_2$), 1.21 (32H, broad m, CH$_2$) and 0.82 (6H, t, CH$_3$).

(iii) **Complex 8(12)**:

Structure of platinum complexes.

Complex **13(12)** (0.11 mmol, 0.100 g) was added to a solution of sodium acetylacetonate monohydrate (0.23 mmol, 0.032 g) in propanone (60 cm^3), and stirred at room temperature for 12 h. After the reaction the solvent was removed by rotary evaporator, the product was solubilised in CH$_2$Cl$_2$ and then filtered. The solvent was removed by rotary evaporator and the crude product was purified by a short chromatography column on silica, using chloroform as eluent. Yield 0.086 g (0.93 mmol, 85%).

^{1}H-NMR δ_H (270 MHz, CDCl$_3$): 8.75 (1H, s, $^3J_{HPt}$ = 37.2 Hz, H^6), 7.45 (1H, d, $^3J_{HH}$ = 8.6 Hz, H^9), 7.30 (2H, d, J = 8.7 Hz, AA'XX'), 7.12 (1H, d, $^4J_{HH}$ = 2.6 Hz, H^7), 6.92 (2H, d, J = 8.7 Hz, AA'XX'), 6.59 (1H, dd, $^3J_{HH}$ = 8.6 Hz, $^4J_{HH}$ = 2.6 Hz, H^8), 5.38 (1H, s, CO-CH-CO), 4.01 (2H, t, OCH$_2$), 3.94 (2H, t, OCH$_2$), 3.30 (2H, t, CH$_2$ cyclopentene), 2.95 (2H, t, CH$_2$ cyclopentene), 2.12 (2H, m, CH$_2$ cyclopentene),1.93 (3H, s, CO-CH$_3$), 1.88 (3H, s, CO-CH$_3$), 1.75 (4H, m, CH$_2$), 1,41 (4H, m, CH$_2$), 1.20 (32H, broad m, CH$_2$) and 0.81 (6H, t, CH$_3$). MS-FAB (*m/z*): [M$^+$], for C$_{49}$H$_{71}$NO$_4$Pt found (expected): 932.50 (932.50).

(iv) **Complex 11(12)** not published: Complex **13(12)** (0.03 mmol, 0.06 g) was solubilised in dichloromethane (15 cm^3), to this solution sodium hexafluoroacetylacetonate (0.19 mmol, 0.044 g) was added. The solution was stirred at room temperature for 24 hours, after which time the solvent was removed and the product purified by a silica column chromatography using a chloroform eluent. Yield: 0.025 g, 40.02 %.

^{1}H-NMR δ_H (400 MHz, CDCl$_3$): 8.44 (1H, s, J_{HPt} not found, H^6), 7.43 (1H, d, $^3J_{HH}$ = 8.9 Hz,

H[9]), 7.29 (2H, d, J = 8.8 Hz, AA'XX'), 6.93 (2H, d, J = 8.8 Hz, AA'XX'), 6.85 (1H, d, $^4J_{HH}$ = 2.4 Hz, H[7]), 6.60 (1H, dd, $^3J_{HH}$ = 8.9 Hz, $^4J_{HH}$ = 2.4 Hz, H[8]), 6.13 (1H, s, CO-CH-CO), 3.97 (2H, t , OCH$_2$), 3.95 (2H, t , OCH$_2$), 3.30 (2H, t, CH$_2$ cyclopentene), 3.04 (2H, t, CH$_2$ cyclopentene), 2.15 (2H, m, CH$_2$ cyclopentene), 1.75 (4H, m, CH$_2$), 1.39 (4H, m, CH$_2$), 1.20 (32 H, broad m, CH$_2$), 0.81 (6H, t, CH$_3$).

(v) **Complex 10(12)** not published: Complex **13(12)** (0.11 mmol, 0.10 g) was solubilised in dichloromethane (20 cm^3), to this solution sodium1,1,1-trifluoro-2,4-pentanedionate (0.33 mmol, 0.058 g) was added. The solution was stirred at room temperature for 24 hours, after which time the solvent was removed and the product purified by column chromatography on silica using a chloroform eluent. Yield: 0.078 g, 71.8 %.

^{1}H-NMR δ_H (400 MHz, CDCl$_3$): 8.60 (1H, s, J_{HPt} not found, ^{6}H), 7.44 (1H, d, $^3J_{HH}$ = 8.9, Ar), 7.29 (2H, d, J = 8.7 Hz, AA'XX'), 7.00 (1H, d, $^4J_{HH}$ = 2.4 Hz, Ar), 6.91 (2H, d, J = 8.7 Hz, AA'XX'), 6.60 (1H, dd, $^3J_{HH}$ = 8.9, $^4J_{HH}$ = 2.4, Ar), 5.76 (1H, s, CO-CH-CO), 3.99 (2H, t, OCH$_2$), 3.94 (2H, t, OCH$_2$), 3.29 (2H, t, CH$_2$, cyclopentene), 2.98 (2H, t, CH$_2$, cyclopentene), 2.13 (2H, m, CH$_2$, cyclopentene), 1.96 (3H, s, CO-CH$_3$), 1.75 (4H, m, CH$_2$), 1.40 (4H, m, CH$_2$), 1.20 (32H, broad m, CH$_2$), 0.81 (6H, t, CH$_3$). Anal. For C$_{49}$H$_{68}$F$_3$NO$_4$Pt found (expected): C 59.44 (59.50), H 6.95 (7.13), N 1.40 (1.42).

(vi) **Complex 9(12)** not published: Complex **13(12)** (0.11 mmol, 0.10 g) was solubilised in dichloromethane (20 cm^3), to this solution sodium 3,5-heptanedionate (0.33 mmol, 0.050 g) was added. The solution was stirred at room temperature for 24 hours, after which time the solvent was removed and the product purified by column chromatography on silica using a chloroform eluent. Yield: 0.069 g, 65.3 %.

^{1}H-NMR δ_H (270 MHz, CDCl$_3$): 8.84 (1H, d, $^3J_{HPt}$ = 31.7 Hz, H[6]), 7.44 (1H, d, $^3J_{HH}$ = 8.4 Hz, H[9]), 7.32 (2H, d, J = 8.8 Hz, AA'XX'), 7.17 (1H, d, $^4J_{HH}$ = 2.1 Hz, H[7]), 6.91 (2H, d, J = 8.8 Hz, AA'XX'), 6.59 (1H, dd, $^3J_{HH}$ = 8.4 Hz, $^4J_{HH}$ = 2.1 Hz, H[8]), 5.37 (1H, s, CO-CH-CO), 4.01 (2H,

t, OCH$_2$), 3.93 (2H, t, OCH$_2$), 3.29 (2H, t, CH$_2$ cyclopentene), 2.97 (2H, t, CH$_2$ cyclopentene), 2.17 (2H, m, CH$_2$ cyclopentene),   2.17 (4H, m, O-CH$_2$), 1.74 (4H, m, CH$_2$), 1.40 (4H, m, CH$_2$), 1.22 (32H, broad m, CH$_2$), 1.20 (6H, O-CH$_2$-CH$_3$), 0.80 (6H, t, CH$_3$).

6.2.1.3 Platinum Complexes of 3(12)

All the intermediate complexes, three-chains **16(12)** and DMSO adduct (**14(12)tc**), for the synthesis of complexes **12(12)** were obtained in the same way of the one described above. For these intermediate complexes no characterisation was done.

(i) **Complex 12(12)** not published:
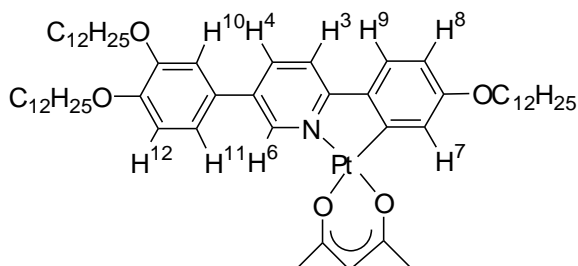
Structure of platinum complex of ligand **3(12)**.

Complex **14(12)tc** (0.092 mmol, 0.10 g) was added to a solution of sodium acetylacetonate monohydrate (1.16 mmol, 0.163 g) in propanone (60 cm^3), and stirred at room temperature for 5 h. After the reaction the solvent was removed by rotary evaporator, washed with water (50 cm^3), and crystallised from propanone. Yield 0.081 g (0.075 mmol, 82%).

^{1}H-NMR δ_H (270 MHz, CDCl$_3$): 9.12 (1H, d, $^4J_{HH}$ = 2.1 Hz, $^3J_{HPt}$ = 32.1 H^6), 7.89 (1H, dd, $^3J_{HH}$ = 8.5 Hz, $^4J_{HH}$ = 1.9 Hz, H^4), 7.47 (1H, d, $^3J_{HH}$ = 8.5 Hz, H^3) 7.35 (1H, d, $^3J_{HH}$ = 8.5 Hz, H^9), 7.12 (3H, m, H^{10} + H^{11} + H^7), 6.97 (1H, d, $^3J_{HH}$ = 8.8 Hz, H^{12}), 6.66 (1H, dd, $^3J_{HH}$ = 8.8 Hz, $^4J_{HH}$ = 2.4 Hz, Ar), 5.47 (1H, s, CO-CH-CO), 4,00 (6H, m, OCH$_2$), 2.00 (3H, s, -CO-

CH$_3$), 1.98 (3H, s, -CO-CH$_3$), 1.83 (6H, m, CH$_2$), 1.48 (6H, m, CH$_2$), 1.26 (48H, broad m, CH$_2$), 0.87 (9H, t, Me).

6.2.2 Iridium(III) Complexes

All the iridium complexes are not published yet.
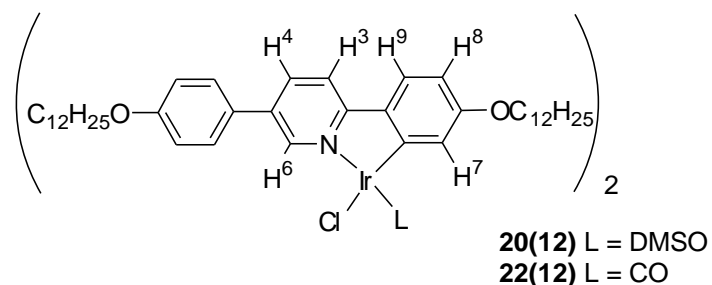
(i) **Complex 19(12)**:
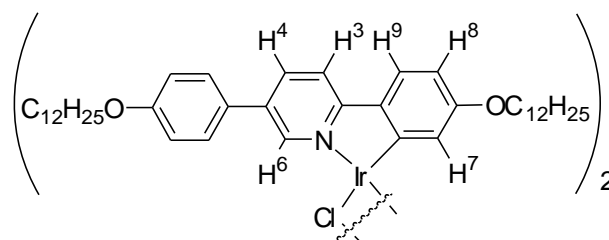
Structure of iridium complex **19(12)**.

IrCl$_3$·3H$_2$O (1.58 mmol, 0.556 g) was added to a solution of **1(12)** (3.00 mmol, 1.799 g) in ethoxyethanol (50 cm^3) and water (10 cm^3); the mixture was stirred and heated under vigorous reflux for 12 h. The solution was cooled to room temperature and the yellow-orange precipitate was collect by filtration. The precipitate was washed with ethanol (20 cm^3) and propanone (20 cm^3). The product was purified on a silica column with CH$_2$Cl$_2$/petroleum ether (60/90) (6:4). Yield 1.49 g (0.52 mmol, 66%).

^{1}H-NMR δ_H (270 MHz, CDCl$_3$): 9.31 (2H, s, H^6), 7.53 (2H, d, $^3J_{HH}$ = 8.9 Hz, Ar), 7.28 (2H, s covered by solvent signal, Ar), 6.97 (2H, d, $^3J_{HH}$ = 8.17 Hz, Ar), 6.52 (4H, d, J = 8.54 Hz, AA'XX'), 6.17 (2H, d, $^3J_{HH}$ = 8.17 Hz, Ar), 5.55 (2H, s,H^7), 3.76 (4H, m, OCH$_2$), 3.47 (4H, t, OCH$_2$), 1.70 (4H, m, CH$_2$), 1.24 (76H, broad m, CH$_2$), 0.80 (12H, m, CH$_3$).

(ii) **Complex 20(12)**:

Structures of Iridium complexes.
The different proton signals of the two ligands are reported, for examples as H^6 and 'H^6.

Complex **19(12)** (0.07 mmol, 0.200 g) was dissolved in the minimum amount of DMSO (~ 20 cm^3). The solution was refluxed for 30 min / 1 h. The solution was cooled at room temperature and the product recovered by filtration. Yield: 0.194 g (0.129 mmol, 92%).

^{1}H-NMR δ_H (270 MHz, CDCl$_3$): 10.27 (1H, d, $^4J_{HH}$ = 1.86 Hz, H^6), 9.99 (1H, d, $^4J_{HH}$ = 1.86 Hz, 'H^6), 7.97 (2H, m, Ar), 7,68 (6H, m, Ar), 7.47 (2H, d, J = 8.91 Hz, AA'XX'), 7.26 (2H, covered by solvent signal, Ar), 6.99 (2H, d, J_{HH} = 8.54 Hz, Ar), 6.45 (2H, m), 6.00 (1H, d, $^4J_{HH}$ = 2.23 Hz, H^7), 5.41 (1H, d, $^4J_{HH}$ = 2.23 Hz, 'H^7), 3.98 (4H, m, OCH$_2$), 3.59 (4H,broad m, OCH$_2$), 3.16 (3H, s, S-CH$_3$), 2,06 (3H, s, S-CH$_3$), 1.79 (4H, broad m, CH$_2$), 1.25 (76H, broad m, CH$_2$), 0.80 (12H, t, CH$_3$).

(iii) **Complex 22(12)**: Complex **20(12)** (0.07 mmol, 0.050 g) was dissolved in dichloromethane (15 cm^3). The solution was stirred under an atmosphere of CO for 3 h. The solvent was removed under vacuum to yield a quantitative amount of the desired product (0.047 g).

^{1}H-NMR δ_H (270 MHz, CDCl$_3$): 10.30 (1H, d, $^4J_{HH}$ = 1.86 Hz, H^6), 9.16 (1H, d, $^4J_{HH}$ = 1.86 Hz, 'H^6), 8.06 (1H, dd, $^3J_{HH}$ = 8.5 Hz, $^4J_{HH}$ = 2.2 Hz, Ar), 7,98 (1H, dd, $^3J_{HH}$ = 8.5 Hz, $^4J_{HH}$ = 2.2 Hz, Ar), 7.79 (2H, m, Ar), 7.60 (6H, m, Ar), 7.00 (3H, m, Ar), 6.49 (3H, m, Ar), 5.96 (1H,

d, $^4J_{HH}$ = 2.3 Hz, H^7), 5.55 (1H, d, $^4J_{HH}$ = 2.25 Hz, 'H^7), 4.00 (4H, m, OCH$_2$), 3.62 (4H,broad m, OCH$_2$), 1.81 (4H, broad m, CH$_2$), 1.25 (76H, broad m, CH$_2$), 0.86 (12H, t, CH$_3$).

(iv) **Complex 21(12)**:
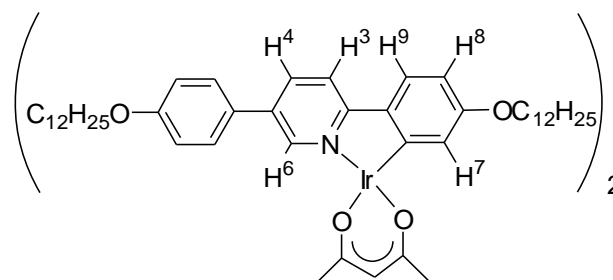
Structure of complex **21(12)**

Complex **20(12)** (0.168 mmol, 0.250 g) was suspended in acetone (35 cm^3), then sodium acetylacetonate (1.68 mmol, 0.205 g) was added to this solution. The mixture was heated under reflux for 6 h; afterwards the solvent was reduced in volume under vacuum, and the product precipitated by the addition of water. The solid was recovered by filtration and washed with ethanol (15 cm^3) and petroleum ether 60/90 (15 cm^3). The yellow-orange precipitate was purified on a silica column with CH$_2$Cl$_2$. Yield: 0.223 g (0.150 mmol, 89%).

^{1}H-NMR δ_H (270 MHz, CDCl$_3$): 8.66 (2H, d, $^4J_{HH}$ = 2.1 Hz, H^6), 7.85 (2H, dd, $^3J_{HH}$ = 8.5 Hz, $^4J_{HH}$ = 2.1 Hz, H^4), 7.72 (2H, d $^3J_{HH}$ = 8.5 Hz, H^3), 7.51 (4H, d, J = 9.1 Hz, AA'XX'), 7.46 (2H, d, $^3J_{HH}$ = 8.8 Hz, H^9), 6.98 (4H, d, J = 8.8 Hz, AA'XX'), 6.39 (2H, dd, $^3J_{HH}$ = 8.5 Hz, $^4J_{HH}$ = 2.4 Hz, H^8), 5.83 (2H, d, $^4J_{HH}$ = 2.4 Hz, H^7), 5,29 (1H, s, CO-CH-CO), 3.99 (4H, t, OCH$_2$), 3.64 (4H, m, OCH$_2$), 1.78 (6H, s, CO-CH$_3$), 1,46 (4H, m, CH$_2$), 1.25 (76H, broad m, CH$_2$), 0.87 (12H, m, CH$_3$).
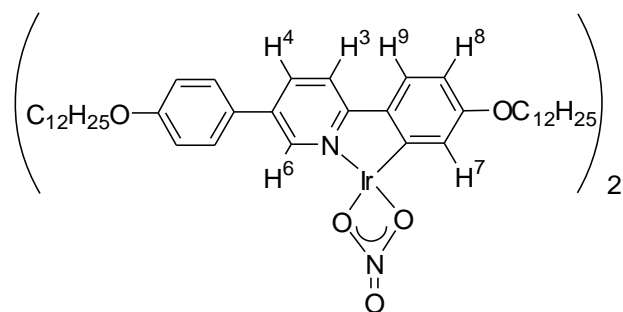
(v) **Complex 23(12)**:

Structure of complex **23(12)**
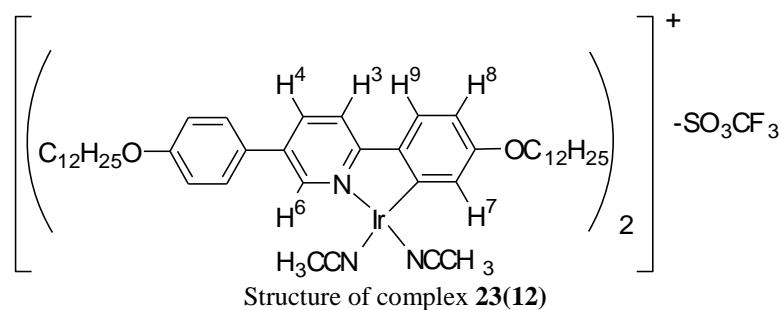
Complex **19(12)** (0.049 mmol, 0.140 g) was dissolved in acetonitrile (25 cm^3) and AgSO$_3$CF$_3$ (0.10 mmol 0.025 g) was added to this solution. The mixture was stirred at room temperature for 7 h and after this time the solvent was removed in cold condition. The product was the solubilised in CH$_2$Cl$_2$ and filtered through celite, then the product was precipitate by the addition of acetone, filtered and washed with methanol (20 cm^3). Yield: 0.055 g (0.034 mmol, 70%)

^{1}H-NMR δ_H (270 MHz, CDCl$_3$): 8.07 (2H, d, $^4J_{HH}$ = 1.8 Hz, H^6), 8.00 (2H, dd, $^3J_{HH}$ = 8.6 Hz, $^4J_{HH}$ = 1.9 Hz, H^4), 7.77 (2H, d $^3J_{HH}$ = 8.7 Hz, H^3), 7.70 (4H, d, J = 8.5 Hz, AA'XX'), 7.47 (2H, d, $^3J_{HH}$ = 8.2 Hz, H^9), 7.07 (4H, d, J = 8.5 Hz, AA'XX'), 6.46 (2H, dd, $^3J_{HH}$ = 8.4 Hz, $^4J_{HH}$ = 1.9 Hz, H^8), 5.62 (2H, d, $^4J_{HH}$ = 2.2 Hz, H^7), 4.02 (4H, m, OCH$_2$), 3.63 (4H, m, OCH$_2$), 2.42 (6H, s, NC-CH$_3$), 1.79 (4H, m, CH$_2$), 1,50 (4H, m, CH$_2$), 1.25 (72H, broad m, CH$_2$), 0.86 (12H, m, CH$_3$).

(vi) **Complex 25(12)**:

Structure of complex **25(12)**.

Complex **19(12)** (0.049 mmol, 0.140 g) was dissolved in acetonitrile (25 cm^3) and AgNO$_3$ (0.10 mmol 0.017 g) was added to this solution. The mixture was stirred at room temperature for 7 h and after this time was heated under reflux overnight. The product was precipitated by the addition of water, filtered and washed with methanol (20 cm^3). Yield: 0.053 g (0.036 mmol, 74%)

^{1}H-NMR δ_H (270 MHz, CDCl$_3$): 8.85 (2H, d, $^4J_{HH}$ = 2.0 Hz, H^6), 7.96 (2H, dd, $^3J_{HH}$ = 8.6 Hz, $^4J_{HH}$ = 2.1 Hz, H^4), 7.78 (2H, d $^3J_{HH}$ = 8.5 Hz, H^3), 7.53 (4H, d, J = 8.6 Hz, AA'XX'), 7.46 (2H, d, $^3J_{HH}$ = 8.6 Hz, H^9), 6.99 (4H, d, J = 8.5 Hz, AA'XX'), 6.44 (2H, dd, $^3J_{HH}$ = 8.6 Hz, $^4J_{HH}$ = 2.5 Hz, H^8), 5.65 (2H, d, $^4J_{HH}$ = 2.3 Hz, H^7), 3.99 (4H, t, OCH$_2$), 3.65 (4H, m, OCH$_2$), 1.79 (4H, m, CH$_2$), 1.25 (76H, broad m, CH$_2$), 0.87 (12H, m, CH$_3$).

6.3 Analytical Data

All the synthesised compounds were analysed with an elemental analyser, unfortunately no good result were obtained for the Ir^{III} complexes. In the Table 1 are reported all the results.

Table 1 Analytical data for the synthesized compounds

Compound	Found (Expected) / %		
	C	H	N
1(6)	80.6 (80.7)	8.7 (8.6)	3.4 (3.3)
1(8)	81.3 (81.1)	9.3 (9.3)	2.7 (2.9)
1(10)	81.8 (81.7)	10.0 (9.8)	2.5 (2.6)
1(12)	82.2 (82.1)	10.8 (10.3)	2.1 (2.3)
2(6)	81.5 (81.9)	8.7 (8.8)	3.2 (3.0)
2(8)	81.7 (81.9)	10.0 (9.4)	2.7 (2.7)
2(10)	82.3 (82.1)	9.8 (9.9)	2.4 (2.8)
2(12)	82.4 (82.6)	10.4 (10.2)	2.3 (2.2)
3(12)	81.2 (81.2)	10.8 (10.9)	1.8 (1.8)
4(6)	56.2 (56.3)	5.8 (6.0)	2.1 (1.9)
4(8)	58.1 (58.5)	6.2 (6.6)	2.0 (1.8)
4(10)	60.3 (60.7)	7.1 (7.4)	1.7 (1.5)
4(12)	61.9 (62.0)	7.6 (7.7)	1.6 (1.5)
5(6)	57.0 (57.3)	6.2 (6.5)	1.7 (1.9)
5(8)	59.0 (59.2)	6.8 (7.1)	1.7 (1.7)
5(10)	61.0 (60.9)	7.3 (7.6)	1.6 (1.6)
5(12)	62.1 (62.4)	7.7 (8.0)	1.5 (1.5)
6(6)	52.1 (52.3)	5.1 (5.4)	1.6 (1.8)
6(8)	54.0 (54.4)	5.8 (6.0)	1.5 (1.7)
6(10)	56.6 (56.5)	6.3 (6.5)	1.6 (1.6)
6(12)	58.3 (58.2)	6.8 (7.0)	1.4 (1.5)
7(12)	54.9 (55.2)	6.1 (6.1)	1.3 (1.4)
14(6)	52.4 (52.6)	5.8 (6.0)	2.2 (2.0)
14(10)	56.9 (57.2)	6.8 (7.1)	1.9 (1.7)

8(6)	57.9 (58.1)	6.0 (6.2)	2.0 (1.8)
8(8)	60.3 (60.0)	6.4 (6.8)	1.9 (1.7)
8(10)	61.6 (61.6)	7.5 (7.2)	1.7 (1.6)
8(12)	62.7 (63.1)	8.0 (7.7)	1.5 (1.5)
9(12)	63.6 (63.6)	7.8 (8.1)	1.4 (1.5)
10(12)	59.4 (59.5)	7.0 (7.1)	1.4 (1.4)
11(12)	56.5 (56.5)	6.3 (6.3)	1.3 (1.4)
13(6)	50.9 (50.7)	4.2 (4.3)	2.3 (2.4)
13(10)	58.3 (58.4)	7.4 (7.5)	1.5 (1.5)
12(12)	63.6 (64.5)	8.4 (8.3)	1.3 (1.3)
15(12)*	56.9 (58.7)	7.3 (7.1)	1.5 (1.6)
18(12)	58.1 (58.5)	7.4 (8.0)	1.5 (1.4)
19(12)**	66.4 (67.1)	8.3 (8.5)	1.8 (1.9)

* Data reported from the MChem student Tabitha Petchey

** Probable presence of complex **29**.

References

1   Nakamaru, K. *Bull. Chem. Soc. Jpn.*, **1982**, *55*, 2697

2   Murov, S. L.; Carmichael, I.; Hug, G. L. *Handbook of Photochemistry,* 2nd ed., Marcel Dekker: New York, **1993**.

3   "SMART" - control software Bruker SMART Apex X-ray Diffractometer. v5.625, Bruker-AXS GMBH, Karlsruhe, Germany.

4   "SAINT+" - integration software for Bruker SMART detectors. v6.45, Bruker-AXS GMBH, Karlsruhe, Germany.

5   "SADABS" - program for absorption correction. v2.10. G. M. Sheldrick, Bruker AXS Inc., Madison, Wisconsin, USA, 2007.

6   "SHELXS-97" - program for structure solution. G. M. Sheldrick, University of Göttingen, Göttingen, Germany, 1997.

7   "SHELXL-97" - program for the Refinement of Crystal Structures. G. M. Sheldrick, University of Göttingen, Göttingen, Germany, 1997.

8   (a) A. Santoro, M. Wegrzyn, A. C. Whitwood, B. Donnio, and D. W. Bruce, *J. Am. Chem. Soc.*, 2010, **132**, 10689; (b) A. Santoro, A. C. Whitwood, J. A. G. Williams, V. K. Kozhevnikov and D. W. Bruce, *Chem. Mater.* 2009, **21**, 3871.

9   J. H. Price,J. H. Williamson, R. F. Schramm, B. B. Wayland, *Inorg. Chem.*, 1972, **11**, 1280.

Appendix

In the electronic version, uploaded on http://etheses.whiterose.ac.uk, it is possible to find the x-Ray details and the published articles of the author.